[1] *Praise the LORD.*
Praise the LORD from the heavens,
praise him in the heights above.

[2] *Praise him, all his angels,*
praise him, all his heavenly hosts.

[3] *Praise him, sun and moon,*
praise him, all you shining stars.

[4] *Praise him, you highest heavens*
and you waters above the skies.

[5] *Let them praise the name of the LORD,*
for he commanded and they were created.

[6] *He set them in place for ever and ever;*
he gave a decree that will never pass away.

[7] *Praise the LORD from the earth,*
you great sea creatures and all ocean depths,

[8] *lightning and hail, snow and clouds,*
stormy winds that do his bidding,

[9] *you mountains and all hills,*
fruit trees and all cedars,

[10] *wild animals and all cattle,*
small creatures and flying birds,

[11] *kings of the earth and all nations,*
you princes and all rulers on earth,

[12] *young men and maidens,*
old men and children.

[13] *Let them praise the name of the LORD,*
for his name alone is exalted;
his splendor is above the earth and the heavens.

[14] *He has raised up for his people a horn,*
the praise of all his saints,
of Israel, the people close to his heart.
Praise the LORD.

– Psalm 148, The Bible (New International Version)

University of Alberta

Quantum Chemistry of Confinement: Studies of Structural and Spectral Properties of Small Molecules

by

John Ming Hong Lo 

A thesis submitted to the Faculty of Graduate Studies and Research in partial fulfillment of the requirements for the degree of **Doctor of Philosophy**.

Department of Chemistry

Edmonton, Alberta
Spring 2006

Your file Votre référence
ISBN: 0-494-14012-7
Our file Notre référence
ISBN: 0-494-14012-7

To My Family and Friends.

Abstract

The studies of electrons, atoms and ions captured by external electric and magnetic fields have recently become a mainstream in the research of semi-conductor physics and nanotechnology; however, similar investigations concerning confined molecules are rather limited. Therefore, the present thesis aims at filling this missing link by exploring the cavity effects on the physical and chemical properties of small molecules when they are enclosed by an external potential.

The thesis is composed of two sections. The first part, consisting of the first two chapters, deals with the theoretical background of the modeling of confinement. All the *ab initio* techniques employed in this project are reviewed in Chapter 1, followed by a general introduction to various models of confinement and a detailed discussion of the parabolic model in Chapter 2.

The subsequent chapters form the second part of the thesis which is concerned with the applications of the harmonic model potential to a number of diatomic

molecules with different unique characteristics. It starts with the analysis of the simplest neutral molecule, H_2, and a comparison with the scenario when H_2 is subjected to a strong magnetic field, followed by the investigations into a wide variety of exotic phenomena induced by the presence of a confining potential: the reorganization of dissociation channels and the alternation of the ground-state terms of alkaline-earth dimers (Chpaters 4 and 5), facilitated field-induced autoionization of Rydberg molecules (Chapters 6 and 7), interplay of relativity, electron correlation, and spatial confinement (Chapter 8) and cavity-modulation of opto-electronic properties of small molecules (Chapter 9). Explanations for all these observations are proposed and discussed in terms of the configuration interactions caused by the spatial confinement. Meanwhile, the applicability of the perturbational approach, a cheaper alternative to variational configuration interaction-type methods, to the studies of confinement effects for weakly-bound systems is also verified.

Acknowledgements

The completion of the present work is not the achievement of a single person but a group of people whose efforts, contributions and support I am always indebted.

First of all, I must express my most sincere gratitude to my Ph.D. supervisor, Professor Mariusz Klobukowski. He has offered all kinds of help, both academic and spiritual, whenever I was desperate and feeling helpless. He showed me the correct attitude towards scientific research: critical, persistent, and enthusiastic. I am grateful he provided me the greatest flexibility in my research so that I could carry out the projects of my own interest. Being knowledgeable, cheerful and gentle, he is always an excellent supervisor, colleague, and friend of mine. It is truly my priviledge to have worked for him in the past five years.

My groupmates have also been the source of support for me during the course of my research. To all the people in Klobukowski's group, past and present, whom I have been working with: Dr. Chris Lovallo, Jonathan Mane, Lara Silkin, Nazanin Jamshidi, Jesse Kadosh, Melissa Gajewski, Toby Tsang, and Evan Kelly - I owe them heartful thanks. They are wonderful friends and colleagues, and they have always provided me with joyful time in the laboratory. I treasure all the moments I have spent with these great colleagues.

In the past several years, I have also had precious opportunities to collaborate with a number of famous quantum chemists and molecular physicists in the world, namely Drs. Dorota Bielińska-Wąż, Geerd H. F. Diercksen, and Andrzej J. Sadlej. Working with these first-rank scientists is such a marvelous experience as I could earn so much invaluable knowledge from them.

I would also like to extend my thanks to the Information Technology Group

of the Department of Chemistry, and the Computing and Network Services of the University of Alberta for the computing facilities and assistance they offered. Computers are one of the most determining factors in computational research. In this aspect, I am fortunate that these poeple have done a great job. Furthermore, I would like to thank all the financial supports from the Department of Chemistry, Faculty of Science and Natural Science and Engineering Research Council of Canada (NSERC) which helped me survive in the past several years.

In this renowned Department and University, I have known a lot of good friends who not only helped me in my research and studies but also supported and guided me in my life journey. In particular, my acknowledgements go to Thanh Luu and Sandra Chan for our mutual inspiration and encouragement. We are forever friends! I am cordially thankful to my parents Frankie and Theresa, my sister Assunta and my brother-in-law Frankie, and my lifelong friends Ida Ling, Aileen Poon, Sappho Mak, Franco Tam and Hugo Lok for all their patience, concern, care, love, hopes, and prayers. Hey, I am done! I have finally accomplished my wish I have had since I was a kid!

Finally, and most importantly, I would like to give thanks to my Lord, Jesus Christ, for He is my Savior, my Helper, and the Creator of the world. Without Him and His grace, I would not have gone this far. He made the world so wonderful and my research so meaningful as, through which, I can appreciate the amazement of His creation, and admire His might. May His name be glorified forever and ever!

Table of Contents

List of Tables

List of Figures

List of Abbreviations

AEA	Adiabatic Electron Affinity
AIMP	*Ab Initio* Model Potential
AM1	Austin Model 1
ANO	Atomic Natural Orbitals
B3LYP	Hybrid Becke-3 and Lee-Yang-Parr Functional
BO	Born-Oppenheimer
BSSE	Basis Set Superposition Error
CASPT	Complete Active Space Perturbation Theory
CASPT2	Second-Order Complete Active Space Perturbation Theory
CASSCF	Complete Active Space Self-Consistent Field
CC	Coupled Cluster
cc	correlation-consistent
CCD	Coupled Cluster Doubles
CCSD	Coupled Cluster Singles and Doubles
CCSDT	Coupled Cluster Singles, Doubles and Triples
CCSD(T)	Coupled Cluster Singles, Doubles and iterative Triples
CEP	Compact Effective Potential
CHA	Chemical Hamiltonian Approach
CI	Configuration Interaction
CISD	Configuration Interaction with Single and Double Excitations
CISDTQ	Configuration Interaction with Single, Double, Triple and Quadruple Excitations
CP	Counterpoise
CSF	Configurational State Function
DFT	Density Functional Theory
DK	Douglas-Kroll
DKH	Douglas-Kroll-Heß
DK1	First-Order Douglas-Kroll
DK2	Second-Order Douglas-Kroll
DK3	Third-Order Douglas-Kroll

ECP	Effective Core Potential
EFG	Electric Field Gradient
FCI	Full Configuration Interaction
FIR	Far-Infrared
FSOCI	Full Second-Order Configuration Interaction
FW	Foldy-Wouthuysen
GTF	Gaussian-Type Function
HF	Hartree-Fock
HFRH	Hartree-Fock-Roothaan-Hall
HMO	Hückel Molecular Orbital
HO	Harmonic Oscillator
HOMO	Highest-Occupied Molecular Orbital
IPM	Independent Particle Model
ISA	Intruder State Avoidance
LUMO	Lowest-Unoccupied Molecular Orbital
MCP	Model Core Potential
MCPT	Multi-Configuration Perturbation Theory
MCSCF	Multi-Configurational Self-Consistent Field
MNDO	Modified Neglect of Differential Overlap
MO	Molecular Orbital
MP2	Second-Order Møller-Plesset
MPPT	Møller-Plesset Perturbation Theory
MRCI	Multi-Reference Configuration Interaction
MRMP	Multi-Reference Møller-Plesset
MRMP2	Second-Order Multi-Reference Møller-Plesset
MRPT	Multi-Reference Perturbation Theory
NMR	Nuclear Magnetic Resonance
NQR	Nuclear Quadrupole Resonance
PEC	Potential Energy Curve
PIB	Particle-In-a-Box
PM3	Parametrized Model 3
PPP	Pople-Parr-Pariser
PT	Perturbation Theory
PW91	Perdew-Wang 91 Functional

RASSCF	Restricted Active Space Self-Consistent Field
RESC	Relativistic Elimination of Small Component
RHF	Restricted Hartree-Fock
RKR	Rydberg-Klein-Rees
ROHF	Restricted Open-shell Hartree-Fock
RSPT	Rayleigh-Schrödinger Perturbation Theory
SCF	Self-Consistent Field
SCRF	Self-Consistent Reaction Field
STF	Slater-Type Function
SOCI	Second-Order Configuration Interaction
SO-MCQDPT2	Spin-Orbit Second-Order Multi-Configuration Quasi-Degenerate Perturbation Theory
TDGI	Time-Dependent Gauge Invariant
TDHF	Time-Dependent Hartree-Fock
TDSE	Time-dependent Schrödinger Equation
TISE	Time-independent Schrödinger Equation
UHF	Unrestricted Hartree-Fock
VEA	Vertical Electron Affinity
VEDE	Vertical Electron Detachment Energy
VWN	Vosko-Wilk-Nusair Functional
ZORA	Zero-Order Regular Approximation

Chapter 1

Introduction

Computational quantum chemistry is a rapidly growing branch of theoretical chemistry which has become an integral part of the modern chemical research. The interface between mathematical, physical and chemical sciences, quantum chemistry is concerned with the applications of the fundamental principles of quantum mechanics to chemical problems. Utilizing advanced numerical techniques, the problems of interest described in the form of various mathematical models are solved, and the desired quantities are evaluated thereafter.

At the dawn of quantum chemistry, where computers were still not present, calculations could only be performed on paper which consumed a humongous amount of time and an immense effort; consequently, within the limited available capability of time and manpower, only the smallest systems, such as hydrogen molecule, could be practically investigated with the semi-quantitative or quantitative level of accuracy. The emergence of computing machines after the World War II provided an effective tool of resolving the limitations of the previously laborious quantum chemical calculations. Taking advantage of the high-speed processing of arithmetic operations, many rather complex mathematical equations in quantum chemistry could be solved by computers within more reasonable time. The unprecedented, rapid growth of hardware technology and high-level programming languages in the past twenty years, alongside the advances in developing more sophisticated theories in molecular quantum mechanics and more efficient numerical algorithms, have

further catalyzed the progress of computational quantum chemistry and made it a well-established phylum of science.

Nowadays, computational quantum chemistry has become a powerful research tool in chemistry. On one hand, the astonishing data-processing ability of modern computers enables large-scale calculations involving a vast number of atoms in a relatively routine fashion. On the other hand, the high accuracy offered by the delicate quantum chemical methods can provide some insight into the design of experiments and establish benchmarks for the reliability of the experimental results. Accordingly, the techniques of computational chemistry have been widely employed in real-world research such as computer-aided drug design and protein modeling [1].

In the following sections, the basic concepts and approximations of quantum chemistry are reviewed, and the computational techniques that have been used in the completion of this project are described. The details concerning the model of confinement, the derivation of necessary formulas and their implementation will be presented in Chapter 2. Excellent monographs on different topics of fundamental quantum chemistry and advanced methods of computational chemistry are widely available. Good references can be found from, for example, the followings: Szabo and Ostlund [2], Jensen [3], Cramer [4], Levine [5] and Helgaker, Jørgensen and Olsen [6].

1.1 The Schrödinger Equation

The central part of the modern quantum theory is the elegant, time-dependent Schrödinger equation (TDSE)

$$\mathcal{H}(\mathbf{r},t)\Psi(\mathbf{r},t) = -\frac{\hbar}{i}\frac{\partial}{\partial t}\Psi(\mathbf{r},t) \tag{1.1}$$

postulated by Schrödinger in 1926 [7], inspired by classical mechanics. In this equation, the Hamiltonian operator $\mathcal{H}$ contains all the terms concerning the interactions between various kinds of particles in the system and the surrounding. The solution $\Psi(\mathbf{r},t)$ of the Schrödinger equation is called the wavefunction from which the information regarding the system can be deduced. The above time-dependent

Schrödinger equation can be reduced to the corresponding time-independent Schrödinger equation (TISE) when only the stationary states are to be considered

$$\mathcal{H}\Psi(\mathbf{r}) = E\Psi(\mathbf{r}), \tag{1.2}$$

in which the Hamiltonian operator bears no time-dependent terms, and the wave-function in eq. (1.1) can simply be written as a product of a stationary-state wave-function (which is space-dependent only) and the time-dependent term: $\Psi(\mathbf{r},t) = \Psi(\mathbf{r})\psi(t)$. The TISE was used throughout this project since only the stationary-state solutions of the Schrödinger equation were of interest.

For an N-electron and M-nuclei molecular system in a free space, the non-relativistic time-independent Hamiltonian operator can be written as:

$$\begin{aligned}\mathcal{H}(\mathbf{r},\mathbf{R}) &= -\frac{\hbar^2}{2m_e}\sum_{i=1}^{N}\nabla_i^2 - \frac{\hbar^2}{2}\sum_{A=1}^{M}\frac{1}{M_A}\nabla_A^2 - \sum_{i=1}^{N}\sum_{A=1}^{M}\frac{Z_A e^2}{4\pi\epsilon_0}\frac{1}{|\mathbf{r}_i-\mathbf{R}_A|} \\ &+ \sum_{i=1}^{N}\sum_{i<j}^{N}\frac{e^2}{4\pi\epsilon_0}\frac{1}{|\mathbf{r}_i-\mathbf{r}_j|} + \sum_{A=1}^{M}\sum_{A<B}^{M}\frac{Z_A Z_B e^2}{4\pi\epsilon_0}\frac{1}{|\mathbf{R}_A-\mathbf{R}_B|},\end{aligned} \tag{1.3}$$

where $\mathbf{r}_i$ and $\mathbf{R}_A$ denote, respectively, the spatial coordinates of electron i and nucleus A, m_e is the mass of an electron, e is the elementary charge, M and Ze are the mass and charge of nucleus, and ϵ_0 is the vacuum permittivity. The first two terms of the Hamiltonian are the kinetic energy operators of the electrons and nuclei, respectively, while the remaining terms describe the electron-nucleus attraction, electron-electron repulsion, and nucleus-nucleus repulsion. The expression for Hamiltonian can be greatly simplified by using the atomic units, in which the following are defined: $\hbar = m_e = e = 4\pi\epsilon_0 = 1$. The resulting Hamiltonian, in atomic units, is given by

$$\begin{aligned}\mathcal{H}(\mathbf{r},\mathbf{R}) &= -\frac{1}{2}\sum_{i=1}^{N}\nabla_i^N - \frac{1}{2}\sum_{A=1}^{M}\frac{1}{M_A}\nabla_A^2 - \sum_{i=1}^{N}\sum_{A=1}^{M}\frac{Z_A}{|\mathbf{r}_i-\mathbf{R}_A|} \\ &+ \sum_{i=1}^{N}\sum_{i<j}^{N}\frac{1}{|\mathbf{r}_i-\mathbf{r}_j|} + \sum_{A=1}^{M}\sum_{A<B}^{M}\frac{Z_A Z_B}{|\mathbf{R}_A-\mathbf{R}_B|}\end{aligned} \tag{1.4}$$

1.1.1 The Born-Oppenheimer Approximation

Because of the presence of a cross term $\frac{1}{|\mathbf{r}-\mathbf{R}|}$, the solution of the TISE utilizing the Hamiltonian in eq. (1.4) will be dependent on both the positions of electrons and nuclei. In quantum chemistry, however, it is reasonable to assume that the motions of electrons and nuclei are not coupled (recall that $M/m_e \approx 1837$); therefore, electrons can be considered as moving in the electrostatic potential generated by the nuclei of fixed configuration. Born and Oppenheimer have shown that, neglecting a small error introduced to the ground state electronic states, the complete wavefunction can be approximated as a product of electronic and nuclear wavefunctions [8]:

$$\Psi(\mathbf{r},\mathbf{R}) = \Psi_{el}(\mathbf{r};\mathbf{R})\Psi_N(\mathbf{R}). \tag{1.5}$$

The electronic wavefunction $\Psi(\mathbf{r};\mathbf{R})$ depends parametrically on the nuclear positions $\mathbf{R}$. Applying the Born-Oppenheimer (BO) approximation, one can demonstrate that the purely electronic Hamiltonian can be expressed, in atomic units, as,

$$\mathcal{H}_{el} = -\frac{1}{2}\sum_{i=1}^{N}\nabla_i^2 - \sum_{i=1}^{N}\sum_{A=1}^{M}\frac{Z_A}{|\mathbf{r}_i-\mathbf{R}_A|} + \sum_{i=1}^{N}\sum_{i<j}^{N}\frac{1}{|\mathbf{r}_i-\mathbf{r}_j|} \tag{1.6}$$

and the total electronic energy is thus given by the purely electronic energy plus the internuclear repulsion energy $U = E_{el} + V_{NN}$ where

$$V_{NN}(\mathbf{R}) = \sum_{A}^{M}\sum_{A<B}^{M}\frac{Z_A Z_B}{|\mathbf{R}_A-\mathbf{R}_B|} \tag{1.7}$$

1.1.2 The Variational Method

Except for several special systems, for instance, harmonic oscillator and hydrogen atom, the TISE is generally not solvable analytically, and only approximate solutions can be achieved. There are three commonly used approximation methods in quantum chemistry: variational method, perturbation theory, and WKB (Wentzel-Kramers-Brillouin) approximation. In this section, the variational method is outlined; the details concerning the perturbation theory will be given in Section 1.3.

The main idea of the variational method is the minimum energy principle which guarantees that the expectation value (or energy of the system) of the Hamiltonian $\mathcal{H}$, calculated using a trial function ψ is always greater than or equal to the true ground state energy of the system E_0, i.e.,

$$\tilde{E} = \frac{\int \psi^* \mathcal{H} \psi d\tau}{\int \psi^* \psi d\tau} \geq E_0. \tag{1.8}$$

This method is powerful since a better solution ψ, and energy $\tilde{E}$, can be obtained by varying ψ until the minimum energy is yielded. An advantage of the variational method is that the real form of the ground state wavefunction should not necessarily be known; the trial wavefunction that gives the lowest energy could serve as the best approximate ground state wavefunction of the system.

1.2 Hartree-Fock Method

The electron interaction term $\frac{1}{|\mathbf{r}_i - \mathbf{r}_j|}$ in the BO Hamiltonian (eq. (1.6)) makes finding the exact solution of the TISE impossible. In order to alleviate the problem, Hartree proposed the independent particle model (IPM) which states that the electron repulsion term can be instead described as the interaction between an electron j at the position $\mathbf{r}_j$ and the mean electrostatic field generated by the other electrons [9]. i.e.,

$$\sum_{i}^{N} \sum_{i<j}^{N} \frac{1}{|\mathbf{r}_i - \mathbf{r}_j|} \rightarrow \sum_{i \neq j}^{N} \int \frac{|\psi_i(\mathbf{r}_i)|^2}{|\mathbf{r}_i - \mathbf{r}|} d\tau_i \tag{1.9}$$

The electronic wavefunction Ψ_{el} associated with this form of electron interaction term can adopt the form of a product (called the Hartree product) of one-electron wavefunctions $\psi_i(\mathbf{r}_i)$, or orbitals. As the eq. (1.10) is dependent on $\psi_i(\mathbf{r}_i)$, the corresponding TISE can only be solved in an iterative, self-consistent field (SCF) method. That is, the initial guess of $\psi_i^{(0)}$ has to be first provided, followed by the substitution of $\Psi_{el}^{(0)}$ into the TISE. The generated $\Psi_{el}^{(1)}$ will be back substituted into the TISE again and yields another new $\Psi_{el}^{(2)}$. This cycle is repeated until the difference between two consecutive sets of Ψ_{el}, $\Psi_{el}^{(n-1)}$ and $\Psi_{el}^{(n)}$, is smaller than the preset threshold of tolerance.

A serious problem of the Hartree product is that it is not anti-symmetric with respect to the interchange of electron positions, as required by the Pauli principle for all fermion particles. Therefore, Fock [10] and Slater [11] modified the Hartree product, and expressed the N-electron wavefunction in the determinantal form:

$$\Psi_{el} = \frac{1}{\sqrt{N!}} \begin{vmatrix} \psi_1(\mathbf{x}_1) & \psi_1(\mathbf{x}_2) & \cdots & \psi_1(\mathbf{x}_N) \\ \psi_2(\mathbf{x}_1) & \psi_2(\mathbf{x}_2) & \cdots & \psi_2(\mathbf{x}_N) \\ \vdots & \vdots & \ddots & \vdots \\ \psi_N(\mathbf{x}_1) & \psi_N(\mathbf{x}_2) & \cdots & \psi_N(\mathbf{x}_N) \end{vmatrix}. \tag{1.10}$$

$\psi_i(\mathbf{x}_i)$ in the Slater determinant eq. (1.11) are called spin-orbitals which are composed of both the spatial part $\phi_i(\mathbf{r}_i)$ and spin part ω:

$$\psi_i(\mathbf{x}_i) = \phi_i(\mathbf{r}_i) \times \begin{cases} \omega(\alpha) = \phi_i(\mathbf{x}_i) \\ \omega(\beta) = \bar{\phi}_i(\mathbf{x}_i) \end{cases} \tag{1.11}$$

Employing the Slater-determinant wavefunction, the energy of the system can be computed as the expectation value of the molecular electronic Hamiltonian (eq. (1.6)):

$$\begin{aligned} E &= \langle \Psi_{el} | \mathcal{H}_{el} | \Psi_{el} \rangle \\ &= \sum_{i=1}^{N} \langle \psi_i | \hat{h}(\mathbf{x}) | \psi_i \rangle + \frac{1}{2} \sum_{i=1}^{N} \sum_{j=1}^{N} \left[\langle \psi_i \psi_j | \psi_i \psi_j \rangle - \langle \psi_i \psi_j | \psi_j \psi_i \rangle \right]. \end{aligned} \tag{1.12}$$

The $\hat{h}(\mathbf{r}_i)$ operator is the one-electron core-Hamiltonian operator containing the first two terms of the electronic Hamiltonian in eq. (1.6). The one-electron integral $\langle \psi_i | \hat{h}(\mathbf{r}) | \psi_i \rangle$ is defined as

$$\langle \psi_i(\mathbf{x}_1) | \hat{h}(\mathbf{r}_1) | \psi_i(\mathbf{x}_1) \rangle = \int d\mathbf{x}_1 \psi_i^*(\mathbf{x}_1) \left(-\frac{1}{2} \nabla_1^2 - \sum_A^M \frac{Z_A}{|\mathbf{r}_1 - \mathbf{R}_A|} \right) \psi_i(\mathbf{x}_1) \tag{1.13}$$

The two-electron integral $\langle \psi_i \psi_j | \psi_i \psi_j \rangle$ is defined as follows:

$$\langle \psi_i \psi_j | \psi_i \psi_j \rangle = \int \int \frac{\psi_i^*(\mathbf{x}_1) \psi_j^*(\mathbf{x}_2) \psi_i(\mathbf{x}_1) \psi_j(\mathbf{x}_2)}{|\mathbf{r}_1 - \mathbf{r}_2|} d\mathbf{x}_1 d\mathbf{x}_2 \tag{1.14}$$

The variational treatment is applied to the energy expression eq. (1.13) to obtain the wavefunction corresponding to the minimum ground state energy of the system.

In this fashion, the electronic Schrödinger equation is transformed into a system of one-electron integro-differential Hartree-Fock (or Fock) equations:

$$\hat{f}(\mathbf{r}_1)\psi_i(\mathbf{x}_1) = \epsilon_i\psi_i(\mathbf{x}_1) \quad , \quad i = 1, 2, \cdots, N \tag{1.15}$$

where the Fock operator $\hat{f}(\mathbf{r}_1)$ for electron 1 is given by

$$\hat{f}(\mathbf{r}_1) = \hat{h}(\mathbf{r}_1) + \sum_j^N \left(J_j(\mathbf{r}_1) - K_j(\mathbf{r}_1)\right). \tag{1.16}$$

The terms $J_j(\mathbf{r}_1)$ and $K_j(\mathbf{r}_1)$ in the Fock operator are, respectively, the Coulomb and exchange operators defined in the following way:

$$J_j(\mathbf{r}_1)\psi_i(\mathbf{x}_1) = \left(\int \psi_j^*(\mathbf{x}_2)\frac{1}{|\mathbf{r}_1 - \mathbf{r}_2|}\psi_j(\mathbf{x}_2)d\mathbf{x}_2\right)\psi_i(\mathbf{x}_1) \tag{1.17}$$

$$K_j(\mathbf{r}_1)\psi_i(\mathbf{x}_1) = \left(\int \psi_j^*(\mathbf{x}_2)\frac{1}{|\mathbf{r}_1 - \mathbf{r}_2|}\psi_i(\mathbf{x}_2)d\mathbf{x}_2\right)\psi_j(\mathbf{x}_1) \tag{1.18}$$

The Coulomb operator $J_j(\mathbf{r}_1)$, as implied by its name, considers the electrostatic interaction of electron 1 and the electron density created by electron 2 in the orbital ϕ_j. The exchange operator $K_j(\mathbf{r}_1)$, however, arises solely from the anti-symmetric property of the wavefunction, and has no classical analog.

1.2.1 Restricted Hartree-Fock Method

The HF equation in eq. (1.15) is derived for a general N-electron system. For the special case of closed-shell systems where all electrons are paired, and only $N/2$ orbitals are occupied, the restricted Hartree-Fock (RHF) equations would retain the same form as eq. (1.15) except that the Fock operators are instead written as

$$\hat{f}(\mathbf{r}_1) = \hat{h}(\mathbf{r}_1) + \sum_j^{N/2} \left(2J_j(\mathbf{r}_1) - K_j(\mathbf{r}_1)\right). \tag{1.19}$$

where the operators are defined in terms of orbitals ϕ_i.

The eigenvalue ϵ_i of the Hartree-Fock equations (1.15) corresponds to the energy of orbital ϕ_i. Unfortunately, the determination of ϵ_i is not straightforward since the Fock operator depends on ϕ_i which is the eigenfunction of the Hartree-Fock equation. Solving the orbital Hartree-Fock equations (1.15) is very difficult, especially

for molecules. In order to simplify the calculations, Roothaan [12] and Hall [13] suggested that the orbital $\phi_i(\mathbf{r}_1)$ be expanded in a set of basis functions $\chi_i(\mathbf{r}_1)$:

$$\phi_i(\mathbf{r}_1) = \sum_{q=1}^{k} c_{iq}\chi_q(\mathbf{r}_1) \quad , \quad i = 1, 2, \cdots, N/2. \tag{1.20}$$

The resulting Hartree-Fock-Roothaan-Hall (HFRH) equations, obtained by substituting eqs. (1.19) and (1.20) into eq. (1.15):

$$\hat{f}(\mathbf{r}_1) \sum_{q=1}^{k} c_{iq}\chi_q(\mathbf{r}_1) = \epsilon_i \sum_{q=1}^{k} c_{iq}\chi_q(\mathbf{r}_1), \tag{1.21}$$

multiplying $\phi(\mathbf{r}_1)$ from the left and integrating, can be written in matrix notation:

$$\mathbf{FC} = \mathbf{SCE}, \tag{1.22}$$

where $\mathbf{F}$ is the Fock matrix, $\mathbf{S}$ is the overlap matrix, and $\mathbf{C}$ is the coefficient matrix. The Fock matrix elements F_{pq} and overlap matrix elements S_{pq} are given by

$$F_{pq} = \langle \chi_p(\mathbf{r}_1) | \hat{f}(\mathbf{r}_1) | \chi_q(\mathbf{r}_1) \rangle; \tag{1.23}$$

$$S_{pq} = \langle \chi_p(\mathbf{r}_1) | \chi_q(\mathbf{r}_1) \rangle. \tag{1.24}$$

Similarly to the Hartree-Fock equation, this HFRH matrix equation can be solved using the SCF technique since the Fock matrix is dependent upon the expansion coefficient matrix $\mathbf{C}$. The RHF electronic energy in terms of the basis functions can be deduced from the HFRH equation as:

$$\begin{aligned} E_{el}^{RHF} &= \sum_p \sum_q \left(2 \sum_i c_{ip}^* c_{iq} \right) \langle \chi_p | \hat{h}(\mathbf{r}_i) | \chi_q \rangle \\ &+ \sum_p \sum_q \sum_r \sum_s \left(\sum_i c_{ip}^* c_{iq} \right) \left(\sum_j c_{jr}^* c_{js} \right) \left[2\langle \chi_p \chi_q | \chi_r \chi_s \rangle - \langle \chi_p \chi_q | \chi_s \chi_r \rangle \right]. \end{aligned} \tag{1.25}$$

It is worth-noting that the RHF energy is not equal to the sum of the orbital energies ϵ_i because the electron repulsion has been counted twice in the Fock operators.

1.2.2 Open-shell Systems

The preceding discussion is concerned only with the systems having closed-shell electronic configurations. However, in many cases, the molecules may possess different numbers of α (spin-up) and β (spin-down) electrons, and some of the molecular orbitals may be occupied by a single electron only. There are two common approaches to deal with these open-shell systems: unrestricted Hartree-Fock (UHF) method and restricted open-shell Hartree-Fock (ROHF) method.

The UHF [14] method assumes that the spatial orbitals of α and β electrons could be different; therefore, the determinantal electronic wavefunction can be rewritten, in shorthand notation, as

$$\Psi_{el} = \frac{1}{\sqrt{M+N!}} \det |\phi_1^\alpha \phi_2^\alpha \dots \phi_M^\alpha \phi_{M+1}^\beta \phi_{M+2}^\beta \dots \phi_{M+N}^\beta| \tag{1.26}$$

where M and N are the numbers of α and β electrons, respectively, and $M > N$. The energy associated with the UHF wavefunction can be deduced in the similar way as for the RHF wavefunction (eqs. (1.13) and (1.25)), but the exchange interaction now consists of two terms, one for α electrons and one for β electrons. Because of the different spatial parts of α and β spin-orbitals, the UHF wavefunction is no longer the eigenfunction of the $\hat{S}^2$ operator, and very often the spin-contaminations of different spin states are observed [15].

Unlike the UHF method where the α and β electrons can occupy different spatial orbitals, the ROHF method requires that a spatial orbital be paired up for both an α and β electron [16]. In other words, there is a constraint: $\phi_{M+i} = \phi_i$ imposed on eq. (1.26). The ROHF wavefunction, compared to the RHF counterpart, can be considered as a system of N closed shells and $M - N$ non-closed open shells. The resulting ROHF wavefunction would again be an eigenfunction of the spin operator $\hat{S}^2$. However, the Fock operators are not invariant under the unitary transformation on the complete orbital space. Furthermore, the ROHF method is applicable only for the high-spin half-filled open-shell, either non-degenerate or degenerate, systems, and the calculated energy is usually higher than the corresponding value obtained using the UHF method.

1.3 Electron Correlation Methods

The Slater-determinant representation of the wavefunction used in HF methods accurately describes their antisymmetry as required by the Pauli exclusion principle, and eliminates the problems of having two electrons of parallel spins occupy the same spatial orbital. However, the HF formalism ignores the instantaneous interaction of two electrons of anti-parallel spins. Recall that the Coulomb integral defined in eqs. (1.10) and (1.17) assumes the electrostatic repulsion of an electron and the averaged field generated by the other electrons, and two anti-parallel electrons are implicitly allowed to simultaneously occupy the same position in space, which is in fact incorrect. As a consequence, an error due to this electron correlation is present in the HF energy, calculated at the limit of the basis set, E_{lim}^{HF}, which makes E_{lim}^{HF} always higher than the exact energy of the system. The energy difference between E_{lim}^{HF} energy and the exact non-relativistic energy ξ_0 is termed the correlation energy E_{corr}:

$$E_{corr} = \xi_0 - E_{lim}^{HF} \tag{1.27}$$

Another drawback of the HF method lies in the fact that the HF wavefunction does not describe the proper dissociation of a bond. Due to the assumption of the RHF method that all orbitals be either occupied by a pair of anti-parallel electrons or empty, the dissociation of, for example, a diatomic molecule will lead to the wrong asymptotic products of closed-shell ions instead of neutral, open-shell atoms. In addition to the inaccurate behavior near the dissociation, the HF method is also inappropriate for the weakly-interacting systems such as van der Waals complexes since the dispersion interaction is completely absent in the HF formalism.

In order to more accurately describe the motion of electrons and their interactions, and recover the correlation energy, approximations beyond the HF method have to be employed. A variety of such electron correlation methods have been formulated and applied (for references, see e.g. [2, 3, 6]). In this section, the details of a number of methods of treating the electron correlation that have been used in this project will be briefly discussed. They include configuration interaction (CI), per-

turbation theory (PT) and coupled-cluster theory (CC), and multi-reference (MR) methods.

1.3.1 Configuration Interaction

The configuration interaction (CI) method is conceptually the easiest among all the electron correlation methods. The main idea of this method is to express the wavefunction by, instead of a single determinant, a linear combination of Slater-determinant. Symbolically, one can write the CI wavefunction as

$$\Psi = \sum_K C_K |\Phi_K\rangle \tag{1.28}$$

where the $|\Phi_K\rangle$ is the configurational state function (CSF) in form of determinants, and C_K is the associated coefficient. Since, in general, the HF method can recover approximately 90% of the total energy, the HF wavefunction is usually chosen as the first term in the CI wavefunction. The other CSF's can then be generated by exciting electrons from the HF occupied orbitals to the virtual orbitals according to the spin and symmetry restrictions. Based on the number of electrons excited, the CI wavefunction can be expressed in a general way as

$$\Psi = C_0|\Phi_0\rangle + \sum_a^{occ}\sum_r^{virt} C_a^r|\Phi_a^r\rangle + \sum_{ab}^{occ}\sum_{rs}^{virt} C_{ab}^{rs}|\Phi_{ab}^{rs}\rangle + \sum_{abc}^{occ}\sum_{rst}^{virt} C_{abc}^{rst}|\Phi_{abc}^{rst}\rangle + \cdots \tag{1.29}$$

The Φ_a^r is the CSF resulting from a single-electron excitation from the occupied orbital a to the virtual orbital r. Similarly, Φ_{ab}^{rs} can be obtained by a two-electron excitation from orbitals a and b to orbitals r and s. The associated coefficients C are determined by the variational method.

As can be seen, the CI wavefunction contains a tremendous number of CSFs. The total number of CSFs that can be generated in CI wavefunction is determined by the Weyl's formula [17]:

$$K(n,N,S) = \frac{2S+1}{n+1}\begin{pmatrix} n+1 \\ \frac{1}{2}N - S \end{pmatrix}\begin{pmatrix} n+1 \\ \frac{1}{2}N + S + 1 \end{pmatrix} \tag{1.30}$$

where n is the number of molecular orbitals, N is the number of electrons, and S is the spin quantum number. The eq. (1.29) describes the full CI (FCI) wavefunction

if all possible excitations are included. FCI method is the most accurate method that yields the exact non-relativistic energy within the orbital space spanned by the given finite basis set. However, it is also the most time-consuming and resource-demanding method which makes it applicable only for very small systems.

It is recognized that high-order excitations (such as fifth-order) in fact contribute only a small portion to the total correlation energy; therefore, the CSFs resulting from those excitations could be removed from the CI wavefunction while retaining most of the correlation energy. Depending on the order of excitations up to which the CI wavefunction is truncated, two subsets of FCI method are commonly used: configuration interaction with single and double excitations (CISD) and configuration interaction with single, double, triple and quadruple excitations (CISDTQ).

The CISD method is the simplest version of truncated CI wavefunction in which only up to the level of double excitations are included. The resulting CISD wavefunction is thus written as

$$\Psi_{CISD} = C_0|\Phi_0\rangle + \sum_{a}^{occ}\sum_{r}^{virt} C_a^r|\Phi_a^r\rangle + \sum_{ab}^{occ}\sum_{rs}^{virt} C_{ab}^{rs}|\Phi_{ab}^{rs}\rangle. \tag{1.31}$$

Brillouin showed [18] that the singly-excited determinants $|\Phi_a^r\rangle$ do not interact directly with the HF ground state reference $|\Phi_0\rangle$. In other words, the single excitation terms have only a small effect on the ground state energy. On the other hand, the double excitations $|\Phi_{ab}^{rs}\rangle$ play an important role in determining the correlation energy as they directly mix with the ground state HF wavefunction. Since the single and double excitations interact with each other, as allowed by Slater's rule, and there are only a small number single excitations compared to the double excitations that have to be considered, the single excitations are normally included in the CISD calculations.

Despite the relatively fast generations of configurations (it scales as N^6, where N is the number of basis functions), the CISD method neglects the contribution from the quadruple excitations which in fact, for many-electron systems, are more important than single and triple excitations. To solve this problem, the configurations resulting from the triple and quadruple excitations can be added to the CISD

wavefunction, giving rise to the so-called CISDTQ wavefunction

$$\Psi_{CISDTQ} = \Psi_{CISD} + \sum_{abc}^{occ} \sum_{rst}^{virt} C_{abc}^{rst} |\Phi_{abc}^{rst}\rangle + \sum_{abcd}^{occ} \sum_{rstu}^{virt} C_{abcd}^{rstu} |\Phi_{abcd}^{rstu}\rangle. \tag{1.32}$$

The triple excitations are included, although they again do not interact with the ground state HF wavefunction due to Slater's rule, because they mix with both the double and quadruple excitation terms. This CISDTQ method has the performance comparable to the full CI method, but it is computationally too expensive (scaling as N^{10}). Consequently, it is of little practical value, and is only applicable to very small systems described with basis sets of modest sizes.

Many variants of CI methods, except for the full CI, suffer from two vital problems: size consistency and size extensivity. The first one refers to the condition that the energy of a many-particle system is the same as the sum of the individual, non-interacting particles. The second one is very similar but a more general concept. It requires that the method scales proportionally to the number of particles [3]. Both problems can be accounted for by the fact that some of the configurations are omitted in the CI wavefunctions, and these missing terms contribute unequal amounts of correlation energy for different sizes of systems and nuclear configurations. In order to regain the properties of size consistency and extensivity without using the full CI wavefunction, an approximation called the Davidson correction [19] can be used, in which the contribution from the quadruple excitations to the correlation energy can be estimated by

$$\Delta E_{Davidson} = \left(1 - C_0^2\right) E_{CISD} \tag{1.33}$$

where C_0 is the coefficient of the HF wavefunction, i.e., $|\Phi_0\rangle$, in the normalized CISD wavefunction (eq. (1.31)).

In addition to the problem of size inconsistency, the practical CI calculations are also limited by the slow convergence in the SCF iterations because of the cusp condition [20] of wavefunctions. Even so, the large flexibility of the wavefunctions, the applicability to both closed- and open-shell systems, and the feasibility of simultaneous treatment for both ground and excited states still make the CI methods among the most popular electron correlation methods in modern computational chemistry.

1.3.2 Perturbation Theory

Since solving the Schrödinger equation and obtaining the exact solutions are impossible in most of the quantum chemical problems, the use of approximations becomes necessary. The variational principle introduced previously is one of the most common techniques to obtain the approximate solutions. Another method that is widely used is called perturbation theory (PT).

The basic assumption of perturbation theory is that the Hamiltonian of a system $\mathcal{H}$ is separable:

$$\mathcal{H} = \mathcal{H}^0 + \lambda\mathcal{H}' \tag{1.34}$$

where $\mathcal{H}^0$ is a Hamiltonian whose eigenfunctions and eigenvalues are known, λ is a perturbation parameter and $\mathcal{H}'$ is called the perturbing Hamiltonian. λ is the factor illustrating the extent the system is perturbed. When λ is zero, the perturbed Hamiltonian is reduced to the unperturbed one; when $\lambda = 1$, it is said that the perturbation is ultimately turned on.

Suppose that the Schrödinger equation corresponding to the Hamiltonian $\mathcal{H}^0$ is given as follows:

$$\mathcal{H}^0|\Psi_n^{(0)}\rangle = E_n^{(0)}|\Psi_n^{(0)}\rangle \tag{1.35}$$

and $|\Psi_n^{(0)}\rangle$ form a complete solution set. Suppose also that the Schrödinger equation for the perturbed Hamiltonian is:

$$\mathcal{H}|\Psi_n\rangle = E_n|\Psi_n\rangle. \tag{1.36}$$

Since the perturbed Hamiltonian is dependent on the perturbation parameter λ, its eigenfunctions $|\Psi_n\rangle$ and eigenvalues E_n also depend on λ, and can be expanded in the form of Taylor series:

$$|\Psi_n\rangle = |\Psi_n^{(0)}\rangle + \lambda|\Psi_n^{(1)}\rangle + \lambda^2|\Psi_n^{(2)}\rangle + \cdots \tag{1.37}$$

$$E_n = E_n^{(0)} + \lambda E_n^{(1)} + \lambda^2 E_n^{(2)} + \cdots \tag{1.38}$$

where

$$|\Psi_n^{(k)}\rangle = \frac{1}{k!}\frac{\partial^k |\Psi_n\rangle}{\partial \lambda^k}\bigg|_{\lambda=0} \tag{1.39}$$

$$E_n^{(k)} = \frac{1}{k!}\frac{\partial^k E_n}{\partial \lambda^k}\bigg|_{\lambda=0} \tag{1.40}$$

for $k = 1, 2, \ldots$. Substituting eqs. (1.37) and (1.38) into eq. (1.36) yields the following equation:

$$\begin{aligned}(\mathcal{H}^0 + \lambda\mathcal{H}')\left(|\Psi_n^{(0)}\rangle + \lambda|\Psi_n^{(1)}\rangle + \lambda^2|\Psi_n^{(2)}\rangle + \cdots\right) = \\ + \left(E_n^{(0)} + \lambda E_n^{(1)} + \lambda^2 E_n^{(2)} + \cdots\right)\left(|\Psi_n^{(0)}\rangle + \lambda|\Psi_n^{(1)}\rangle + \lambda^2|\Psi_n^{(2)}\rangle + \cdots\right)\end{aligned} \tag{1.41}$$

Collecting and equating terms with the same powers of λ generates an infinite number of linear equations:

$$\mathcal{H}^0|\Psi_n^{(0)}\rangle = E_n^{(0)}|\Psi_n^{(0)}\rangle \tag{1.42}$$

$$\mathcal{H}^0|\Psi_n^{(1)}\rangle + \mathcal{H}'|\Psi_n^{(0)}\rangle = E_n^{(0)}|\Psi_n^{(1)}\rangle + E_n^{(1)}|\Psi_n^{(0)}\rangle \tag{1.43}$$

$$\mathcal{H}^0|\Psi_n^{(2)}\rangle + \mathcal{H}'|\Psi_n^{(1)}\rangle = E_n^{(0)}|\Psi_n^{(2)}\rangle + E_n^{(1)}|\Psi_n^{(1)}\rangle + E_n^{(2)}|\Psi_n^{(0)}\rangle \tag{1.44}$$

$$\vdots$$

The expressions for high-order terms for energy and wavefunction in eqs (1.36) and (1.37) can be deduced from these equations. The first equation (1.42) is the Schrödinger equation corresponding to the unperturbed system. The associated energy and wavefunction are thus said to be the zeroth-order energy and wavefunction. To obtain the first-order correction of energy, the eq. (1.43) is left-projected by $\langle\Psi_n^{(0)}|$:

$$\langle\Psi_n^{(0)}|\mathcal{H}^0|\Psi_n^{(1)}\rangle + \langle\Psi_n^{(0)}|\mathcal{H}'|\Psi_n^{(0)}\rangle = \langle\Psi_n^{(0)}|E_n^0|\Psi_n^{(1)}\rangle + \langle\Psi_n^{(0)}|E_n^1|\Psi_n^{(0)}\rangle \tag{1.45}$$

$$E_n^{(0)}\langle\Psi_n^{(0)}|\Psi_n^{(1)}\rangle + \langle\Psi_n^{(0)}|\mathcal{H}'|\Psi_n^{(0)}\rangle = E_n^{(0)}\langle\Psi_n^{(0)}|\Psi_n^{(1)}\rangle + E_n^{(1)}\langle\Psi_n^{(0)}|\Psi_n^{(0)}\rangle. \tag{1.46}$$

Two assumptions are used here to simplify the derivation. First, the zeroth-order wavefunction $|\Psi_n^0\rangle$ is normalized, i.e., $\langle\Psi_n^{(0)}|\Psi_n^{(0)}\rangle = 1$. Secondly, the condition of intermediate normalization leads to $\langle\Psi_n^{(k)}|\Psi_n^{(l)}\rangle = \delta_{kl}$. As a result, the first order correction to the energy is given by

$$E_n^{(1)} = \langle\Psi_n^{(0)}|\mathcal{H}'|\Psi_n^{(0)}\rangle. \tag{1.47}$$

It is now assumed that the unperturbed Hamiltonian $\mathcal{H}^0$ possesses a complete orthonormal set of eigenfunctions. Hence, the first-order correction to the wavefunction can be expanded as:

$$|\Psi_n^{(1)}\rangle = \sum_{\mu \neq n} C_{n\mu}^{(1)} |\Psi_\mu^{(0)}\rangle \tag{1.48}$$

Inserting this expression into eq. (1.43) yields

$$\mathcal{H}^0 \left(\sum_{\mu \neq n} C_{n\mu}^{(1)} |\Psi_\mu^{(0)}\rangle \right) + \mathcal{H}' |\Psi_n^{(0)}\rangle = E_n^{(0)} \left(\sum_{\mu \neq n} C_{n\mu}^{(1)} |\Psi_\mu^{(0)}\rangle \right) + E_n^{(1)} |\Psi_n^{(0)}\rangle. \tag{1.49}$$

Multiplying $\langle \Psi_\nu^{(0)}|$ from the left gives:

$$\begin{aligned} &\sum_{\mu \neq n} C_{n\mu}^{(1)} E_\mu^{(0)} \langle \Psi_\nu^{(0)} | \Psi_\mu^{(0)} \rangle + \langle \Psi_\nu^{(0)} | \mathcal{H}' | \Psi_n^{(0)} \rangle \\ &\quad = \sum_{\mu \neq n} C_{n\mu}^{(1)} E_n^{(0)} \langle \Psi_\nu^{(0)} | \Psi_\mu^{(0)} \rangle + E_n^{(1)} \langle \Psi_\nu^{(0)} | \Psi_n^{(0)} \rangle, \end{aligned} \tag{1.50}$$

which, due to the condition of intermediate normalization, leads to

$$C_{n\nu}^{(1)} E_\nu^{(0)} + \langle \Psi_\nu^{(0)} | \mathcal{H}' | \Psi_n^{(0)} \rangle = C_{n\nu}^{(1)} E_n^{(0)} \tag{1.51}$$

and, finally,

$$C_{n\nu}^{(1)} = \frac{\langle \Psi_\nu^{(0)} | \mathcal{H}' | \Psi_n^{(0)} \rangle}{E_n^{(0)} - E_\nu^{(0)}}. \tag{1.52}$$

Therefore, the first-order correction to the wavefunction is

$$|\Psi_n^{(1)}\rangle = \sum_{\mu \neq n} \left(\frac{\langle \Psi_\mu^{(0)} | \mathcal{H}' | \Psi_n^{(0)} \rangle}{E_n^{(0)} - E_\mu^{(0)}} \right) |\Psi_\mu^{(0)}\rangle. \tag{1.53}$$

The second-order correction to the energy can be derived from the eq. (1.44) in a similar way as used for $E_n^{(1)}$. Projection of $\langle \Psi_n^{(0)}|$ from the left yields the following

$$\begin{aligned} &\langle \Psi_n^{(0)} | \mathcal{H}^0 | \Psi_n^{(2)} \rangle + \langle \Psi_n^{(0)} | \mathcal{H}' | \Psi_n^{(1)} \rangle \\ &\quad = \langle \Psi_n^{(0)} | E_n^{(0)} | \Psi_n^{(2)} \rangle + \langle \Psi_n^{(0)} | E_n^{(1)} | \Psi_n^{(1)} \rangle + \langle \Psi_n^{(0)} | E_n^{(2)} | \Psi_n^{(0)} \rangle \end{aligned} \tag{1.54}$$

which is simplified as

$$E_n^{(2)} = \langle \Psi_n^{(0)} | \mathcal{H}' | \Psi_n^{(1)} \rangle \tag{1.55}$$

according to the intermediate normalization condition. Using the expression of the first-order correction to the wavefunction in eq. (1.53), the final expression for the second-order correction to energy can be achieved:

$$E_n^{(2)} = \sum_{\mu \neq n} \frac{\langle \Psi_n^{(0)} | \mathcal{H}' | \Psi_\mu^{(0)} \rangle \langle \Psi_\mu^{(0)} | \mathcal{H}' | \Psi_n^{(0)} \rangle}{E_n^{(0)} - E_\mu^{(0)}}. \tag{1.56}$$

Since the perturbing Hamiltonian $\mathcal{H}'$ is Hermitian, the above expression can be rewritten simply as

$$E_n^{(2)} = \sum_{\mu \neq n} \frac{|\langle \Psi_n^{(0)} | \mathcal{H}' | \Psi_\mu^{(0)} \rangle|^2}{E_n^{(0)} - E_\mu^{(0)}}. \tag{1.57}$$

The corresponding second-order correction to the wavefunction is, without showing the details of derivation,

$$|\Psi_n^{(2)}\rangle = \left(\sum_{\mu \neq n} \frac{\langle \Psi_\nu^{(0)} | \mathcal{H}' | \Psi_\mu^{(0)} \rangle \langle \Psi_\mu^{(0)} | \mathcal{H}' | \Psi_n^{(0)} \rangle}{\left(E_n^{(0)} - E_\mu^{(0)}\right)\left(E_n^{(0)} - E_\nu^{(0)}\right)} - \frac{\langle \Psi_\nu^{(0)} | \mathcal{H}' | \Psi_n^{(0)} \rangle \langle \Psi_n^{(0)} | \mathcal{H}' | \Psi_n^{(0)} \rangle}{\left(E_n^{(0)} - E_\nu^{(0)}\right)^2} \right) |\Psi_\mu^{(0)}\rangle. \tag{1.58}$$

The higher-order corrections can be obtained in the similar procedures, although the derivations are much more tedious and the expressions very complicated. The above-mentioned development is the time-independent version of Rayleigh-Schrödinger perturbation theory (RSPT) [21, 22] which is designed for the systems with non-degenerate ground states. As can be seen, if the ground state of a system is degenerate, the denominators in eqs (1.53), (1.57) and (1.58) will vanish for certain μ and ν. The corresponding treatment for degenerate systems has been developed as well, and both methods have been extended to incorporate the time-dependence effects. These have been shown very powerful in the studies of, for instance, Stark effect of hydrogen atom [23, 24].

The RSPT formalism is a general treatment of the perturbation effects on the energies and the associated wavefunctions of a system, and thus it is applicable to any quantum mechanical systems with bound-state eigenfunctions. In the regime of quantum chemistry, Møller and Plesset devised an analog of the RSPT which deals with the electron correlation effects [25]. In the Møller-Plesset perturbation theory

(MPPT), the unperturbed Hamiltonian is taken as the sum of one-electron Fock operators (eq. (1.16))

$$\mathcal{H}^0 = \sum_{i=1}^{N} \left\{ \hat{h}(i) + \sum_{i<j}^{N} (J_j(i) - K_j(i)) \right\}. \tag{1.59}$$

Therefore, the perturbing Hamiltonian $\mathcal{H}'$ is simply the difference between $\mathcal{H}^0$ and the multi-electron Hamiltonian:

$$\begin{aligned} \mathcal{H}' &= \mathcal{H} - \mathcal{H}^0 \\ &= \sum_{i=1}^{N} \hat{h}(i) + \sum_{i=1}^{N} \sum_{i<j}^{N} \frac{1}{|\mathbf{r}_i - \mathbf{r}_j|} - \sum_{i=1}^{N} \left\{ \hat{h}(i) + \sum_{i<j}^{N} (J_j(i) - K_j(i)) \right\} \\ &= \sum_{i=1}^{N} \sum_{i<j}^{N} \frac{1}{|\mathbf{r}_i - \mathbf{r}_j|} - \sum_{i=1}^{N} \sum_{i<j}^{N} (J_j(i) - K_j(i)) . \end{aligned} \tag{1.60}$$

The formulas for the energy and wavefunction corrections in the MPPT scheme are based on those derived in the general RSPT. The zeroth-order energy is merely the sum of orbital energies

$$E_0^{(0)} = \sum_{i=1}^{N/2} \left\{ \langle \phi_i | \hat{h}(i) | \phi_i \rangle + \sum_{j=1}^{N/2} \left(\langle \phi_i \phi_j | \phi_i \phi_j \rangle - \langle \phi_i \phi_j | \phi_j \phi_i \rangle \right) \right\} = \sum_{i=1}^{N/2} \epsilon_i \tag{1.61}$$

since ϵ_i are the eigenvalues of the Fock equations (1.16). From eq. (1.47) the first-order energy correction can be computed:

$$\begin{aligned} E_0^{(1)} &= \langle \Psi_{el} | \mathcal{H}' | \Psi_{el} \rangle \\ &= \frac{1}{2} \sum_{i=1}^{N} \sum_{j=1}^{N} \langle \Psi_{el} | \frac{1}{|\mathbf{r}_i - \mathbf{r}_j|} | \Psi_{el} \rangle - \sum_{i=1}^{N} \langle \Psi_{el} | \sum_{i<J}^{N} (J_j(i) - K_j(i)) | \Psi_{el} \rangle \\ &= -\frac{1}{2} \sum_{i=1}^{N/2} \sum_{j=1}^{N/2} \left(\langle \phi_i \phi_j | \phi_i \phi_j \rangle - \langle \phi_i \phi_j | \phi_j \phi_i \rangle \right). \end{aligned} \tag{1.62}$$

The total energy up to the first-order correction is thus

$$E_0^{(0)} + E_0^{(1)} = \sum_{i=1}^{N/2} \left\{ \langle \phi_i | \hat{h}(i) | \phi_i \rangle + \frac{1}{2} \sum_{j=1}^{N/2} \left(\langle \phi_i \phi_j | \phi_i \phi_j \rangle - \langle \phi_i \phi_j | \phi_j \phi_i \rangle \right) \right\} \tag{1.63}$$

which is equal to eq. (1.13), which is the HF energy. In other words, no correlation has been yet introduced in the first-order MPPT. Using eq (1.57), the second-order correction to the energy can be easily found:

$$E_0^{(2)} = 2\sum_{ijkl}^{N/2} \frac{\langle\phi_i\phi_j|\phi_k\phi_l\rangle\langle\phi_k\phi_l|\phi_i\phi_j\rangle}{\epsilon_i+\epsilon_j-\epsilon_k-\epsilon_l} - \sum_{ijkl}^{N/2} \frac{\langle\phi_i\phi_j|\phi_k\phi_l\rangle\langle\phi_k\phi_l|\phi_j\phi_i\rangle}{\epsilon_i+\epsilon_j-\epsilon_k-\epsilon_l} \tag{1.64}$$

for a closed-shell system. The expression contains only the HF and doubly excited determinants because of the Brillouin theorem. The second-order Møller-Plesset (MP2) energy is thus:

$$E_0^{MP2} = E_0^{(0)} + E_0^{(1)} + E_0^{(2)} = E^{HF} + E_0^{(2)}. \tag{1.65}$$

Working equations of higher-order MPPT can be derived in the similar fashion, but, like the RSPT counterpart, the expressions of energy corrections are complicated and rather difficult to be used efficiently.

There are several advantages of the MPPT over the variational CI method. The most important one is the size-consistent and size-extensive nature of MPPT, regardless of the orders of correction. Furthermore, the computational expense of MPPT, especially MP2, is smaller than the CI methods (N^5 for MP2 versus N^6 for CISD) which usually suffer the problem of convergence. Contrary to other popular correlation methods, MPPT is not variational; the MPPT energy is not guaranteed to be the upper bound to the exact energy. Consequently, the calculations results of the MPPT have to be viewed with caution. In general, the MPPT energy converges with increasing orders of correction. However, this is not always the case, and in some circumstances, higher-order corrections may lead to the divergent total energy [26]. Since, in most quantum chemical calculations, the property of size consistency is generally more important than being variational, MPPT, in particular MP2, remains the most common post-HF method for the approximation of electron correlation.

1.3.3 Coupled Cluster Method

The coupled cluster (CC) method has recently emerged as one of the most accurate computational methods for electronic structure calculations. First applied in nuclear

physics [27, 28], the use of the CC theory in chemistry was initially very limited because of the highly complicated formalism using the sophisticated mathematical concepts such as Feynman diagrams and second quantization. The efforts of Čížek [29, 30], Paldus [31], Hurley [32] and Sinanoğlu [33] on reformulation and interpretation of the CC theory made this method understandable and, more importantly, applicable to effectively solving chemical problems.

The central idea of the CC method is to generate all possible determinants from the HF wavefunction using the exponential ansatz. That is, the CC wavefunction is written as

$$\Psi_{CC} = e^{\mathbf{T}}|\Phi_0\rangle \tag{1.66}$$

where the exponential ansatz, when expanding, is given by

$$e^{\mathbf{T}} = \mathbf{1} + \mathbf{T} + \frac{1}{2!}\mathbf{T}^2 + \frac{1}{3!}\mathbf{T}^3 \cdots = \sum_{k=0}^{\infty} \frac{1}{k!}\mathbf{T}^k. \tag{1.67}$$

The operator $\mathbf{T}$ is called the cluster operator which is a sum of i-particle operators:

$$\mathbf{T} = \mathbf{T}_1 + \mathbf{T}_2 + \mathbf{T}_3 + \cdots, \tag{1.68}$$

each of which defined as, for example,

$$\mathbf{T}_1|\Phi_0\rangle = \sum_{i}^{occ}\sum_{a}^{vir} t_i^a|\Phi_i^a\rangle \tag{1.69}$$

$$\mathbf{T}_2|\Phi_0\rangle = \sum_{i<j}^{occ}\sum_{a<b}^{vir} t_{ij}^{ab}|\Phi_{ij}^{ab}\rangle. \tag{1.70}$$

The coefficients t associated with the excited determinants are called amplitudes. Substituting eqs. (1.67) and (1.68) into eq. (1.66) yields the complete CC wavefunction:

$$\begin{aligned}\Psi_{CC} = &\left\{\mathbf{1} + \mathbf{T}_1 + \left(\mathbf{T}_2 + \frac{1}{2}\mathbf{T}_1^2\right) + \left(\mathbf{T}_3 + \mathbf{T}_2\mathbf{T}_1 + \frac{1}{6}\mathbf{T}_1^3\right)\right. \\ &\left. + \left(\mathbf{T}_4 + \mathbf{T}_3\mathbf{T}_1 + \frac{1}{2}\mathbf{T}_2^2 + \frac{1}{2}\mathbf{T}_2\mathbf{T}_1^2 + \frac{1}{24}\mathbf{T}_1^4\right) + \cdots\right\}|\Phi_0\rangle. \end{aligned} \tag{1.71}$$

The CC energy can then be computed by substituting the CC wavefunction into the Schrödinger equation.

If eq. (1.69) is used, then the resulting wavefunction will contain all possible excited determinants; in this case, the CC wavefunction is equivalent to the full CI wavefunction. However, as mentioned earlier, the calculations using wavefunctions at the full CI level are possible only for small systems. Therefore, for practical reasons, the cluster operator has to be truncated. If only $\mathbf{T}_2$ is present in the exponential ansatz, the method is referred to as the coupled cluster doubles (CCD). The $\mathbf{T}_1$ term is missing because of the Brillouin's theorem. The more common variant is the coupled cluster singles and doubles (CCSD) method where $\mathbf{T} = \mathbf{T}_1 + \mathbf{T}_2$. The exponential ansatz corresponding to this cluster operator is

$$e^{\mathbf{T}_1+\mathbf{T}_2} = \mathbf{1}+\mathbf{T}_1+\left(\mathbf{T}_2+\frac{1}{2}\mathbf{T}_1^2\right)+\left(\mathbf{T}_1\mathbf{T}_2+\frac{1}{6}\mathbf{T}_1^3\right)+\left(\frac{1}{2}\mathbf{T}_2^2+\frac{1}{2}\mathbf{T}_2\mathbf{T}_1^2+\frac{1}{24}\mathbf{T}_1^4\right)+\cdots. \tag{1.72}$$

There are several unique features of the CCSD wavefunction that are notable. Despite the cluster operator truncated at the double excitation level, the expanded CCSD wavefunction contains terms that result from triple and quadruple excitations, such as $\mathbf{T}_1^3$ and $\mathbf{T}_2^2$. The CISD wavefunction, in which the excited determinants are generated by the linear ansatz, omits all these terms. In other words, the CCSD method employing the exponential ansatz is able to recover all the geminal terms in the pair-correlation theory [34]. These disconnected terms in fact account for the size inconsistency of the CISD, and all other truncated CI methods. Another feature is that the amplitudes for these high-order excitation terms are not determined independently; instead they are related to the amplitudes of the singly and doubly excited determinants. Accordingly, the iterative determination of the singles and doubles amplitudes can simultaneously resolve the contribution of the higher-order excited determinants.

Normally, the CCSD method enables the recovery of 95% of the correlation energy. The performance of the CCSD wavefunction can be determined by the so-called T_1-diagnostic [35], which is defined as the norm of the singles amplitude vector divided by the square root of the number of electrons:

$$T_1 = \frac{|\mathbf{t}_1|}{\sqrt{N}}. \tag{1.73}$$

Since, from the Brillouin's theorem, singly excited determinants do not directly interact with the ground state, the values of $\mathbf{t}_1$, and in turn T_1, are expected to be small. Hence, the magnitude of computed T_1 gives an indication of how adequate the HF reference wavefunction is. Typically, the values smaller than 0.02 imply the performance of CCSD method comparable to the full CI limit.

Besides the pure CCSD method, the one augmented with triples through perturbative approach (CCSD(T)) [36] and full approach (CCSDT) [37] are also available. As the scaling factors of these methods (N^6 for CCSD and N^7 for CCSD(T)) are similar to that of CISD (N^6) and the size-consistent and size-extensive properties, CCSD(T), or even CCSDT, has already become the standard for high-level computational quantum chemistry. Still, it has to be mentioned that CC methods are not variational; therefore, the CC energies are, like the MPPT energies, not necessarily the upper bound of the true energies.

1.3.4 Multi-Configurational Self Consistent Field Methods

For the electron correlation methods introduced in the previous sections (CI,MPPT, and CC), the reference wavefunction from which excited determinants are generated is the HF determinant, with the closed-shell HF wavefunction represented by a single determinant. Accordingly, these correlation methods can be referred to as single-reference correlation methods. As can be easily seen, the performance of these methods in recovering the correlation energy is partly dependent upon the quality of the HF reference function. Poor results are to be expected if the HF determinant is not able to nicely describe (or approximate) the electronic configuration of the system. A typical example is the system where the ground state is degenerate. In such case HF fails to describe the wavefunction properly using a single determinant (or more precisely, CSF).

A straightforward way to solve this problem is to allow the HF wavefunction to contain more than one CSF. This is the reason the multi-configurational self-consistent field (MCSCF) was first developed [38]. This method is very similar to the CI methods in the way that the wavefunction is written as a linear combination

of configurations, i.e.,

$$\Psi_{MCSCF} = \sum_{i=1}^{K} C_i |\Phi_i\rangle. \tag{1.74}$$

The coefficients C_i of the configurations are determined variationally by the SCF procedures. There are a number of differences between the MCSCF and CI wavefunctions. First, while all possible configurations are generated and included automatically in the CI wavefunction according to the constraint on the order of excitations, in MCSCF only a limited number of configurations is actually included, and the configurations that are present in the MCSCF wavefunction are specified on the basis of chemical understanding of the system of interest. Secondly, instead of optimizing solely the coefficients as done in the CI methods, both the coefficients of configurations and the molecular orbitals with which the configurations are constructed are optimized in MCSCF calculations. Therefore, a greater flexibility is provided in the MCSCF scheme which, however, creates an additional problem of difficult convergence, and often solutions are obtained which do not correspond to real minima.

The MCSCF wavefunctions containing more than one configuration are advantageous because the static correlation can be recovered; i.e., the degenerate (or resonant) configurations can be treated on the same footing, and no artificial error will be introduced by neglecting certain important configurations. A downside of the idea of MCSCF, however, is the proper choice of configurations. Very often it is difficult to select the necessary configurations that have to be included in the MCSCF wavefunction. A possible approach is to include all possible configurations arising from a group of pre-selected molecular orbitals called the active space. In the complete active space self-consistent field (CASSCF) method [39, 40, 41], molecular orbitals are separated into two groups: active and inactive spaces. Orbitals in the inactive space are considered frozen; no electron excitations are allowed between these orbitals. In the active space, on the other hand, different configurations are generated by full CI calculations and enter the MCSCF wavefunction (Figure 1.1). Though smaller orbital space than the genuine full CI, CASSCF method still generates a huge number of configurations which makes the calculations impractical.

The reduction of the configurations in MCSCF wavefunctions can be achieved by employing the restricted active space self-consistent field (RASSCF) method [42], which is a variant of CASSCF. In RASSCF, the active space is further divided into three subspaces, as illustrated in Figure 1.1. RAS2 is the space in which full CI calculations are still performed to generate all possible configurations. Furthermore, additional single and double excitations from RAS1 and to RAS3 are allowed, giving rise to a CISD in these spaces. By doing so, the accuracy of the resulting wavefunction is slightly deteriorated, but the number of necessary configurations is largely reduced.

The main advantage of MCSCF and related methods is the proper treatment of the static (or non-dynamical) correlation effects which deal with the degeneracy (or near-degeneracy) of configurations. By expanding the wavefunction from single-determinantal to multi-determinantal, different configurations (or CSFs) of same chemical importance can be considered equally, and the balanced description of degenerate, or quasi-degenerate, orbitals can be attained. Unfortunately, the design of chemically active space is problematic and a prior knowledge of the systems of interest is required. In addition, the dynamical correlation is not considered in MCSCF methods, so that the resulting energies are worse than those obtained by MPPT and CC methods. The MCSCF methods clearly serve as an excellent starting point for the improvement of HF reference wavefunctions in the electron correlation methods, although their calculations are not as mechanical as HF and MPPT methods.

1.3.5 Multi-Reference Methods

Due to the lack of treating the dynamical correlation effects, the MCSCF and related methods are only suitable for computing the potential energy curves and obtaining the spectroscopic constants. In order to capture most of the correlation energy, MCSCF methods have to be incorporated with other electron correlation methods, so that both the static and dynamical correlation effects can be dealt with equally. Attempts have been made to combine the MCSCF methods with, for example,

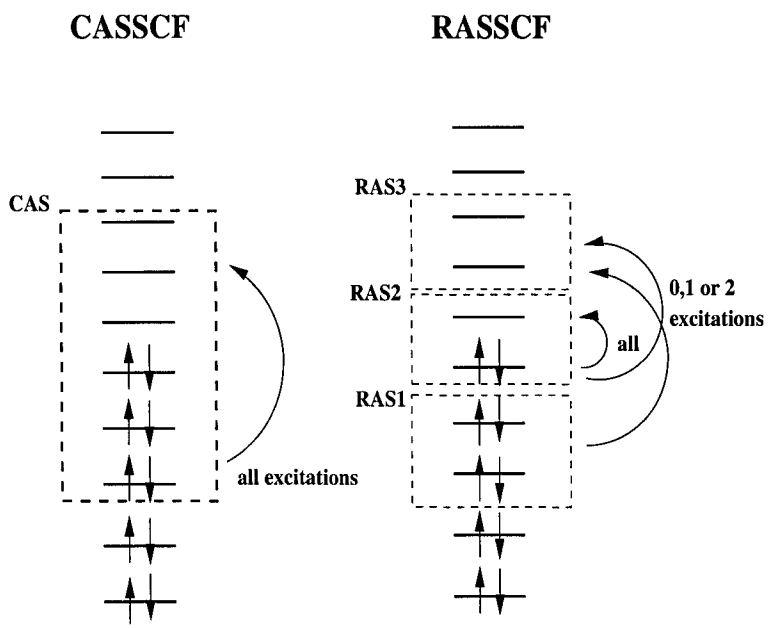

Figure 1.1: Illustration of the CAS and RAS orbital partitions

CI, MP2 and CCSD methods, and satisfactory results have been obtained. In the following section, several such combined approaches will be outlined.

The method of multi-reference configuration interaction (MRCI) was first introduced in mid 1970's [43], and by now it has become one of the standard electron correlation methods employed in routine computational studies of ground and excited state potential energy surfaces. The basic idea behind the MRCI method is simple: instead of the excited determinants generated from the HF wavefunction, they are generated from a reference space consisting of a number of configurations. The CISD wavefunction in eq. (1.31) can be rewritten, in second quantization format, as

$$\Psi_{CISD} = \left(C_0 + \sum_{a}^{occ} \sum_{r}^{virt} C_a^r \mathbf{a}_r^+ \mathbf{a}_a + \sum_{ab}^{occ} \sum_{rs}^{virt} C_{ab}^{rs} \mathbf{a}_s^+ \mathbf{a}_r^+ \mathbf{a}_b \mathbf{a}_a + \cdots \right) |\Phi_0\rangle \qquad (1.75)$$

where $\mathbf{a}^+$ and $\mathbf{a}$ are creation and annihilation operator, respectively, acting on the HF wavefunction $|\Phi_0\rangle$. In MRCI scheme, the HF wavefunction is replaced by a

CISD wavefunction. That is,

$$\Psi_{MRCI} = \left(C_0 + \sum_{a}^{occ} \sum_{r}^{virt} C_a^r \mathbf{a}_r^+ \mathbf{a}_a + \sum_{ab}^{occ} \sum_{rs}^{virt} C_{ab}^{rs} \mathbf{a}_s^+ \mathbf{a}_r^+ \mathbf{a}_b \mathbf{a}_a + \cdots \right) \Psi_{CISD}. \quad (1.76)$$

By choosing the CISD wavefunction as the reference, higher-order excitation terms can be included. For instance, the missing quadruple excitations in the CISD wavefunction, which make the method size-inconsistent, can be generated in the MRCI method, therefore significantly improving both the wavefunction and energy. In general, this method is able to recover a much larger portion of the correlation energy than the CISD method, while requiring only a small amount of extra computer resources. Normally, the expression inside the bracket in eq (1.73) is truncated at the double excitation level since the contributions from higher-order terms are negligibly small. This gives rise to the so-called MRCISD (or MRSDCI) method. As the other truncated CI methods, the MRCI method is not size-consistent, and Davidson correction is still required to recover the contribution from the missing higher-order configurations.

A closely-related method to MRCI is known as the second-order configuration interaction (SOCI) [44]. This method differs from the general MRCI in the way that the MCSCF or CASSCF wavefunction is taken as the reference, from which excited configurations are generated by CISD. An important factor determining the accuracy of MRCI is the choice of molecular orbitals with which the wavefunction constructed. Note that these orbitals are generated by the single-reference HF method which is incapable of dealing with the effects of degeneracy. Thus, this set of HF orbitals is certainly not able to properly describe the systems with degenerate ground states, although this problem can partly be solved by including a large number of configurations in the MRCI wavefunction. However, the resulting wavefunction will suffer a serious problem of convergence. The use of an MCSCF-type reference, on the other hand, can avoid the potential problem of degeneracy, as both the orbitals and coefficients in the MCSCF wavefunction are optimized, and all chemically significant configurations are manually chosen in the reference space. Consequently, both static and dynamical correlations can be considered while only

smaller number of configurations, compared to MRCI, have to be included. This method has been applied fairly successfully on heavy systems such as LaH [45], PbBr [46], WF_4 [47] and $[Mo_2Cl_9]^{3-}$ [48].

Both MRCI and SOCI inherit the property of size-inconsistency from the truncated CI wavefunction, although the problem of non-dynamical correlation is to certain extent solved. The multi-reference perturbation theory (MRPT), however, does not encounter the same situation because perturbational method is, as mentioned in the previous sections, both size-consistent and size-extensive. Unfortunately, the development of MRPT is much more difficult than MRCI and SOCI. Recall that in perturbational approach, the complete Hamiltonian of the system is separated into two parts, with the zeroth-order Hamiltonian being solvable. Generally, the zeroth-order Hamiltonian in MPPT method is the sum of one-electron Fock operators, whose eigenfunctions are simply the HF wavefunction. This is not true in the case of MCSCF wavefunctions since they are not the eigenfunctions of the Fock operators. Therefore, the zeroth-order Hamiltonian and wavefunction in the general multi-configuration perturbation theory (MCPT) [49] should be constructed from both the HF and excited configurations:

$$|\Psi_n^{(0)}\rangle = C_0|\Phi_0\rangle + \sum_{k\neq 0} C_k|\Phi_k\rangle \tag{1.77}$$

$$\mathcal{H}^{(0)} = E_0|\Psi_n^{(0)}\rangle\langle\Psi_n^{(0)}| + \sum_{k'\neq 0} E_k|\Phi_{k'}\rangle\langle\Phi_{k'}|. \tag{1.78}$$

An additional requirement in the zeroth-order Hamiltonian is that the ground state $|\Psi_n^{(0)}\rangle$ is projected out of the excited configurational space $\{|\Phi_{k'}\rangle\}$. Using the same technique as shown for RSPT, the second-order correction to energy can be deduced:

$$E_n^{(2)} = -\sum_{k\neq 0} \frac{\langle\Psi_n^{(0)}|\mathcal{H}|\Phi_{k'}\rangle\langle\Phi_{k'}|\mathcal{H}|\Psi_n^{(0)}\rangle}{E_k^{(0)} - E_n^{(0)}}. \tag{1.79}$$

The multi-reference Møller-Plesset method developed by Hirao and co-workers [50] divides the state space into three sections: CAS reference space $|\Phi_n\rangle$, excited determinants $|\Phi_k\rangle$ from the CAS space, and orthogonal determinants $|\Phi_q\rangle$ outside

the CAS space. Symbolically, the Hamiltonian is written as

$$\mathcal{H}^{(0)} = E_\alpha^{(0)}|\Psi_n^{(0)}\rangle\langle\Psi_n^{(0)}| + \sum_k E_k^{(0)}|\Phi_k\rangle\langle\Phi_k| + \sum_q E_q^{(0)}|\Phi_q\rangle\langle\Phi_q|. \tag{1.80}$$

The second-order MRMP (MRMP2) energy is thus

$$E_n^{(2)} = -\sum_q \frac{|\langle\Phi_q|\mathcal{H}|\Psi_n^{(0)}\rangle|^2}{E_q^{(0)} - E_n^{(0)}}. \tag{1.81}$$

The complete active space perturbation theory (CASPT) is another popular MRPT developed by Roos et al. [51], in which the zeroth-order Hamiltonian is further transformed into block-diagonal matrix based on the order of excitations from the CAS reference space. The second-order CASPT (CASPT2) is identical to MRMP2 when only the ground state energy and wavefunction are to be calculated.

Despite the size-consistent property that makes MRPTs promising techniques in electron correlation calculations, they all suffer from the singularity problem arising from the diminishing denominators in eqs. (1.79) and (1.81). This so-called intruder states problem [52] is particularly important for excited states since their energies in the CAS space are usually quasi-degenerate. Several proposals dealing with the intruder states have been reported; the most commonly used scheme is the intruder state avoidance (ISA) [53] in which an energy-denominator shift is added to the energy correction terms so as to remove all $|\Phi_q\rangle$ which are quasi-degenerate to $|\Psi_n^{(0)}\rangle$.

1.3.6 Other Methods

In the previous sections the basic information of HF and electron correlation methods such as CI, MP2 and CC was introduced. These methods are categorized as *ab initio* wavefunction methods because no *a priori* assumptions are made in the computations of the wavefunction: The wavefunction of the system of interest is determined from the correct Hamiltonian without using any experimental data. Since all the integrals have to be evaluated, the efficiency of such methods is greatly dependent on the number of basis functions that are used to build the wavefunctions.

This limitation strongly hinders the applicability of these methods, and restricts them to only small atomic and molecular systems.

There are two quantum chemical approaches which allow for the calculations involving relatively large systems. The first one is semi-empirical approach [54], in which the Hamiltonian is somehow simplified by introducing parameters that are pre-determined to fit experimental data or *ab initio* values. In this family of methods, certain types of molecular integrals are replaced by parameters which are adjusted so that the energies and other molecular properties agree with the experimental values or the results from the *ab initio* calculations. Depending on the underlying approximations and parameters, various semi-empirical methods such as Pople-Parr-Pariser (PPP) method [55, 56], Hückel molecular orbital (HMO) method [12], modified neglect of differential overlap (MNDO) [57] method, Austin Model 1 (AM1) method [58] and Parametrized Model 3 (PM3) method [59] have been developed.

Another completely different approach to the electronic structure calculations is to employ the electron density rather than the wavefunction. This method, known as density functional theory (DFT) [60], stems from two revolutionary papers from Hohenberg and Kohn [61], and Kohn and Sham [62] which showed that the ground state energy (and other molecular properties) can be uniquely determined by the ground state electron density, and this relation can be expressed in terms of a density functional

$$E_0[\rho] = \int \rho(\mathbf{r}) v(\mathbf{r}) d\mathbf{r} + \bar{T}_s[\rho] + \frac{1}{2} \int \int \frac{\rho(\mathbf{r}_1)\rho(\mathbf{r}_2)}{\mathbf{r}_{12}} d\mathbf{r}_1 d\mathbf{r}_2 + E_{xc}[\rho]. \qquad (1.82)$$

In this equation, $\rho(\mathbf{r})$ is the electron density of the system, $v(\mathbf{r})$ is the electrostatic potential energy of electrons, $\bar{T}_s[\rho]$ is the kinetic energy of electrons and $E_{xc}[\rho]$ is the exchange-correlation functional. This energy expression is very similar to those derived in HF and other wavefunction methods; its exact form, unfortunately, is not known. Many forms of the exchange-correlation functionals $E_{xc}[\rho]$ have been developed (for example, X_α [63], VWN [64], PW91 [65] and B3LYP [66]) and their performance has been extensively tested. In general, the computational resources required in the DFT calculations are much smaller than wavefunction methods since

the problem has been reduced to finding the electron density of a system in x, y and z coordinates. Therefore, DFT can be utilized in the molecular modeling for large systems such as clusters or solids. However, a problem associated with the DFT formalism is the use of "empirical" functionals which may not work equally well for all systems; in some circumstances, the DFT even predicts wrong geometries and binding energies [67, 68]. For a comprehensive comparison of the performance of various DFT methods, see Ref. [69].

1.4 Relativistic Effects

Relativistic effects, generally speaking, refer to the consequences of changes of physical and chemical properties of atomic or molecular systems when electrons are moving at the speed comparable to the speed of light. In classical mechanics, the speed of light is assumed infinite and there is no interaction between light and particles. Accordingly, the masses of particles are conserved in Newtonian mechanics. However, the proposition and verification of the special theory of relativity developed by Einstein [70] completely revised this idea. In the relativistic mechanics, the rule of the conservation of mass does not hold; instead, the mass of a moving particle is related to its speed via the following relation:

$$m_v = \frac{m_0}{\sqrt{1 - \left(\frac{v}{c}\right)^2}} \tag{1.83}$$

in which m_0 is the rest mass of a particle, and m_v is the corresponding mass of the particle moving at the speed v. Furthermore, the special theory of relativity also suggests the mass-energy equivalence which reveals that both energy and mass are not conserved; they can be transformed from and to each other.

These two fundamental principles of relativity, though widely adopted already in several areas of modern physics, were found not very useful in chemistry until 1970's when it was discovered that the relativistic effects are in fact substantial in the systems containing heavy atoms. The most known and fascinating examples of relativistic effects in chemistry are the yellow glitter of gold [71], the liquid phase of mercury and the existence of mercurous ion [72], and the weak binding of heavy

main-group dimers such as Tl_2 and Pb_2 [73]. Nowadays, the relativistic effects have become the central part of the research on the electronic structure and properties of systems composed of heavy elements.

All relativistic quantum chemistry centers on the Dirac equation for particle in an arbitrary external scalar field, which is the relativistic version of the Schrödinger equation:

$$\left(c\boldsymbol{\alpha}\cdot\mathbf{p}+\beta mc^2+V\right)\Psi=E\Psi \tag{1.84}$$

where $\boldsymbol{\alpha}$ is a (4×4) matrix expressed in terms of the (2×2) Pauli spin matrix $\boldsymbol{\alpha}$ in Cartesian coordinates, β is expressed in terms of two (2×2) identity matrices:

$$\boldsymbol{\alpha}=\begin{pmatrix} 0 & \boldsymbol{\sigma} \\ \boldsymbol{\sigma} & 0 \end{pmatrix} \quad , \quad \beta=\begin{pmatrix} 1 & 0 & 0 & 0 \\ 0 & 1 & 0 & 0 \\ 0 & 0 & -1 & 0 \\ 0 & 0 & 0 & -1 \end{pmatrix}, \tag{1.85}$$

and $\mathbf{p}$ is the momentum of particle. Since the Dirac equation is a four-dimension equation, the resulting Dirac wavefunction thus contains four components, which are generally written as

$$\Psi=\begin{pmatrix} \Psi_{L\alpha} \\ \Psi_{L\beta} \\ \Psi_{S\alpha} \\ \Psi_{S\beta} \end{pmatrix} \tag{1.86}$$

where Ψ_L and Ψ_S refer to the large and small components respectively. Using this four-component wavefunction, the Dirac equation can be rewritten as a system of two coupled equations:

$$c\left(\boldsymbol{\alpha}\cdot\mathbf{p}\right)\Psi_S+V\Psi_L = E\Psi_L \tag{1.87}$$

$$c\left(\boldsymbol{\alpha}\cdot\mathbf{p}\right)\Psi_L+(V-2mc^2)\Psi_S = E\Psi_S \tag{1.88}$$

In the non-relativistic case, the large components for electrons will be reduced to the solutions of the Schrödinger equation, and the small components disappear. For electrons, the small components are needed only for the coupling with the positronic states.

For the many-particle systems, the Dirac operator is written as the so-called Dirac-Coulomb Hamiltonian [74]

$$\mathcal{H} = \sum_i h_D(i) + \sum_{i<j} \frac{1}{r_{ij}}. \tag{1.89}$$

The first term is the summation of one-electron Dirac operator defined, in atomic units, as:

$$h_D(i) = \left(\boldsymbol{\alpha}_i \cdot \mathbf{p}_i + \beta_i c^2 - \frac{Z}{r_i} \right). \tag{1.90}$$

The second term is a generic non-relativistic Coulomb two-electron operator. The full relativistic two-electron term is very complicated because of the presence of retardation effects that can be dealt with only by quantum electrodynamics. Consequently, this term is usually written as the Taylor expansion up to the order of $1/c$, giving the following Coulomb-Breit operator [75]:

$$V^{CB}(\mathbf{r}_{12}) = \frac{1}{r_{12}} - \frac{1}{2r_{12}} \left[\boldsymbol{\alpha}_1 \cdot \boldsymbol{\alpha}_2 + \frac{(\boldsymbol{\alpha}_1 \cdot \mathbf{r}_{12})(\boldsymbol{\alpha}_2 \cdot \mathbf{r}_{12})}{r_{12}^2} \right]. \tag{1.91}$$

The presence of the two-electron interactions may lead to problems in finding suitable solution [76], as the negative-energy states may interfere with the positive-energy ones [77]. A discussion of the approaches that avoid these problems in practical calculations is given by Grant and Quiney [78].

1.4.1 Pauli Approximation

The ideal way of studying the relativistic effects on molecular structures and properties is to solve the Dirac equation directly and obtain the four-component wavefunctions (or spinors). However, the mathematics involved and the practical implementation of such procedures into computer programs are very tedious. Therefore, simplifications were sought by decoupling the large and small components in the spinors and looking only at the large-component solutions of the Dirac equation which correspond to the electronic motions. The large and small components couple through one-electron operators in the Dirac Hamiltonian; therefore, the decoupling can be achieved by transforming only the one-electron terms in the Dirac Hamiltonian. A number of decoupling schemes have been proposed. The first method is to

substitute to the large-component equation (1.87) the expansion of $\mathbf{K}$ defined as

$$\mathbf{K} = \left(1 + \frac{E - V}{2mc^2}\right)^{-1} \approx 1 - \frac{E - V}{2mc^2} + \cdots . \tag{1.92}$$

Assuming the Coulomb potential V, the one-electron Dirac equation can be transformed to the Pauli equation:

$$\left[\frac{\mathbf{p}^2}{2m} + V - \frac{\mathbf{p}^4}{8m^3c^2} + \frac{Z\mathbf{s}\cdot\mathbf{l}}{2m^2c^2r^3} + \frac{Z\pi\delta(\mathbf{r})}{2m^2c^2}\right]\Psi_L = E\Psi_L. \tag{1.93}$$

The first two terms in the Pauli equation constitute the non-relativistic Hamiltonian, and the remaining terms account for the relativistic effects. The third term is called the mass-velocity term dealing with the dependence of mass of electron on its velocity. The fourth term is the spin-orbit term concerning the interaction of the spin and orbital angular momenta. It is worth noting, in passing, that spin emerges as a consequence of relativity. The last term, called the Darwin correction, is sometimes called *Zwitterbewegung*. This term has no definite physical meaning, but can be considered as arising from the high oscillations of an electron at its mean position or the smearing of electron charge due to its relativistic motion [79]. The third and fifth terms are often collectively called the scalar relativistic correction as they do not contain spin terms.

A major problem in the Pauli approach is the singularity at regions close to the nucleus which arises from the constraint that $|V - E| << 2mc$ in order for the expansion to be valid. The violation of this assumption will cause the phenomenon of variational collapse, which strongly prohibits applications of the Pauli approximation to the variational calculations in the relativistic quantum chemistry.

1.4.2 Zero-Order Regular Approximation

In the zero-order regular approximation (ZORA) [80], the Dirac Hamiltonian for the large component is expanded, to the zeroth-order, in the similar way as the Pauli approximation except that the factor $\mathbf{K}$ is modified as the following

$$\mathbf{K} = \left(1 + \frac{E}{2mc^2 - V}\right)^{-1} \approx 1 - \frac{E}{2mc^2 - V} + \cdots , \tag{1.94}$$

such that the problem of divergence near the nuclear position can be eliminated [81]. The resulting ZORA Hamiltonian slightly differs form from the Pauli Hamiltonian:

$$\left[\mathbf{p}\frac{c^2}{2m^2c^2 - V}\mathbf{p} + \left(\frac{c^2}{2m^2c^2 - V}\right)^2 \frac{Z\mathbf{s}\cdot\mathbf{l}}{r^3} + V\right]\Psi_L = E\Psi_L. \tag{1.95}$$

An interesting feature of the ZORA Hamiltonian is that the spin-orbit coupling term exists even at the zero-order correction, which enables the description of relativistic effects in the region close to the nucleus. However, this Hamiltonian is gauge-dependent; the shift of potential V results in non-constant shift of energy.

1.4.3 Relativistic Elimination of Small Component

Another popular approximate method is the relativistic elimination of small component (RESC) method proposed by Hirao and Nakajima [82]. This method starts with the equation for the large component obtained by the substitution of eq. (1.88) into eq. (1.87):

$$\left[V + (\boldsymbol{\alpha}\cdot\mathbf{p})\frac{c}{2mc^2 - (V - E)}(\boldsymbol{\alpha}\cdot\mathbf{p})\right]\Psi_L = E\Psi_L, \tag{1.96}$$

with the $(V - E)$ in the denominator replaced by the relativistic kinetic energy T:

$$T = \sqrt{m^2c^4 + p^2c^2} - mc^2. \tag{1.97}$$

Expanding the Hamiltonian in the powers of $(p/mc)^2$ yields the RESC Hamiltonian as a sum of spin-free and spin-dependent parts:

$$\mathcal{H}^{sf} = T + OQ\mathbf{p}\cdot V\mathbf{p}QO^{-1} + 2mcOQ^{1/2}VQ^{1/2}O^{-1} \tag{1.98}$$

$$\mathcal{H}^{sd} = iOQ\boldsymbol{\alpha}\cdot(\mathbf{p}V)\times\mathbf{p}QO^{-1} \tag{1.99}$$

in which

$$O = \frac{1}{E_p + mc^2}\left[1 + \frac{p^2c^2}{(E_p + mc^2)^2}\right]^{1/2} \tag{1.100}$$

$$Q = \frac{c}{E_p + mc^2} \tag{1.101}$$

and $E_p = \sqrt{m^2c^4 + p^2c^2}$. This method contains relativistic correction terms of order higher than the ZORA approach, as it is derived directly from the Dirac equation; however, it has been shown that RESC may suffer from the variational collapse when Z exceeds 80 [83].

1.4.4 Douglas-Kroll Transformation

All the methods introduced previously eliminate the small component of the full four-component spinors by inserting eq. (1.88) into (1.87), and expanding the large-component equation in different terms. Another way of reducing the four-component Dirac Hamiltonian is to diagonalize the Dirac equation. As demonstrated by Foldy and Wouthuysen [84], this decoupling scheme can be achieved by the unitary transformation of the Dirac Hamiltonian using the unitary operator S defined as

$$\Psi' = e^{iS}\Psi \quad , \quad S = \frac{i\beta\boldsymbol{\alpha}\cdot\mathbf{p}}{2mc}. \tag{1.102}$$

Unfortunately, the Foldy-Wouthuysen (FW) transformed Hamiltonian cannot be applied in variational calculations as both the mass-velocity and Darwin terms are singular. In order to solve this problem, Douglas and Kroll, and later Heß, developed a modified approach, in which a successive FW transformations are to be performed so that all operators become bound from below. In the Douglas-Kroll (DK), or Douglas-Kroll-Hess (DKH) method [85, 86], the free-particle FW unitary operator is instead defined as

$$U_0 = A(1+\beta R) \tag{1.103}$$

in which

$$A = \sqrt{\frac{E_p + mc^2}{2E_p}}, \tag{1.104}$$

$$R = \frac{c\boldsymbol{\alpha}\cdot\mathbf{p}}{E_p + mc^2}, \tag{1.105}$$

$$E_p = c\sqrt{p^2 + m^2c^2}. \tag{1.106}$$

Acting with this operator on eq. (1.84) generates the first-order DK (DK1) Hamiltonian:

$$\mathcal{H}_{DK1} = \beta E_p + \xi_1 + \mathcal{O}_1 = \beta E_p + A(V + RVR)A + \beta A(RV - VR)A. \tag{1.107}$$

The second FW transformation, using the unitary operator:

$$U_1 = \sqrt{1 + W_1^2} + W_1 \tag{1.108}$$

is carried out on the first-order DK Hamiltonian with the commutation constraint:

$$[\beta E_p, W_1] = \mathcal{O}_1 \tag{1.109}$$

and the kernel of W_1 defined as:

$$W_1(\mathbf{p}, \mathbf{p}') = \beta \frac{\mathcal{O}_1(\mathbf{p}, \mathbf{p}')}{E_{p'} + E_p}. \tag{1.110}$$

The final second-order DK (DK2) Hamiltonian has the form

$$\mathcal{H}_{DK2} = \beta E_p + \xi_1 - \frac{1}{2}[W_1, \mathcal{O}_1]. \tag{1.111}$$

Similar procedures can be repeated to generate the higher-order DK Hamiltonians. Here, only the third-order DK (DK3) Hamiltonian is given as an example:

$$\mathcal{H}_{DK3} = \beta E_p + \xi_1 - \frac{1}{2}[W_1, \mathcal{O}_1] + \frac{1}{2}[W_1, [W_1, \xi_1]]. \tag{1.112}$$

There are several advantages of DK method. The method remains regular for the Coulomb potential so that the problem of variational collapse can be avoided. During the decoupling process, the influence of the small component on the large-component solutions is reduced by the factor of v/c [87]; hence, in theory the effect of small component (or negative-energy states) can be completely diminished when a sufficiently high-order DK transformation is performed on the Dirac Hamiltonian. One limitation of the DK method is the complicated form of high-order DK Hamiltonians. In the presence of an external potential V, all the operators in the Hamiltonian are well-defined only in the momentum space, and those containing V are represented as integral operators specified by their kernels. Therefore, the applications of DK method at the high-order levels ($n \geq 3$) to atomic and molecular calculations are still rather limited.

1.4.5 Practical Computations of Relativistic Effects

The above-mentioned elimination methods are not limited to the single-electron system, i.e., hydrogen atom. They can be easily extended to multi-electron systems, by modifying the potential term to include electron-electron repulsion, or multi-nuclear

systems. The full transformation including the Dirac one-electron Hamiltonian and the Coulomb-Breit two-electron operator in eq. (1.91) leads to at least fourteen different terms pertaining to Zeeman effects and all kinds of relativistic effects such as spin-spin interaction, spin-orbit coupling, etc [3]. The calculations involving such Hamiltonians are impractical. Hence, one usually treats relativistic effects as perturbations, assuming that the influence of these factors on the total energies is small. The terms that are generally considered are mass-velocity, Darwin and spin-orbit corrections which constitute the so-called scalar relativistic (only the first two terms) or quasi-relativistic (including also spin-orbit term) Pauli Hamiltonian.

The incorporation of both relativistic and electron correlation effects in quantum chemical calculations is straightforward since only the one-electron operators have to be transformed relativistically while the correlation effects are determined solely by the two-electron operators. As a consequence, there are relativistic counterparts of almost all post-HF methods available in a variety of *ab initio* packages.

Although the two-component methods form the mainstream in the area of relativistic quantum chemistry, the calculations applying four-component Dirac Hamiltonian have become more popular due to the improving computer capability and the advance in the theoretical development [88]. Some remarkable calculations on the properties of atoms, molecules and solids containing heavy elements have already been published (for example: Refs [89, 90, 91, 92]).

1.5 Basis Sets

The main task of quantum chemical calculations is to solve the Schrödinger equation concerning the system of interest and find the wavefunctions associated with it, from which the properties of the system can be deduced. As described, the analytical solution of the Schrödinger equation is in fact impossible to find except for some special models such as harmonic oscillator, particle-in-a-box, or hydrogen atom. In other words, only approximate solutions of the Schrödinger equation may be obtained.

One difficulty connected with solving the Schrödinger equation using standard

quantum chemical methods is that the transformed Hartree-Fock equation is an eigenvalue problem in which the Fock operator is dependent on the eigenvectors, and the equations can be solved only iteratively. Therefore, initial guesses of the eigenvectors have to be provided in order to obtain self-consistent solutions. Unfortunately, the exact form of the solution is not known; recall that the Schrödinger equations for multi-electron and molecular systems are not solvable.

To facilitate the solution of the approximate equations, it was proposed that the unknown solutions be expanded in terms of some known functions, called basis functions, the contribution of each determined via the self-consistent field procedures subjected to the constraint of minimum total energy. There are two types of commonly used basis functions: Slater-type functions (STF) and Gaussian-type functions (GTF).

1.5.1 Slater-type and Gaussian-type Functions

It is known that, when solving the non-relativistic Schrödinger equation for hydrogen atom, the wavefunctions can be expressed as a product of spherical harmonics and radial functions which are exponential functions in terms of the position of electron r. Slater therefore assumed that atomic orbitals of many-electron elements could also be well represented by the hydrogen-like orbitals, or Slater-type functions [93]. In general, STFs possess the following form, in spherical coordinates:

$$\chi_{\alpha,n,l,m}(r,\theta,\phi) = NY_{l,m}(\theta,\phi)r^{n-1}e^{-\alpha r}, \tag{1.113}$$

where N is the normalization constant and $Y_{l,m}$ stands for the spherical harmonics. Here, n, l, m determine the type of the orbital that the STF represents. A major difference between hydrogen-like orbitals and STFs is that the latter ones are nodeless; the nodal feature of real atomic orbitals could be retained only by using a linear combination of properly chosen STFs. Calculations using STFs have been found fairly difficult, particularly in the multi-center two-electron molecular integral evaluations. Consequently, the applications of STFs are quite restricted to atomic, diatomic, or semi-empirical calculations.

In order to speed up the calculations of molecular integrals, Boys proposed the use of Gaussian-type functions whose form is very similar to the STFs [94]:

$$\chi_{\alpha,n,l,m}(r,\theta,\phi) = NY_{l,m}(\theta,\phi)r^{(2n-2-l)}\exp\left\{-\alpha r^2\right\} \quad \text{(Spherical)} \tag{1.114}$$

$$\chi_{\alpha,l_x,l_y,l_z}(x-X_A, y-Y_A, z-Z_A) = N(x-X_A)^{l_x}(y-Y_A)^{l_y}(z-Z_A)^{l_z} \times \exp\left\{-\alpha((x-X_A)^2+(y-Y_A)^2+(z-Z_A)^2)\right\} \quad \text{(Cartesian)} \tag{1.115}$$

where X_A, Y_A and Z_A are the coordinates of the point with respect to which the basis is defined. The sum of indices l_x, l_y, and l_z in eq. (1.115), like n, l, m in eq. (1.114), determines the type of orbital. The GTFs are inferior to the STFs in two aspects. A GTF has a zero slope when $r \to 0$ while the STF correctly possesses a non-zero gradient at the nucleus. The missing cusp condition in the GTFs leads to the error in representing the behavior near the nucleus. In addition, the GTFs decays more rapidly than the STFs at large r, as they depend exponentially on r^2, consequently leading to a poorer representation of wavefunctions at distances far from the nucleus. To overcome these deficiencies, one has to use several GTFs with different exponents α to mimick the behavior of a single STF, leading to the contracted basis functions. This, unfortunately, will very rapidly increase the number of integrals to be evaluated.

On the other hand, there is a peculiar feature of the GTFs that can compensate for the increased number of molecular integrals needed to be evaluated: the product of two GTFs is a new GTF; i.e., for example, for $1s$ GTFs,

$$\chi_\alpha^{1s}(r-R_A)\chi_\beta^{1s}(r-R_B) = \left(\frac{2\alpha\beta}{(\alpha+\beta)\pi}\right)^{3/4}\exp\left[-\frac{\alpha\beta}{\alpha+\beta}|R_A-R_B|^2\right]\chi_{\alpha+\beta}^{1s}(r-R_P) \tag{1.116}$$

where R_p is given by

$$R_P = \frac{\alpha R_A + \beta R_B}{\alpha+\beta}. \tag{1.117}$$

In other words, the product of two GTFs centered at A and B, respectively, is in fact a GTF centered at a new position P. This is an invaluable relation since all the four-center molecular integrals can now be converted immediately to two-center

integrals which can be evaluated very efficiently. Therefore, the total time required to perform calculations using the GTFs is significantly reduced compared to the cases using the STFs.

1.5.2 Common Types of Basis Sets

A basis set is the collection of basis functions used to expand molecular orbitals in quantum chemical calculations. The smallest basis set is the one in which each occupied orbital is represented by one contracted basis function; this type of basis is called minimal or single-zeta basis set, where ζ is the symbol of Slater atomic orbital. A typical family of single-zeta basis sets is the STO-nG set, where n stands for the number of GTFs in the contraction, developed by Pople and co-workers [95]. Obviously, the single-zeta basis sets are not good choices in accurate calculations as they are unable to describe any deviation of electron density caused by the neighboring atoms in a molecule.

The performance of single-zeta basis sets can be improved simply by increasing the number of contracted basis functions describing an atomic orbital, leading to the development of double-zeta, triple-zeta, and so on, basis sets. (For example, the DZ and TZ basis sets developed by Dunning and Hay [96, 97, 98]) These expansions allow for a better representation of electron density in both core and valence regions by selecting appropriate GTF exponents. Furthermore, the larger number of basis functions better accounts for the different electron distribution in different directions. Besides increasing the number of basis functions for all the atomic orbitals, the shell splitting can be done merely for the valence orbitals, with the argument being that mostly chemical reactivity of an atom is determined by the valence electrons. This kind of splitting scheme produces the split-valence basis set [99]. Pople and co-workers have designed a series of such split-valence basis sets such as double split-valence 4-31G and 6-31G and triple split-valence 6-311G basis sets for the first, second, and third-row elements [100, 101, 102, 103].

In parallel to the expansion of zeta, the angular correlation (i.e., the distortion of electron density from its original direction) can be considered by adding basis

functions with angular momenta higher than those of the occupied atomic orbitals. Such polarization functions are important in the electron correlation calculations and the geometry optimizations of hypervalent compounds [104]. In the cases where the electron density is spread out far away from the nuclei, such as in molecular anions, a set of GTFs with very small exponents, called diffuse functions, have to be added to the atomic basis sets so as to well describe the extended electron distribution in the outer region.

Another logical way of improving the performance of basis sets is to increase the number of GTFs in the contraction, so as to enhance the flexibility of the basis set. However, the large number of GTFs causes the slow convergence in the optimization. Therefore, the contraction coefficients are usually pre-defined based on variational atomic calculations. It has been observed that the ratios of two successive exponents in the best optimized basis sets are nearly constant. This provides a route to expanding a basis set if more GTFs are to be added. Two approaches are commonly employed: the even-tempered basis set [105]

$$\zeta_i = \alpha\beta^i \quad , \quad i = 1, 2, \cdots, M \tag{1.118}$$

$$\ln(\ln\beta) = b\ln M + b' \tag{1.119}$$

$$\ln\alpha = a\ln(\beta - 1) + a', \tag{1.120}$$

and the well-tempered basis set [106]

$$\zeta_i = \alpha\beta^{i-1}\left(1 + \gamma\left(\frac{i}{M}\right)^{\delta}\right) \quad , \quad i = 1, 2, \cdots, M. \tag{1.121}$$

in which a, a', b, b', α, β, γ, and δ are optimized for each atom. The even-tempered formula shares the same ratio of exponent for the whole range of i, so that the generation of contraction coefficients is fast. On the other hand, the well-tempered formula guarantees the better even-tempered behavior for the valence region than the core region, which is more sensible in chemical consideration. In addition, the orbitals of different angular momenta will have the same exponents and thus the same radial part in the well-tempered basis set.

There are two more popular classes of basis sets, besides the ones just mentioned, widely used in quantum chemical calculations. The first class is the atomic natural orbitals (ANO) basis sets which are constructed using a large number of GTFs optimized based on the natural orbitals obtained from CISD calculations [107, 108]. These ANO basis sets are very accurate and may be easily extended to approach the basis set limit. However, a major disadvantage of this family of basis sets is the huge number of GTFs which makes the computations very time-consuming unless the integral code is specifically designed to handle such basis sets. The second class is the correlation-consistent (cc) basis sets [109, 110] which aim at yielding results comparable to those for ANO basis sets with smaller set of GTFs. The features of the cc-type basis sets are that the GTFs which contribute the similar amount of correlation energy, regardless their type, are included at the same stage, and that the correlation energy from the valence electrons is recovered. Accordingly, the polarization functions can be augmented in a systematic fashion, for example: $1d$, $2d1f$, $3d2f1g$, and so on. Similarly to the ANO basis sets, the cc-type basis sets can be easily extended towards the basis set limit.

1.5.3 Pseudopotential Methods

It has been generally accepted that the chemical properties of an element are determined mainly by its valence electrons. A representative example is the elements belonging to the same group in the periodic table that exhibit very similar behavior such as preferred oxidation states, redox properties, and chemical reactivities. These observations stimulated the idea that the chemically "unreactive" core electrons of an atom be replaced by an effective electrostatic potential, by which a great computer time saving can be achieved since now only the basis functions for the valence electrons should be explicitly present in the basis set.

The central concept of pseudopotentials is to divide the electrons of a system into two groups: core electrons and valence electrons, in accordance to some sort of chemical intuition. The valence Hamiltonian describing the resulting many-electron

system can be expressed in a general form, in atomic units, as:

$$\mathcal{H}_v = V_{cc} + \sum_{i=1}^{n_v} h_v(i) + \sum_{i=1}^{n_v} \frac{1}{r_{ij}} \tag{1.122}$$

where n_v is the number of valence electrons. The last term in eq. (1.122) is the usual Coulomb repulsion between valence electron. The first term concerns the repulsion between shielded nuclei; explicitly, this term is given by, for a K-nuclei system,

$$V_{cc} = \sum_{\lambda<\mu}^{K} \frac{Q_\lambda Q_\mu}{R_{\lambda\mu}} \tag{1.123}$$

in which λ and μ denote the nuclei and Q_λ is the core charge associated with the nucleus λ. The effective one-electron operator is

$$h_v(i) = -\frac{1}{2}\nabla_i^2 + U_{cv}(i) \tag{1.124}$$

where $U_{cv}(i)$ is called the effective core potential (ECP), or pseudopotential, which describes the Coulomb interaction between valence electrons and the core. The general form of ECP is:

$$U_{cv}(i) = \sum_{\lambda}^{K} \left\{ -\frac{Q_\lambda}{r_{\lambda i}} + \Delta U_{cv}^{\lambda}(\mathbf{r}_{\lambda i}) \right\}. \tag{1.125}$$

Many forms of the ECP operator $U_{cv}^{\lambda}(\mathbf{r})$ have been proposed. The most popular one is the shape-consistent ECP [111] which adopts the form of ECP operator as follows:

$$U_{cv}^{\lambda}(\mathbf{r}) = \sum_k A_k r^{n_k} \exp(-\alpha_k r^2) + \sum_{l=0}^{L-1} \left(\sum_k B_k r^{m_k} \exp(-\beta_k r^2) \right) \left(\sum_{m=-1}^{l} |\lambda l m\rangle\langle \lambda l m| \right), \tag{1.126}$$

where L is the maximum angular momentum of the core orbitals. The last term is the projection operator which guarantees the orthogonality between core and valence orbitals of the same angular momentum. The parameters in the ECP operators, i.e., A, B, m, n, α, β, are determined by the fitting with the orbitals obtained in all-electron calculations. The numerical pseudo-valence orbitals determined using this ECP Hamiltonian are nodeless and retain the same shapes as the true

valence orbitals only at the region beyond their outermost maximum R_m. In the core region, i.e., $r < R_m$, the pseudo-orbitals are adjusted so that the normalization integral yields the same value as that of the real valence orbitals. These semi-local pseudopotentials assume the complete separation of the core and valence electrons; therefore, the core-polarization effect on the valence electrons is ignored. In addition, the nodeless ECP orbitals induce a large error when properties of inner-core electrons are to be calculated. Therefore, the use of ECPs in the calculations of nuclear shielding tensors and spin-orbit coupling constants, for instance, will be inappropriate. The numerical potentials of the pseudo-orbitals are generated by the Phillips-Kleinman transformation [112], and are fitted with an analytical pseudopotential, for example,

$$r^2 V_l(r) = \sum_k A_{l,k} r^{n_{l,k}} \exp\left(-B_{l,k} r^2\right), \tag{1.127}$$

in which A_l, $n_{l,k}$ and $B_{l,k}$ are optimized for each value of angular momentum l. There are several ways of performing the fitting of the numerical pseudopotential to the analytical form. For example, Hay and Wadt did the accurate least-square fitting with a large number of terms [113, 114, 115]. In the Stuttgart approach, the fitting is performed based on the constraint that the parameters should yield the best fit for the valence electron excitation spectrum [116]. On the other hand, Stevens and co-workers developed the compact effective potentials (CEPs) [117] by fitting the pseudopotentials with the all-electron HF potentials generated from very large valence basis sets, by which only a relatively small number of parameters are needed.

A way to get rid of the nodeless feature of the pseudo-valence orbitals is to define the effective potential in a nonlocal fashion. Huzinaga and co-workers [118, 119] have proposed the *ab initio* model potential (AIMP), or model core potentials (MCP), in which the ECP operator $U^{\lambda}_{cv}(\mathbf{r})$ is written as

$$U^{\lambda}(\mathbf{r}) = \sum_k T^{\lambda}_l r^{n^{\lambda}_k}_{\lambda i} \exp\left(-\alpha^{\alpha}_k r^2_{\lambda i}\right) + \sum_{c\in\lambda} B_c |\phi^{\lambda}_c\rangle\langle\phi^{\lambda}_c|. \tag{1.128}$$

In the operator, the nonlocal projection is present to maintain the orthogonality between the valence and core orbitals, and to prevent the collapse of the valence

orbitals onto the core. Since no orbital transformation is needed, the resulting pseudo-orbitals retain all the nodal structure of the true valence orbitals. Like the ECPs, the parameters in the MCP operators, i.e., T_l^λ, n_k^λ and α_k^λ are determined by the fitting to the all-electron potentials. Depending on the methods the reference potentials are generated, a number of different types of MCPs such as well-tempered MCPs [120] and improved MCPs [121] have recently been produced.

The relativistic effects can be incorporated into the pseudopotentials by utilizing the reference all-electron potentials obtained from the Dirac-Hartree-Fock calculations in which the relativistic Hamiltonian is used. On the other hand, the inclusion of core-polarization and spin-orbit effects can be achieved by adding the appropriate potential terms to the effective one-electron operators [122, 123, 124], and determining the necessary parameters via matching with the all-electron potentials.

1.5.4 Basis Set Superposition Errors

In most of the molecular calculations, the basis sets used to construct the molecular wavefunctions are atomic basis sets which are centered at the positions of atoms. The performance of an atomic basis set is not constant; it changes when the geometry of the molecule changes. Recall that all the basis sets discussed so far are finite and incomplete. Therefore, errors will be introduced when the two atoms come so close during the geometry optimization that the basis functions from one atom are used by the other atom. These "borrowed" basis functions will artificially lower the energy of the system since the basis set becomes apparently larger and more flexible. The error associated with such borrowing of basis functions is referred to as the basis set superposition error (BSSE). The BSSE could be a serious problem in the calculations of the hydrogen-bonded and weakly interacting systems [6].

Various approaches have been proposed to eliminate the BSSE. The counterpoise correction (CP) is by far the most frequently used method [125]. However, it still overestimates the BSSE since, in certain situations, the BSSE truly reflects the partial charge transfer between atoms. Other attempts such as the chemical hamiltonian approach (CHA) [126] and linear-scaling local correlation methods [127] have

been made to exclude the BSSE directly from the calculations; however, these methods are not yet widely used because of the rather complicated formalisms.

1.6 Molecular Properties

Computing the properties of a molecule is the main objective of electronic structure calculations. Molecular properties can be generally divided into two categories: primary and induced properties, according to the Boys and Cook's definitions [128]. Various methods have been developed for determining molecular properties, but they can be grouped generally into three main approaches: (1) to evaluate the molecular property as the expectation value:

$$O = O_{nuc} + \int \Psi_e^* \left(\sum_{i=1}^{m} \hat{O}_i \right) \Psi_e d\tau, \tag{1.129}$$

in which $\hat{O}$ is the quantum mechanical operator that defines the property, O_{nuc} is the contribution from the nuclei, and Ψ_e is the electronic wavefunction, (2) to measure the molecular property as a response to a particular type of external fields such as electric or magnetic radiation which are considered as a perturbation, and (3) to extract the properties of a molecule directly from its Born-Oppenheimer potential energy hypersurface.

1.6.1 Spectroscopic Properties

Potential energy hypersurface is the collection of energies of the molecule at different nuclear configurations. This hypersurface for an N-particle molecular system will be multi-dimensional and highly complicated for visualization and analysis. The situation for diatomic molecules, however, becomes very simple since now the system contains only one degree of freedom, and the potential energy curve can be represented in terms of only internuclear distances and energies.

Though it is merely a trivial low-dimensional plot, the potential energy curve for a diatomic molecule is informative, and many interesting, spectroscopy-related quantities can be determined from it. To obtain the spectroscopic constants, the analytical form of the potential is required. Since only the numerical potential

can be calculated from *ab initio* calculations, least-square fitting of the *ab initio* potential to a pre-defined potential functions is necessary. The most common form of the potential functions is the Taylor expansion at equilibrium bond distance R_e derived by Dunham [129] using the perturbation theory:

$$V(R) = V(R_e) + \frac{1}{2!}\left(\frac{d^2V(R)}{dR^2}\right)_{R_e}(R-R_e)^2 + \frac{1}{3!}\left(\frac{d^3V(R)}{dR^3}\right)_{R_e}(R-R_e)^3 + \cdots . \tag{1.130}$$

This function can be simplified to:

$$V(R) = V(0) + \frac{1}{2}f^2(R-R_e)^2 + \frac{1}{6}f^3(R-R_e)^3 + \frac{1}{24}f^4(R-R_e)^4 + \cdots \tag{1.131}$$

in which f^2, f^3 and f^4 are the second, third and fourth-order force constants that are related to the spectroscopic constants such as harmonic frequency ω_e, rotational constant B_e, reduced mass μ, vibration-rotation coupling constant α_e, and anharmonic constant $\omega_e x_e$ in the following way:

$$f^2 = 4\pi^2\mu\omega_e^2c^2 \tag{1.132}$$

$$f^3 = -\frac{3f^2}{R_e}\left(1+\frac{\alpha_e\omega_e}{6B_e^2}\right) \tag{1.133}$$

$$f^4 = \frac{f^2}{R_e^2}\left[15\left(1+\frac{\alpha_e\omega_e}{6B_e^2}\right)^2 - \frac{8\omega_e x_e}{B_e}\right]. \tag{1.134}$$

Other popular potential functions that are widely used include the Morse potential [130]:

$$V(R) = D_e\left\{\exp(-2\alpha(R-R_e)) - 2\exp(-\alpha(R-R_e))\right\} \tag{1.135}$$

where D_e is the binding energy and $f^2 = 2D_e\alpha^2$, and the Lennard-Jones potential [131]:

$$V(R) = 4\epsilon\left[\left(\frac{\sigma}{R}\right)^{12} - \left(\frac{\sigma}{R}\right)^{6}\right] \tag{1.136}$$

where ϵ and σ are binding energy and the inner zeros of the potential, respectively. Recently, the potential function proposed by Murrell and Sorbie [132] has attracted a considerable attention of spectroscopists as it has demonstrated its superior performance in both the repulsive and attractive regions compared to other available

potential functions, and in the matching with the experimental potential deduced by the Rydberg-Klein-Rees (RKR) inversion [133, 134, 135] for more than a hundred diatomic molecules. The general form of Murrell-Sorbie potential is:

$$V(R) = -D_e \left(1 + \sum_{k=1} a_k (R - R_e)^k\right) \exp\left(-\gamma(R - R_e)\right). \tag{1.137}$$

In most of the cases, the five-parameter (i.e., $k = 3$) Murrell-Sorbie potential is used. The relations between the force constants of different orders and the parameters in the Murrell-Sorbie potential function are as follows:

$$D_e a_1^4 - 6f^2 a_1^2 - 4f^3 a_1 - f_4 = 0 \tag{1.138}$$

$$a_2 = \frac{1}{2}\left(a_1^2 - \frac{f^2}{D_e}\right) \tag{1.139}$$

$$a_3 = a_1 a_2 - \frac{1}{3}a_1^3 - \frac{f^3}{6D_e}. \tag{1.140}$$

Once the analytical form of the potential energy curve is known, the rotational, vibrational and electronic Schrödinger equations can be solved, yielding the corresponding wavefunctions that can be used in the calculations of transition probabilities between different states. In the vibronic spectrum, the intensity of a transition is proportional to the integral

$$I = \int \psi_{v'}'^* \psi_{v''}'' dV_v \int \psi_e'^* \vec{\mu}_e \psi_e'' dV_e, \tag{1.141}$$

in which ψ_v and ψ_e are the vibrational and electronic wavefunctions. ψ' and ψ'' refer to, respectively, the final and initial states involved in the transition. The square of the first integral is commonly called the Frank-Condon factor [136] which measures the degree of overlap between the two vibrational wavefunctions. The second integral is the electric dipole integral from which the selection rules of electronic transitions are deduced. The determination of Frank-Condon factors is essential since these values reveal the relative positions of the equilibrium internuclear distances of the two states and the spacing of their vibrational levels.

Another quantity that is closely related to the electric dipole integral is the oscillator strength which is defined as [137]:

$$f_{v''\to v'} = \frac{8\pi^2 m_e}{3he^2} \omega_{v''\to v'} \left| \int \psi_e'^* \vec{\mu}_e \psi_e'' dV_e \right|^2 \tag{1.142}$$

where $\omega_{v''\to v'}$ is the frequency of radiation. This value shows the transition probability of a electronic transition; therefore, it can be used in the determinations of, for example, the rate of radiative decay of an excited state and the fluorescence lifetime of an organic dye.

1.6.2 Electric Properties

When a molecule is placed in a static electric field, the equilibrium electron density will be distorted according to the orientation of the field. The modified electron density will thus create an induced electric dipole $\mu_i^{ind}(E_j)$ which is related to the original electric dipole moment $\mu_i(0)$ by:

$$\mu_i^{ind}(E_j) = \mu_i(E_j) - \mu_i(0) = \alpha_{ij}E_j + \frac{1}{2}\beta_{ijk}E_jE_k + \frac{1}{6}\gamma_{ijkl}E_jE_kE_l + \cdots . \quad (1.143)$$

In the equation, (i, j, k, l) designate the Cartesian coordinates, α, β and γ denote the molecular polarizabilities, first hyperpolarizabilities and second hyperpolarizabilities, respectively. The polarizability α is a crucial factor determining the strength of a transition in the Raman spectroscopy. The hyperpolarizabilities β and γ are of great importance in nonlinear optics since large third-order nonlinearity effects on the intensity dependence of the refractive index are required for a good material to be utilized in optical-switching components in photonics [138].

In the *ab initio* calculations, the energy of a molecule in the presence of an electric field is computed by treating the electric field interaction as a small perturbation. As this energy can be expressed in terms of α, β and γ:

$$E(\vec{E}) = E(0) - \mu_iE_i - \frac{1}{2}\alpha_{ij}E_iE_j - \frac{1}{6}\beta_{ijk}E_iE_jE_k - \frac{1}{24}\gamma_{ijkl}E_iE_jE_kE_l - \cdots , \quad (1.144)$$

the different components of α, β and γ can be determined using the finite-difference techniques [139], where, for example, α_{ii} and β_{iii} are given by:

$$\alpha_{ii}E_i^2 = \frac{5}{2}E(0) - \frac{4}{3}\left(E(E_i) + E(-E_i)\right) + \frac{1}{12}\left(E(2E_i) + E(-2E_i)\right) \quad (1.145)$$

$$\beta_{iii}E_i^3 = \left(E(E_i) - E(-E_i)\right) + \frac{1}{2}\left(E(2E_i) - E(-2E_i)\right). \quad (1.146)$$

A by-product of the *ab initio* calculations of molecules is the electric field gradient (EFG) tensor, the second derivative of the electrostatic potential generated by the

neighboring charges. The different components of the EFG tensor can be directly computed from the electron distribution determined by the electronic wavefunction or via the response theory of molecular properties. Though mainly important in the studies of the nuclear quadrupole interactions in the solid-state nuclear quadrupole resonance (NQR) spectra, the hyperfine splitting of pure rotational spectra and line-broadening effects of the nuclear magnetic resonance (NMR) spectra [140], the EFG tensors are in fact valuable parameters that provide paramount information related to the orientation-dependent charge distribution of a molecule.

1.7 Scope of The Thesis

The central theme of this thesis is the study, using *ab initio* quantum chemical techniques, of simple molecular systems enclosed in external electrostatic potentials of different strengths and symmetries, and their behavior under such influence. The thesis is composed of two major parts. The first part, consisting of the first two chapters, presents the theoretical background of the model of confinement. The basic outline of the quantum chemical methods that have been employed in this research project and the necessary knowledge required to interpret the results are given in Chapter 1. Chapter 2 is devoted to the theory of confinement, including the historical review of the early development and recent advances in the studies of confinement effects, the discussion of the harmonic oscillator model utilized in the present project, and some technical information concerning the derivations and computer implementation of the confinement integrals.

The subsequent chapters comprise the second part of the thesis which centers on the applications and case studies of the model of confinement. For simplicity, only diatomic molecules have been chosen in all calculations. The presentation starts with the full CI studies of hydrogen molecule, the smallest diatomic neutral molecule, for its ground and several low-lying excited states (Chapter 3). This study serves as a starting point of the investigation of different behavior of electronic states with different symmetries to the application of an external potential, and their relations to the orbital responses. The results from the current confinement model are also

compared to those from the modeling of the hydrogen molecule magnetized by a parallel ultra-strong magnetic field on the surface of neutron stars.

The main focus of Chapters 4 and 5 is on the effects of confinement on a peculiar molecule, beryllium dimer, and its molecular ions. These chapters report the results of the comprehensive studies of the low-lying electronic states of these systems. In particular, there are two important issues that have been discussed in details. The first one is the decreasing electron affinity of Be_2 molecule as a result of the instability of the anion relative to the neutral counterpart. The second one is the rearrangement of dissociation channels which are caused by the significant orbital re-ordering of the confined Be atom.

In Chapters 6 and 7, the attention is switched to the noble-gas hydrides, the group of Rydberg molecules, being only weakly-bound, that exhibit intriguing properties in their excited states. Chapter 6 describes the full CI studies the effects of confinement on the electronic structure and spectral properties of the HeH molecule. The transition dipole moments and oscillator strengths were computed for the first three excited states, and their variations with respect to the strengths of the applied potentials have been rationalized in terms of the induced changes of the electronic structure. Chapter 7 summarizes the work performed on a heavier NeH molecule, and the emphasis is on the analysis of the unprecedented state crossings that are caused by the external potential.

In additional to the respective focal points, there are two common objectives that are shared by both Chapters 6 and 7. As the valence electrons of Rydberg molecules are usually diffuse and not strongly held by the ion core, they should be very sensitive to the presence of the repulsive electrostatic potential. The first objective is thus to investigate the field-induced ionization process of these molecules, and to find the field-strength dependence of the valence electrons in different Rydberg energy levels. The second objective is to verify the applicability of the Rayleigh-Schrödinger perturbation theory as an effective alternative for the studies of the effects of confinement, since a small external potential is already sufficient to cause noticeable changes on the structural and spectral behaviors of these molecules.

Theoretical analysis of the relativistic effects in the compounds containing heavy elements is one of the most popular topics in modern quantum chemistry. Many remarkable results have already been published. Nevertheless, the study of the relativistic properties of confined molecules and their interactions with the environmental constraints is still a fairly untouched area. In order to gain an insight into the interplay of the relativity, electron correlation, and confinement effects, DK3-MRMP2 calculations of AgH and AuH molecules confined in a cylindrical harmonic potentials were performed, and the results are presented and discussed in Chapter 8.

Chapter 9 deals with a more specific topic concerning the influence of the applied potential to a number of one-electron properties of LiH molecule. In this study, the electric dipole moments, dipole polarizability and electric field gradients of the ground and first two excited states of LiH, subjected to various strengths of the confining potential, were computed. Analysis of the relations between the changes of these electric properties and the geometry and strengths of the spatial confinement was undertaken.

Finally, a general conclusion of this project is given in Chapter 10, along with some perspectives of the possible research projects in the studies of quantum confinement.

Bibliography

[1] A. R. Leach, *Molecular Modelling: Principles and Applications*, 2nd edition, Prentice-Hall, New York, 2001; Chapter 10 and 12.

[2] A. Szabo, N. S. Ostlund, *Modern Quantum Chemistry: Introduction to Advanced Electronic Structure Theory*, McGraw-Hill Inc., New York, 1989.

[3] F. Jensen, *Introduction to Computational Chemistry*, Wiley, New York, 1999.

[4] C. J. Cramer, *Essentials of Computational Chemistry: Theories and Models*, Wiley, New York, 2002.

[5] I. N. Levine, *Quantum Chemistry*, 5th edition, Prentice-Hall, 2000.

[6] T. Helgaker, P. Jørgensen, J. Olsen, *Molecular Electronic Structure Theory*, Wiley, New York, 2000.

[7] E. Schrödinger, *Ann. Phys.* **81**, 109 (1926).

[8] M. Born, J. R. Oppenheimer, *Ann. Phys.* **84**, 457 (1927).

[9] D. R. Hartree, *Proc. Cambridge Phil. Soc.* **24**, 89; 111 (1928).

[10] V. Fock, *Z. Phys.* **61**, 126 (1930).

[11] J. C. Slater, *Phys. Rev.* **35**, 210 (1930).

[12] C. C. J. Roothann, *Rev. Mod. Phys.* **23**, 69 (1951).

[13] G. C. Hall, *Proc. Roy. Soc. A* **205**, 541 (1951).

[14] J. A. Pople, R. K. Nesbet, *J. Chem. Phys.* **22**, 571 (1954).

[15] P. O. Löwdin, *Adv. Chem. Phys.* **2**, 201 (1959).

[16] C. C. J. Roothaan, *Rev. Mod. Phys.* **32**, 179 (1960).

[17] H. Weyl, *The Theory of Groups and Quantum Mechanics*, Methuen, London, 1931.

[18] L. Brillouin, *J. Phys.* **3**, 373 (1932).

[19] S. R. Langhoff, E. R. Davidson, *Int. J. Quantum Chem.* **8**, 61 (1974).

[20] T. Kato, *Comm. Pure Appl. Math. 10*, 151 (1957).

[21] L. Rayleigh, *Phil. Mag.* **34**, 481 (1892).

[22] E. Schrödinger, *Ann. Physik* **80**, 437 (1926).

[23] G. Wentzel, *Z. f. Phys.* **38**, 518 (1926).

[24] S. Doi, Y. Ishida, S. Hiyama, *Sci. Papers Tokyo* **9**, 1 (1928).

[25] C. Møller, M. S. Plesset, *Phys. Rev.* **46**, 618 (1934).

[26] M. L. Leininger, W. D. Allen, H. F. Schaefer, C. D. Sherrill, *J. Chem. Phys.* **112**, 9213 (2000).

[27] W. Macke, *Z. Naturforsch* **5a**, 192 (1950).

[28] H. A. Bethe, *Phys. Rev.* **103**, 1353 (1956).

[29] J. Čížek, *J. Chem. Phys.* **45**, 4256 (1966).

[30] J. Čížek, *Adv. Chem. Phys.* **14**, 35 (1969).

[31] J. Čížek, J. Paldus, *Int. J. Quantum Chem.* **5**, 359 (1971).

[32] A. C. Hurley, *Electron Correlation in Small Molecules*, Academic Press, London, 1976.

[33] O. Sinanoğlu, *Adv. Chem. Phys.* **6**, 315 (1964).

[34] R. Ahlrich, W. Kutzelnigg, *J. Chem. Phys.* **48**, 1819 (1968).

[35] T. L. Lee, P. R. Taylor, *Int. J. Quantum Chem.* **S23**, 199 (1989).

[36] K. Raghavachari, G. W. Trucks, J. A. Pople, M. Head-Gordon, *Chem. Phys. Lett.* **157**, 479 (1989).

[37] J. Noga, R. J. Bartlett, *J. Chem. Phys.* **86**, 7041 (1987).

[38] A. Veillard, *Theor. Chim. Acta* **4**, 22 (1966).

[39] B. O. Roos, P. R. Taylor, P. E. M. Siegbahn, *Chem. Phys.* **48**, 157 (1980).

[40] P. E. M. Siegbahn, J. Almlöf, A. Heiberg, B. O. Roos, *J. Chem. Phys.* **74**, 2384 (1981).

[41] B. O. Roos, *Int. J. Quantum Chem. Sym.* **14**, 175 (1980).

[42] J. Olsen, B. O. Roos, P. Jørgensen, H. J. Aa. Jensen, *J. Chem. Phys.* **89**, 2185 (1998).

[43] R. J. Buenker, S. D. Peyerimhoff, *Theoret. Chim. Acta* **35**, 33 (1974).

[44] H. F. Schaefer, *Ph.D. Thesis*, Stanford University, 1969.

[45] K. K. Das, K. Balasubramanian, *J. Phys. Chem.* **95**, 42 (1991).

[46] M. Benavides-Garcia, K. Balasubramanian, *Chem. Phys. Lett.* **211**, 631 (1993).

[47] V. V. Sliznev, V. G. Solomonik, *J. Struct. Chem.* **41**, 11 (2000).

[48] K. Tanaka, M. Sekiya, Y. Tawada, E. Miyoshi, *J. Chem. Phys.* **122**, A214315 (2005).

[49] Z. Rolik, Á. Szabados, P. R. Surján, *J. Chem. Phys.* **119**, 1922 (2003).

[50] K. Hirao, *Chem. Phys. Lett.* **201**, 59 (1993).

[51] P.-Å. Malmqvist, A. Rendell, B. O. Roos, *J. Phys. Chem.* **94**, 5477 (1990).

[52] T. H. Schucan, H. Weidenmüller, *Ann. Phys. N.Y.* **73**, 108 (1972).

[53] H. A. Witek, Y. K. Choe, J. P. Finley, K. Hirao, *J. Comput. Chem.* **23**, 957 (2002).

[54] J. Sadlej, I. L. Cooper, *Semi-Empirical Methods of Quantum Chemistry*, Ellis Horwood Ltd., Chichester, 1985.

[55] J. A. Pople, *Trans. Faraday Soc.* **49**, 1375 (1953).

[56] R. Pariser, R. G. Parr, *J. Chem. Phys.* **21**, 769 (1953).

[57] M. J. S. Dewar, W. Thiel, *J. Am. Chem. Soc.* **99**, 4899 (1977).

[58] M. J. S. Dewar, E. G. Zoebisch, E. F. Healy, J. J. P. Stewart, *J. Am. Chem. Soc.* **107**, 3902 (1985).

[59] J. J. P. Stewart, *J. Comput. Chem.* **10**, 209, 221 (1989).

[60] R. Parr, W. T. Yang, *Density-Functional Theory of Atoms and Molecules*, Oxford University Press, London, 1988.

[61] P. Hohenberg, W. Kohn, *Phys. Rev.* **136**, B864 (1964).

[62] W. Kohn, L. J. Sham, *Phys. Rev.* **140**, A1133 (1965).

[63] J. C. Slater, *Phys. Rev.* **81**, 385 (1951).

[64] S. J. Vosko, L. Wilk, M. Nusair, *Can. J. Phys.* **58**, 1200 (1980).

[65] J. P. Perdew, J. A. Chevary, S. H. Vosko, K. A. Jackson, M. R. Pederson, D. J. Singh, C. Fiohais, *Phys. Rev. B* **46**, 6671 (1992).

[66] P. J. Stephen, F. J. Devlin, C. F. Chabalowski, M. J. Frisch, *J. Chem. Phys.* **98**, 11623 (1994).

[67] C. J. Cramer, S. E. Barrow, *J. Org. Chem.* **63**, 5523 (1998).

[68] O. Wiest, D. C. Montiel, K. N. Houk, *J. Phys. Chem. A* **101**, 8378 (1997).

[69] W. Koch, M. C. Holthausen, *A Chemist's Guide to Density Functional Theory*, Wiley-VCH, New York, 2000.

[70] A. Einstein, *Ann. Physik* **17**, 891 (1905).

[71] P. Pyykkö, J. P. Desclaux, *Acc. Chem. Res.* **12**, 276 (1979).

[72] R. Niesler, K. S. Pitzer, *J. Phys. Chem.* **91**, 1084 (1987).

[73] K. Balasubramanian, K. S. Pitzer, *J. Chem. Phys.* **78**, 321 (1983).

[74] J. Sucher, *Phys. Rev. A* **22**, 348 (1980).

[75] H. Bethe, E. E. Salpeter, *Quantum Mechanics of One and Two-Electron Atoms*, Springer, Berlin, 1957.

[76] G. W. Brown, D. G. Ravenhall, *Proc. Roy. Soc. (London) A* **208**, 552 (1951).

[77] J. Sucher, *Phys. Rev. Lett.* **55**, 1033 (1985).

[78] I. P. Grant, H. M. Quiney, *Adv. Atomic Molec. Phys.* **23**, 37 (1988).

[79] K. Balasubramanian, *Relativistic Effects in Chemistry: Part A*, Wiley, New York, 1997.

[80] E. van Lenthe, E. J. Baerends, J. G. Snijder, *J. Chem. Phys.* **99**, 4597 (1993).

[81] E. van Lenthe, *Ph.D. Thesis*, Vrije Universiteit, 1996.

[82] T. Nakajima, K. Hirao, *Chem. Phys. Lett.* **302**, 383 (1999).

[83] M. Barysz, *J. Chem. Phys.* **113**, 4003 (2000).

[84] L. L. Foldy, S. A. Wouthuysen, *Phys. Rev.* **78**, 29 (1950).

[85] M. Douglas, N. M. Kroll, *Ann. Phys. N.Y.* **82**, 89 (1974).

[86] B. A. Heß, *Phys. Rev. A* **33**, 3742 (1986).

[87] A. Wolf, *Ph.D. Thesis*, Friedrich-Alexander-Universität Erlangen-Nürnberg, 2004.

[88] B. A. Heß, *Relativistic Effects in Heavy-Element Chemistry and Physics*, Wiley, New York, 2003.

[89] O. Christiansen, J. Gauss, B. Schimmelpfennig, *Phys. Chem. Chem. Phys.* **2**, 965 (2000).

[90] J. Thyssen, J. K. Laerdahl, P. Schwerdtfeger, *Phys. Rev. Lett.* **85**, 3105 (2000).

[91] L. Visscher, E. van Lenthe, *Chem. Phys. Lett.* **306**, 357 (1999).

[92] A. Hu, P. Otto, J. Ladik, *Chem. Phys. Lett.* **320**, 6 (2000).

[93] J. C. Slater, *Phys. Rev.* **36**, 57 (1930).

[94] S. F. Boys, *Proc. R. Soc. (London) A* **200**, 542 (1950).

[95] W. J. Hehre, R. F. Stewart, J. A. Pople, *J. Chem. Phys.* **51**, 2657 (1969).

[96] T. H. Dunning Jr., *J. Chem. Phys.* **53**, 2823 (1970).

[97] T. H. Dunning Jr., P. J. Hay, *Methods of Electronic Structure Theory*, Plenum Press, Ney York, 1977; Chapter 1.

[98] T. H. Dunning Jr., *J. Chem. Phys.* **55**, 716 (1971).

[99] A. Schafer, H. Horn and R. Ahlrichs, *J. Chem. Phys.* **97**, 2571 (1992).

[100] R. Ditchfield, W. J. Hehre, J. A. Pople, *J. Chem. Phys.* **54**, 724 (1971).

[101] M. S. Gordon, J. S. Binkley, J. A. Pople, W. J. Pietro, W. J. Hehre, *J. Am. Chem. Soc.* **104**, 2797 (1983).

[102] W. J. Hehre, R. Ditchfield, J. A. Pople, *J. Chem. Phys.* **56**, 2257 (1972).

[103] R. Krishnan, J. S. Binkley, R. Seeger, J. A. Pople, *J. Chem. Phys.* **72**, 650 (1980).

[104] J. B. Collins, P. von R. Schleyer, J. S. Binkley, J. A. Pople, *J. Chem. Phys.* **64**, 5142 (1976).

[105] M. W. Schmidt, K. Ruedenberg, *J. Chem. Phys.* **71**, 3951 (1979).

[106] S. Huzinaga, M. Klobukowski, H. Tatewaki, *Can. J. Chem.* **63**, 1812 (1985).

[107] J. Almlöf, P. R. Taylor, *J. Chem. Phys.* **92**, 551 (1990).

[108] J. Almlöf, P. R. Taylor, *Adv. Quantum. Chem. 22*, 301 (1991).

[109] T. H. Dunning Jr., *J. Chem. Phys.* **90**, 1007 (1989).

[110] A. K. Wilson, T. van Mourik, T. H. Dunning Jr., *J. Mol. Struct.* **388**, 339 (1996).

[111] L. R. Kahn, P. Baybutt, D. G. Truhlar, *J. Chem. Phys.* **65**, 3826 (1976).

[112] J. C. Phillips, L. Kleinman, *Phys. Rev.* **116**, 880 (1959).

[113] P. J. Hay, W. R. Wadt, *J. Chem. Phys.* **82**, 270 (1985).

[114] P. J. Hay, W. R. Wadt, *J. Chem. Phys.* **82**, 284 (1985).

[115] P. J. Hay, W. R. Wadt, *J. Chem. Phys.* **82**, 299 (1985).

[116] P. Fuentealba, H. Preuss, H. Stoll, L. v. Szentpaly, *Chem. Phys. Lett.* **89**, 418 (1982).

[117] W. J. Stevens, H. Basch, M. Krauss, *J. Chem. Phys.* **81**, 6026 (1984).

[118] V. Bonifacic, S. Huzinaga, *J. Chem. Phys.* **60**, 2779 (1973).

[119] M. Klobukowski, S. Huzinaga, Y. Sakai, *Comput. Chem.* **3**, 49 (2000).

[120] J. Y. Mane, M. Klobukowski, *Theor. Chem. Acc. 112*, 33 (2004).

[121] C. C. Lovallo, M. Klobukowski, *J. Comput. Chem.* **25**, 1206 (2004).

[122] W. Müller, J. Flesch, W. Meyer, *J. Chem. Phys.* **80**, 3297 (1984).

[123] P. Hafner, W. H. E. Schwarz, *Chem. Phys. Lett. 65*, 537 (1979).

[124] R. M. Pitzer, N. W. Winter, *J. Chem. Phys.* **92**, 3061 (1988).

[125] G. Chalasinski, M. M. Szczesniak, *Chem. Rev.* **94**, 1723 (1994).

[126] I. Meyer, A. Vibok, *Mol. Phys.* **92**, 503 (1997).

[127] M. Schütz, G. Rauhut, H. J. Werner, *J. Phys. Chem. A* **102**, 5997 (1998).

[128] S. F. Boys, G. B. Cook, *Rev. Mod. Phys.* **32**, 285 (1960).

[129] J. L. Dunham, *Phys. Rev.* **41**, 721 (1932).

[130] P. M. Morse, *Phys. Rev.* **34**, 29 (1927).

[131] J. E. Lennard-Jones, *Proc. Roy. Soc. A 106*, 463 (1924).

[132] J. N. Murrell, K. S. Sorbie, *J. Chem. Soc. Faraday Trans. II 70*, 1552 (1974).

[133] R. Rydberg, *Z. Phys.* **73**, 376 (1931).

[134] O. Klein, *Z. Phys.* **76**, 226 (1932).

[135] A. G. L. Rees, *Proc. Phys. Soc.* **59**, 998 (1947).

[136] E. U. Condon, *Phys. Rev.* **32**, 858 (1928).

[137] D. R. Bates, *J. Chem. Phys.* **19**, 1122 (1951).

[138] D. R. Kanis, M. A. Ratner, T. J. Marks, *Chem. Rev.* **94**, 195 (1994).

[139] H. A. Kurtz, J. J. P. Stewart, K. M. Dieter, *J. Comput. Chem.* **11**, 82 (1990).

[140] J. D. Graybeal, *Molecular Spectroscopy*, Revised 1st edition, McGraw-Hill, Inc., New York, 1988; Chapter 10.

Chapter 2

Model of Confinement

2.1 Overview

In many electronic structure calculations of atoms and molecules, the system of interest is assumed to be isolated from the surrounding; that is, the system is said to be present in the free space. This approximation, incorporated with the currently available quantum chemical methods, usually works very well in reproducing the experimentally measured structural and energetic quantities, especially in the gas-phase reactions and spectroscopy. However, the same performance is not achieved in the cases where the systems is either in the solution or in solid phase. Very often the interaction of the system with the neighboring particles, either atoms or molecules, is not negligible and will cause substantial changes in the geometric and electronic properties. For instance, the B3LYP/6-31G* investigation of formamide, $HCONH_2$, revealed significant differences in the vibrational modes of this molecule in gas-phase and water [1]. The presence of surrounding molecules may even lead to the change on the reaction profile, as demonstrated by Frisch and co-workers in their studies of the keto-enol tautomerization of 2-pyridone in cyclohexane and acetonitrile [2].

The examples mentioned above illustrate two major types of influence experienced by a trapped atom or molecule. The first one is called the boxing effect, proposed by Jaskólski et al. [3], which deals with the spatial constraints on the confined system exerted by the environment which result in the modified physical and chemical properties of the system. Some interesting work of this type include

simulations of the properties of hydrogen molecule adsorbed on a surface [4], adsorption and dynamics of acetonitrile molecules in mordenite zeolite [5], aromatic benzene, naphthalene and anthracene on a mica sheet [6], and the production of hydroxyl radicals from confined water [7]. Another type of confinement effect concerns the interaction of the system with the electric field produced by the environment. Modeling of the solvent environment using the self-consistent reaction field (SCRF) method is a representative case, in which the solvation effect on the system (solute) is approximated simply as the Coulomb interaction with the reaction field created by the solvent molecules.

In fact, the studies of confinement effects on quantum systems have long been a subject in quantum mechanics since the pioneering study of the confinement by a magnetic field by Fock [8]. The particle-in-a-box (PIB) and the harmonic oscillator models are among the most well-known examples. Progress in this area was initially slow, and most of the research centered on some solvable or quasi-solvable systems such as an electron and hydrogen atom [9, 10, 11, 12, 13]. However, a change of this situation took place in 1970's because of three important breakthroughs in condensed-matter physics and astronomy. On one hand, the development of new techniques in semi-conductor manufacture allowed one to synthesize exotic objects such as quantum wells, quantum wires and quantum dots, in which electrons are spatially confined in different dimensions [14, 15, 16], which, to some extent, revolutionized the understanding of quantum systems. In parallel to the production of nano-scale objects, the discovery of quantum Hall effects [17] also stimulated the establishment of new theories which are capable of explaining the extraordinary behavior of the systems in such small scales. Finally, the location of neutron stars and white dwarfs [18, 19] opened up a completely new area of research regarding the atomic and molecular physics in super-strong electric and magnetic fields. Since the Lorentz force becomes comparable to the Coulomb force in such circumstances, the Zeeman interaction can no longer be treated as a perturbation, and a new set of computational methods has to be constructed in order to study these heavily magnetized systems. The rationalization of the behavior of quantum systems under

such extreme conditions is essential to the analysis and identification of various interstellar media and the composition of the atmospheres of planets. For the reviews of what has been accomplished, one can consult the reports by Jaskólski [20] and Karwowski [21].

In the present chapter, the formalism of confinement will be introduced by describing several confinement models that are widely used, and their correspondence with different areas of physics and chemistry. The details regarding the model of harmonic oscillator, which is employed in the present research project, will be emphasized. The derivations of the one-electron confinement operator and the associated energy integrals will also be presented, together with some technical information concerning the program implementations and the actual computations.

2.2 Common Models of Confinement

In the non-relativistic quantum mechanics, the Hamiltonian for a confined N-electron system in the Born-Oppenheimer approximation can be written as a sum of several interaction terms:

$$\mathcal{H}(\mathbf{r}) = \mathcal{T}(\mathbf{r}) + \mathcal{V}(\mathbf{r}) + \mathcal{G}(\mathbf{r}) + \mathcal{W}(\mathbf{r}) \tag{2.1}$$

where $\mathbf{r} \equiv \{\mathbf{r}_1, \mathbf{r}_2, \cdots, \mathbf{r}_N\}$. The first two terms, $\mathcal{T}$ and $\mathcal{V}$, describe the kinetic energy and nuclear attraction of the electrons respectively. The third term $\mathcal{G}$ is the two-electron interactions where the electron correlation effect comes into play. The last term $\mathcal{W}(\mathbf{r})$ is a generic confinement potential that is applied to the system. Generally speaking, this potential is assumed to be a one-electron operator, that is, it is completely separable from the electron-electron Coulomb interaction. Therefore, no modification of the electron correlation methods is necessary when they are used in the calculations involving confinement effects.

The choice of the functional form of $\mathcal{W}$ is arbitrary. Depending on the nature of the physical systems for which the model of confinement is employed, there are several different model potentials $\mathcal{W}$ that have been proposed. Usually, the resulting Schrödinger equation is not analytically solvable, except for certain special systems with specific forms of the confinement potentials for which the closed-form energy

expressions and wavefunctions can be obtained. In the following, only the systems where analytical solutions exist will be described. They include particle-in-a-box, cotangent and power potentials.

2.2.1 Particle-In-a-Box

This is perhaps the most popular model system that is introduced in elementary quantum mechanics and physical chemistry. This model is conceptually straightforward, and the solution can be worked out very easily. Meanwhile, this is the model that best illustrates the idea of quantum confinement.

In the PIB model, the confinement potential is defined as

$$\mathcal{W}(r) = \begin{cases} 0, & |r| < R, \\ \infty, & |r| \geq R \end{cases} . \tag{2.2}$$

In other word, the particles are bound within the rectangular, infinite and impenetrable potential with the width $2R$. The solutions for such systems can be derived from the solutions for particles in free space, plus the additional boundary condition that the wavefunction should vanish at both $r = -R$ and $r = R$. The well-known time-independent solutions of PIB can be expressed as a linear combination of sine functions:

$$f(x) = \sqrt{\frac{2}{a}} \sum_{n=1}^{\infty} c_n \sin\left(\frac{n\pi}{a}x\right). \tag{2.3}$$

In this solution, a is the width of the box, and n is the parameter that specifies the energy level. The exact form of the energy associated with the wavefunction $f(x)$ is:

$$E_n = \frac{n^2\pi^2\hbar^2}{2ma^2}. \tag{2.4}$$

Though more for academic purposes, this simple example has been found very useful in the first-approximation calculations of the electronic spectra of conjugated molecules such as organic dyes in which π-electrons are assumed to be trapped within the conjugated orbitals [22].

Assuming the separability of the motion of particles in different orientation, this model can be easily extended to two and three-dimensions, giving rise to the so-called particle-in-a-plane and particle-in-a-cube models. The PIB model is not

restricted to rectangular potentials. Calculations have recently been conducted by Jung and Alvarellos [23] in which they found the exact solution and investigated the strong correlations for the two interacting electrons confined in a spherical three-dimensional PIB model.

The situation becomes more complicated in the presence of a nucleus, in which the Coulomb attraction $\mathcal{V}$ is added to the PIB Hamiltonian. This equation has been solved, respectively, by Satpathy [24] and Kovalenko et al. [25] using prolate spheroidal coordinate transformation. Numerous interesting features have been found in this system that are completely different from those in the PIB. For example, degeneracy is noticed at both asymptotes $r \to 0$ and $r \to R$, and more energy levels exist at $r = R$ which correspond to higher symmetry orbitals of the free hydrogen atom. This Coulomb potential has been widely used in the studies of the effects of impurities inside the semiconductors and zeolite cages.

2.2.2 Cotangent-type Potentials

The PIB model is an ideal case, in which the particle is assumed to move freely inside the impenetrable potential well. However, it becomes unrealistic when the model is applied to the cases such as doping in semiconductors, or guest atoms in zeolites. In these cases, the potential inside the well is finite while the boundary conditions at the asymptotes are still fulfilled. Therefore, a cotangent potential has been proposed by Zicovich et al. [26] which takes the following form:

$$\mathcal{W}(r) = -\frac{Z\pi}{R} \cot \frac{r\pi}{R}, \tag{2.5}$$

where Z is the nuclear charge. The equation having this confinement potential possesses analytical solutions for the s states but not for $l \neq 0$ [27]. Despite the absence of compact solutions, the energies for different values of n can be written as:

$$E_n = \frac{x_l^2}{2R^2} - \frac{Z^2}{2n^2}. \tag{2.6}$$

where $x_l = n = 0, 1, 2, \ldots$ for $l = 0$, and it equals to some non-integer number for $l \neq 0$. A rather surprising observation in this model is that for the same parameter

n,

$$E_{n,l+1}(R) = E_{n,l}(R) \tag{2.7}$$

which is a result of the spatial confinement effects that overwhelm the Coulomb interaction with the nucleus.

2.2.3 Power Potentials

Apart from the model potentials mentioned in the previous sections, the power-series potential is another popular model used in describing a variety of confinement effects because of its flexibility. Such potentials are mainly adopted in the modeling of interactions in elementary particle physics. For example, the Cornell-type potential [28]

$$\mathcal{W}(r) = \frac{1}{2}\omega^{3/2} r \tag{2.8}$$

can be used to model the Stark effect and spectra of multiquark systems. Usually, the power potential is used in a combination with the Coulomb potential, giving rise to the combined potentials such as:

$$\mathcal{W}(r) = -\frac{4}{3}\frac{\alpha_s(r)\hbar c}{r} + k \cdot r \tag{2.9}$$

or

$$\mathcal{W}(r) = \frac{\kappa}{r} + \frac{r}{a^2} \tag{2.10}$$

which may be used to describe the strong interaction of quarks in hadrons in the charmomium model [29]. Another popular type of combined potential is the one constructed by Coulomb and Yukawa potentials [30]:

$$\mathcal{W}(r) = g \cdot \frac{\exp\left(-\frac{mc}{\hbar}r\right)}{r} \tag{2.11}$$

which describes the exchange of mesons of mass m in the internuclear forces.

2.3 Hooke-law Potential

Recall that the general form of the power potentials can be written as [31]

$$\mathcal{W}(r) = \frac{1}{2}\sum_{t=x,y,z} \omega_t^{n_t+1}\left(t - b_t\right)^{2n_t} \tag{2.12}$$

where $r \equiv \{x, y, z\}$, t denotes the coordinate axes, ω_t is the scaling coefficient, and b_t is the position corresponding to the center of the power potential. n_t is the power which defines the curvature of the potential. Often $b_t = 0$ for all t for simplicity. When $n_t = 1$, the power potential is reduced to an anisotropic harmonic oscillator potential:

$$\mathcal{W}(r) = \frac{1}{2}\left(\omega_x^2 x^2 + \omega_y^2 y^2 + \omega_z^2 z^2\right). \tag{2.13}$$

The potential can be further simplified by assuming that $\omega_x = \omega_y = \omega_z = \omega$, leading to the symmetrical, isotropic, one-parameter harmonic oscillator potential:

$$\mathcal{W}(r) = \frac{1}{2}\omega^2 r^2 \tag{2.14}$$

where $r^2 = x^2 + y^2 + z^2$.

2.3.1 Harmonic Oscillator

The Harmonic oscillator (HO), like the particle-in-a-box, is one of the simplest models that are introduced in the elementary quantum mechanics. Despite its simplicity, this model is of great value in, among others, solid-state physics, nanotechnology, molecular spectroscopy, and electrodynamics.

The Hamiltonian for a free particle moving in a one-dimensional symmetric parabolic potential characterized by a parameter ω is given by

$$\mathcal{H}(x) = \frac{p^2}{2m} + \frac{1}{2}m\omega^2 x^2, \tag{2.15}$$

and the corresponding time-independent Schrödinger equation is

$$\left[-\frac{\hbar^2}{2m}\frac{d^2}{dx^2} + \frac{1}{2}m\omega^2 x^2\right]\psi(x) = E\psi(x). \tag{2.16}$$

This second-order differential equation can be easily solved using either standard techniques or algebraic method [32]. With the constraint that the solutions be finite and square-integrable, the solutions have the following form [33]:

$$\psi_n(x) = \frac{1}{\sqrt{2^n n!\sqrt{\pi}x_0}} \exp\left\{-\frac{1}{2}\left(\frac{x}{x_0}\right)^2\right\} H_n\left(\frac{x}{x_0}\right), \tag{2.17}$$

in which $x_0 = \sqrt{\frac{\hbar}{\omega m}}$ and H_n is the Hermite polynomial:

$$H_n(x) = (-1)^n e^{x^2} \frac{d^n}{dx^n} e^{-x^2}. \tag{2.18}$$

The energy spectrum corresponding to the wavefunction $\psi_n(x)$ is surprisingly simple:

$$E_n = \hbar\omega \left(n + \frac{1}{2}\right). \tag{2.19}$$

2.3.2 Applications of The Harmonic Oscillator Potentials

In the case of one-particle systems, the HO potential describes very well the far-infrared spectral properties [34] and other electronic and optical properties of laterally confined, small quantum dots without scattering states [35, 36]. For the systems of more than one electron, the model becomes so complicated that not all systems are solvable. System of interest is the two-electron system, called harmonium, for which the analytical solution can be obtained. This model offers the possibility that comparisons can be made with approximate methods in order to verify their correctness.

The exact solution for harmonium has been obtained by Singh, Biswas and Datta [37], Znoil [38] and Taut [39], and recently reviewed by Karwowski [21]. The external harmonic potential of the following form was assumed:

$$\mathcal{W}(\mathbf{r}_1, \mathbf{r}_2) = \frac{1}{2}\omega^2 \left(m_1 \mathbf{r}_1^2 + m_2 \mathbf{r}_2^2\right) = \frac{1}{2}\omega^2 \left(M\mathbf{R}^2 + \mu \mathbf{r}^2\right), \tag{2.20}$$

where $M = m_1 + m_2$ and μ is the reduced mass of the two-electron system. If the Hamiltonian is rearranged in terms of the center-of-mass coordinate $\mathbf{R}$ and the relative coordinate $\mathbf{r}$, then the resulting radial equation describing the relative motion will be

$$\left[-\frac{1}{2\mu}\frac{d^2}{dr^2} + \frac{l(l+1)}{2\mu r^2} + \frac{\mu\omega^2 r^2}{2} + V(r)\right] \phi_{nl}(r) = E^r_{nl}\phi_{nl}(r). \tag{2.21}$$

Assuming the Coulomb-type interaction between the two electrons in the harmonium system, i.e., $V(r) = \frac{1}{r}$, the above-mentioned radial equation is solvable, yielding the corresponding energy [40]

$$E^r_{nl}(\omega) = \left(n + \frac{1}{2}\right)\omega \tag{2.22}$$

for $n = 2, 3, \ldots$.

The radial equation of harmonium is also exactly or quasi-analytically solvable for a number of different interaction potentials $V(r)$. This is possible, for instance, for a positronium ($V(r) = -1/r$), confined helium-like atoms ($V(r) = -Z/r_1 - Z/r_2 + e^2/r_{12}$) [31], and atoms in plasma ($V(r) = e^{-dr}/r$) [41].

2.3.3 Cylindrical Harmonic Oscillator Potentials

In the present project, an isotropic HO potential (eq. (2.14)) for a multi-electron system is used; the potential is written as a sum of one-electron contribution:

$$\mathcal{W}(\mathbf{r}) = \sum_i W(r_i) = \frac{\omega^2}{2} \sum_i r_i^2. \tag{2.23}$$

Again, for simplicity, the center of the potential is assumed to overlap the origin of the Cartesian coordinate system, so that all coefficients b_t in eq. (2.12) vanish. This type of HO potential has been extensively used in the recent studies of quantum dots and confined atoms by Diercksen and co-workers [42, 43, 44]. In those studies, the electronic properties of several simple systems such as harmonium, hydrogen atom, and helium atom confined by spherical and elliptical HO potentials were computed and compared. In the present work, however, the HO potential of cylindrical symmetry is employed; in other words, the three-dimensional HO potential is reduced to a two-dimensional, laterally confining parabolic potential. The final form of the cylindrical HO potential is thus given by

$$\mathcal{W}(\mathbf{r}) = \frac{\omega^2}{2} \sum_i \left(x_i^2 + y_i^2\right). \tag{2.24}$$

The orientation of the principal axis of the confining potential is chosen so that it always overlaps the molecular axis of the diatomic systems trapped inside the potential.

The rationale on which the HO potential of such symmetry is preferred is that the problem of non-homogeneous and uneven potential along the molecular bond can be avoided. In the cases where a spherical or elliptical HO potential centered at the origin of the coordinate system is used, the Coulomb interaction experienced

by the electrons at the two ends of the diatomic molecule is stronger than those in the midpoint between the two nuclei. Since the confining potential is assumed acting on solely electrons, the applications of the potentials without the tubular symmetry will cause a spurious accumulation of electron density in the bonding area, giving rise to the artificial shortening of the chemical bond. In contrast, the isotropic cylindrical potential eliminates this obstacle by ensuring that the HO potential is axially equivalent in all directions with respect to the principal axis, and is independent of its position along the molecular bond. It should be mentioned that Sako, Cernusak and Diercksen [45] argued that the Coulomb potential strong enough to penetrate the shielding electrons and be experienced by the nucleus will be outside the energy range of interest in physics and chemistry. This argument is apparently well justified for many-electron systems such as heavy-metal compounds, but not equally true for small molecules like hydrogen molecule which has only two electrons. Therefore, more detailed investigations are definitely necessary for the final judgment of the uses of the confining potentials of arbitrary shapes in the electronic structure calculations of confined polyatomic molecules.

2.3.4 Confinement Basis Sets

As shown in eq. (2.17), the general solutions of HO model is a composite of Hermite polynomial and a Gaussian function, both expressed in terms of the displacement x. The resulting HO wavefunctions for a several values of n are given in Table 2.1:

Table 2.1: Wavefunctions of one-dimensional Harmonic Oscillator (A_n are the normalization constants).

n	ψ_n
0	$A_0 \exp\left\{-\frac{1}{2}(x/x_0)^2\right\}$
1	$A_1(2x) \exp\left\{-\frac{1}{2}(x/x_0)^2\right\}$
2	$A_2(4x^2-2) \exp\left\{-\frac{1}{2}(x/x_0)^2\right\}$
3	$A_3(8x^3-12x) \exp\left\{-\frac{1}{2}(x/x_0)^2\right\}$
4	$A_4(16x^4-48x^2+12) \exp\left\{-\frac{1}{2}(x/x_0)^2\right\}$

One can easily notice that the wavefunctions for one-dimensional HO are indeed the linear combinations of Gaussian basis functions. Consequently, using Gaussian basis functions in the calculations of confined atomic and molecular systems is justified as they are able to properly describe the distortion in electron density due to the presence of the external HO potential.

There are three criteria in choosing the good basis set for the calculations of confinement effects. As the applied HO potential is repulsive in nature, electron density in the atomic core region is expected to be larger; thus Gaussian basis functions with large exponents are required for the core electrons. Meanwhile, basis functions with small exponents are also needed so as to describe the diffuse electron density for the excited states of the confined systems which have a high probability of undergoing pressurized auto-ionization. Finally, a new set of basis functions, called confinement functions, should be included whose exponents are determined by the strength ω of the confining potential. This set of new functions serves to more appropriately account for the contracted electron density within the bonding region, the task the normal atomic basis functions may fail to perform well. Diercksen and co-workers have demonstrated that the choices of the types and numbers of confinement basis functions are crucial in the convergence of the energy spectrum to the electronic states of appropriate order [42].

2.4 Confinement Integral Evaluation

According to the definitions of eqs. (2.1) and (2.14), the confining potential is treated as a one-electron operator, and it is assumed transparent to the nuclei. Therefore, the inclusion of the confinement effects into all-electron *ab initio* calculations is straightforward; only the one-electron term $\hat{h}(\mathbf{r})$ in eq. (1.19) needs to be modified while the Coulomb and exchange terms retain their standard form. The formalism of confinement effects can be incorporated with all kinds of electron correlation methods which deal mainly with the two-electron terms, as well as relativistically transformed two-component Hamiltonians. It is worth-noting that the combined treatment of relativistic and confinement effects is by no means equivalent to the

formal treatment for relativistic HO model as the exact solutions for the latter show a stronger dependence on the momentum due to the Lorentz contraction [46].

2.4.1 Transformation of Confinement Operator

The Schrödinger equation for an N-electron confined system is:

$$[\mathcal{H}(\mathbf{r}) + \mathcal{V}(\mathbf{r})]\,\Psi(1,2,\ldots,N) = E\Psi(1,2,\ldots,N) \tag{2.25}$$

where $\mathbf{r} = \{\vec{r}_1, \vec{r}_2, \ldots, \vec{r}_N\}$. As defined in eq. (2.23), the confinement operator $\mathcal{V}(\mathbf{r})$ can be written as a sum of one-electron terms:

$$\mathcal{V}(\mathbf{r}) = \sum_{i=1}^{N} V(\vec{r}_i) = \sum_{i=1}^{N} V_i, \tag{2.26}$$

in which the one-electron operator is given explicitly by

$$V(\vec{r}_i) = \frac{1}{2}\left[\omega_x^{v_x+1}(x_i - C_x)^{2v_x} + \omega_y^{v_y+1}(y_i - C_y)^{2v_y} + \omega_z^{v_z+1}(z_i - C_z)^{2v_z}\right]. \tag{2.27}$$

In this expression, (C_x, C_y, C_z) is the center of the confining potential, and (x_i, y_i, z_i) is the position of the i-th electron. Eq. (2.27) is indeed equivalent to the power potential in eq. (2.12). For an isotropic three-dimensional harmonic oscillator centered at the origin of the coordinate system, eq. (2.27) can be simplified to the following:

$$V(\vec{r}_i) = \frac{1}{2}\omega^2 \vec{r}_i^{\,2} \tag{2.28}$$

since $\omega_x = \omega_y = \omega_z = \omega$, $v_x = v_y = v_z = 1$ and $C_x = C_y = C_z = 0$. In general, the $V(\vec{r}_i)$ operator can be factorized into three Cartesian components:

$$V(\vec{r}_i) = V_x(i) + V_y(i) + V_z(i), \tag{2.29}$$

with each component (for example, the x component) given by

$$V_x(i) = \frac{1}{2}\omega_x^{v_x+1}(x_i - C_x)^{2v_x} \tag{2.30}$$

as shown in eq. (2.27). One may introduce a new parameter D_x, which is defined as:

$$\frac{1}{D_x} = \left(\frac{1}{2}\omega_x^{v_x+1}\right)^{1/2v_x}. \tag{2.31}$$

Substituting D_x into eq. (2.30) yields a more compact expression of $V_x(i)$:

$$V_x(i) = \frac{1}{2}\omega_x^{v_x+1}(x_i - C_x)^{2v_x} = \left(\frac{x_i - C_x}{D_x}\right)^{2v_x}, \tag{2.32}$$

and this operator is invariant under the translation with arbitrary displacement ζ_x:

$$V_x(i) = \left(\frac{x_i - C_x}{D_x}\right)^{2v_x} = \left[\frac{(x_i - \zeta_x) - (C_x - \zeta_x)}{D_x}\right]^{2v_x}. \tag{2.33}$$

Using the binomial expansion

$$(a-b)^n = \sum_{j=1}^{n}(-1)^j \begin{pmatrix} n \\ j \end{pmatrix} a^{n-j}b^j = \sum_{j=1}^{n}(-1)^{n-j} \begin{pmatrix} n \\ j \end{pmatrix} a^j b^{n-j} \tag{2.34}$$

where

$$\begin{pmatrix} n \\ j \end{pmatrix} = \frac{n!}{j!(n-j)!}, \tag{2.35}$$

the confinement operator $V_x(i)$ can be expressed in form of a series:

$$V_x(i) = \left(\frac{1}{D_x}\right)^{2v_x} \sum_{k=0}^{2v_x} (x_i - \zeta_x)^{2v_x-k} (C_x - \zeta_x)^k (-1)^k \begin{pmatrix} 2v_x \\ k \end{pmatrix}. \tag{2.36}$$

Consequently, the Cartesian components of the one-electron confinement operator can be defined in binomial form in terms of the five parameters: x, C_x, ξ_x, D_x and v_x

$$\begin{aligned} V_x^c &\equiv V_x^c(x, C_x, \xi_x, D_x, v_x) \\ &\equiv \left(\frac{1}{D_x}\right)^{2v_x} \sum_{k=0}^{2v_x} (x_i - \zeta_x)^k (C_x - \zeta_x)^{2v_x-k} (-1)^{2v_x-k} \begin{pmatrix} 2v_x \\ k \end{pmatrix}. \end{aligned} \tag{2.37}$$

This transformation allows the confinement operator to be written in the polynomial form which facilitates the subsequent evaluations of the molecular integrals over Gaussian basis functions.

2.4.2 Confinement Integrals

Let assume that two atoms are located at positions $A = (A_x, A_y, A_z)$ and $B = (B_x, B_y, B_z)$ which are defined, respectively, by the position vectors **A** and **B**, as illustrated by figure 2.1. The center of the confining potential is assumed at the

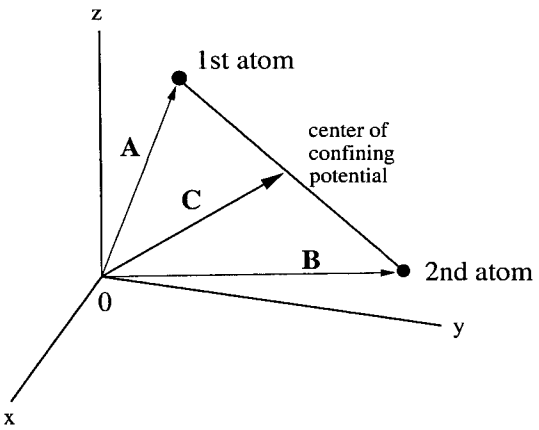

Figure 2.1: Molecular Coordinate System

position $C = (C_x, C_y, C_z)$ with the corresponding position vector **C**. The confinement integral over the general, uncontracted Cartesian Gaussian basis functions (eq. (1.115)) that are centered at the atomic positions is:

$$\begin{aligned} V_{AB} &= \iiint (x-A_x)^{n_x^A}(y-A_y)^{n_y^A}(z-A_z)^{n_z^A} e^{-\xi_A(x-A_x)^2} e^{-\xi_A(y-A_y)^2} e^{-\xi_A(z-A_z)^2} \\ &\times (x-B_x)^{n_x^B}(y-B_y)^{n_y^B}(z-B_z)^{n_z^B} e^{-\xi_B(x-B_x)^2} e^{-\xi_B(y-B_y)^2} e^{-\xi_B(z-B_z)^2} \\ &\times \left[V_x^c + V_y^c + V_z^c\right] dxdydz, \end{aligned} \tag{2.38}$$

which, using $g_i^A(i, A_i, \xi_i)$ to denote the i-component Gaussian basis function of atom A, can be simplified and rearranged as follows:

$$\begin{aligned} V_{AB} &= \iiint g_x^A(x, A_x, \xi_A) g_y^A(y, A_y, \xi_A) g_z^A(z, A_z, \xi_A) \left[V_x^c + V_y^c + V_z^c\right] \\ &\times g_x^B(x, B_x, \xi_B) g_y^B(y, B_y, \xi_B) g_z^B(z, B_z, \xi_B) dxdydz \end{aligned} \tag{2.39}$$

$$\begin{aligned} &= \iiint g_x^A g_y^A g_z^A V_x^c g_x^B g_y^B g_z^B dxdydz + \iiint g_x^A g_y^A g_z^A V_y^c g_x^B g_y^B g_z^B dxdydz \\ &+ \iiint g_x^A g_y^A g_z^A V_z^c g_x^B g_y^B g_z^B dxdydz \end{aligned} \tag{2.40}$$

$$\begin{aligned} &= \int g_x^A V_x^c g_x^B dx \int g_y^A g_y^B dy \int g_z^A g_z^B dz + \int g_x^A g_x^B dx \int g_y^A V_y^c g_y^B dy \int g_z^A g_z^B dz \\ &+ \int g_x^A g_x^B dx \int g_y^A g_y^B dy \int g_z^A V_z^c g_z^B dz \end{aligned} \tag{2.41}$$

Therefore, one can see that there are two types of integrals that have to be evaluated in order to determine the confinement integral: the overlap integral of

two Gaussian basis functions, and the confinement potential integral which involves the confinement operator.

The explicit form of the overlap integral is:

$$\int_{-\infty}^{\infty} g_x^A g_x^B dx = \int_{-\infty}^{\infty} (x - A_x)^{n_x^A} (x - B_x)^{n_x^B} e^{-\xi_A (x-A_x)^2} e^{-\xi_B (x-B_x)^2} dx. \quad (2.42)$$

Utilizing the Gaussian product theorem [47], the overlap integral can be rewritten as:

$$\int_{-\infty}^{\infty} g_x^A g_x^B dx = \int_{-\infty}^{\infty} (x - A_x)^{n_x^A} (x - B_x)^{n_x^B} e^{-\frac{\xi_A \xi_B}{\xi_A + \xi_B}(A_x - B_x)^2} e^{-(\xi_A + \xi_B)(x - P_x)^2} dx \quad (2.43)$$

where

$$P_x = \frac{\xi_A A_x + \xi_B B_x}{\xi_A + \xi_B}. \quad (2.44)$$

Therefore, the overlap integral becomes

$$\int_{-\infty}^{\infty} g_x^A g_x^B dx = e^{-\frac{\xi_A \xi_B}{\xi_A + \xi_B}(A_x - B_x)^2} \int_{-\infty}^{\infty} (x - A_x)^{n_x^A} (x - B_x)^{n_x^B} e^{-(\xi_A + \xi_B)(x - P_x)^2} dx. \quad (2.45)$$

In order to simplify the exponential term in the integral, the following transformations are performed:

$$t \equiv x - P_x \ , \ \bar{A} \equiv P_x - A_x \ , \ \bar{B} \equiv P_x - B_x \ , \ \bar{Z} \equiv \xi_A + \xi_B, \quad (2.46)$$

which lead to the new form of the overlap integral

$$\int_{-\infty}^{\infty} g_x^A g_x^B dx = e^{-\frac{\xi_A \xi_B}{\xi_A + \xi_B}(A_x - B_x)^2} \int_{-\infty}^{\infty} (t + \bar{A})^{n_x^A} (t + \bar{B})^{n_x^B} e^{-\bar{Z} t^2} dt. \quad (2.47)$$

Again, the binomial expansion is carried out for $(t + \bar{A})^{n_x^A}$ and $(t + \bar{B})^{n_x^B}$:

$$(t + \bar{A})^{n_x^A} = \sum_{i=1}^{n_x^A} \binom{n_x^A}{i} t^i \bar{A}^{n_x^A - i} \quad (2.48)$$

$$(t + \bar{B})^{n_x^B} = \sum_{j=1}^{n_x^B} \binom{n_x^B}{j} t^j \bar{B}^{n_x^B - j}. \quad (2.49)$$

Substituting these expressions back into the overlap integral yields

$$\int_{-\infty}^{\infty} g_x^A g_x^B dx = e^{-\frac{\xi_A \xi_B}{\xi_A + \xi_B}(A_x - B_x)^2} \sum_{i=1}^{n_x^A} \sum_{j=1}^{n_x^B} \binom{n_x^A}{i} \binom{n_x^B}{j} \bar{A}^{n_x^A - i} \bar{B}^{n_x^B - j} \int_{-\infty}^{\infty} t^{i+j} e^{-\bar{Z} t^2} dt. \quad (2.50)$$

The last integral is a standard integral whose solution is given by

$$\int_{-\infty}^{\infty} t^{i+j} e^{-\bar{Z}t^2} dt = \begin{cases} 2\left(\frac{1\cdot 3\cdot 5\cdots(i+j-1)}{2^{(i+j)/2+1}\bar{Z}^{(i+j)/2}}\sqrt{\frac{\pi}{2}}\right) & , i+j = \text{even} \\ 0 & , i+j = \text{odd} \end{cases} . \tag{2.51}$$

The evaluation of the confinement potential integrals is slightly more complicated. The integrals can be written explicitly as:

$$\int_{-\infty}^{\infty} g_x^A V_x^c g_x^B dx = \int_{-\infty}^{\infty} (x-A_x)^{n_x^A} V_x^c(x, C_x, \zeta_x, D_x, v_x)(x-B_x)^{n_x^B} e^{-\xi_A(x-A_x)^2} e^{-\xi_B(x-B_x)^2} dx. \tag{2.52}$$

Using the transformed confinement operator in eq. (2.37), one can get, assuming $\zeta_x = A_x$,

$$\begin{aligned} \int_{-\infty}^{\infty} g_x^A V_x^c g_x^B dx &= \int_{-\infty}^{\infty} \left[\left(\frac{1}{D_x}\right)^{2v_x} \sum_{k=0}^{2v_x} (x_i - \zeta_x)^k (C_x - \zeta_x)^{2v_x-k} (-1)^{2v_x-k} \begin{pmatrix} 2v_x \\ k \end{pmatrix} \right] \\ &\times (x-A_x)^{n_x^A} (x-B_x)^{n_x^B} e^{-\xi_A(x-A_x)^2} e^{-\xi_B(x-B_x)^2} dx \qquad (2.53) \\ &= \int_{-\infty}^{\infty} \left[\left(\frac{1}{D_x}\right)^{2v_x} \sum_{k=0}^{2v_x} (x_i - A_x)^k (C_x - A_x)^{2v_x-k} (-1)^{2v_x-k} \begin{pmatrix} 2v_x \\ k \end{pmatrix} \right] \\ &\times (x-A_x)^{n_x^A} (x-B_x)^{n_x^B} e^{-\xi_A(x-A_x)^2} e^{-\xi_B(x-B_x)^2} dx \qquad (2.54) \\ &= \left(\frac{1}{D_x}\right)^{2v_x} \sum_{k=0}^{2v_x} (C_x - A_x)^{2v_x-k} (-1)^{2v_x-k} \begin{pmatrix} 2v_x \\ k \end{pmatrix} \\ &\times \int_{-\infty}^{\infty} (x-A_x)^{n_x^A+k} (x-B_x)^{n_x^B} e^{-\xi_A(x-A_x)^2} e^{-\xi_B(x-B_x)^2} dx. \qquad (2.55) \end{aligned}$$

Notice that the integral appearing in eq. (2.55) is in fact the overlap integral in eq. (2.42). Therefore, one can adopt the expression derived for the overlap integral and easily deduce the final expression of the confinement potential integral:

$$\begin{aligned} \int_{-\infty}^{\infty} g_x^A V_x^c g_x^B dx &= \left(\frac{1}{D_x}\right)^{2v_x} \sum_{k=0}^{2v_x} (C_x - A_x)^{2v_x-k} (-1)^{2v_x-k} \begin{pmatrix} 2v_x \\ k \end{pmatrix} \\ &\times e^{-\frac{\xi_A\xi_b}{\xi_A+\xi_B}(A_x-B_x)^2} \sum_{i=0}^{n_x^A+k} \sum_{j=0}^{n_x^B} \begin{pmatrix} n_x^A+k \\ i \end{pmatrix} \begin{pmatrix} n_x^B \\ j \end{pmatrix} \bar{A}^{n_x^A+k-i} \bar{B}^{n_x^B-j} \\ &\times \begin{cases} 0 & \text{if i + j = odd} \\ \frac{1\cdot 3\cdot 5\cdots(i+j-1)}{(2\bar{Z})^{(i+j)/2}} \left(\frac{\pi}{2}\right)^{1/2} & \text{if i + j = even} \end{cases} . \qquad (2.56) \end{aligned}$$

The complete integral V_{AB} can thus be calculated by computing the integrals in eqs. (2.50), (2.51) and (2.56) and substituting them into the expression in eq. (2.41).

2.4.3 Implementation

Since the calculations of confinement effects require the evaluation of only one-electron molecular integrals, the implementation of this feature to *ab initio* quantum chemistry packages is straightforward, and only relatively small modification is needed. The code has been developed and added to the program GAMESS-US [48]. An independent coding of the confinement integrals was incorporated into the OPENMOL program [49] by his research group. Both programs were utilized in the present project.

In general, the procedure of performing a calculation including the confinement effects consists of the following steps:

1. Define the coordinates of the molecular system and the parameters of the confining potential (such as the geometry, strength, and the origin).

2. Calculate the required molecular integrals: overlap integrals $\mathcal{S}_{pq}$, one-electron integrals $\mathcal{H}_{pq}$ and two-electron integrals $\langle\phi_p\phi_q|\phi_r\phi_s\rangle$.

3. Calculate the one-electron confinement integrals $\mathcal{V}_{pq}$.

4. Construct the density matrix $\mathcal{P}$.

5. Calculate the two-electron contributions $\mathcal{G}$ from the density matrix and two-electron integrals: $G_{pq} = \sum_r \sum_s P_{pq} \left[\langle\phi_p\phi_q|\phi_r\phi_s\rangle - \langle\phi_p\phi_q|\phi_s\phi_r\rangle\right]$

6. Form the Fock matrix: $\mathcal{F}_{pq} = \mathcal{H}_{pq} + \mathcal{V}_{pq} + \mathcal{G}_{pq}$.

7. Perform the Unitary transformation and diagonalize the Fock matrix to find the orbital coefficient matrix $\mathcal{C}$.

8. Form a new density matrix and check for the convergence.

9. Use the optimized SCF wavefunctions in other post-Hartree-Fock calculations.

Bibliography

[1] V. Barone, M. Cossi, J. Tomasi, *J. Comput. Chem.* **19**, 404 (1998).

[2] M. W. Wong, K. B. Wiberg, M. J. Frisch, *J. Am. Chem. Soc.* **114**, 1645 (1992).

[3] C. Zicovich-Wilson, J. H. Planelles, W. Jaskólski, *Int. J. Quantum Chem.* **50**, 429 (1994).

[4] A. F. Kovalenko, E. N. Sovyak, M. F. Holovko, *Int. J. Quantum Chem.* **42**, 321 (1992).

[5] K. S. Smirnov, F. Thibault-Starzyk, *J. Phys. Chem. B* **103**, 8595 (1999).

[6] L. Z. Zhang, P. Cheng, *Phys. Chem. Comm.* **6**, 62 (2003).

[7] S. Foley, P. Rotureau, S. Pin, G. Baldacchino, J.-P. Renault, J.-C. Mialocq, *Angew. Chem. Int. Ed.* **44**, 110 (2005).

[8] V. Fock, *Z. Phys.* **47**, 446 (1928).

[9] C. G. Darwin, *Proc. Cam. Phil. Soc.* **27**, 86 (1930).

[10] A. Sommerfeld, H. Welker, *Ann. Phys.* **32**, 56 (1938).

[11] N. R. Kestner, O. Sinanoğlu, *Phys. Rev.* **128**, 2687 (1962).

[12] J. Jortner, N. R. Kestner, S. A. Rice, M. H. Cohen, *J. Chem. Phys.* **43**, 2614 (1965).

[13] R. J. White, W. B. Brown, *J. Chem. Phys.* **53**, 3869 (1970).

[14] L. L. Chang, L. Esaki, R. Tsu, *Appl. Phys. Lett.* **24**, 593 (1974).

[15] P. M. Petroff, A. C. Gossard, R. A. Logan, W. Wiegmann, *Appl. Phys. Lett.* **41**, 635 (1982).

[16] M. A. Reed, R. T. Bate, K. Bradshaw, W. M. Duncan, W. M. Frensley, J. W. Lee, H. D. Smith, *J. Vacuum Sci. Technol. B* **4**, 358 (1986).

[17] K. von Klitzing, G. Dorda, M. Pepper, *Phys. Rev. Lett. 45*, 494 (1980).

[18] J. R. P. Angel, E. F. Borra, J. D. Landstreet, *Astrophys. J. Suppl. Ser.* **45**, 457 (1981).

[19] J. Trümper, W. Pietsch, C. Reppin, W. Voges, R. Staubert, E. Kendziorra, *Astrophys. J.* **219**, L105 (1978).

[20] W. Jaskólski, *Phys. Rep.* **271**, 1 (1996).

[21] J. Karwowski, *J. Mol. Struct.: THEOCHEM* **727**, 1 (2005).

[22] D. A. McQuarrie, J. D. Simon, *Physical Chemistry: A Molecular Approach*, University Science Books, California, 1997: Chapter 3.

[23] J. Jung, J. E. Alvarellos, *J. Chem. Phys.* **118**, 10825 (2003).

[24] S. Sapathy, *Phys. Rev. B* **28**, 4585 (1983).

[25] A. F. Kovalenko, E. N. Sovyak, M. F. Golovko, *Phys. Stat. Sol. b* **155**, 549 (1989).

[26] C. Zicovich-Wilson, J. Planelles, W. Jaslólski, *Int. J. Quantum Chem.* **50**, 429 (1994).

[27] L. Infeld, T. E. Hull, *Rev. Mod. Phys.* **23**, 21 (1951).

[28] E. Eichten, K. Gottfried, T. Kinoshita, K. D. Lane, T. M. Yan, *Phys. Rev. D* **17**, 3090 (1978).

[29] B. Povh, K. Rith, C. Scholz, F. Zetsche, *Particles and Nuclei: An Introduction to the Physical Concepts*, 3rd edition, Springer, New York, 2002; Chapter 13.

[30] H. Yukawa, *Proc. Phys. Math. Soc. Japan* **17**, 48 (1935).

[31] D. Bielińska-Wąż, J. Karwowski, G. H. F. Diercksen, *J. Phys. B: At. Mol. Opt. Phys.* **34**, 1987 (2001).

[32] T. H. Cooke, J. L. Wood, *Am. J. Phys.* **70**, 945 (2002).

[33] F. Schwabl, *Quantum Mechanics*, 3rd edition, Springer, New York, 2002; Chapter 3.

[34] A. Kumar, S. E. Laux, F. Stern, *Phys. Rev. B* **42**, 5166 (1990).

[35] P. Hawrylak, A. Wójs, J. A. Brum, *Phys. Rev. B* **54**, 11346 (1996).

[36] P. A. Maksym, T. Chakraborty, *Phys. Rev. Lett.* **65**, 108 (1990).

[37] V. Singh, S. N. Biswas, K. Datta, *Phys. Rev. D* **18**, 1901 (1978).

[38] M. Znoil, *J. Phys. A: Math. Gen.* **15**, 2111 (1982).

[39] M. Taut, *Phys. Rev. A* **48**, 3561 (1993).

[40] J. Cioslowski, K. Pernal, *J. Chem. Phys.* **113**, 8434 (2000).

[41] P. K. M. Mukherjee, J. Karwowski, G. H. F. Diercksen, *Chem. Phys. Lett.* **363**, 323 (2002).

[42] T. Sako, G. H. F. Diercksen, *J. Phys. B: At. Mol. Opt. Phys.* **36**, 1433 (2003).

[43] T. Sako, G. H. F. Diercksen, *J. Phys. B: At. Mol. Opt. Phys.* **36**, 1681 (2003).

[44] T. Sako, G. H. F. Diercksen, *J. Phys. B: At. Mol. Opt. Phys.* **36**, 3743 (2003).

[45] T. Sako, I. Cernusak, G. H. F. Diercksen, *J. Phys. B: At. Mol. Opt. Phys.* **37**, 1091 (2004).

[46] Y. B. Dong, A. Faessler, T. Morii, *Nucl. Phys. A* **651**, 209 (1999).

[47] S. F. Boys, *Proc. Roy. Soc. London Ser. A 200*, 542 (1950).

[48] M. W. Schmidt, K. K. Baldridge, J. A. Boatz, S. T. Elbert, M. S. Gordon, J. H. Jensen, S. Koseki, N. Matsunaga, K. A. Nguyen, S. Su, T. L. Windus, M. Dupuis, J. A. Montgomery, *J. Comput. Chem.* **14**, 1347 (1993).

[49] G. H. F. Diercksen, G. Hall, *Comput. Phys.* **8**, 215 (1994).

Chapter 3

Low-lying Excited States of the Hydrogen Molecule in Cylindrical Harmonic Confinement

In the following seven chapters, the results of applications of the parabolic confinement model to several diatomic molecules are presented. The results concerning the studies of hydrogen molecule confined by a cylindrical harmonic potential are discussed in this chapter first [1].

3.1 Introduction

The study of atoms and molecules in external fields is a fascinating area of research that has attracted much attention from different areas of science and engineering. Following the influential work of Loudon in 1959, in which he performed the quantum mechanical analysis of the behavior of a one-dimensional hydrogen atom in various Coulomb potentials [1], many studies have been carried out to understand the physics of excitons (hydrogen-like electron-hole pair) and some related systems (e.g. Refs.[2, 3, 4, 5]). The discovery of neutron stars and white dwarf stars further motivated rapid development of this field since it stimulated the interest of

[1] A version of this chapter was published in *Adv. Quantum Chem.* **48**, 59 (2005).

studying the variation of electronic structure and behavior of atomic and molecular systems when they are under the magnetic field in which the Lorentz force outweighs the Coulombic interaction [6, 7]. Besides the exploration of the process of star evolution, several areas of condensed-matter physics, in particular the studies of quantum Hall effects and quantum dots, also require an in-depth theoretical framework that explains the motion of electrons and particles in strong electric and magnetic fields [8]. Electrons, when being spatially localized in either quasizero-, one-, or two-dimensions by means of an applied electric or magnetic field, exhibit unique properties that are absent without external confinement [9]. Extensive investigations, both theoretical and experimental, have been performed, and some useful results have been obtained. The advances in the technology of lithographic etching [10] allow for the facile creation of quantum dots, wires, and wells of various sizes and numbers of electrons, which greatly assist the intense experimental research of these intriguing objects. To date, quantum dots and wells have already been widely used in electronic and opto-electronic devices, such as compact discs and microwave antennas, as well as in medical science, for instance, as imaging biosensors of living cells [11].

Despite being the simplest neutral molecule, dihydrogen molecule (H_2) is of great importance to astrophysics, atomic and molecular physics, solid-state physics, plasma physics, catalysis and fuel cell studies. Hydrogen is the first element synthesized in the formation of a star, and is found to exist in the interstellar space and in a wide range of cosmic objects. It is the most abundant molecular species and constitutes approximately 92% of the matter in the Universe [12, 13]. Hence, the studies of magnetized hydrogen provide a vital information for the mapping of the life-cycle of a star and the evolution of the Universe. From the theoretical viewpoint, hydrogen molecule is the best candidate for the benchmarking calculations when testing new theories due to its structural simplicity and the availability of highly accurate experimental spectroscopic constants [14]. Since the first qualitative quantum mechanical calculation performed in 1927 [15], hydrogen molecule has been extensively studied using various methods, in which the computation carried

out by Kolos and Wolniewicz was the most remarkable [16].

In contrast to a large number of studies on H_2 in field-free environment, the investigations of H_2 in the presence of strong fields are rather limited. Most of these calculations center on the H_2^+ molecular ion (e.g. Refs [17, 18, 19, 20]). Recently, the behaviour of H_2 in strong to superstrong magnetic fields has became a topic of considerable interest, and several calculations have been performed concerning the explanation of some unusual phenomena of hydrogen molecules in superstrong fields ($B \geq 10^{11}$G)[21, 22]. Calculations performed by Lai and co-workers using Hartree-Fock method suggested the existence of long-chain polymers of hydrogen on the surface of neutron stars where the magnetic field is as strong as 10^{12} G [23]. A subsequent study by Demeur et al. also supported the stability of finite chains of hydrogen in very intense magnetic fields [24]. In addition, a number of changes in both the electronic structure and geometry of H_2 were proposed. Korolev and Liberman found that the total spin of the hydrogen molecule in an ultra-high magnetic field becomes one as a result of a triplet ground state [22]. The analysis by Ortiz and co-workers using variational quantum Monte Carlo method proved that the hydrogen molecule possesses the ground state symmetry of $^3\Pi_0$ in superstrong magnetic fields [25]. On the other hand, the studies conducted by Detmer and co-workers using configuration interaction method predicted that the $^3\Sigma_u$ state would be the ground state when the magnetic field strength is moderate ($B \approx 0.2$ a.u.) [26]. These investigations also showed that both the ground and excited states of H_2 will be more strongly bound and in certain circumstances local maxima appear at large internuclear distances which have no counterparts in the field-free situation [26, 27, 28]. Moreover, different vibrational excitation levels were obtained when the orientation of the applied magnetic field was changed, which gives rise to a continuum opacity in the photoionization of excited-state H_2 on neutron star [29]. The chaotic behavior of the energy levels of H_2 in Rydberg state may also result from the linear and quadratic Zeeman interaction induced by the application of a magnetic field [30].

The laterally confining potential of a small quantum dot can be approximated

by a smooth parabolic well in the cases where the scattering states are to be neglected due to the generalized Kohn theorem [31]. Maksym and Chakraborty [32], and Bakshi et al. [33] demonstrated, using far-infrared spectroscopy (FIR), that the resonance energy of a quantum dot is independent of the number of confined electrons, which is a unique characteristic of a parabolic potential. The Hartree-Fock modeling of a GaAs quantum dot (300 $\times$ 300 nm) with $N \leq 10$ electrons revealed that the parabolic confining potential that is approximately circularly symmetric, with the diameter of about 100 nm, leads to the observed magnetic-field-dependence of energy levels [34].

In the present work a cylindrical harmonic potential has been adopted as a model potential of a 2-dimensional quantum well. The potential energy curves (PEC) of the ground and low-lying excited states of H_2 aligned along the axis of the potential have been calculated using the method of configuration interaction with single and double substitutions (CISD) (in the case of H_2 this corresponds to full configuration interaction method) and the results of computations are reported below together with analysis of the associated wavefunctions. Comparison with the results from the studies of hydrogen molecule in a parallel magnetic field [22, 25, 26, 27] has been made. Several similarities as well as differences are observed for the excited states of hydrogen molecule when it is embedded in the two potentials and they are discussed in the following sections.

3.2 Method of Computation

The potential energy curves (PECs) of confined hydrogen molecule were calculated using the configuration interaction (CI) method implemented in the modified version of GAMESS-US program [35]. Preliminary calculations were carried out using the object-oriented OpenMol program [36]. The configuration state functions (CSFs) were generated by the Graphical Unitary Group Approach (GUGA) [37] in which all possible single and double excitations from the occupied to virtual one-electron orbitals were included. The canonical orbitals obtained by solving the Hartree-Fock-Roothaan equations were used. The total energies of the molecule in different

symmetry states were computed as the eigenvalues of the full CI matrix. The virtual space was not truncated.

In the present work, the confining potential was assumed to be in form of a cylindrical, laterally parabolic potential as described in Chapter 2. This potential was co-axial to the hydrogen molecule aligned along the z-axis of the coordinate system. In addition, the center of confining potential was chosen to coincide with the center of mass of the molecule, i.e., the confining HO potential took the form of eq. (2.24).

The basis set adopted in the calculations was optimized to yield good values of both the ground and excited state energies of hydrogen atom. Detailed analysis of the basis set will be given in the following section. In addition to the atom-centered Gaussian basis set, a set of basis functions (1s1p1d), with the exponents of $\omega/2$, was added at the mid-bond position of the hydrogen molecule in order to appropriately account for the distortion of electron density due to the external harmonic potential. This mixed basis set strategy has been tested on numerous atomic systems such as confined two-electrons quantum dots, negative hydrogen ion, helium atom and lithium atom [38, 39], and satisfactory results have been obtained. It is expected that these confinement functions should behave equally well in the molecular cases. The recent study of lithium dimer confined in an ellipsoidal harmonic potential [40] showed that the use of the confinement functions ensures the proper description of avoided crossings between the electronic states and of their correct dissociation limits.

3.3 Results and Discussion

3.3.1 Basis set

One of the bottlenecks of the modern quantum chemical calculations is the large number of integrals that have to be evaluated. Depending on the nature of the formalism, the scaling may vary from K^5 to K^{10}, where K is the number of basis functions, which makes the calculations including explicit treatment of electron correlation very expensive computationally. The full CI method, which is size-

consistent, can yield the variationally exact eigenvalues within the space spanned by the given basis set. However, it suffers from the fact that a tremendous number of determinants will be generated and this number grows factorially with respect to the number of basis functions. Therefore, the application of full CI calculations is limited to very small systems. As a two-electron system, hydrogen molecule is the best candidate for the benchmark calculation of different sophisticated post-Hartree-Fock methods because rather small number of integrals must be computed even when a comparatively large basis set is used. Another advantage of employing the hydrogen molecule in calculations is that experimental data of high precision are available that allow for verification of a method. Consequently, the hydrogen molecule has been extensively studied by various quantum chemical methods (e.g. Refs [16, 41, 42, 43, 44, 45, 46, 47]), and an enormous number of basis sets have been designed for accurate computations of structures and properties of hydrogen-containing compounds.

Recently, Tachikawa and Osamura have applied the fully variational molecular orbital method (FVMO), combined with the full CI wavefunctions, to obtain very accurate geometries and excitation energies of the ground and excited states of hydrogen molecule [48]. Their study also showed that full CI calculations using large correlation-consistent basis sets do not necessarily yield results that agree very well with the experiment. Severe problems appeared in the estimations of excitation energies T_e, which for the $^1\Pi_u$ state was about 6325 cm^{-1} ($\sim$ 6.3 %) overestimated. Due to the limitations of the correlation-consistent basis sets for the excited state studies, a new atomic basis set has been designed in the present work for the accurate calculation of the PECs of the low-lying excited states as well as the ground state of hydrogen molecule. The exponents and coefficients of the basis set were obtained by the least-square fitting to the radial distribution functions of the 1s, 2s, 2p, 3d, and 4f orbitals. The basis set, denoted by H-73, consists of 11 s-, 7 p-, 6 d- and 4 f-type basis functions contracted to [11s7p4d3f]. The s- and p-type functions are fully uncontracted to allow for the greatest flexibility in the molecular calculations. The exponents and coefficients are given in Table 3.1.

Table 3.1: H-73 Basis set of hydrogen

Symmetry	Exponent	Coefficient
s	418.55081	1.00
	62.745349	1.00
	14.279584	1.00
	4.0418170	1.00
	1.3163895	1.00
	0.47346186	1.00
	0.18279991	1.00
	0.072884362	1.00
	0.039056541	1.00
	0.019077672	1.00
	0.0097350280	1.00
p	65.554593	1.00
	4.4119074	1.00
	1.4101801	1.00
	0.31641648	1.00
	0.10161790	1.00
	0.038707113	1.00
	0.015936506	1.00
d	22.213281	0.15854785
	2.5916309	0.47406581
	0.41870791	0.71413682
	0.67153126	1.00
	0.12927862	1.00
	0.034247992	1.00
f	7.2151367	0.40231477
	0.88389643	0.79963606
	0.33897511	1.00
	0.063826911	1.00

Table 3.2: Equilibrium internuclear distances of selected electronic states of H_2 (in Å)

Basis set	X $^1\Sigma_g^+$	B $^1\Sigma_u^+$	C $^1\Pi_u$	a $^3\Sigma_g^+$	c $^3\Pi_u$
6-31++G**[a]	0.7389	1.1232	0.7846	0.9502	0.7215
6-311++G**[a]	0.7434	1.1567	0.8944	0.9726	0.8136
aug-cc-pVDZ[a]	0.7617	1.2670	0.9838	0.9884	1.0197
aug-cc-pVTZ[a]	0.7431	1.2822	0.9976	0.9870	1.0211
aug-cc-pVQZ[a]	0.7419	1.2845	1.0245	0.9874	1.0476
FV-OPT/[8s4p2d][a]	0.7417	1.2828	1.0330	0.9887	1.0375
H-36[b]	0.7419	1.2747	1.0287	0.9857	1.0321
H-73	0.7414	1.2840	1.0319	0.9887	1.0375
Numerical limit[a]	0.7408	1.2859	1.0330	0.9885	
Experiment[c]	0.7414	1.2928	1.0327	0.9887	1.0370

[a] Ref [48]. [b] Ref [50]. [c] Ref [14].

The H-73 basis set has been tested in the atomic calculation for hydrogen. The total energy of hydrogen atom in ^2S state was -0.4999951 a.u., which is superior to the results obtained by employing aug-cc-pVTZ and aug-cc-pVQZ basis sets, and comparable to the values from aug-cc-pV5Z and aug-cc-pV6Z calculations.

To test the validity of the basis set in molecular calculations, CI calculations for the ground and several low-lying excited states of the hydrogen molecule have been performed. Figure 3.1 depicts the *ab initio* PECs of H_2 and H_2^+ ion and Tables 3.2 and 3.3 show the calculated equilibrium bond distances and excitation energies of different electronic states of the hydrogen molecule.

It may be seen that the bond distances calculated using H-73 basis set agree better with experiment than those obtained using aug-cc-pVQZ or aug-cc-pVTZ basis set, and are close to the highly accurate values computed using FVMO method.

It is noticeable that correlation-consistent basis sets are not able to accurately reproduce the bond distances and energies of the excited states in Π symmetry, which may be attributed to the relatively inadequate p-space. The problem was eliminated in the case of H-73 basis set. The polarization set that was purposefully optimized to correlate with the 2p orbitals of hydrogen atoms greatly improved the bond lengths and excitation energies, and reduced the errors to be within 100 cm^{-1}

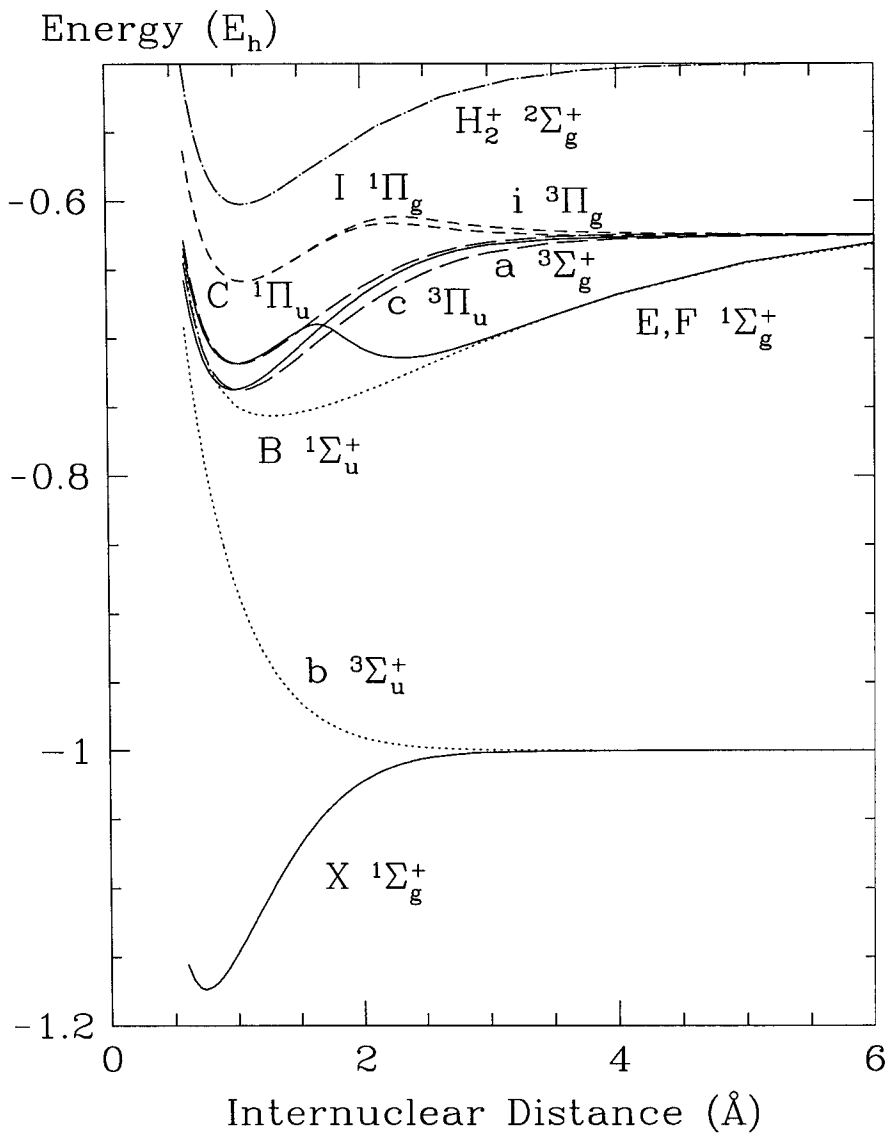

Figure 3.1: Potential energy curves of the ground and low-lying excited states of H_2 and of the ground state of H_2^+. Solid lines: Σ_g^+ states; dotted lines: Σ_u^+ states; short-dashed lines: Π_g states; long-dashed lines: Π_u state; dotted-short-dashed line: H_2^+ ground state. For the Π_g manifold, the $^3\Pi_g$ state lies slightly above the $^1\Pi_g$ state. The opposite is observed for the Π_u manifold.

Table 3.3: Excitation energies of selected electronic states of H_2 (in cm^{-1})

Basis set	B $^1\Sigma_u^+$	C $^1\Pi_u$	a $^3\Sigma_g^+$	c $^3\Pi_u$
aug-cc-pVQZ[a]	91660.9	106414.5	95935.4	99095.4
FV-OPT/[8s4p2d][a]	91670.1	100067.1	95884.3	95828.4
H-36[b]	91372.4	99964.9	95437.5	95603.5
H-73	91612.4	99990.6	95844.3	95763.8
Numerical limit[a]	91694.2	100104.3	95981.4	
Experiment[c]	91700.0	100089.8	95936.1	95838.5

[a] Ref [48]. [b] Ref [50]. [c] Ref [51].

of exact values.

3.3.2 General features of the potential energy curves

Due to the superior performance of the H-73 basis set in the CI calculations of structures and energies for the excited states of hydrogen molecule, it was used in the subsequent studies of H_2 enclosed in a cylindrical harmonic potential. The PECs of the ground and eight low-lying excited states of H_2 encapsulated in a cylindrical potential have been calculated. Several confining potential strengths ω have been utilized: 0.00, 0.05, 0.10, 0.15 and 0.20 a.u. The mapping of PECs was done in the range from 0.6 Å to 8.0 Å so as to capture the dissociation limits.

Figs. 3.2(a) to 3.2(d) display the PECs of several electronic states of H_2 and of the ground state of the H_2^+ ion in the presence of a confining potential. Several features may be observed when compared to the situation where no potential is applied. Firstly, the energy corresponding to a dissociation limit, $E_{lim} = E(r \rightarrow \infty)$, shifts up for all the states when the strength of the potential increases. For instance, in the dissociation channel for the X $^1\Sigma_g^+$ and b $^3\Sigma_u^+$ (channel I), E_{lim} = -1.0000 a.u. for ω = 0.00 a.u.

This value increases to -0.9808 a.u. for ω = 0.10 a.u., and -0.9292 a.u. for ω = 0.20 a.u. In other words, all the dissociation channels are destabilized by the harmonic repulsive potential that acts on electrons. The electron density of H_2 is compressed by the potential and the increased Coulomb interaction destabilizes the molecule. Secondly, the dissociation channel that leads to H(1s) + H(2s or 2p) in

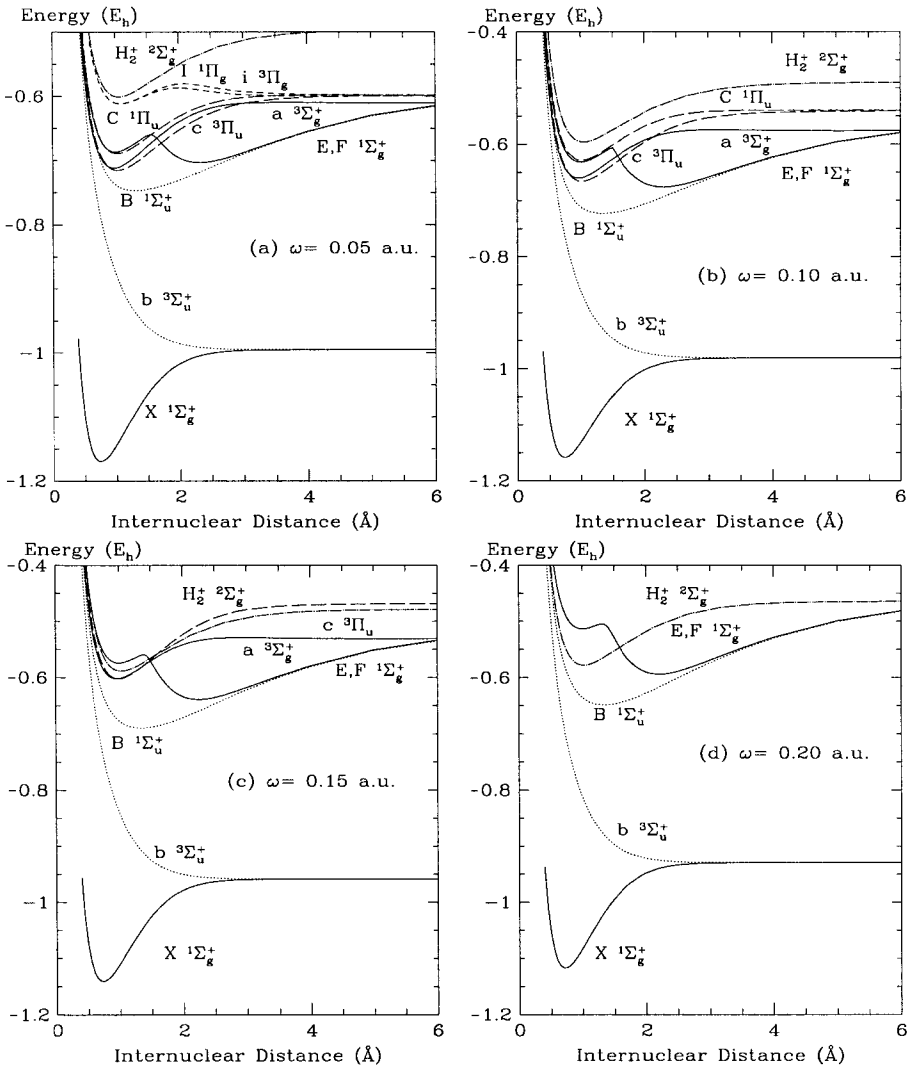

Figure 3.2: Potential energy curves of H_2 and H_2^+ in confinement. Solid lines: Σ_g^+ states; dotted lines: Σ_u^+ states; short-dashed lines: Π_g states; long-dashed lines: Π_u state; dotted-short-dashed line: H_2^+ ground state. For the Π_g manifold, the $^3\Pi_g$ state lies slightly above the $^1\Pi_g$ state. The opposite is observed for the Π_u manifold.

Table 3.4: Atomic calculations of hydrogen atom in confinement[a]

Configuration	$\omega = 0.00$	$\omega = 0.05$	$\omega = 0.10$	$\omega = 0.15$	$\omega = 0.20$
1s	-0.499995	-0.497521	-0.490376	-0.479179	-0.464588
2s	-0.124999	-0.097968	-0.047714	0.006649	0.062849
$2p_x/2p_y$	-0.124991	-0.100749	-0.050135	0.011405	0.081274
$2p_z$	-0.124991	-0.112215	-0.084665	-0.050641	-0.012044

[a] All values in a.u.

a field-free environment (channel II) splits into two when the potential is turned on. The states of Σ symmetry correlate to the channel, which is lower in energy, that corresponds to H(1s) + H($2p_z$), while those of Π symmetry correlate to the higher channel that leads to the limit of H(1s) + H($2p_x/2p_y$). The energy separation between these two channels becomes larger when a stronger potential is used. The peculiar nature of the channel II within the harmonic potential can be rationalized via the atomic calculations of hydrogen atom for various confining potential strengths. Figure 3.3 shows the energies corresponding to different configurations of the hydrogen atom (see also Table 3.4).

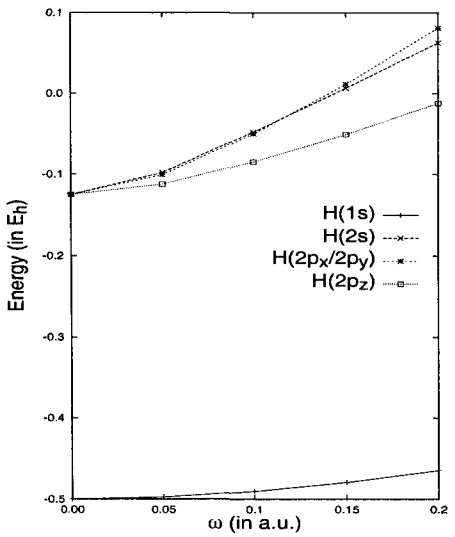

Figure 3.3: Atomic energies of hydrogen atom in confinement

The data show that H($2p_z$) configuration becomes more stable relative to the

$H(2p_x)$ and $H(2p_y)$ counterparts in the harmonic potential. It can be attributed to the fact that the potential is laterally circular about the z-axis which enhances the electrostatic interaction along the x-and y-directions. As a consequence, the p-shell degeneracy is removed, and the channel II splits, with the one corresponding to H(1s) and $H(2p_z)$ becoming lower in energy.

Finally, it should be noticed that the energy of the one-electron system H_2^+ increases less rapidly than the system of the states of the two-electron H_2. In consequence, for the larger values of ω, the energy of the ionized system H_2^+ will be lower than the energy of some of the excited electronic states of H_2. In cylindrical confinement, in contrast to spherical [49] or ellipsoidal [38] confinements, there is a possibility of escape of an electron when the repulsive influence of confinement exceeds the attractive interaction with the nuclei. In the following sections, in order to compare qualitative behaviour of our results with those previously published, we sometimes discuss the results obtained for very large values of ω. However, in the tables and the figures we show only those data that relate to the excited states whose energies are below the ground-state energy of H_2^+ in the confinement of a given strength ω.

X $^1\Sigma_g^+$ and b $^3\Sigma_u^+$ states

Both the X $^1\Sigma_g^+$ and b $^3\Sigma_u^+$ states of the H_2 molecule correlate to the limit of H(1s) + H(1s) (channel I). The ground state X $^1\Sigma_g^+$ arises from the configuration $|1\sigma_g^2\rangle$ while the b $^3\Sigma_u^+$ state results from the configuration $|1\sigma_g 1\sigma_u\rangle$. The configurations of these states remain the same for the applied potential with various strengths. It has been suggested that the hydrogen molecule, under the influence of a parallel ultrastrong magnetic field, undergoes a transition of the ground state symmetry from $^1\Sigma_g$ to $^3\Pi_0$ (see e.g., Refs. [22, 23, 24, 25, 26]). In the intermediate regime, Detmer et al. [26] and Kravchenko and Liberman [52] showed, using numerical Hartree-Fock approach, that the $^3\Sigma_u$ state would appear as the ground state, although the existence of this weakly bound Bose-particle superfluid phase is still controversial. Nevertheless, such transitions do not happen in the present case even up to the

field strength of 0.20 a.u. The ground state retains the symmetry $^1\Sigma_g^+$ and the PECs of these two states still lead to the same dissociation limit of channel I. The difference between these two situations can be accounted for by considering the different nature of the external fields. The potential adopted in the present study is purely electrostatic and repulsive to the electrons. The first-order Stark effect will not split the species in channel I because it corresponds to a non-degenerate ground-state hydrogen atoms whose orbital angular momentum is zero. In the case of magnetic field, however, the spin-orbit interaction and the coupling between the canonical momentum and the vector field have to be taken into account. As a result, the influence of the magnetic field on the electronic structures of different states of H_2 becomes orientation-dependent, and the Zeeman effects (linear and quadratic) split the dissociation channel I according to the different spin states of $^1\Sigma_g$ and $^3\Sigma_u$.

Despite the difference in the asymptotic limits, some features characteristic for molecules in magnetic fields can also be seen in the present work. Table 3.5 shows that the binding energy of the ground state H_2 increases with the strength of the potential and the equilibrium internuclear distance r_e decreases. Meanwhile, the monotonically increasing ν_e suggests that the potential well becomes much steeper.

Similar observations have been made when H_2 was placed in a parallel magnetic field [26]. The shorter bond distance and stronger binding interaction in the ground state H_2 are the consequences of the increased electron density between the two nuclei that is induced by the potential.

The lowest triplet state, b $^3\Sigma_u^+$, possesses interesting characteristics that are worth noting. According to the early work of Kolos and Wolniewicz [53], the b $^3\Sigma_u^+$ state is predominantly repulsive except for a shallow van der Waals minimum around $R \approx 7.8$ a.u. (4.1 Å) with the estimated binding energy of about 4 cm^{-1}. Other computations [54, 55, 56], that included electron correlation, confirmed the existence of a van der Waals minimum. In the present work a minimum was also found and its parameters are shown in Table 3.6. The analysis of the PEC in the region of $3.0 \leq R \leq 5.0$ Å including the correction for the basis set superposition error (BSSE), which is significant for such a weak binding, yielded $r_e = 4.1608$ Å

Table 3.5: Spectroscopic parameters of X $^1\Sigma_g^+$ and b $^3\Sigma_u^+$ states[a,b]

State	Parameter	$\omega = 0.00$	$\omega = 0.05$	$\omega = 0.10$	$\omega = 0.15$	$\omega = 0.20$
X $^1\Sigma_g^+$	r_e	0.7414 (0.7414)[c]	0.7368	0.7273	0.7202	0.7156
	ν_e	4404.6 (4401.2)[c]	4428.4	4503.3	4635.5	4737.8
	B_e	60.857 (60.853)[c]	61.620	63.242	64.491	65.318
	$\nu_e x_e$	147.262 (121.336)[c]	145.819	150.791	233.272	123.788
	α_e	3.2393 (3.0622)[c]	3.2497	3.2325	4.1626	3.1167
	D_e	38111.9 (38292.8)[d]	38328.4	39103.2	40072.8	41328.1
b $^3\Sigma_u^+$	r_e	4.1608 (4.13)[e]	4.1379	4.0842	4.0305	3.9846
	ν_e	34.65	35.17	36.02	35.53	35.31
	B_e	1.932	1.954	2.005	2.059	2.107
	$\nu_e x_e$	102.005	106.100	110.776	116.817	122.854
	α_e	3.8806	3.8700	3.8589	4.3257	4.4514
	D_e	4.148 (4.20)[e]	4.280	4.236	3.995	3.622

[a] Experimental values in parentheses. [b] r_e in Å, all other values in cm^{-1}. [c] Ref [51]. [d] Ref [16]. [e] Ref [55].

Table 3.6: Spectroscopic parameters of van der Waals minima of selected states[a,b]

State	Parameter	$\omega = 0.00$	$\omega = 0.05$	$\omega = 0.10$	$\omega = 0.15$	$\omega = 0.20$
b $^3\Sigma_u^+$	r_e	4.1608 (4.13)[c]	4.1379	4.0842	4.0305	3.9846
	ν_e	34.65	35.17	36.02	35.53	35.31
	B_e	1.932	1.954	2.005	2.059	2.107
	$\nu_e x_e$	102.005	106.100	110.776	116.817	122.854
	α_e	3.8806	3.8700	3.8589	4.3257	4.4514
	D_e	4.148 (4.20)[c]	4.280	4.236	3.995	3.622
a $^3\Sigma_g^+$	r_e		5.5335	5.0862	4.7692	
	ν_e		83.21	104.68	129.09	
	B_e		1.092	1.293	1.471	
	D_e		94.1	156.6	194.2	
I $^1\Pi_g$	r_e	4.3089 (4.2)[d]	4.0112			
	ν_e	123.1	154.2			
	B_e	1.802	2.079			
	D_e	173.3 (177)[d]	214.7			

[a] Experimental values in parentheses. [b] r_e in Å, all other values in cm^{-1}. [c] Ref [55]. [d] Ref [88].

and $D_e = 4.15$ cm^{-1}, as illustrated by Figure 3.4. The results are in good agreement with the available theoretical values. Similarly to the situation of the ground state, the application of an external potential causes the contraction of the internuclear distance. However, the change of dissociation energy is drastically different. Initially, the potential well depth increases when a potential of $\omega = 0.05$ a.u. is imposed. However, the potential becomes shallower when the potential strength exceeds 0.10 a.u. and the binding energy decreases monotonically. Same situation has also been seen for the hydrogen molecule in a magnetic field [26], in which the van der Waals minimum eventually vanished when the magnetic field strength became greater than 100 a.u. (corresponding to about 10^{11} G).

B $^1\Sigma_u^+$ and a $^3\Sigma_g^+$ states

Being the lowest stable excited state, the electronic structure of the B $^1\Sigma_u^+$ state of H_2 has been of considerable interest. The calculation of Kolos and Wolniewicz using the variational method with elliptic coordinates [57] showed that the wavefunction

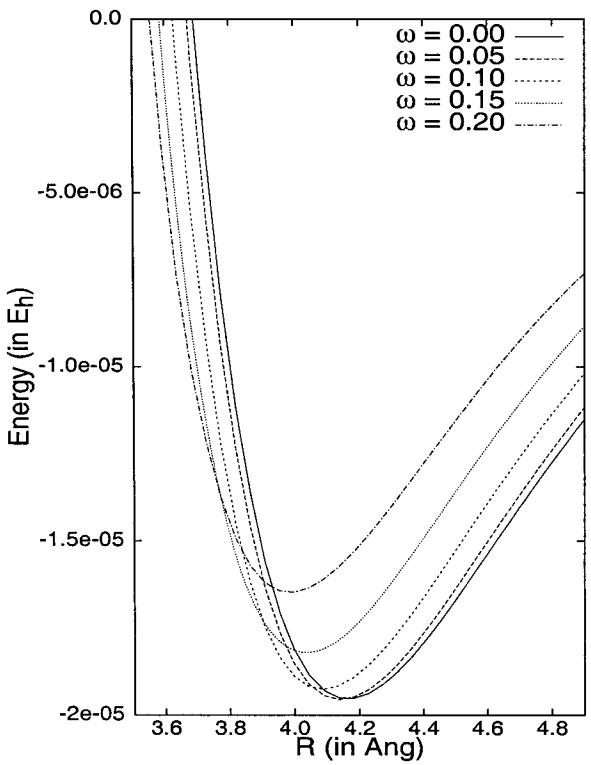

Figure 3.4: b $^3\Sigma_u^+$ state in confinement

is well represented by a mixture of three configurations: ionic, $|1s2s\rangle$ and $|1s2p_\sigma\rangle$. The analysis of the wavefunction indicated that for the region of $3 \leq R \leq 7$ a.u. the nature of the B $^1\Sigma_u^+$ state is essentially ionic. For the small internuclear distances, however, the most important contribution comes from the Heitler-London type $|1s2p_\sigma\rangle$ function. Yet for the large values of R both the $|1s2s\rangle$ and $|1s2p_\sigma\rangle$ functions become important, leading to the asymptotic limit of H(1s) + H(2p) in the field-free space. Because of the strong ionic character, the B state potential energy curve exhibits a very broad minimum. The dihydrogen molecule in the B $^1\Sigma_u^+$ state is paramagnetic [58] and can form stable compounds with noble gases [59].

The spectroscopic constants obtained by polynomial fitting to the calculated *ab initio* PECs for the B $^1\Sigma_u^+$ state are given in Table 3.7. The values are in a very good agreement with the experiment except for the binding energy being underestimated by about 1%. The relatively large discrepancy of r_e results from the flat minimum of the potential which increases the uncertainty in the evaluation of r_e. Change of configurations with R was noticed in the wavefunction analysis. The contribution from the ionic wavefunction drops from about 80 % at $R \approx 4.00$ a.u. to about 20 % at $R \approx 12$ a.u.; meanwhile, the contribution of $|1s2p_\sigma\rangle$ wavefunction grows from 5 % to 62 %.

Under the influence of the external harmonic potential, two changes occur: an elongation of the internuclear distance and the accompanying reduction of the vibrational constant. These variations could be attributed to the increasing contribution of $|1s2s\rangle$ wavefunction with the strength of the potential, which diminishes the ionic interaction and stretches the internuclear separation. Similar to the case where no potential is applied, when $R \to \infty$, the configuration of $|1s2p_\sigma\rangle$ dominates and leads to H(1s) + H($2p_z$) as this is the function that gives non-vanishing dispersion at the dissociation limit. For $\omega \geq 0.15$ a.u. unusual changes occur in the B state, in which the equilibrium internuclear distance starts to decrease and the vibrational constant increases. These unexpected differences have also been predicted for the hydrogen molecule placed in a parallel magnetic field of strength larger than 0.20 a.u. [26],

Table 3.7: Spectroscopic parameters of B $^1\Sigma_u^+$ and a $^3\Sigma_g^+$ states[a,b]

State	Parameter	$\omega = 0.00$	$\omega = 0.05$	$\omega = 0.10$	$\omega = 0.15$	$\omega = 0.20$
B $^1\Sigma_u^+$	r_e	1.2840 (1.2928)[c]	1.3163	1.3383	1.3469	1.3413
	ν_e	1365.8 (1358.1)[c]	1472.3	1360.4	1423.6	1507.0
	B_e	20.290 (20.015)[c]	19.305	18.675	18.438	18.593
	$\nu_e x_e$	24.330 (20.888)[c]		10.548	8.403	6.739
	α_e	1.3219 (1.1845)[c]	0.9516	0.5665	0.3622	0.2584
	D_e	28812.3 (28852.7)[d]	29956.7	32331.8	34904.0	37630.0
	T_e	91612.4 (91700)[c]	92908.8	95710.5	99113.8	102927.2
a $^3\Sigma_g^+$	r_e	0.9887 (0.9887)[c]	0.9736	0.9625	0.9634	
	ν_e	2664.8 (2664.8)[c]	2747.9	2778.7	2719.4	
	B_e	34.219 (34.216)[c]	35.286	36.109	36.036	
	$\nu_e x_e$	82.061 (71.65)[c]	80.943	96.870	99.888	
	α_e	1.7192 (1.671)[c]	1.8673	2.0239	2.2410	
	D_e	24581.4 (24615.3)[e]	22246.5	18584.4	15727.3	
	T_e	95844.3 (95936.1)[c]	100635.8	109471.3	118310.0	

[a] Experimental values in parentheses. [b] r_e in Å, all other values in cm^{-1}. [c] Ref [51]. [d] Ref [91]. [e] Ref [92].

although the effect is more pronounced in the latter case. The shortening of r_e could be a consequence of the induced interaction due to the polarized electron density, within the internuclear vicinity, caused by the harmonic potential.

In contrast to channel I, which remains non-degenerate in the field, channel II splits into three dissociation branches due to the Stark effect. Atomic calculations of the H atom in a cylindrical potential oriented along the z-axis show that the energy levels of 2p-orbitals split and H($2p_z$) becomes more stable relative to H($2p_x$) and H($2p_y$). Because of the lateral symmetry of the potential, the degeneracy of H($2p_x$) and H($2p_y$) persists. For small values of ω, H(2s) is slightly less stable than H($2p_x$) and H($2p_y$) while the ordering reverses when ω exceeds 0.15 a.u. As a result, there exist three dissociation limits for channel II, with a non-zero cylindrical potential, which correspond to H(2s), H($2p_z$), and H($2p_x$)/H($2p_y$).

Besides the B $^1\Sigma_u^+$ state, the a $^3\Sigma_g^+$ state also possesses the asymptotic limit of H(1s) + H($2p_z$) in the presence of a harmonic electrostatic potential. The PEC of the a $^3\Sigma_g^+$ state has already been extensively studied (see e.g. Refs. [60, 61, 62, 63, 64]), and both highly accurate adiabatic and non-adiabatic *ab initio* PECs have been calculated. The PEC and the corresponding spectroscopic constants determined in the present study are in very good agreement with the experiment except for the excitation energy where the calculated value is about 90 cm^{-1} smaller than the experimental one. Zung and Duncan, using orthonormal molecular orbitals with variable orbital parameters, showed that the contribution of $|1s2p_z\rangle$ to the total energy near the potential minimum is negligible [61]. On the other hand, Mulliken has demonstrated that for $R \geq r_e$ the MO configuration becomes a mixture of $|1s2s\rangle$ and $|1s2p_z\rangle$ and when $R \to \infty$ the function $|1s2p_z\rangle$ predominates and correlates to the dissociation of H(1s) + H(2p) [65]. A detailed analysis of the relative contributions of various configurations in the a $^3\Sigma_g^+$ state wavefunction confirms their conclusions. It is found that the main component of the state at the region around the minimum is a mixture of $|1s2s\rangle$ and $|1s3s\rangle$ which then changes to $|1s2s\rangle$ and $|1s2p_z\rangle$ when R increases. For very large R, the predominant configuration is $|1s2p_z\rangle$ which leads to the appropriate dissociation limit of H(1s) + H(2p).

In the presence of the confining harmonic potential, several interesting changes of the a $^3\Sigma_g^+$ state occur. In contrast to the other states, where the binding energy increases with the stronger potential strength, the dissociation energy for the a $^3\Sigma_g^+$ state exhibits a decreasing trend. The D_e value reduces from 24578 cm^{-1} for $\omega = 0.00$ a.u. to 15727 cm^{-1} for $\omega = 0.15$ a.u. For $\omega = 0.20$ a.u., the energy of the a $^3\Sigma_g^+$ state is greater than the energy of the ground state of H_2^+. Detmer et al. have observed similar behavior of the a $^3\Sigma_g^+$ state of H_2 in a parallel magnetic field with the strength below 0.5 a.u. [26] and they have found that upon further increasing the field, the well starts becoming deeper and more pronounced. In order to verify the existence of the same phenomenon in the present case, the dissociation energy has been evaluated for the potential strength of 1.0, 2.0 and 5.0 a.u., respectively. The calculations show that the binding energy further reduces to about 9060 cm^{-1} when $\omega \approx 1.0$ a.u. However, a turnover appears for $\omega \geq 1.0$ a.u. in which the dissociation energy drastically increases to about 30000 cm^{-1} for $\omega = 2.0$ a.u. and 68000 cm^{-1} for $\omega = 5.0$ a.u. The development of a $^3\Sigma_g^+$ state under an extremely strong potential can be rationalized by considering the variation of configurations with the confinement strength. For the field-free and weak-field regime (i.e., $\omega \leq 1.0$ a.u.) the contribution from the function $|1s2s\rangle$ increases progressively from 60 % ($\omega = 0.00$ a.u.) to 98 % ($\omega = 1.0$ a.u.) while that from the function $|1s2p_z\rangle$ diminishes very rapidly. The domination of the configuration of $|1s2s\rangle$ weakens the exchange interaction between the two parallel-spin electrons in 1s and 2s orbital respectively [66], which counteracts the enhanced binding due to the applied potential. For the strong-field regime, however, the contribution from the function $|1s2p_z\rangle$ suddenly increases and dominates the state wavefunction. The better orbital overlap between 1s and $2p_z$ orbitals under the influence of an applied potential increases the exchange energy [67] which in turn strengthens the binding interaction. On the other hand, the main configuration for the a $^3\Sigma_g^+$ state at large R is $|1s2p_z\rangle$ and its contribution grows very rapidly when the potential strength increases. For $\omega \geq 0.20$ a.u. the configuration becomes exclusively $|1s2p_z\rangle$. As mentioned, the larger involvement of the $2p_z$ orbital can increase the binding interaction via the enhanced exchange energy contribution.

Consequently, the dissociation limit of H(1s) + H($2p_z$) is stabilized relative to the potential minimum, and the binding energy is reduced.

Besides the abrupt change of binding energy, Detmer and coworkers have observed the development of a second minimum at large R which has no counterpart in the field-free space [26]. This additional minimum becomes more pronounced when the magnetic field increases to 1.0 a.u. The further increase in the field starts to diminish the potential well. The minimum eventually vanishes when the field is greater than 50.0 a.u. The calculated PEC of the a $^3\Sigma_g^+$ state in the present study also exhibits a shallow minimum. As shown in Table 3.6, for a confining potential of $\omega = 0.05$ a.u., the second minimum appears at about 5.5 Å with the binding energy of 94.1 cm^{-1} which accommodates one vibrational level. The position of this minimum moves towards a smaller value of R, accompanying the increase of the binding energy and number of vibrational levels when the potential strength increases. Using the above-mentioned argument, the existence of the second minimum and the increase of its binding energy with the increasing ω can be accounted for by the strong exchange interaction of 1s and $2p_z$ orbitals which constitute the major contribution to the a $^3\Sigma_g^+$ state at large R.

C $^1\Pi_u$, c $^3\Pi_u$, I $^1\Pi_g$ and i $^3\Pi_g$ states

Experimental studies of the Π-manifold excited states of H_2 began with the extensive investigations of the emission spectra of molecular hydrogen from the near infrared to extremely ultraviolet regions (e.g. Refs. [68, 69, 70, 71]). After the observation by Lichten, using molecular beam resonance spectroscopy technique, that the c $^3\Pi_u$ state is metastable [72, 73], a lot of work has been devoted to accurate theoretical calculations of the Π_u PECs of H_2 which helped to assist the assignments and confirmation of emission bands. Meanwhile, the studies of the Π_g counterparts emerged rapidly because of the problem of 3d ΣΠΔ complex of states that leads to the breakdown of Born-Oppenheimer approximation in the computation of the excited states involving 3d orbitals [74]. The wrong prediction of singlet-triplet splitting for Π_g states also stimulated the calculations of reliable PECs that cover

a very wide range of R [75]. Up to now highly accurate PECs for these states have already been obtained (e.g. Refs. [75, 76, 77, 78]) and precise spectroscopic constants have been determined which are in excellent agreement with the experiment (e.g. Refs. [79, 80, 81]). All of these states correlate to the dissociation limit of H(1s) + H(2p) as $R \rightarrow \infty$. Despite the same asymptotic behavior, they exhibit very different characteristics for the small to medium-R region that are of interest to discuss.

The C $^1\Pi_u$ state has attracted much attention from spectroscopists because the state was believed to be the upper state of the ultraviolet absorption band which can help establish the accurate dissociation energy of the ground state of H_2 [82]. Therefore, several attempts have been made to obtain the complete PEC for the C state [53, 76, 83, 84]. The calculations by Browne revealed that there exists a suspicious maximum at $R \approx 8$ a.u. which is about 160 cm^{-1} above the dissociation limit [76]. This observation was consistent with the conclusion of Herzberg and Monfils that a maximum might exist in the vicinity of $R \approx 13$ a.u. [82]. The subsequent calculations by Kolos and Wolniewicz [53], and Namioka [77] refined the barrier to be about 105.5 cm^{-1} at $R \approx 9$ a.u. The computed PEC for the C $^1\Pi_u$ state and the fitted spectroscopic parameters (r_e, ν_e, $\nu_e x_e$, α_e) in the present study agree well with the experiment, as demonstrated by Table 3.8.

The hump is located at $R \approx 9.03$ a.u. being 106.3 cm^{-1} higher than the dissociation limit, which differs by only 1 cm^{-1} from the value determined by Kolos and Wolniewicz. The estimated excitation energy for the C state is far superior than the value obtained by CI calculation using aug-cc-pVQZ basis set [48], which overestimated T_e by 6300 cm^{-1}.

The PEC of the c $^3\Pi_u$ state has been studied, although less thoroughly than the C state, in order to get insight into the metastable behavior of the $v = 0$ vibrational level that decays to the B $^1\Sigma_u^+$ with the lifetime in the range of milliseconds [73]. Browne [76] and Hoyland [78] have computed the PEC for the c $^3\Pi_u$ state and showed that it resembles very much that for the singlet counterpart except that there is no local maximum at large R. The same observations have been made in the present study where, due to the different electron-nuclear interaction [85], the

Table 3.8: Spectroscopic parameters of C $^1\Pi_u$ and c $^3\Pi_u$ states[a,b]

State	Parameter	$\omega = 0.00$	$\omega = 0.05$	$\omega = 0.10$	$\omega = 0.15$
C $^1\Pi_u$	r_e	1.0319 (1.0327)[c]	1.0202	1.0033	
	ν_e	2445.3 (2443.8)[c]	2497.0	2584.2	
	B_e	31.346 (31.363)[c]	31.964	32.977	
	$\nu_e x_e$	79.039 (69.524)[c]	79.113	96.862	
	α_e	1.6616 (1.6647)[c]	1.7640	1.7889	
	D_e	20435.1 (20488.6)[d]	19932.2	19383.7	
	T_e	99990.6 (100089.8)[c]	105600.8	116397.0	
c $^3\Pi_u$	r_e	1.0358 (1.037)[c]	1.0274	1.0105	0.9896
	ν_e	2466.7 (2466.9)[c]	2522.4	2633.1	2765.8
	B_e	31.077 (31.07)[c]	31.545	31.583	33.968
	$\nu_e x_e$	71.365 (63.51)[c]	77.493	75.341	54.905
	α_e	1.525 (1.425)[c]	1.477	1.515	1.480
	D_e	24666.6 (24816.8)[c]	25604.0	27437.3	29437.1
	T_e	95763.8 (95838.5)[c]	99836.9	108257.5	118264.0

[a] Experimental values in parentheses. [b] r_e in Å, all other values in cm^{-1}. [c] Ref [51]. [d] Ref [91].

triplet state is lower in energy than the singlet state by about 4232 cm^{-1} at r_e, which is comparable to the experimental value of 4251.3 cm^{-1} [51]. The spectroscopic constants determined using the calculated PEC have excellent agreement with the experimental values. Similarly to the C $^1\Pi_u$ state, the calculated T_e for the c state is closer to the experiment than that obtained by using aug-cc-pVQZ basis set [48].

The natural orbital analysis indicated that the major configuration for both Π_u states is $|1s_{\sigma_g}2p_{\pi_u}\rangle$ near the minimum [86]. While this configuration remains dominant for the c $^3\Pi_u$ state throughout the whole range of R, the C $^1\Pi_u$ state undergoes a configuration mixing at large R where the repulsive $|1s_{\sigma_u}2p_{\pi_g}\rangle$ dominates, resulting in the small potential maximum [87]. Wavefunction analysis in the present work corroborates these observations. A drastic change of the relative contributions of $|1s_{\sigma_g}2p_{\pi_u}\rangle$ and $|1s_{\sigma_u}2p_{\pi_g}\rangle$ states along the potential curve is observed. The former one is paramount ($\sim$ 50 %) while the latter one is absent in the region close to the minimum. For the region of large R, however, a sharp increase of the contribution from $|1s_{\sigma_u}2p_{\pi_g}\rangle$ is noticed, especially at $7.00 \leq R \leq 12.00$ a.u. where its weight

Table 3.9: Spectroscopic parameters of I $^1\Pi_g$ and i $^3\Pi_g$ states[a,b]

State	Parameter	$\omega = 0.00$	$\omega = 0.05$
I $^1\Pi_g$	r_e	1.0658 (1.0693)[c]	1.0839
	ν_e	2252.8 (2259.2)[c]	2114.8
	B_e	29.445 (29.259)[c]	28.473
	$\nu_e x_e$	91.675 (78.41)[c]	111.864
	α_e	1.919 (1.584)[c]	2.208
	D_e	7324.4 (7576.8)[d]	2853.3
	T_e	113096.5 (113142)[c]	122523.8
i $^3\Pi_g$	r_e	1.0653 (1.0700)[c]	1.0805
	ν_e	2260.8 (2253.6)[c]	2154.9
	B_e	29.475 (29.221)[c]	28.653
	$\nu_e x_e$	89.075 (67.05)[c]	100.194
	α_e	1.880 (1.506)[c]	2.021
	D_e	7373.5 (7493.4)[e]	2957.6
	T_e	113083.8 (113132)[c]	122502.4

[a] Experimental values in parentheses. [b] r_e in Å, all other values in cm^{-1}. [c] Ref [51]. [d] Ref [89]. [e] Ref [93].

raises from 5 % to 20 %. Simultaneously, the contribution from the attractive term $|1s_{\sigma_g}2p_{\pi_u}\rangle$ drops rapidly to 25 %. Interestingly, the higher excitation terms, such as $|1s3p_{\sigma}\rangle$, have a significant interaction with these states ($\sim$ 46 % at $R = 20.00$ Å). Therefore, a basis set that is optimized not only for 2p space but also for 3p space is necessary for the proper description of the Π states at large internuclear distances.

Accurate PECs of I $^1\Pi_g$ and i $^3\Pi_g$ states have been computed using highly flexible wavefunctions in elliptical coordinates containing explicit r_{12} terms [88]. The presently calculated potential curves for these states, as illustrated by Figure 3.1 and Table 3.9, are in good agreement with those results except for $\nu_e x_e$ which are all overestimated by 10 %. The estimated singlet-triplet splitting for the Π_g states at r_e is about 12.7 cm^{-1}, with the triplet state being lower in energy, which is consistent with the value of 10.8 cm^{-1} determined by Kolos and Rychlewski. A crossing between the states is found at $R \approx 1.25$ Å where the triplet state becomes higher in energy than the singlet state. For both states a maximum appears at $2.25 \leq R \leq 2.30$ Å which are 1870 cm^{-1}, for the singlet state, and 2942 cm^{-1}, for

the triplet state, above the asymptote. These values match the values estimated by Kolos and Rychlewski [88], Dressler and Wolniewicz [80] and Wolniewicz [89]. The existence of maxima for the two Π_g states is attributed to the avoided crossing between the $|1\sigma_g 1\pi_g\rangle$ and $|1\sigma_u 1\pi_u\rangle$ states where the latter one is repulsive [87]. To verify this argument the wavefunctions for the Π_g states have been analyzed. For the singlet state, the contribution of $|1\sigma_g 1\pi_g\rangle$ function declines quickly from 73 % at r_e to 18 % at 6.00 Å, while the that for the $|1\sigma_u 1\pi_u\rangle$ function increases from 0 to 25 %. A similar variation of configurations is observed as well for the triplet state although the change is slightly more significant, which is anticipated due to the fact that the valence repulsion in the triplet state is enhanced by the repulsive resonance interaction, giving rise to the broader and higher hump at large R [88]. Therefore, this strong configuration interaction at large internuclear distances is indicative of the crossing between $|1\sigma_g 1\pi_g\rangle$ and $|1\sigma_u 1\pi_u\rangle$ for the Π_g states that leads to the local maxima.

The attractive resonance interaction for the $^1\Pi_g$ state overcomes the valence repulsion at large R and causes the formation of a second minimum, which is not found in the triplet state [88]. The resonance interaction in the triplet state is instead repulsive which further strengthens the valence repulsion at large internuclear distances. The second minimum for the $^1\Pi_g$ state is found at 8.14 a.u. which has the depth of 173 cm^{-1} and accommodates several vibrational levels in the present study. These values are only moderately different from the values reported by Wolniewicz including the adiabatic corrections [89], who found the second minimum at $R \approx 8.25$ a.u. with the depth of 178 cm^{-1}.

The four Π states behave in substantially different ways in accordance to the applied confining potential. For these highly excited states, the Π_g energies are above the energy of the $^2\Sigma_g^+$ state of H_2^+ already for $\omega = 0.10$ a.u., while the lower Π_u energies are placed above that of H_2^+ at $\omega = 0.15$ a.u. For the potential strength $\omega \leq 0.10$ a.u. the equilibrium internuclear distance of the $^1\Pi_u$ state decreases from 1.0319 Å to 1.0033 Å. Simultaneously, the binding energy drops from 20435 cm^{-1}, for $\omega = 0.00$ a.u., to 19384 cm^{-1}, for $\omega = 0.10$ a.u. On the other hand,

a trend opposite to the change of binding energy is noticed for the well-known maximum at large R. While this hump is shifted towards smaller values of R, its height with respect to the dissociation limit increases rapidly for $0.00 \leq \omega \leq 0.15$ a.u. and then decreases. Detmer et al. have also observed similar behavior of the $^1\Pi_u$ state in the presence of a parallel magnetic field [27]. The inverse relation between ω and D_e could be accounted for by considering the deformation of π orbitals within a repulsive cylindrical potential. Due to the symmetry restriction exerted by the applied potential, the np orbital sets loses the degeneracy, with p_x and p_y components being more destabilized. The distorted $1\pi_u$ MO, which is more localized in the region between the two nuclei, has better overlap with the $1\sigma_g$ MO, thus strongly enhancing the Coulomb interaction. However, the overlap between $1\sigma_u$ and $1\pi_g$ is remarkably diminished. Consequently, the dissociation limit is greatly stabilized with respect to the potential minimum, giving rise to the decreasing binding energy for the $^1\Pi_u$ state. The induced stabilization effect on the repulsive $|1\sigma_u 1\pi_g\rangle$ function also explains the larger barrier of the large-R maximum for $\omega \geq 0.00$ a.u. since it intensifies the coupling between the $|1\sigma_u 1\pi_g\rangle$ and $|1\sigma_g 1\pi_u\rangle$ configurations, resulting in a higher potential hump. When ω increases, the single-reference $|1\sigma_u 1\pi_g\rangle$ potential curve is more stabilized and crosses the single-reference $|1\sigma_g 1\pi_u\rangle$ potential curve at smaller R. This explains the shift of the maximum towards smaller R with the increasing ω.

On the contrary, the PEC of the $^3\Pi_u$ state evolves in a way similar to that of the X $^1\Sigma_g^+$ state: the potential well becomes increasingly deeper, and the equilibrium internuclear distance contracts continuously. As in the case of the singlet C $^1\Pi_u$ state, the overlap between $1\sigma_g$ and $1\pi_u$ MOs is enhanced due to the distortion from the confining potential. Apart from the stronger Coulomb interaction, the exchange energy between the two parallel electrons is introduced which cancels out the Coulomb repulsion [65]. Therefore, the $|1\sigma_g 1\pi_u\rangle$ configuration, which dominates in the region near the minimum, is more stabilized than the $|1\sigma_u 1\pi_g\rangle$ configuration in which the orbital overlap is less efficient, and this exchange effect contributes towards the increasing well depth of the $^3\Pi_u$ state when an external potential is

applied.

The PECs of the highest states in the Π manifold, $^1\Pi_g$ and $^3\Pi_g$ states, exhibit drastic changes in the presence of a cylindrical potential. The changes of the PECs of these states with confinement are shown in Figure 3.5 and Figure 3.6. For

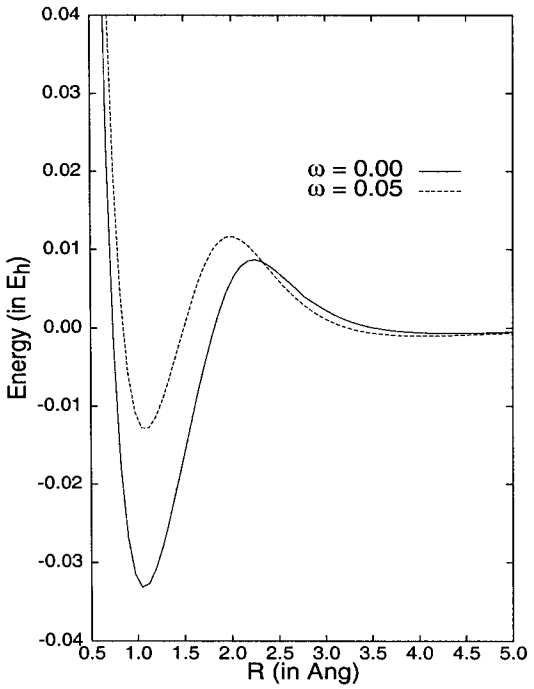

Figure 3.5: I $^1\Pi_g$ state in confinement. The energy is shown with respect to the dissociation limit.

both cases, the equilibrium internuclear distances increase with ω. Concurrently, the binding energies of both states decrease, with the change in the singlet state being more pronounced. Both of the Π_g states correlate to the united-atom limit of He(1s3d) [65]. For $R \approx r_e$, the wavefunctions of $^1\Pi_g$ and $^3\Pi_g$ are composed of $|1\sigma_g 3d_{\pi_g}\rangle$, which is treated as a Rydberg state, and $|1\sigma_g 2p_{\pi_g}\rangle$, respectively. The latter function becomes more important when R is larger until eventually it dominates at very large R and leads to the asymptote of H(1s) + H(2p). When the hydrogen molecule is encapsulated in a cylindrical potential, not only the p-shell but also the d-shell orbital degeneracy is removed, and those involved in $3d_{\pi_g}$ MOs, i.e., $3d_{xz}$

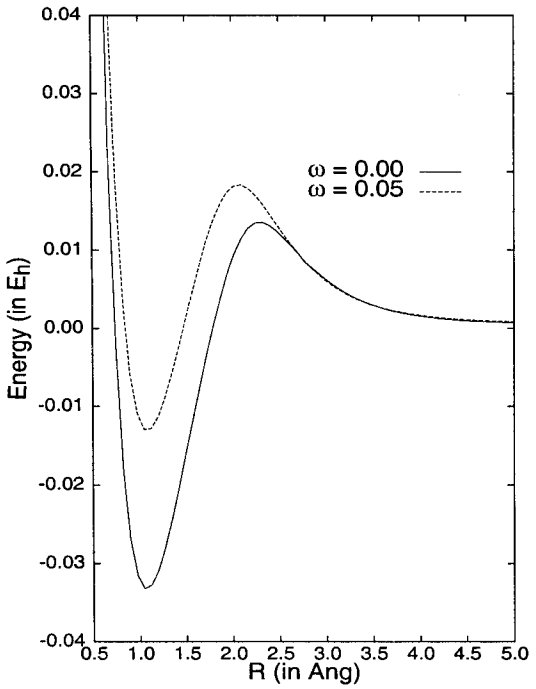

Figure 3.6: i $^3\Pi_g$ state in confinement. The energy is shown with respect to the dissociation limit.

and $3d_{yz}$ orbitals which are very diffuse, will be very intensely destabilized. As a consequence, in the region close to the minimum, their contribution to the $^1\Pi_g$ and $^3\Pi_g$ states, as measured by squares of coefficients in the CI expansion, is reduced. The destabilization of 3d orbitals causes the attractive potential of $|1\sigma_g 3d_{\pi_g}\rangle$ to be shifted upward in energy relative to the repulsive potential of $|1\sigma_g 2p_{\pi_g}\rangle$, resulting in the decreasing binding energy. Simultaneously, the maximum is shifted towards smaller values of R and becomes higher in energy with respect to the dissociation limit due to the fact that the two potential curves of $|1\sigma_g 2p_{\pi_g}\rangle$ and $|1\sigma_g 3d_{\pi_g}\rangle$ cross at smaller R. The slight stretching of the equilibrium internuclear distances also reflects a larger contribution of the $|1\sigma_g 2p_{\pi_g}\rangle$ function.

It may be seen from Figure 3.5 and Figure 3.6 that the $^1\Pi_g$ state is more susceptible to the influence of the external potential than the $^3\Pi_g$ state. Unlike the first minimum at small R the second van der Waals minimum of the $^1\Pi_g$ becomes more

pronounced with the increasing strength of the harmonic potential. The corresponding binding energy (see Table 3.6) increases from 173 cm^{-1} for $\omega = 0.00$ a.u. to 215 cm^{-1} for $\omega = 0.05$ a.u. and the minimum moves to smaller values of R. Detmer et al. have observed a similar trend [27] and they found that the second minimum will vanish when the magnetic field strength is larger than 10.0 a.u. Mulliken ascribed the second minimum to the first-order London dispersion interaction between H(1s) and H($2p_\pi$) which yields a net stabilization for the $^1\Pi_g$ state at large R [90]. As the contribution of $|1\sigma_g 2p_{\pi_g}\rangle$ function to the $^1\Pi_g$ state increases with the application of a cylindrical confining potential, this long-range attraction is significantly enhanced, giving rise to a deeper potential well in the region $6 \leq R \leq 8$ a.u.

E,F $^1\Sigma_g^+$ state

The first excited $^1\Sigma_g^+$ state is characterized by the double-minimum potential which is manifested in a very complicated vibrational-rotational spectrum [94]. The PEC of the E,F $^1\Sigma_g^+$ state has been extensively studied by Davidson [95, 96], Gerhauser and Taylor [62], and Kolos and Wolniewicz [97]. The peculiar double minimum is the result of an avoided crossing of the potential curves for the, in MO notation, $|1\sigma_g 2\sigma_g\rangle$ and $|1\sigma_u^2\rangle$ configurations. The inner minimum originates from the covalent $|1\sigma_g 2\sigma_g\rangle$ configuration while the outer minimum is composed mainly of ionic $|1\sigma_u^2\rangle$ configuration. These configurational alterations along R and multiple-minimum potential have also been observed for higher excited $^1\Sigma_g^+$ states, and were attributed to the H^+H^- separate atom level that intervenes in all the $|1sns\rangle$ levels below $|1s5s\rangle$ [95]. The calculated PEC of E,F $^1\Sigma_g^+$ state is plotted in Figure 3.7 and the corresponding spectroscopic constants are summarized in Table 3.10. Very good agreement with the experiment is achieved except that the discrepancies in vibrational frequencies are moderately large. The detailed analysis of the CI wavefunction has been performed in order to comprehend the nature of the state, and it reveals a complicated change of configurations with R. Figure 3.8(a) illustrates the variation of contributions of configurations involved in the E,F $^1\Sigma_g^+$ state. For $R \leq 1.5$ Å the state is well represented by the covalent $|1\sigma_g 2\sigma_g\rangle$ configuration ($\sim$

Table 3.10: Spectroscopic parameters of the E,F $^1\Sigma_g^+$ state[a,b]

State	Parameter	$\omega = 0.00$	$\omega = 0.05$	$\omega = 0.10$	$\omega = 0.15$	$\omega = 0.20$
E $^1\Sigma_g^+$	r_e	1.0114 (1.011)[c]	0.9966	0.9940	0.9986	
	ν_e	2541.1 (2588.9)[c]	2626.8	2615.2	2542.9	
	B_e	32.698 (32.68)[c]	32.679	33.853	33.542	
	$\nu_e x_e$	124.879 (130.5)[c]	148.904	146.964	167.952	
	α_e	1.909 (1.818)[c]	1.969	1.961	2.226	
	T_e	100018.9 (100082)[c]	106018.4	115651.0	124419.7	
F $^1\Sigma_g^+$	r_e	2.3227 (2.31)[c]	2.3193	2.2913	2.2491	2.2039
	ν_e	1248.1 (1199)[c]	1289.1	1349.9	1419.9	1486.2
	B_e	6.198	6.218	6.372	6.613	6.886
	$\nu_e x_e$	30.365	26.909	26.993	27.574	27.957
	α_e	0.1202	0.1529	0.1657	0.1701	0.17841
	T_e	100879.7 (100911)[c]	102488.6	105999.7	110231.2	114884.1

[a] Experimental values in parentheses. [b] r_e in Å, all other values in cm^{-1}. [c] Ref [51].

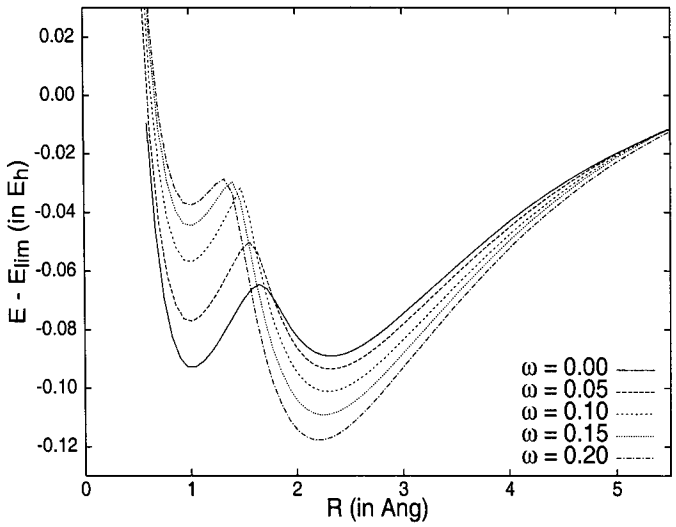

Figure 3.7: E,F $^1\Sigma_g^+$ state in confinement. The energy is shown with respect to the dissociation limit.

90 %) whose PEC rises very rapidly to the asymptote corresponding to H(1s) + H(2s). When R approaches the point of avoided crossing ($\sim$ 1.65 Å), an intrusion of the ionic potential happens that causes a drastic increase in the weight of $|1\sigma_u^2\rangle$ and forms a deep minimum at fairly large R ($\sim$ 2.3 Å).

These observations confirm the molecular orbital analysis of the E,F $^1\Sigma_g^+$ state carried out by Kolos and Wolniewicz in which the ionic part of the total wavefunction dominates the region from 3 to 6 a.u. [97]. At still larger R, the $|1\sigma_g 2\sigma_g\rangle$ configuration, which is a mixture of $|1s2s_\sigma\rangle$ and $|1s2p_\sigma\rangle$, becomes predominant again due to a second avoided crossing with the ionic potential. This avoided crossing allows for the proper dissociation of the state into the separate atom limit of H(1s) and H(2s) [65].

The evolution of the PEC of E,F $^1\Sigma_g^+$ state under the effect of a cylindrical harmonic potential is illustrated in Figure 3.7. The two minima have considerably different behavior in response to the applied potential, and several characteristics are noticeable. The inner minimum becomes less pronounced when the potential strength is increased from 0.00 a.u. to 0.15 a.u. However, this monotonic change

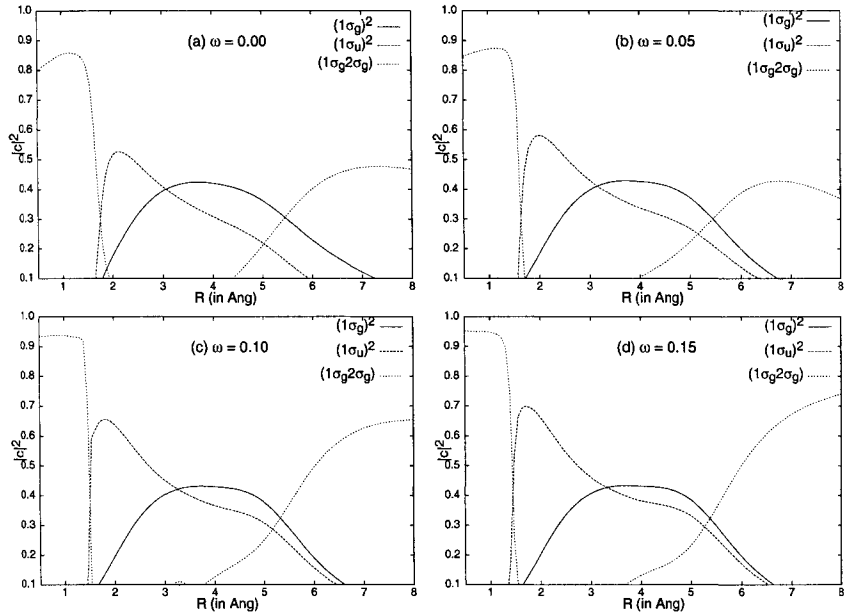

Figure 3.8: Decomposition of wavefunction of E,F $^1\Sigma_g^+$ state in confinement

is not seen in r_e, which first decreases for $\omega \leq 0.10$ a.u. and then increases for larger ω. On the other hand, the outer minimum is shifted monotonically towards the inner minimum accompanied by the increasing potential depth. Schmelcher et al. have studied the $^1\Sigma$ excited states of the hydrogen molecule in a parallel magnetic field for the field strength ranging from 0 to 100 a.u. [98], and they observed qualitatively very similar trends of the inner and outer minima evolving in the field with strengths smaller than 0.5 a.u. The unusual behavior can be explained in terms of the different extent of configuration mixing with respect to the strength of confining potential. Figs. 3.8(b)-(d) display the weight of each configuration in the total CI wavefunction that corresponds to the E,F $^1\Sigma_g^+$ state when a harmonic potential is present. At the region close to the inner minimum $|1\sigma_g 2\sigma_g\rangle$ remains as the dominant configuration. However, the associated potential well becomes more shallow because the $|1\sigma_g 2\sigma_g\rangle$ configuration is strongly destabilized due to the involvement of 2s orbitals and the PEC is shifted up relative to the ionic PEC. This PEC shifting leads to the transition point where the $|1\sigma_g 2\sigma_g\rangle$ PEC crosses the ionic

PEC moving to smaller R, as implied by the observation that the contribution of $|1\sigma_g 2\sigma_g\rangle$ configuration vanishes more rapidly for $\omega = 0.15$ a.u. (Figure 3.8(d)) when compared to the field-free case (Figure 3.8(a)).

Another feature of the E,F $^1\Sigma_g^+$ state wavefunction is the increase in weight of the ionic character in the intermediate-R region. The contribution of ionic wavefunction increases from 50 % to 70 % when a potential of the strength $\omega = 0.20$ a.u. is applied. This is not unexpected because the competing $|1\sigma_g 2\sigma_g\rangle$ configuration becomes less and less important due to the 2s destabilization. Furthermore, the $|1\sigma_u^2\rangle$ configuration is less destabilized as the smaller electron density within the internuclear vicinity reduces the repulsive interaction between electrons. Thus, the depth of the outer minimum which is formed from the $|1\sigma_u^2\rangle$ configuration increases monotonically for $\omega \leq 0.15$ a.u. The greater ionic character of the E,F $^1\Sigma_g^+$ state enhances the coupling with the G,K $^1\Sigma_g^+$ state, as shown in Figure 3.9, giving rise to a smaller energy difference between these two states at the point of avoided crossing, that may indicate a possibility of the failure of the Born-Oppenheimer approximation in the calculations of low-lying excited states in the presence of a confining potential. Shi and coworkers have shown recently that for a diatomic molecule two

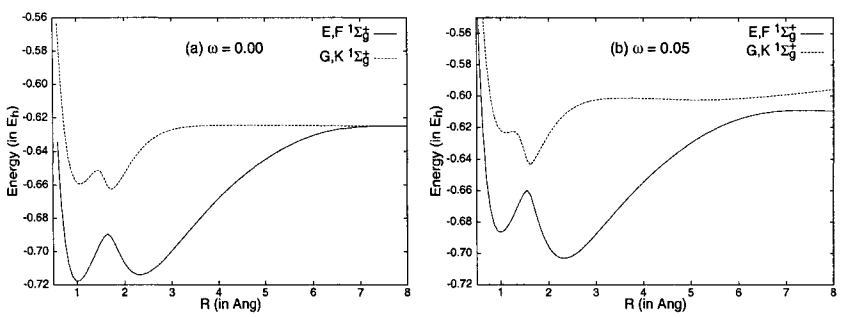

Figure 3.9: The E,F and G,K $^1\Sigma_g^+$ states in confinement

electronic states of the same spatial symmetry may intersect in multi-parameter space because additional symmetry elements appear in the perturbation operator in the adiabatic approximation that may result in zero off-diagonal matrix elements even though the two states have the same spatial symmetry [99]. In the present case,

the external harmonic potential can be viewed as a perturbation to the Hamiltonian of the hydrogen molecule in free space. Hence, the perturbation operator will be expressed in terms of not only the internuclear distance R but also the strength of confining potential ω, and the assumption that the off-diagonal coupling matrix elements are zero if two states are of the same symmetry may no longer be valid. A thorough understanding of this phenomenon requires a more detailed analysis of conical intersection in both theoretical and experimental aspects, a subject of intensive recent studies [100, 101].

Compared to the wavefunction in free space, the role of the $|1\sigma_g 2\sigma_g\rangle$ configuration is of greater significance at large R when confining potential is present. Its contribution progressively increases from 45 % to 80 % when ω is increased from 0.00 to 0.20 a.u. It suggests that the dissociation channel leading to $H^+ + H^-$ will be strongly destabilized relative to the covalent channels and will lie higher in energy, which confirms the contention of Sako and Diercksen that negative hydrogen ion possesses a fragile electron density that is easily affected by the confinement [38]. Surprisingly, a closer look at the composition of $|1\sigma_g 2\sigma_g\rangle$ configuration at large values of R discloses that the configuration comprises $|1s2s_\sigma\rangle$ and $|1s2p_\sigma\rangle$ (in Heitler-London convention) and the latter one predominates for $\omega \neq 0.00$ a.u., in contrast to the situation without confinement, where the former one dominates the state throughout a wide range of R till the asymptote. Concurrently, the dissociation limit of the E,F $^1\Sigma_g^+$ state merges to that of B $^1\Sigma_u^+$ and a $^3\Sigma_g^+$ states that corresponds to H(1s)+ H($2p_z$) for $\omega \geq 0.00$ a.u. These observations can be explained by noting the fact that the 2s and 2p energy levels of the hydrogen atom, which are degenerate when there is no external field, split in a cylindrical harmonic potential, as depicted by Figure 3.3, and $2p_z$ orbital becomes lower in energy relative to 2s orbital, resulting in the splitting of the channel II into three routes: $1s2p_z \leq 1s2s \leq 1s2p_x$, $1s2p_y$.

3.3.3 Molecules in magnetic fields

The results of calculations carried out in the present study show similarity to the results obtained using the cylindrical harmonic potential and those obtained from the numerical calculations of hydrogen molecule in parallel magnetic field. On the other hand, there exist a number of differences between these two models such as the switch of ground state symmetry in an intermediate- to ultrahigh-field regime. In order to understand the origin of the interesting similarities, it is worthwhile to review the basic formalism of a molecule in magnetic field.

From the classical electrodynamics, the Dirac Hamiltonian of a hydrogen molecule moving in a constant magnetic field $\vec{B}$ is [102]:

$$\mathcal{H}_{mag} = \sum_{i=1}^{2} \frac{1}{2m_e} \left[\sigma_i \cdot \left(\vec{p}_i + \frac{e}{c}\vec{A}\right)\right]^2 - \sum_{i=1}^{2}\sum_{\alpha=1}^{2} \frac{Ze^2}{R_{i\alpha}} + \frac{e^2}{r_{12}} + \frac{e^2}{R} \tag{3.1}$$

where the adiabatic approximation is employed to assume that the kinetic energy of nuclei is zero. R is the internuclear distance, r_{12} is the distance between the two electrons, and $R_{i\alpha}$ is the distance between the i-th electron and the α-th nucleus. $\vec{A}$ is the vector potential of the magnetic field that obeys the relation

$$\vec{B} = \nabla \times \vec{A}, \tag{3.2}$$

and σ_i is the Pauli spin matrix. It is assumed that the molecular axis is along the z-direction and $\vec{B} = B\hat{z}$ where $\hat{z}$ is the corresponding unit vector. The Schrödinger equation is gauge-invariant and any gauge can be selected if eq. (3.2) is fulfilled. Hence, a symmetric Coulomb gauge, $\nabla \cdot \vec{A} = 0$, is used which is defined as $\vec{A} = \frac{B}{2}(-y, x, 0)$. The substitution of $\vec{A}$ into eq. (3.1) yields the Hamiltonian

$$\begin{aligned} \mathcal{H}_{mag} &= \frac{1}{2m_e}\sum_{i=1}^{2}\left\{\left(p_{ix} - \frac{eBy}{2c}\right)^2 + \left(p_{iy} + \frac{eBx}{2c}\right)^2 + p_{iz}^2\right\} \\ &- \sum_{i=1}^{2}\sum_{j=1}^{2}\frac{Ze^2}{R_{ij}} + \frac{e^2}{r_{12}} + \frac{e^2}{R} - \sum_{i=1}^{2}\mu_{is}\cdot\vec{B} \end{aligned} \tag{3.3}$$

where the last term deals with the interaction between an electron spin and the field $\vec{B}$. The simplification of eq. (3.3) is straightforward; expanding and rearranging the

terms leads to the following

$$\begin{aligned}
\mathcal{H}_{mag} &= \sum_{i=1}^{2} \frac{p_i^2}{2m_e} - \sum_{i=1}^{2}\sum_{j=1}^{2} \frac{Ze^2}{R_{ij}} + \frac{e^2}{r_{12}} + \frac{Z^2e^2}{R} \\
&+ \frac{e^2B^2}{8m_ec^2} \sum_{i=1}^{2} \left(x_i^2 + y_i^2\right) + \frac{eB}{2m_ec} \sum_{i=1}^{2} \ell_{iz} + \frac{eB}{m_ec} \sum_{i=1}^{2} \mathcal{S}_{iz} \qquad (3.4) \\
&= \sum_{i=1}^{2} \frac{p_i^2}{2m_e} - \sum_{i=1}^{2}\sum_{j=1}^{2} \frac{Ze^2}{R_{ij}} + \frac{e^2}{r_{12}} + \frac{Z^2e^2}{R} \\
&+ \frac{1}{2}m_e\gamma^2 \sum_{i=1}^{2} \left(x_i^2 + y_i^2\right) + \gamma \left(\sum_{i=1}^{2} \ell_{iz} + 2\sum_{i=1}^{2} \mathcal{S}_{iz} \right), \qquad (3.5)
\end{aligned}$$

where $\gamma = \frac{eB}{2m_ec}$. The first part of eq. (3.5) is the Hamiltonian of a hydrogen molecule in free space, while the second part deals with the interaction of the molecule with the field. Comparing eq. (3.5) and eqs. (1.4) and (2.24), it is seen that the two Hamiltonians are very similar except that eq. (3.5) contains two extra terms which constitute the longitudinal kinetic energy Hamiltonian [24]

$$\mathcal{H}_1 = \sum_{i=1}^{2} T_{iz} = \gamma \sum_{i=1}^{2} \left(\ell_{iz} + 2\mathcal{S}_{iz}\right) \qquad (3.6)$$

that corresponds to the Zeeman effect [103]. The transverse magnetic Hamiltonian

$$\mathcal{H}_2 = \sum_{i=1}^{2} h_i^{\perp} = \frac{1}{2}m_e\gamma^2 \sum_{i=1}^{2} \left(x_i^2 + y_i^2\right) \qquad (3.7)$$

is equivalent to eq. (2.24) when $\omega^2 = \gamma^2$ in atomic units.

Hence, the Hamiltonian constructed from eqs. (1.4) and (2.24) is suitable for the evaluation of the transverse magnetic effect on a hydrogen molecule, due to the presence of a parallel magnetic field, that gives rise to the fine features of PECs. Since eq. (3.6) commutes with the total Hamiltonian $\mathcal{H}_{mag}$, the correction for the longitudinal component of the total magnetic effect on the molecule can be calculated as the energy eigenvalue of the Hamiltonian $\mathcal{H}_1$ acting on the hydrogen molecular wavefunction, and the corrected total energy is given by:

$$E^{\mathcal{H}_{mag}} = E^{\mathcal{H}_{el}} + \Delta E^{\mathcal{H}_1} \qquad (3.8)$$

The GUGA-CI wavefunctions are spatial and spin symmetry-adapted, thus the projections of total orbital angular momentum and total spin of a hydrogen molecule in a particular electronic state are conserved for all the values of R. Therefore, the term $\Delta E^{\mathcal{H}_1}$ remains constant for an electronic state, and it causes a shift of the corresponding PEC depending on the spin configuration. For the Σ states the orbital contribution to $\Delta E^{\mathcal{H}_1}$ is zero since the total orbital angular momentum is zero. Similarly, for the singlet states the spin contribution is zero as $S_z = 0$. Accordingly, it is expected that the ground X $^1\Sigma_g^+$ state would be identical if either the Hamiltonian $\mathcal{H}$ or $\mathcal{H}_{mag}$ is used because the term $\Delta E^{\mathcal{H}_1}$ vanishes. However, the term becomes non-zero for the triplet states, and the spin configuration has to be taken into account. A triplet state will be split into three sub-levels since there are three possible values of $S_z = -1, 0, 1$. If only the lowest state, i.e., $S_z = -1$ is considered, the term $\Delta E^{\mathcal{H}_1}$ will become negative, thus lowering the complete PEC. This explains the change of ground-state symmetry of the hydrogen molecule in a magnetic field. Since the term $\Delta E^{\mathcal{H}_1}$ is always negative for both b $^3\Sigma_u^+$ and c $^3\Pi_u$ states, for a sufficiently strong magnetic field, these states would be lowered in energy until they cross successively the X $^1\Sigma_g^+$ state and become the ground state.

3.4 Final remarks and conclusions

Molecules exhibit versatile behavior in response to the application of various forms of external potentials. In the present study, different electronic states of a hydrogen molecule enclosed in a cylindrical harmonic potential have been investigated and it has been found that states with different spatial symmetry and spins behave in different manner. In general, the applied potential shrinks the molecule and makes the minima on the PECs more pronounced. However, the symmetries of atomic orbitals that constitute the configuration of an electronic state also play a crucial role, and some unexpected shallow van der Waals minima and interchanges of dissociation limits that are caused by the orbital reordering under the influence of confinement have been observed. Moreover, a near intersection has been seen between the excited $^1\Sigma_g^+$ states through which a possible breakdown of the Born-

Oppenheimer approximation may occur. Interestingly, it is found that a hydrogen molecule, when confined in a cylindrical potential, behaves in a very similar way as it does under the influence of a parallel magnetic field, which stimulates a further study regarding the use of this model potential to the electrodynamic studies of molecules in external fields.

Bibliography

[1] R. Loudon, *Am. J. Phys.* **27**, 649 (1959).

[2] H. Hasegawa, R. E. Howard, *J. Phys. Chem. Solids* **21**, 179 (1961).

[3] D. Cabib, E. Fabri, G. Fiorio, *Solid State Commun.* **9**, 1517 (1971).

[4] E. R. Smith, R. J. W. Henry, G. L. Surmelian, R. F. O'Connell, A. K. Rajagopal, *Phys. Rev. D* **6**, 3700 (1972).

[5] G. H. Garstang, S. B. Kemic, *Astrophys. Space Sci.* **31**, 103 (1974).

[6] J. R. P. Angel, E. F. Borra, J. D. Landstreet, *Astrophys. J. Suppl. Ser.* **45**, 457 (1981).

[7] J. Trümper, W. Pietsch, C. Reppin, W. Voges, R. Staubert, E. Kendziorra, *Astrophys. J.* **219**, L105 (1978).

[8] D. Yoshioka, *The Quantum Hall Effect*, Springer, New York, 2002.

[9] L. Jacak, P. Hawrylak, A. Wójs, *Quantum Dots*, Springer, New York, 1998.

[10] M. Reed, R. T. Bate, K. Bradshaw, W. M. Duncan, W. M. Frensley, J. W. Lee, H. D. Smith, *J. Vacuum Sci. Technol. B* **4** 358 (1986).

[11] J. K. Jaiswal, H. Mattoussi, J. M. Mauro, S. M. Simon, *Nature Biotech.* **21**, 47 (2003).

[12] F. Combes, G. Pineau des Forêts, *Molecular Hydrogen in Space*, Cambridge University Press, UK, 2000.

[13] A. G. Massey, *Main Group Chemistry*, 2nd edition, Wiley, New York, 2000.

[14] G. Herzberg, *Phys. Rev. Lett.* **23**, 108 (1969).

[15] W. Heitler, F. London, *Z. Physik* **44**, 455 (1927).

[16] W. Kolos, L. Wolniewicz, *J. Chem. Phys.* **49**, 404 (1968).

[17] D. M. Larsen, *Phys. Rev. A* **25**, 1295 (1982).

[18] U. Wille, *J. Phys. B: At. Mol. Phys.* **20**, L417 (1987).

[19] U. Kappes, P. Schmelcher, *Phys. Rev. A* **51**, 4542 (1995).

[20] U. Kappes, P. Schmelcher, *Phys. Rev. A* **54**, 1313 (1996).

[21] S. Basile, F. Trombetta, G. Ferrante, *Nuovo Cimento* **9**, 457 (1987).

[22] A. V. Korolev, M. A. Liberman, *Phys. Rev. A* **45**, 1762 (1992).

[23] D. Lai, E. E. Salpeter, S. L. Shapiro, *Phys. Rev. A* **45**, 4832 (1992).

[24] M. Demeur, P. H. Heenen, M. Godefroid, *Phys. Rev. A* **49**, 176 (1994).

[25] G. Ortiz, M. D. Jones, D. M. Ceperley, *Phys. Rev. A* **52**, R3405 (1995).

[26] T. Detmer, P. Schmelcher, F. K. Diakonos, L. S. Cederbaum, *Phys. Rev. A* **56**, 1825 (1997).

[27] T. Detmer, P. Schmelcher, L. S. Cederbaum, *Phys. Rev. A* **57**, 1767 (1998).

[28] K. Runge, J. R. Sabin, *Int. J. Quantum Chem.* **64**, 561 (1997).

[29] D. Lai, E. E. Salpeter, *Phys. Rev. A* **53**, 152 (1996).

[30] T. S. Monteiro, K. T. Taylor, *J. Phys. B: At. Opt. Phys.* **23** 427 (1990).

[31] W. Kohn, *Phys. Rev.* **123**, 1242 (1961).

[32] P. Maksym, T. Chakraborty, *Phys. Rev. Lett.* **65**, 108 (1990).

[33] P. Bakshi, D. A. Broido, K. Kempa, *Phys. Rev. B* **42**, 7416 (1990).

[34] A. Kumar, S. E. Laux, F. Stern, *Phys. Rev. B* **42**, 5166 (1990).

[35] M. W. Schmidt, K. K. Baldridge, J. A. Boatz, S. T. Elbert, M. S. Gordon, J. H. Jensen, S. Koseki, N. Matsunaga, K. A. Nguyen, S. J. Su, T. L. Windus, M. Dupuis, J. A. Montgomery, *J. Comput. Chem.* **14**, 1347 (1993).

[36] G. H. F. Diercksen, G. Hall, *Comput. Phys.* **8**, 215 (1994).

[37] B. R. Brooks, H. F. Schaefer, *J. Chem. Phys.* **70**, 5092 (1979).

[38] T. Sako, G. H. F. Diercksen, *J. Phys. B: At. Mol. Opt. Phys.* **36** 1681 (2003).

[39] T. Sako, G. H. F. Diercksen, *J. Phys. B: At. Mol. Opt. Phys.* **36** 1433 (2003).

[40] T. Sako, I. Cernusak, G. H. F. Diercksen, *J. Phys. B: At. Mol. Opt. Phys.* **37** 1091 (2004).

[41] U. Kaldor, *J. Chem. Phys.* **62**, 4634 (1975).

[42] L. Wolniewicz, *J. Chem. Phys.* **109**, 2254 (1998).

[43] R. Bukowski, B. Jeziorski, K. Szalewicz, *J. Chem. Phys.* **110**, 4165 (1999).

[44] O. V. Gritsenko, S. J. A. van Gisbergen, A. Görling, E. J. Baerends, *J. Chem. Phys.* **113**, 8478 (2000).

[45] K. Yokoyama, H. Nakano, K. Hirao, J. P. Finley, *Theor. Chem. Acc.* **110**, 185 (2003).

[46] P. R. Surjan, D. Kohalmi, A. Szabados, *Collection of Czechoslovak Chem. Commun.* **68**, 331 (2003).

[47] B. O. Roos (ed.), *Lecture Notes in Quantum Chemistry*, Springer-Verlag, New York, 1992, pp. 177-255.

[48] M. Tachikawa, Y. Osamura, *J. Chem. Phys.* **113**, 4942 (2000).

[49] D. Bielińska-Wąż, G. H. F. Diercksen, M. Klobukowski, *Chem. Phys. Lett.* **349**, 215 (2001).

[50] E. W. S. Schreiner, Ph.D. Thesis, Technische Universität München, 1996.

[51] K. P. Huber, G. Herzberg, *Molecular Spectra and Molecular Structure Constants of Diatomic Molecules*, Van Nostrand Reinhold, New York, 1979.

[52] Y. P. Kravchenko, M. A. Liberman, *Phys. Rev. A* **57**, 3403 (1998).

[53] W. Kolos, L. Wolniewicz, *J. Chem. Phys.* **43**, 2429 (1965).

[54] J. W. Liu, S. Hagstrom, *J. Phys. B: At. Mol. Opt. Phys.* **27**, L729 (1994).

[55] D. Frye, G. C. Lie, E. Clementi, *J. Chem. Phys.* **91**, 2366 (1989).

[56] F. Borondo, F. Martin, M. Yanez, *J. Chem. Phys.* **86**, 4982 (1986).

[57] W. Kolos, L. Wolniewicz, *J. Chem. Phys.* **45**, 509 (1966).

[58] J. Rychlewski, W. T. Raynes, *Mol. Phys.* **50**, 1335 (1983).

[59] S. C. Farantos, G. Theodorakopoulos, C. A. Nicolaides, *Chem. Phys. Lett.* **100**, 263 (1983).

[60] H. M. James, A. S. Coolidge, *J. Chem. Phys.* **6**, 730 (1939).

[61] T. Zung, A. B. F. Duncan, *J. Chem. Phys.* **36**, 2140 (1962).

[62] J. Gerhauser, H. S. Taylor, *J. Chem. Phys.* **42**, 3621 (1965).

[63] W. Kolos, J. Rychlewski, *Chem. Phys. Lett.* **59**, 183 (1978).

[64] D. M. Bishop, L. M. Cheung, *Chem. Phys. Lett.* **79**, 130 (1981).

[65] R. S. Mulliken, *J. Am. Chem. Soc.* **88**, 1849 (1966).

[66] P. Schmelcher, M. V. Ivanov, W. Becken, *Phys. Rev. A* **59**, 3424 (1999).

[67] J. E. Avron, I. W. Herbst, B. Simon, *Phys. Rev. A* **20**, 2287 (1979).

[68] T. Hori, *Zeits. f. Physik* **44**, 838 (1927).

[69] G. H. Dieke, J. J. Hopfield, *Phys. Rev.* **30**, 400 (1927).

[70] H. H. Hyman, *Phys. Rev.* **36**, 187 (1930).

[71] C. R. Jeppesen, *Phys. Rev.* **44**, 165 (1933).

[72] W. Lichten, *J. Chem. Phys.* **26**, 306 (1957).

[73] W. Lichten, *Phys. Rev.* **120**, 848 (1960).

[74] Y. N. Chiu, *J. Chem. Phys.* **41**, 3235 (1964).

[75] W. M. Wright, E. R. Davidson, *J. Chem. Phys.* **43**, 840 (1965).

[76] J. C. Browne, *J. Chem. Phys.* **40**, 43 (1964).

[77] T. Namioka, *J. Chem. Phys.* **43**, 1636 (1965).

[78] J. R. Hoyland, *J. Chem. Phys.* **45**, 3928 (1966).

[79] L. Y. Chow Chiu, *Phys. Rev.* **137**, A384 (1965).

[80] K. Dressler, L. Wolniewicz, *Can. J. Phys.* **62**, 1706 (1984).

[81] K. Dressler, L. Wolniewicz, P. Quadrelli, *Int. J. Quantum Chem.* **29**, 185 (1986).

[82] G. Herzberg, A. Monfils, *J. Mol. Spectry.* **5**, 482 (1960).

[83] G. H. Brigman, S. J. Brient, F. A. Matsen, *J. Chem. Phys.* **34**, 958 (1961).

[84] A. Amemiya, *Proc. Phys. Math. Soc. (Japan)* **21**, 394 (1939).

[85] E. R. Davidson, *J. Chem. Phys.* **42**, 4199 (1965).

[86] S. Rothenberg, E. R. Davidson, *J. Chem. Phys.* **45**, 2560 (1966).

[87] W. T. Zemke, P. G. Lykos, A. C. Wahl, *J. Chem. Phys.* **51**, 5635 (1969).

[88] W. Kolos, J. Rychlewski, *J. Mol. Spectrosc.* **66**, 428 (1977).

[89] L. Wolniewicz, *J. Mol. Spectrosc.* **169**, 329 (1995).

[90] R. S. Mulliken, *Phys. Rev.* **120**, 1674 (1960).

[91] G. Herzberg, L. L. Howe, *Can. J. Phys.* **37**, 636 (1957).

[92] W. Kolos, *J. Mol. Struct.* **46**, 73 (1978).

[93] J. Rychlewski, *Theor. Chim. Acta.* **83**, 249 (1995).

[94] G. H. Dieke, *J. Mol. Spectrosc.* **2**, 494 (1958).

[95] E. R. Davidson, *J. Chem. Phys.* **33**, 1577 (1960).

[96] E. R. Davidson, *J. Chem. Phys.* **35**, 1189 (1961).

[97] W. Kolos, L. Wolniewicz, *J. Chem. Phys.* **50**, 3228 (1969).

[98] P. Schmelcher, T. Detmer, L. S. Cederbaum, *Phys. Rev. A* **61**, 043411 (2000).

[99] Q. Shi, S. Kais, F. Remacle, R. D. Levine, *J. Chem. Phys.* **114**, 9697 (2001).

[100] B. E. Applegate, T. A. Barckholtz, T. A. Miller, *Chem. Soc. Rev.* **32**, 38 (2003).

[101] G. A. Worth, L. S. Cederbaum, *Annu. Rev. Phys. Chem.* **55**, 127 (2004).

[102] A. Messiah, *Quantum Mechanics Vol. II*, North-Holland Publishing Company, Amsterdam, 1986.

[103] E. U. Condon, G. H. Shortley, *The Theory of Atomic Spectra*, Cambridge University Press, Cambridge, 1991.

Chapter 4

MCQDPT Studies of Beryllium Molecule in Cylindrical Harmonic Confining Potential

In Chapters 4 and 5, the observations in the studies of confinement effects on the spectral properties of unstable Be_2 and its molecular ions are given, and rationalizations are proposed to account for the distinctive phenomena. Discussions about the neutral Be_2 are presented in Chapter 4 [1], followed by the analysis for the molecular ions in Chapter 5.

4.1 Introduction

Recent advances in solid state physics and semiconductor technology allow for the studies of the behavior of electrons confined in various forms of electric and magnetic fields. These confined electrons, known as quantum dots or artificial atoms, exhibit special electrical and optical properties which depend on the applied external fields. By manipulating geometry and strengths of the fields, the energy levels of the artificial atoms can be fine-tuned, which opens a new avenue to the design of new materials with desired characteristics for nano-electronic devices and laser diodes [1].

In parallel to the rapid development in technology of creating quantum dots,

[1] A version of this chapter was published in *Mol. Phys.* **102**, 2511 (2004).

the theoretical research towards the understanding of these quantum objects has been commenced and several models have been proposed for studying the effects of the confining potentials on the electronic properties [2, 3] and chemical reactivity [4] of atoms. In most of the investigations the harmonic confining potential was adopted, and the calculations were restricted to the ground-state structures using the Hartree-Fock method [5]. Studies including electron correlation effects have been relatively limited until recently, when several calculations using density functional theory (DFT) and configuration interaction (CI) methods have been reported [6, 7, 8].

In the present study the effects of the harmonic confining potential on the beryllium dimer (Be_2) were investigated. The theoretical analysis of Be_2 has initiated in the early 1930s, when Furry and Bartlett, using valence-bond method, first predicted that the ground state potential of Be_2 is repulsive [9]. Thirty years later the SCF-CI calculations of Ransil and Fraga [10], and of Bender and Davidson [11] also supported the repulsive ground state potential. However, subsequent calculations using DFT [12] and Møller-Plesset (MP2) methods [13], and finally valence full CI [14] approach used by Harrison and Handy suggested that Be_2 has a bound ground state, although the predicted equilibrium bond lengths and binding energies were not consistent - not surprisingly, given the various basis sets and methods used. The controversy about the existence of Be_2 persisted until, following the very accurate theoretical calculations, the first experimental evidence of Be_2 was found by Bondybey [15] using laser-induced fluorescence (LIF). The estimated small binding energy ($\sim$ 790 cm^{-1}) and relatively short equilibrium bond length (2.45 Å) triggered a series of calculations employing various sophisticated electron correlation methods and large basis sets (for example, see [16, 17, 18]), resulting in the conclusion that Be_2 stability could be attributed to the strong core-valence correlation effect due to the near degeneracy of 2s and 2p atomic orbitals of Be [19].

Experimental investigation of the excited states of Be_2 is limited by the small binding energy, and, using LIF, only three singlet excited states have been detected [15, 20]. Recently, several extensive theoretical studies of the excited states of Be_2

have been reported. It was found that the results depend on the methods used [20, 21, 22, 23], and multi-reference techniques are necessary to deal with the non-dynamical correlation due to the interaction between the 2s and 2p orbitals.

Due to the near-degenerate nature of 2s and 2p orbitals, Be_2 was chosen in the present study to demonstrate the effect of harmonic confining potential on molecular geometries and electronic structures. Using perturbation theory, Vorontsova et al. have shown that the atomic S and P states split under the influence of one-dimensional non-uniform electric field [24]. Accordingly, a similar scenario is expected for beryllium as the s-p quasi-degeneracy of Be atom and dimer would be removed by the applied potential and significant changes in both ground and excited states should be observed. In order to deal with both the electron correlation and near-degeneracy, a multi-configurational quasi-degenerate perturbation theory (MCQDPT), developed by Nakano [25], was used in the present study. This method addresses the problem of degeneracy by employing several reference functions obtained by multi-configuration self-consistent-field (MCSCF) calculations. The dynamical correlation is then included by perturbation calculations using the resulting reference wavefunctions. This method has shown to yield results in excellent agreement with the ones obtained by full CI or multi-reference CI for diatomic molecules such as CO, NO, BN and LiF [25], and good accuracy compared to experimental data (e.g. InH [26] and 2-aminopurine [27]). One advantage of MCQDPT over other multi-reference methods is its efficiency. Traditional multi-configurational *ab initio* methods require reference wavefunctions with tremendous numbers of configurations, thus making them less applicable, in particular for large systems, while in MCQDPT the MCSCF reference wavefunctions are generated by complete-active-space configuration interaction (CAS-CI), in which only excitations within the defined active space will be considered, leading to a smaller number of configurations, and higher computational efficiency. In addition, the capability of simultaneous calculations of several states, either degenerate or quasi-degenerate, and the characteristic of size-consistency make this method ideal for the present study of the ground and excited states of Be_2.

4.2 Computational Methodology

This project is mainly concerned with the computations of the potential energy curves of a diatomic Be_2 molecule confined in a two-dimensional harmonic oscillator-type electrostatic potential whose axis coincides the molecular axis of the Be_2 molecule. The potential is defined at the position of the center of mass of the molecule, i.e., the mid-point position. For further details regarding the model of confinement, see Chapter 2.

All the MCQDPT calculations in the present study were performed using the modified version of GAMESS-US [28]. In the CASSCF calculations, the active space included all molecular orbitals constructed from 1s, 2s and 2p atomic orbitals of Be atoms, making the CAS(8e,10o) combination. The chemical core $1\sigma_g$ and $1\sigma_u$ orbitals were included to allow for the complete description of core-valence correlation, which is significant in Be_2. $1\pi_g$ and $1\pi_u$ orbitals were also included to describe the experimentally observed singlet excited states which dissociate to ^{1}S and ^{1}P atomic states. In the subsequent MP2 calculations all the 8 electrons were correlated in order to yield the best correlation energies. Dunning's correlation-consistent valence quadruple-zeta basis set (cc-pVQZ) [29] for Be was employed, augmented with a set of (1s1p1d1f) bond function derived from the contracted [11s,9p,6d,4f,2g] basis set of Røeggen and Almlöf [18]. In addition, (1s1p1d) confinement basis functions, with exponents of $\omega/2$, were added at the center of the potential in order to properly describe the wavefunction in the region of dominated by the harmonic potential [30].

4.3 Results and Discussion

4.3.1 Basis Sets

The Dunning's correlation-consistent basis sets are designed so that results are comparable to using atomic natural orbitals (ANO) while keeping the total number of primitive functions minimum, and the problem of imbalanced polarization space could be avoided [31]. However, the s and p exponents were optimized for the

Table 4.1: MCQDPT Results for X $^1\Sigma_g^+$ State of Be_2

Basis set	cc-pVQZ	cc-pVQZ + (1s1p1d1f)	Expt
Number of basis functions	140	160	
r_e/a_0	4.6051	4.5958	4.6298
D_e/cm^{-1}	770	818	
D_e (corr)/cm^{-1}	597	622	790

Hartree-Fock ground state while the polarization exponents were obtained through configuration interaction with single and double excitations (SD-CI). As the primary goal of the present study is to investigate the effects of confinement on both ground and excited states, full CI calculations of the singlet and triplet excited state energies of Be atom have been performed to test the performance of cc-pVQZ basis set in excited state studies. The calculated ^{3}P state shows excellent agreement with experiment (21972 cm^{-1} vs 21982 cm^{-1} above the ground state) while the calculated ^{1}S-^{1}P transition reasonably matches the observed emission spectrum of Be (43283 cm^{-1} vs 42565 cm^{-1}) [32]. These results indicate that cc-pVQZ basis set could accurately describe the excitation of 2s electrons in Be and be a suitable basis set for the studies of those excited states of Be_2 whose electronic configurations involve 2s-2p excitations.

A set of bond functions was added at the mid-point position of Be_2 to improve the description of the weak interaction between two closed-shell Be atoms. The bond function set was derived from the basis set of Røeggen and Almlöf [18], which was constructed from an even-tempered set of 20 Gaussian-type functions [33] with the expanded diffuse space, by extracting the most diffuse s-, p-, d- and f-type functions without the g-function. The corresponding exponents of the resulting (1s1p1d1f) set are 0.0160584, 0.0353510, 0.0778218 and 0.1713171 respectively. Calculations have also been performed without bond functions, and the results are shown and compared in Table 4.1. The cc-pVQZ basis set yields the binding energy that is too small. A more reasonable value of D_e, after the counterpoise correction for the basis set superposition error (BSSE) was performed, could be obtained when bond functions were used. However, the internuclear distance r_e, calculated using

cc-pVQZ basis set, agrees better with the experiment, and the addition of bond functions induces shorter bond lengths. The bond function set in general shows a good agreement in r_e and could yield fairly good binding energy. Consequently, it was used in the subsequent confinement calculations of the ground and excited states of Be_2.

4.3.2 Spectroscopic Constants

Potential energy curves of four singlet states of Be_2 have been calculated with three different strengths of the external harmonic potentials: ω = 0.0, 0.1, and 0.2 a.u., respectively. Energies were evaluated at about forty points covering the range from r = 2.0 a.u. to r = 10 a.u. The harmonic potential was cylindrical, with its axis aligned along the molecular axis. Spectroscopic parameters were extracted by fitting the *ab initio* total energies into the Murrell-Sorbie (MS) potential function [34]. The MS function is a modified Rydberg function [35], with the pre-exponential term replaced by a power series in (r-r_e):

$$V(r) = -D_e \left(1 + \sum_{k=1} a_k (r - r_e)^k \right) \exp\left(-\gamma (r - r_e)\right) \tag{4.1}$$

The MS potential behaves better than both Morse and Rydberg potentials in the repulsive and attractive regions. Zhu and Huxley demonstrated that the third and fourth-order force constants derived from the MS potentials agreed very well with the spectroscopically determined values for more than a hundred diatomic molecules and ions [34, 36, 37]. In this study the five-parameter version of MS potential was used (i.e., $k = 3$ and $\gamma = a_1$ in eq. (4.1)). The resulting spectroscopic parameters are given in Table 4.2. Fairly good agreement is obtained for r_e and ν_e, while α_e and $\nu_e x_e$ show big discrepancies from the experiment. As these values are strongly dependent on the quality of the potential energy curve, the relatively large differences in α_e and $\nu_e x_e$ could be attributed to the insufficient accuracy of the *ab initio* potentials at the r_e region.

For weakly interacting systems such as Be_2, an accurate binding energy could be obtained only if BSSE correction is taken into account. Pecul and co-workers have

Table 4.2: Spectroscopic parameters in the ground and some excited states[a] of Be_2

State	Parameters	$\omega = 0.0$[b]	$\omega = 0.1$	$\omega = 0.2$
$X\ ^1\Sigma_g^+$	r_e	2.4320(2.4500)	2.2331	2.0784
	B_e	0.633(0.623)	0.750	0.866
	ν_e	257.9(275.8)	419.6	665.6
	α_e	0.037(0.028)	0.025	0.012
	$\nu_e x_e$	17.3(26.0)	14.4	10.0
	D_e	818(790)	2578	7978
	T_e	0(0)	0	0
$B\ ^1\Sigma_u^+$	r_e	2.2063(2.1993)	2.2016	2.1696
	B_e	0.769(0.773)	0.772	0.794
	ν_e	507.8(511.2)	510.4	515.4
	α_e	0.0146	0.0121	0.0123
	$\nu_e x_e$	6.00(4.69)	5.42	5.07
	D_e	16336(15666)	16569	18292
	T_e	27947(27738)	31329	36453
$A'\ ^1\Pi_g$	r_e	1.9893(2.0162)	1.9213	1.8667
	B_e	0.945(0.920)	1.014	1.074
	ν_e	710.1(726.0)	756.5	810.7
	α_e	0.008(0.009)	0.010	0.007
	$\nu_e x_e$	3.7(4.4)	3.4	3.7
	D_e	31106(29693)	32054	32497
	T_e	13163(13711)	15653	21202
$A\ ^1\Pi_u$	r_e	1.9830(1.9781)	1.9404	1.8880
	B_e	0.951(0.956)	0.994	1.050
	ν_e	701.4(685.7)	705.1	805.4
	α_e	0.0097	0.0104	0.0092
	$\nu_e x_e$	4.67(4.85)	2.48	3.93
	D_e	24607(21936)	25480	27171
	T_e	21083(21468)	22056	25902

[a] All constants in cm^{-1} except for r_e in Å. [b] Experimental values in parentheses; Ref [15, 20].

Table 4.3: Dissociation energies[a] of of Be_2 in the X $^1\Sigma_g^+$ state

Harmonic Potential	D_e	D_e (corrected)	Change	% Change
$\omega = 0.0$	818	622	196	24.0%
$\omega = 0.1$	2578	2443	135	5.2%
$\omega = 0.2$	7978	7800	178	2.2%

[a] In cm^{-1}

shown that the errors caused by BSSE in the values of the spectroscopic constants of the strongly-bound low-lying excited states of Be_2 are negligible at the coupled-cluster (CCSD and CC3) levels with very large correlation-consistent basis sets [23]. On the other hand, the binding energy of the weakly-bound ground state of Be_2 is susceptible to BSSE and 30% decrease of D_e was observed upon removal of the BSSE. Thus, the counterpoise (CP) correction [38, 39] was applied only to the ground state X $^1\Sigma_g^+$. The results are summarized in Table 4.3. The percentage change of D_e due to BSSE is decreased by the applied harmonic potential. However, the trend of the absolute change is not apparent, and approximately the same amount of BSSE error is observed for all the four cases. The BSSE-corrected binding energy of Be_2 is reduced to 622 cm^{-1}, which is about 180 cm^{-1} smaller than the experimental binding energy.

The structures and spectroscopic constants of the four lowest singlet states of Be_2 are listed in table B.2. It may be seen that fairly good agreement with experiment is achieved (for $\omega = 0.0$). The largest discrepancy in r_e is 0.03 Å for the $^1\Pi_g$ state, while that for ν_e is 18 cm^{-1} for the $^1\Sigma_g^+$ state. Nevertheless, the errors in $\nu_e x_e$ and α_e are significant. The calculated and experimental values of α_e and $\nu_e x_e$ differ by 36% and 35% respectively. While these errors are fairly large, the PEC should possess sufficiently good quality for the major purpose of this study, that is the general effects of confining potentials on the molecular geometry and spectroscopic constants of the ground and low-lying excited states of Be_2.

Some general trends of the effects of the applied harmonic potentials on the spectroscopic constants can be observed. The internuclear distance r_e decreases when the potential is present, which agrees with the observation of Bielińska-Wąż

et al. that the H_2 molecule shrinks in the confinement of a spherical potential [8]. The shortening of r_e is caused by the increase of electron density in the region between the Be nuclei due to the applied cylindrical potential. Mulliken population analysis reveals that larger electron density is found in the mid-bond region when ω is increased from 0.0 to 0.2 a.u. The accumulation of electron density strengthens the bonding interaction and results in the shorter equilibrium distance. The increase of ν_e with the strength of confinement is the direct consequence of this strengthened Be-Be bond. For the two sigma states (X $^1\Sigma_g^+$ and B $^1\Sigma_u^+$) both α_e and $\nu_e x_e$ decrease with increasing strength of the confinement. The decreasing trends of these parameters indicate that the potential energy curves become less anharmonic and more symmetrical [40].

4.3.3 Electronic Structure

Figures 4.1(a)-(c) show the potential energy curves of the four singlet states studied in the present work. The ground state X $^1\Sigma_g^+$ of Be_2 has the dominant configuration of $(1\sigma_g)^2(1\sigma_u)^2(2\sigma_g)^2(2\sigma_u)^2$ which correlates to two ground state ^{1}S Be atoms. The occupation (0.1829) of the $3\sigma_g$ MCSCF orbital, consistent with the results reported by Heaven and co-workers [20], suggests significant contribution of this orbital to the bonding interaction between closed-shell Be atoms. When the confinement is turned on, this configuration becomes less dominant and a new configuration $(1\sigma_g)^2(1\sigma_u)^2(2\sigma_g)^2(3\sigma_g)^2$ appears, which results from the double excitation of two electrons from $2\sigma_u$ orbital to $3\sigma_g$ orbital. This promotion is facilitated by the fact that the applied potential greatly reduces the $2\sigma_u$-$3\sigma_g$ energy gap (from 0.2382 a.u. to 0.1268 a.u. when ω is increased from 0.0 to 0.2 a.u.). In qualitative terms, the lowering of the $3\sigma_g$ orbital energy could be attributed to the effect of symmetry of the cylindrical potential, through which the $2p_z$ orbital, coaxial with the repulsive potential, is no longer degenerate with the $2p_x$ and $2p_y$ orbitals. Therefore, both the $2p_z$ orbital and the $3\sigma_g$ orbital which is composed of the two $2p_z$ atomic orbitals of Be atoms, are stabilized and the energy gap between $2\sigma_u$ and $3\sigma_g$ orbitals is reduced.

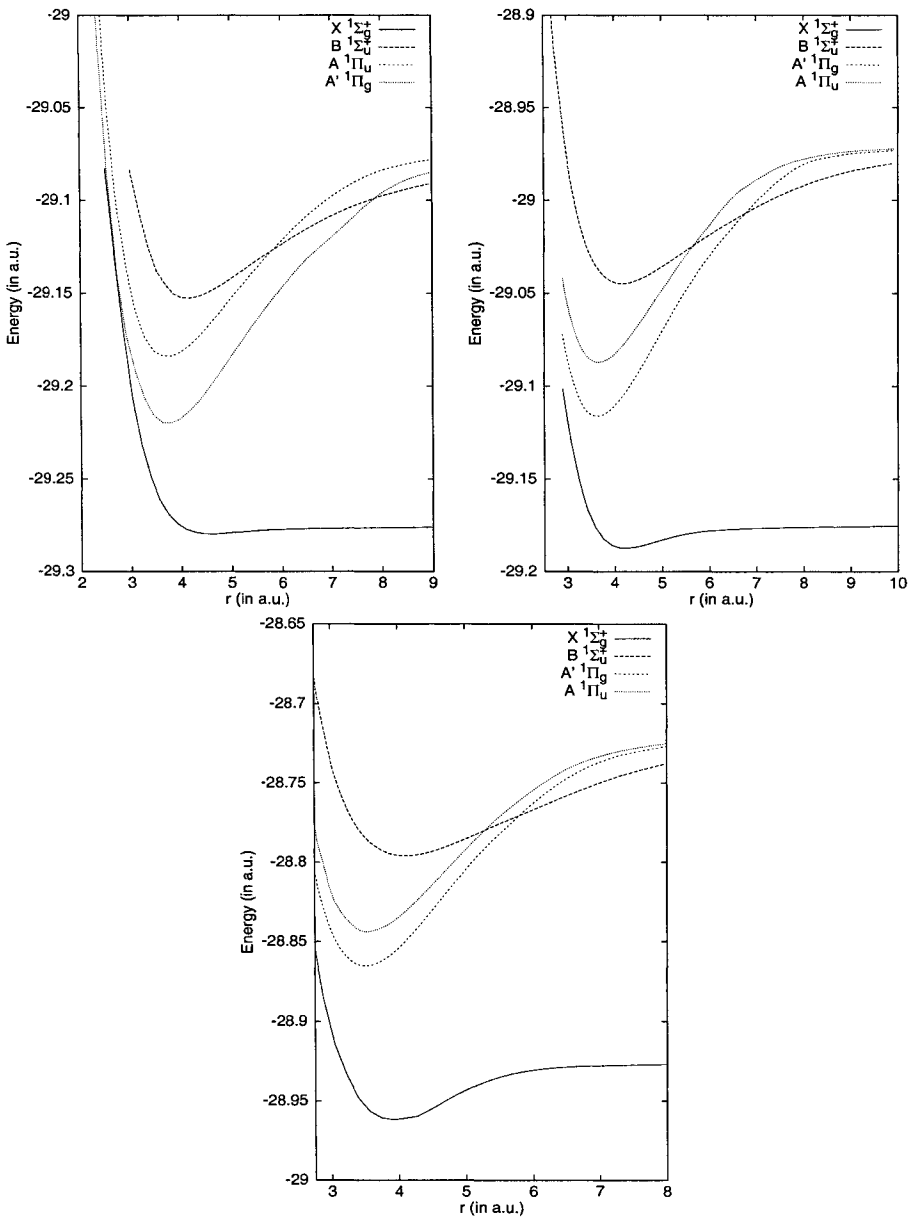

Figure 4.1: Potential energy curves of the four singlet states of Be_2. (a) Top-left: ω = 0.0; (b) Top-right: ω = 0.1; (c) Bottom: ω = 0.2

A similar situation appears also in the B $^1\Sigma_u^+$ state. In the absence of confining potential, the configuration is predominantly $(1\sigma_g)^2(1\sigma_u)^2(2\sigma_g)^2(2\sigma_u)^1(3\sigma_g)^1$, which is derived from the single excitation from $2\sigma_u$ orbital to $3\sigma_g$ orbital. When a harmonic potential is imposed, another excitation from $2\sigma_g$ orbital to $3\sigma_g$ orbital is induced due to the lowering of the $3\sigma_g$ orbital, giving rise to the increase of the weight of $(1\sigma_g)^2(1\sigma_u)^2(2\sigma_g)^1(2\sigma_u)^1(3\sigma_g)^2$. No change of dissociation limit is seen for the B $^1\Sigma_u^+$ state, and it still correlates to the ground-state ^{1}S Be and the excited ^{1}P (^{1}S when confinement is present) Be whose configuration is $(1s)^2(2s)^1(2p_z)^1$. Very likely an avoided crossing would happen, if a stronger confining potential were used, in which the configuration $(1\sigma_g)^2(1\sigma_u)^2(2\sigma_g)^1(2\sigma_u)^1(3\sigma_g)^2$ would become dominant, leading to the dissociation limit of two excited ^{3}S $[(1s)^2(2s)^1(2p_z)^1]$ Be atoms.

The two low-lying $^1\Pi$ states of Be_2 possess fundamentally different characteristics from the $^1\Sigma$ states when enclosed in a cylindrical potential. The A' $^1\Pi_g$ state is well-characterized at the equilibrium internuclear separation by the configuration $(1\sigma_g)^2(1\sigma_u)^2(2\sigma_g)^2(2\sigma_u)^1(1\pi_u)^1$, which results from the single excitation of $2\sigma_u \rightarrow 1\pi_u$. This configuration remains unchanged with various strengths of the confining harmonic potential. Note that the $2p_x$ and $2p_y$ orbitals, which constitute the $1\pi_u$ and $1\pi_g$ sets of molecular orbitals, are destabilized because of the increased electrostatic repulsion with the potential that encapsulates the molecule in the x- and y-directions. This interaction enlarges the 2s-$2p_{x/y}$ separation and supresses the contribution from the configuration $(1\sigma_g)^2(1\sigma_u)^2(2\sigma_g)^1(2\sigma_u)^2(1\pi_g)^1$, as the required excitation $2\sigma_g \rightarrow 1\pi_g$ is less feasible. The larger 2s-$2p_{x/y}$ energy gap is also illustrated by the increase of the excitation energy T_e of A' $^1\Pi_g$ state when the potential is applied (see Table 4.2).

The A $^1\Pi_u$ state, on the other hand, is a mixture of $(1\sigma_g)^2(1\sigma_u)^2(2\sigma_g)^2(3\sigma_g)^1(1\pi_u)^1$ and $(1\sigma_g)^2(1\sigma_u)^2(2\sigma_g)^2(2\sigma_u)^1(1\pi_g)^1$, with the former being the dominant configuration. The first configuration ($\sim$ 70%) could be derived from the A' $^1\Pi_g$ whose electron in $2\sigma_u$ orbital is excited to $3\sigma_g$ orbital, while the second one ($\sim$ 19%) results from the single excitation $2\sigma_u \rightarrow 1\pi_g$ of the ground state Be_2. The weight ratio of these configurations is apparently independent of the strength of the harmonic po-

tential, and approximately the same ratio (0.70:0.19) is found for the three different values of ω.

Application of confinement leads to change of the characteristics of the dissociation limit of the two low-lying Π states. These two states correlate to the same dissociation limit of Be(^{1}S) and Be(^{1}P) without the influence of an external potential. The two configurations of A $^1\Pi_u$ state interact strongly at large internuclear distances, and the avoided crossing causes the domination of the configuration of $(1\sigma_g)^2(1\sigma_u)^2(2\sigma_g)^2(2\sigma_u)^1(1\pi_g)^1$, leading to the Be(^{1}S) and Be(^{1}P) dissociation limit. The A' $^1\Pi_g$ state, however, retains the electronic configuration of $(1\sigma_g)^2(1\sigma_u)^2(2\sigma_g)^2(2\sigma_u)^1(1\pi_u)^1$ until the dissociation limit, giving Be(^{1}S) and Be(^{1}P) atoms. When the molecule is placed in cylindrical harmonic potential, these two states switch to correlate to the ^{3}S(2s2p$_z$) + ^{3}P(2s2p$_{x/y}$) limit. The MCQDPT calculations reveal that the configuration $(1\sigma_g)^2(1\sigma_u)^2(2\sigma_g)^2(3\sigma_g)^1(1\pi_u)^1$ dominates the A $^1\Pi_u$ state for the whole range of internuclear separations, and the avoided crossing with the other $^1\Pi_u$ states disappears. Elimination of the avoided crossing allows for the proper dissociation of this state to two singly excited Be atoms. In contrast with the single-configuration nature of the A $^1\Pi_u$ state in a tubular confining environment, the A' $^1\Pi_g$ state shows variation of configuration with the internuclear distance. At distances close to the equilibrium separation the dominant configuration remains $(1\sigma_g)^2(1\sigma_u)^2(2\sigma_g)^2(2\sigma_u)^1(1\pi_u)^1$, while at larger distances the contribution from $(1\sigma_g)^2(1\sigma_u)^2(2\sigma_g)^1(2\sigma_u)^1(3\sigma_g)^1(1\pi_u)^1$ grows very rapidly and leads to the ^{3}S(2s2p$_z$) + ^{3}P(2s2p$_{x/y}$) limit. The latter configuration represents a one-electron promotion, $2\sigma_g \rightarrow 3\sigma_g$, of the A' $^1\Pi_g$ state. The change of configurations at large internuclear separations suggests the existence of an avoided crossing between the A' $^1\Pi_g$ and $2^1\Pi_g$ states under the effect of the applied potential.

The peculiar asymptotic behavior has also been studied using the full CI/cc-pVQZ approach for beryllium atom encapsulated in the cylindrical potential. Selected results are presented in Table 4.4 and Table 4.5. Several observations are noteworthy. Firstly, the singlet-triplet energy gaps for the P states (2p$_x$, 2p$_y$) and S state (2p$_z$) become larger with a stronger potential. The effect is more pro-

Table 4.4: Atomic energies[a] of Be using FCI/cc-pVQZ

ω	$^1S(2s^2)$	$^1S(2s2p_z)$	$^3S(2s2p_z)$	$^1P(2s2p_x)$	$^3P(2s2p_x)$
0.0	-14.640124	-14.442934	-14.540023	-14.442934	-14.540023
0.1	-14.589412	-14.387449	-14.497212	-14.370203	-14.478794
0.2	-14.463418	-14.255730	-14.390852	-14.215373	-14.331860

[a] In atomic units

Table 4.5: Estimated asymptotic energies[a] of Be_2 using FCI/cc-pVQZ

ω	$^1S(2s^2)$ $+^1S(2s^2)$	$^1S(2s^2)$ $+^1P(2s2p_x)$	$^1S(2s^2)$ $+^1S(2s2p_z)$	$^3P(2s2p_x)$ $+^3S(2s2p_z)$
0.0	-29.280248	-29.083057	-29.083057	-29.080046
0.1	-29.178825	-28.959615	-28.976861	-28.976006
0.2	-28.926835	-28.678790	-28.719148	-28.722713

[a] In atomic units

nounced for the $^1S(2s2p_z)$ configuration. This observation can be rationalized by considering that p_x (as well as p_y) orbitals are more susceptible to the Coulomb repulsion induced by the potential than the p_z orbitals. Similar conclusions have also been reached by Vorontsova and co-workers using perturbation theory [24]. The triplet state is more stable than the singlet state according to the Hund's rule. In the present case, a particular configuration with either the singlet or triplet spin state experiences the same magnitude of Coulomb repulsion with the potential, but the triplet state gains extra stability due to the exchange interaction between two electrons with parallel spins that offsets the destabilization from the Coulomb repulsion, resulting in the triplet state being more stable than the singlet counterpart. Secondly, the energy difference between $^1S(2s^2)$ and $^3S(2s2p_z)$ is reduced by the confinement. In the presence of a confining potential, the excitation energy of an electron from 2s to $2p_z$ orbital is slightly increased by two counteracting interactions. The first one is the relaxation of Coulomb interaction between electrons in the Be atom when one electron is promoted to $2p_z$ orbital which overlaps less with the 2s orbital. The second one is the increased electrostatic repulsion between the $2p_z$ orbital and the potential. The greater energy gap with the stronger applied

Table 4.6: Adiabatic electron affinities (AEA) and vertical electron affinities (VEA) of Be_2 and vertical electron detachment energies (VEDE) and equilibrium internuclear distances r_e of Be_2^- [a]

ω	0.0	0.1	0.2	Experiment[f]
AEA	0.360	-1.116	-3.775	0.450[b], 0.398[c], 0.324[d], 0.337[e]
VEA	0.264	-1.138	-3.864	0.442[b], 0.392[c], 0.316[d], 0.332[e]
VEDE	0.412	-1.095	-3.686	0.467[b], 0.405[c], 0.327[d], 0.341[e]
r_e	2.2303	2.4076	2.2198	2.2384[g]

[a] Affinities in eV and r_e in a.u. [b] MP2 [c] MP4(SDTQ) [d] CCSD(T) [e] CCSDT [f] Ref [41] [g] Ref [44]

potential indicates that the second interaction plays the major role in determining the relative stabilities of $^1S(2s^2)$ and $^1S(2s2p_z)$ states. On the other hand, Be atom with $(2s2p_z)$ configuration favors the triplet state and a large stability is gained from the exchange interaction between the unpaired electrons. The combined effect diminishes the separation of the $^1S(2s^2)$ and $^3S(2s2p_z)$ states, and causes the switch of the ordering of dissociation limits.

4.3.4 Electron Affinities

In addition to the electronic structure calculations of the neutral beryllium dimer, the computations of electron affinities of Be_2 have also been performed. The potential energy curves of the ground-state Be_2^- molecular ion were computed using CASSCF/MCQDPT with the active space identical to that used in the calculations of Be_2 to maintain consistency. Three types of electron affinities have been evaluated: (1) adiabatic electron affinity (AEA), (2) vertical electron affinity (VEA), and (3) vertical electron detachment energy (VEDE). The results are collected in Table 4.6. These quantities have recently been computed in the Møller-Plesset perturbation and coupled-cluster approaches using the 6-311+G(3d2f) basis set [41]. The results from the present study agree fairly well with those data but the computed AEA agrees better with the value calculated by Wright using multi-reference double CI [42]. The positive electron affinities support the conclusion from previous calculations that Be_2 binds an electron to form a stable Be_2^- [43]. However, the electron

affinity values become negative when a potential is applied to the system, indicating that the molecular ion is less stable than the neutral species. This instability may be attributed to the fact that when the electrons are confined within the molecule by the potential, repulsion between electrons is enhanced. Accordingly, addition of an extra electron to Be_2 further destabilizes the system and gives rise to a negative electron affinity. Interestingly, the studies of the Be_2^- ion show that the ground state symmetry switches from $^2\Pi_u$ to $^2\Sigma_g^+$, and r_e increases. These observations are consistent with the results from atomic calculations on beryllium atom that show the set of $2p_x$ and $2p_y$ orbitals being strongly destabilized by the potential; in consequence, the near-degeneracy of π_u-σ_g molecular orbitals is removed and $3\sigma_g$ orbital becomes energetically lower than $1\pi_u$ orbitals.

4.4 Conclusion

Calculations for the ground and several low-lying singlet excited states of Be_2 under the influence of a cylindrical harmonic potential have been performed. The results demonstrate that the applied potential increases the binding energies of all the states, and shortens the bond lengths. In addition, the potential induces the re-ordering of the molecular orbitals, resulting in the change of dissociation limits of the two Π states. The electron affinities of Be_2 have also been computed. The decrease of these quantities shows that Be_2 is unlikely to bind an electron in the presence of the potential because of the increased electron-electron repulsion. The calculations indicate again a possibility to finely manipulate and adjust the properties of a molecule using external potentials.

Bibliography

[1] L. Jacak, P. Hawrylak, A. Wójs, *Quantum Dots*, Springer, New York, 1998.

[2] J. P. Connerade, V. K. Dolmatov, P. A. Lakshmi, S. T. Manson, *J. Phys. B: At. Mol. Opt. Phys.* **32**, L239 (1999).

[3] D. Bielińska-Wąż, J. Karwowski, G. H. F. Diercksen, *J. Phys. B: At. Mol. Opt. Phys.* **34**, 1987 (2001).

[4] P. K. Chattaraj, U. Sarkar, *J. Phys. Chem. A* **107**, 4877 (2003).

[5] S. Bednarek, B. Szafran, J. Adamowski, *Phys. Rev. B* **59**, 13036 (1999).

[6] J. Garza, R. Vargas, A. Vela. K. D. Sen, *J. Mol. Struct. (THEOCHEM)* **501**, 183 (2000).

[7] T. Sako, G. H. F. Diercksen, *J. Phys. B: At. Mol. Opt. Phys.* **36**, 1681 (2003).

[8] D. Bielińska-Wąż, G. H. F. Diercksen, M. Klobukowski, *Chem. Phys. Lett.* **349**, 215 (2001).

[9] W. H. Furry, J. H. Bartlett, Jr., *Phys. Rev.* **38**, 1615 (1931).

[10] B. J. Ransil, S. Fraga, *J. Chem. Phys.* **35**, 669 (1961).

[11] C. F. Bender, E. R. Davidson, *J. Chem. Phys.* **47**, 4972 (1967).

[12] R. O. Jones, *J. Chem. Phys.* **71**, 1300 (1979).

[13] V. Klimo, J. Tino, *Collect. Czech. Chem. Commun.* **46**, 3171 (1981).

[14] R. J. Harrison, N. C. Handy, *Chem. Phys. Lett.* **98**, 97 (1983).

[15] V. E. Bondybey, *Chem. Phys. Lett.* **109**, 436 (1984).

[16] G. A. Peterson, W. A. Shirley, *Chem. Phys. Lett.* **160**, 494 (1989).

[17] W. A. Shirley, G. A. Peterson, *Chem. Phys. Lett.* **181**, 588 (1991).

[18] I. Røeggen, J. Almlöf, *Int. J. Quantum Chem.* **60**, 453 (1996).

[19] J. Stärck, W. Meyer, *Chem. Phys. Lett.* **258**, 421 (1996).

[20] L. A. Kaledin, A. L. Kaledin, M. C. Heaven, V. E. Bondybey, *J. Mol. Struct. (THEOCHEM)* **461-462**, 177 (1999).

[21] P. J. Bruna, J. S. Wright, *Can. J. Chem.* **74**, 998 (1996).

[22] D. Bégué, M. Mérawa, M. Rérat, C. Pouchan, *J. Chem. Phys.* **110**, 2051 (1999).

[23] M. Pecul, M. Jaszuński, H. Larsen, P. Jørgensen, *J. Chem. Phys.* **112**, 3671 (2000).

[24] I. A. Abronin, I. K. Vorontsova, I. D. Mikheikin, *Chem. Phys Lett.* **368**, 523 (2003).

[25] H. Nakano, *J. Chem. Phys.* **99**, 7983 (1993).

[26] W. Zou, M. Lin, X. Yang, B. Zhang, *Phys. Chem. Chem. Phys.* **5**, 1106 (2003).

[27] E. L. Rachofsky, J. B. Alexander Ross, M. Krauss, R. Osman, *J. Phys. Chem. A* **105**, 190 (2001).

[28] M. W. Schmidt, K. K. Baldridge, J. A. Boatz, S. T. Elbert, M. S. Gordon, J. H. Jensen, S. Koseki, N. Matsunaga, K. A. Nguyen, S. J. Su, T. L. Windus, M. Dupuis, J. A. Montgomery, *J. Comput. Chem.* **14**, 1347 (1993).

[29] T. H. Dunning, Jr. *J. Chem. Phys.* **90**, 1007 (1989).

[30] T. Sako, G. H. F. Diercksen, *J. Phys. B: At. Mol. Opt. Phys.* **36**, 1433 (2003).

[31] F. Jensen, *Introduction to Computational Chemistry*, Wiley, New York, 1999.

[32] H. G. Kuhn, *Atomic Spectra*, Longmans, London, 1962.

[33] M. W. Schmidt, K. Ruedenberg, *J. Chem. Phys.* **71**, 3951 (1979).

[34] J. N. Murrell, K. S. Sorbie, *J. Chem. Soc. Faraday Trans. II* **70**, 1552 (1974).

[35] R. Rydberg, *Z. Phys.* **73**, 376 (1931).

[36] Z. H. Zhu, S. Y. Shen, W. M. Mou, L. Li, *J. Mol. Sci. (Wuhan, China)* **2**, 79 (1984).

[37] P. Huxley, J. N. Murrell, *J. Chem. Soc. Faraday Trans. II* **79**, 323 (1983).

[38] F. B. van Duijneveldt, J. G. C. M. van Duijneveldt-van de Rijdt, J. H. van Lenthe, *Chem. Rev.* **94**, 1873 (1994).

[39] S. F. Boys, F. Bernardi, *Mol. Phys.* **19**, 553 (1970).

[40] J. L. McHale, *Molecular Spectroscopy*, Prentice-Hall, Toronto, 1999.

[41] I. G. Kaplan, O. Dolgounitcheva, J. D. Watts, J. V. Ortiz, *J. Chem. Phys.* **117**, 3687 (2002).

[42] P. J. Bruna, G. A. Di Labio, J. S. Wright, *J. Phys. Chem.* **96**, 6269 (1992).

[43] K. D. Jordan, J. Simons, *J. Chem. Phys.* **77**, 5250 (1982).

[44] C. W. Bauschlicher, H. Partridge, *J. Chem. Phys.* **80**, 334 (1984).

Chapter 5

Configuration Interaction Calculations on Beryllium Molecular Ion in Cylindrical Harmonic Confining Potential

This chapter[1] is the continuation of the Chapter 4 in which the discussions are extended to the effects on the molecualr structure and properties of the low-lying electronic states of the molecular ion of Be_2 due to the presence of the harmonic confining potential.

5.1 Introduction

Objects embedded in various forms of one-, two- and three-dimensional confinements are one of the major research areas in condensed-matter physics, nanotechnology and engineering. These systems exhibit novel characteristics with potential applications in such areas as solid-state devices [1], nano-electronics [2] and nonlinear optical materials [3]. A significant effort has been devoted to the syntheses of these materials and the experimental investigations of their properties. Simultaneously, theories have also been developed in order to understand the experimental observations (see e.g. [4, 5, 6]). Confinement effects have been demonstrated also in chemistry where

[1] A version of this chapter was published in *Mol. Phys.* **103**, 2599 (2005).

they result in, for instance, the formation of the neon dimer in a fullerene [7], the increased electronegativity and decreased polarizability of the first-row elements in a spherical cavity [8], pressure-induced variation of the dipole moment of ammonia [9], and the development of hyperpolarized ^{129}Xe NMR technique as a probe to study the structures of mesoporous materials [10].

In most of the theoretical studies of confined systems, the harmonic potential was utilized because it allows the Hamiltonian of systems of two or more particles to become exactly or quasi-exactly solvable under appropriate coordinate transformations [11]; this potential also serves as an excellent model to approximate quantum dots [12]. A series of studies involving two-electron system, helium atom, hydrogen molecule and lithium dimer confined in 3-dimensional harmonic oscillator potentials has recently been conducted by Diercksen and coworkers [13, 14, 15, 16, 17], and some intriguing changes in electronic structures and spectral properties of these systems were observed. In the present work, the studies of the effects of confinement were extended to the molecular cation of beryllium (Be_2^+).

Alkaline-earth dimers are one of the most challenging systems to be studied theoretically. They are formed from two closed s-shell atoms and predicted to have a zero bond-order according to the simple molecular orbital (MO) theory; on the other hand, they have been detected experimentally in the gas phase [18, 19]. Among these species beryllium is the most spectacular since it exhibits an irregularity in the trend of binding energy of Group IIA dimers. Extensive configuration interaction calculations show that satisfactory results could be obtained only if all the correlation effects are included [20].

Despite the extensive studies on Be_2, investigations on the corresponding Be_2^+ are relatively limited. The experimental research on Be_2^+ is to a very large extent restricted by the difficulty in generation and the instability of Be_2. Therefore, only very little is known experimentally about Be_2^+. However, this system has recently been a subject of a number of theoretical studies [21, 22, 23, 24] for several reasons. Firstly, understanding the formation of charged metal clusters plays an important role in solid-state chemistry and condensed-matter physics. Accurate ex-

perimental or *ab initio* dimer potentials are necessary in order to perform molecular dynamic simulations of charged clusters, and explain experimental phenomena such as Coulomb explosion [25] and meta-stability [26]. Secondly, Be_2^+ is an interesting species in electron spin resonance (ESR) spectroscopy as it exists as a three valence-electron radical having low excitation energy. As the isotropic part of the hyperfine coupling constant depends on the s-character of the singly occupied molecular orbital, the strong s-p mixing may give rise to the molecular electron-spin g-factor very different from that of a free electron [27, 28]. Consequently, accurate determination of these parameters requires geometry and excitation energy obtained by the methods that can properly take into account the electron correlation effects.

In the present study we investigated the effects of an external potential on the electronic structure and spectrum of molecular ion. The ground and excited state potential energy curves (PECs) of Be_2^+ enclosed in a harmonic confining potential were computed using valence full configuration interaction (CI) method. The confining harmonic potential is of cylindrical symmetry aligned along the molecular axis. Spectroscopic constants were determined from the computed PECs, and the electronic structures of these states were analyzed. Differences between the PECs in field-free environment and under the confinement were discussed.

5.2 Computational Method

The current model of confining potential is the two-dimensional harmonic potential of cylindrical symmetry as discussed in Chpater 2. This model has been found of great use in several aspects of condensed-matter physics, atomic and molecular physics, and nanotechnology. It has been shown that small, two-dimensional quantum dots can be adequately described using a parabolic potential well [2]. In addition, the Hamiltonian of a molecular system embedded in a cylindrical harmonic potential can be applied to the case of a molecule in a parallel magnetic field [29].

In all calculations a correlation-consistent triple-zeta basis set, cc-pVTZ, was used [30], with the contraction pattern of (10s5p2d1f)/[4s3p2d1f]. In order to properly describe the effects of the harmonic confining potential, a set of (1s1p1d) func-

tions with orbital exponents of $\omega/2$ were added at the midpoint position between two Be nuclei. In all the calculations, the two 1s orbitals of Be were frozen, the complete valence space was included, and the virtual space was not truncated. The MCQDPT2 calculations of Be_2 revealed that the occupation numbers of the first two MOs are essentially 2 for the electronic states studied [31]. Therefore, the inclusion of only valence electrons in the CI calculations should be able to yield qualitative and semi-quantitative description of the electronic states of Be_2^+ that were studied in the present work.

All the CI calculations were performed using a modified version of GAMESS-US [32] and the configuration interaction code implemented by Ivanic and Ruedenberg [33].

5.3 Results and Discussion

5.3.1 Dissociation Channels

Four dissociation channels (I-IV) were investigated. The first channel (channel I) correlates to the ground-state product of Be (^1S_g) and Be^+ (^2S_g) and two molecular states are generated: X $^2\Sigma_u^+$ and 1 $^2\Sigma_g^+$. The next channel (channel II) is formed by the pair of states Be (^3P_u) and Be^+ (^2S_g) which result from the single excitation of Be atom from $1s^22s^2$ to $1s^22s2p$, leading to four pairs of 2 $^2\Sigma_{g,u}^+$, 1 $^2\Pi_{g,u}$, 1 $^4\Sigma_{g,u}^+$ and 1 $^4\Pi_{g,u}$ states. Channel III is composed of Be (^1S_g) and an excited Be^+ (^2P_u) due to the $2s \rightarrow 2p$ excitation. Four states are associated with this channel: 3 $^2\Sigma_{g,u}^+$ and 2 $^2\Pi_{g,u}$. Two possible atomic states can be obtained via $2s^2 \rightarrow 2s2p$ excitation of ground-state Be atom. While the triplet Be (^3P_u) and Be^+ (^2S_g) constitute the channel II, the singlet counterpart leads to the channel IV that correlates to the 4 $^2\Sigma_{g,u}^+$ and 3 $^2\Pi_{g,u}$ states.

The computed PECs of Be_2^+ are plotted in Figures 5.1-5.4 and the corresponding spectroscopic constants are listed in Tables 5.1-5.3.

Diercksen et al. [15, 17] and the present authors [31] predicted that an anisotropic confining potential would give rise to the differentiation of p-orbitals (which are degenerate in field-free space) because prolate-type and cylindrical harmonic potentials

Table 5.1: Spectroscopic Data for Doublet Σ States[a]

		Experiment[b]	$\omega = 0.00$	$\omega = 0.10$	$\omega = 0.20$	$\omega = 0.30$
X $^2\Sigma_u^+$	r_e	4.22	4.2433	4.1507	3.9914	3.8347
	ν_e	502	518.66	555.35	628.20	712.35
	$\nu_e x_e$	4.2	4.750	4.798	5.282	6.949
	D_e	1.97	1.99	2.27	2.85	3.53
	T_e	0.00	0.00	0.00	0.00	0.00
1 $^2\Sigma_g^+$	r_e	4.02	4.0792	4.0130	3.8858	3.7723
	ν_e	517	520.53	562.91	644.31	721.22
	$\nu_e x_e$	13.2	11.522	10.103	8.520	7.905
	D_e	0.39	0.43	0.72	1.53	2.56
	T_e	1.73	1.72	1.61	1.32	0.97
2 $^2\Sigma_g^+$	r_e	5.13	5.0980	4.8507	4.4448	4.2001
	ν_e	283	318.88	373.51	534.26	641.87
	$\nu_e x_e$		8.797	10.042	5.350	2.042
	D_e	0.78	0.84	0.84	1.05	1.62
	T_e	3.89	3.89	3.94	3.77	3.23
2 $^2\Sigma_u^+$	r_e	4.80	4.8529	4.6386	4.3799	4.1768
	ν_e		326.56	430.83	539.22	617.70
	$\nu_e x_e$		38.725	6.515	3.501	2.079
	D_e		0.012	0.16	0.65	1.36
	T_e	5.49	5.49	5.35	4.83	4.01
3 $^2\Sigma_u^+$	r_e	5.71	5.7331	5.8008	5.9604	6.1824
	ν_e	415	424.46	494.36	497.01	525.02
	$\nu_e x_e$		9.767	6.796	4.711	7.482
	D_e	0.14	0.20	0.24	0.40	0.51
	T_e	5.79	5.80	5.79	5.73	5.60
3 $^2\Sigma_g^+$	r_e	3.89	3.8663	3.7694	3.6705	
	ν_e	530	567.86	565.40	476.65	
	$\nu_e x_e$		14.275	22.425	130.182	
	D_e		0.22	0.12	0.013	
	T_e	6.48	6.47	6.91	7.82	

[a] r_e in atomic units, ν_e and $\nu_e x_e$ in cm^{-1}, D_e and T_e in eV.
[b] Experimental values for X $^2\Sigma_u^+$ and 1 $^2\Sigma_g^+$ states from Ref [22], others from Ref [24] for field-free environment.

Table 5.2: Spectroscopic Data for Doublet Π States[a]

		Experiment[b]	$\omega = 0.00$	$\omega = 0.10$	$\omega = 0.20$	$\omega = 0.30$
$1\ ^2\Pi_u$	r_e	3.56	3.5915	3.5283	3.4283	3.3490
	ν_e	818	812.69	849.58	914.48	963.70
	$\nu_e x_e$	6.2	5.975	6.029	6.520	7.272
	D_e	3.33	3.35	3.69	4.27	4.85
	T_e	1.37	1.35	1.59	2.17	3.08
$1\ ^2\Pi_g$	r_e	4.44	4.4378	4.3300	4.1323	3.9357
	ν_e	446	462.77	497.01	558.71	609.97
	$\nu_e x_e$	3.5	4.336	4.181	3.949	3.141
	D_e	1.03	1.10	1.42	2.05	2.87
	T_e	3.66	3.66	3.90	4.41	5.07
$2\ ^2\Pi_g$	r_e		4.0618	4.0078	3.9666	4.2115
	ν_e		600.38	610.05	529.22	375.95
	$\nu_e x_e$		31.396	31.447	67.244	1.832
	D_e		0.08	0.22	0.59	1.20
	T_e	6.00	6.01	6.29	6.77	7.24
$2\ ^2\Pi_u$	r_e	4.25	4.2477	4.1110	3.8890	3.7156
	ν_e	390	425.70	490.80	595.42	683.81
	$\nu_e x_e$		15.836	11.430	7.863	7.798
	D_e		0.13	0.28	0.90	1.80
	T_e	6.04	6.03	6.17	6.36	6.57
$3\ ^2\Pi_g$	r_e	4.48	4.4771	4.3835	4.1767	3.9823
	ν_e	600	780.74	753.95	754.44	810.42
	$\nu_e x_e$		27.113	21.061	13.201	13.032
	D_e	1.03	1.12	1.60	2.00	2.02
	T_e	6.25	6.24	6.55	7.06	7.57
$3\ ^2\Pi_u$	r_e	5.45	5.3571	4.8182	4.3848	4.1739
	ν_e	200	197.69	321.42	515.19	619.03
	$\nu_e x_e$		8.193	19.993	4.320	0.848
	D_e	0.16	0.31	0.75	1.30	1.60
	T_e	7.12	7.15	5.36	5.50	5.74

[a] r_e in atomic units, ν_e and $\nu_e x_e$ in cm^{-1}, D_e and T_e in eV.
[b] Experimental values for $1\ ^2\Pi_{g,u}$ states from Ref [22], others from Ref [24] for field-free environment.

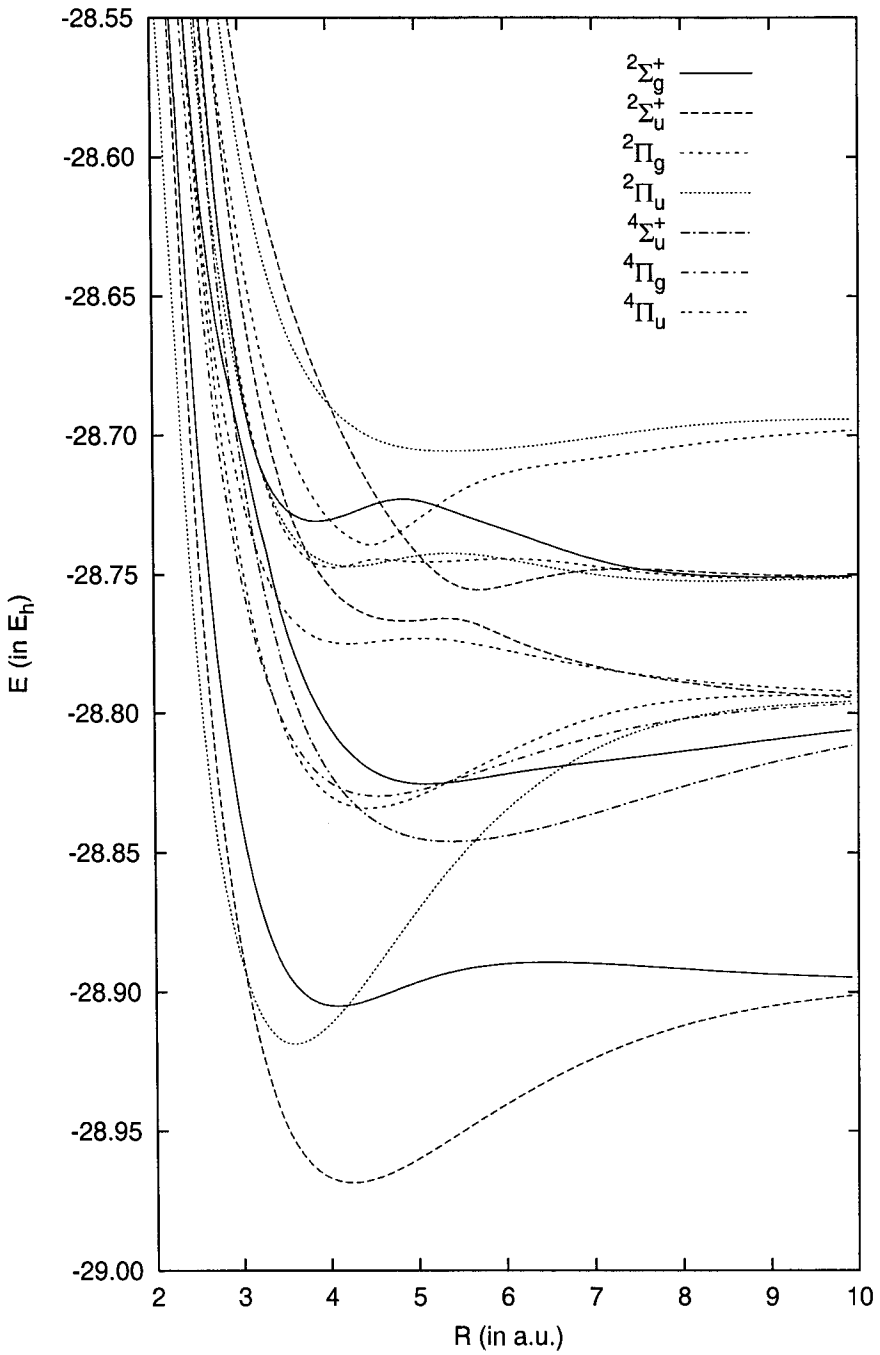

Figure 5.1: Potential energy curves of electronic states of Be_2^+ without confinement.

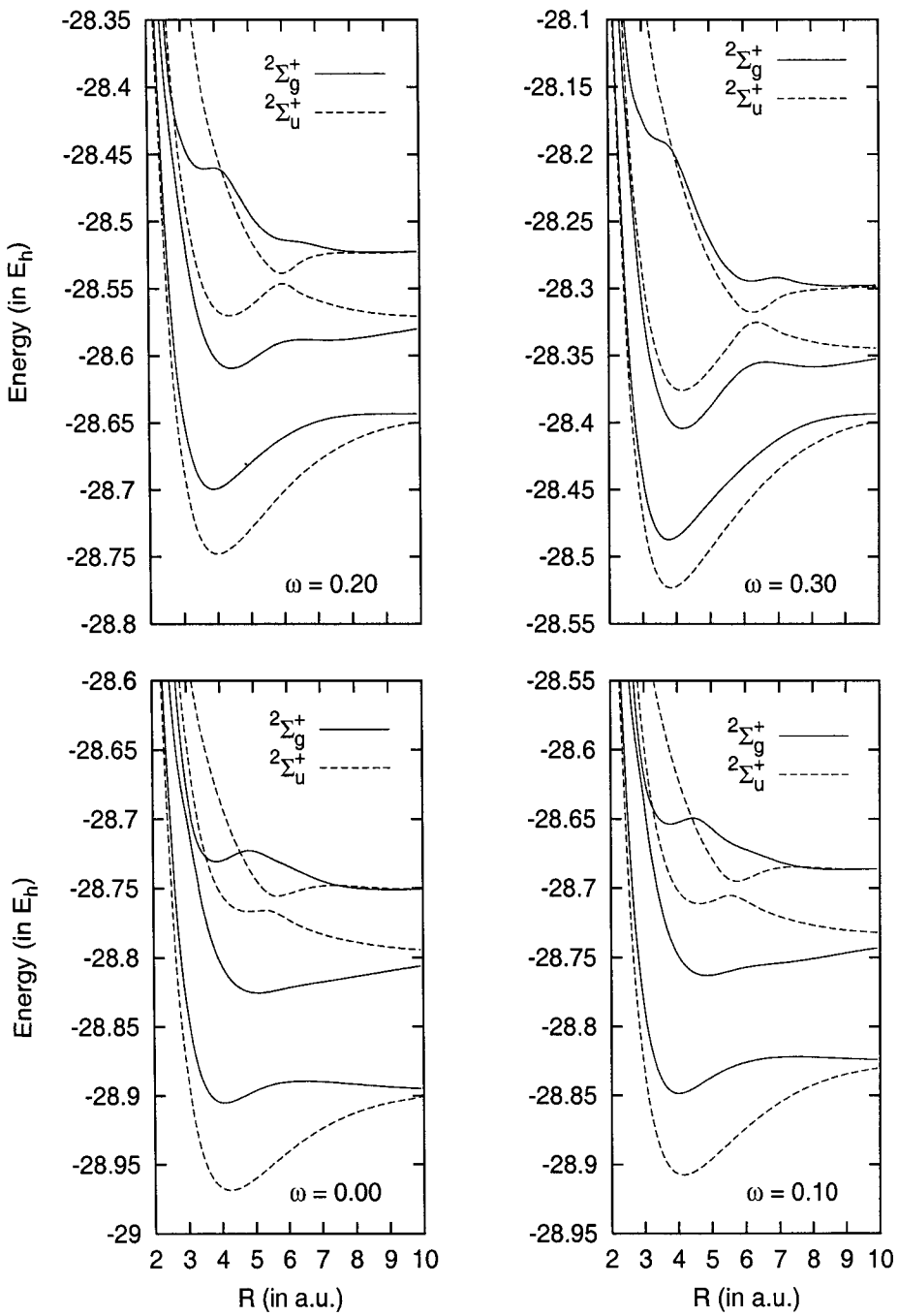

Figure 5.2: Selected $^2\Sigma$ states of Be_2^+ in confinement.

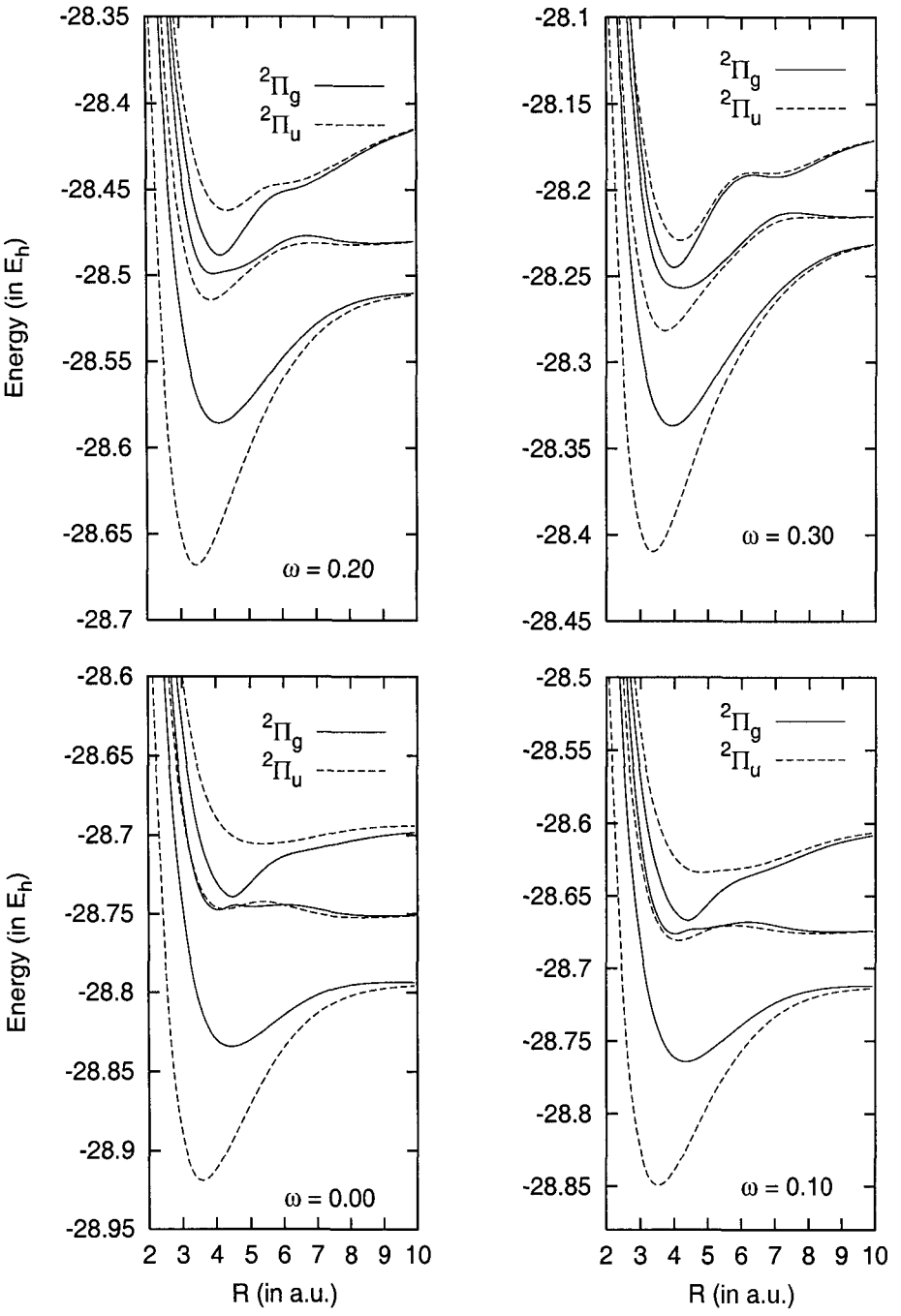

Figure 5.3: Selected $^2\Pi$ states of Be_2^+ in confinement.

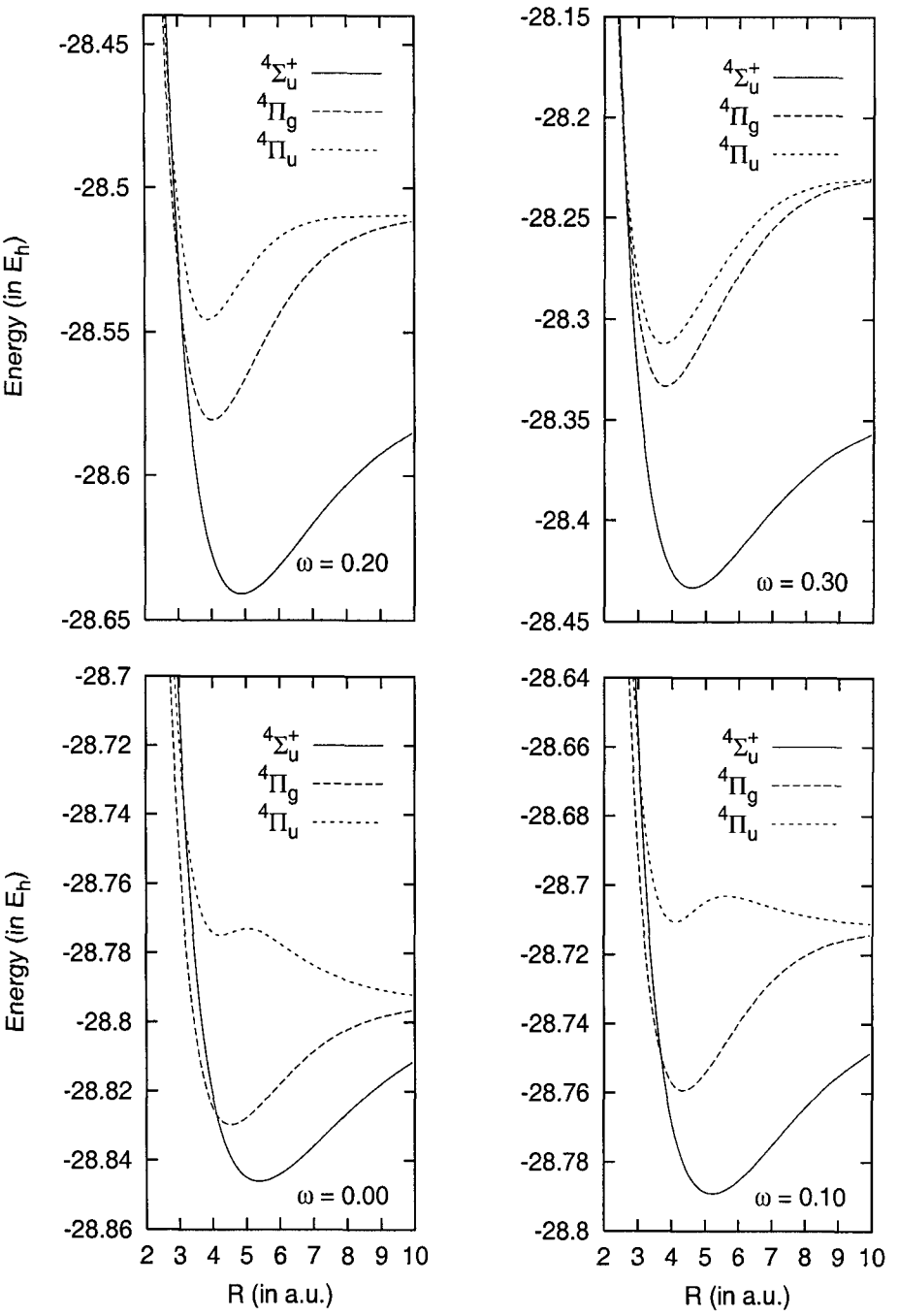

Figure 5.4: Selected quartet states of Be_2^+ in confinement.

Table 5.3: Spectroscopic Data for Selected Quartet States[a]

		Experiment[b]	$\omega = 0.00$	$\omega = 0.10$	$\omega = 0.20$	$\omega = 0.30$
$1\ ^4\Sigma_u^+$	r_e	5.43	5.3814	5.2125	4.8668	4.5741
	ν_e	278	284.61	304.33	371.38	439.63
	$\nu_e x_e$	2.2	2.398	1.809	2.352	2.194
	D_e	1.39	1.40	1.55	1.91	2.41
	T_e	3.30	3.33	3.22	2.91	2.45
$1\ ^4\Pi_g$	r_e	4.57	4.5438	4.3241	4.0134	3.7817
	ν_e	356	373.90	439.46	549.13	647.74
	$\nu_e x_e$	3.4	4.473	4.603	4.696	6.308
	D_e	0.93	0.90	1.23	1.88	2.77
	T_e	3.76	3.78	4.04	4.55	5.17
$1\ ^4\Pi_u$	r_e	4.20	4.2213	4.0819	3.8790	3.7329
	ν_e		363.46	449.25	556.37	626.27
	$\nu_e x_e$		28.563	14.077	7.166	6.002
	D_e		0.05	0.20	0.98	2.23
	T_e	5.25	5.27	5.36	5.50	5.74

[a] r_e in atomic units, ν_e and $\nu_e x_e$ in cm^{-1}, D_e and T_e in eV.
[b] Experimental values from Ref [22] for field-free environment.

with the principal axis overlapping the molecular axis destabilize p_x and p_y orbitals more strongly than the p_z orbitals. Consequently, all the channels that correlate to the dissociation products involving Be or Be^+ in P_u states should split into two subchannels, with the subchannel connected to the Π states lying higher in energy than that connected to the Σ states.

The calculated excitation energies of Be and Be^+ subjected to a confining potential, as measured by the spacing between channels, are summarized in Table 5.4.

Several trends are noticeable. Firstly, the channels II and III split into two subchannels, one corresponding to Σ states and the other Π states. Secondly, the spacings between the channel I (ground-state Be and Be^+) and Π-subchannels increase with increasing strengths of the confining potential, whereas the opposite trend is observed for the Σ-subchannels. These features suggest that the $2p_z$ orbital of Be atom becomes more stable than the $2p_x$ and $2p_y$ orbitals when the molecule

Table 5.4: Dissociation Channels of $Be_2^{+(a)}$

Channels	Experiment	$\omega = 0.00$	$\omega = 0.10$	$\omega = 0.20$	$\omega = 0.30$
Channel I	0.00	0.00	0.00	0.00	0.00
Σ-subchannel II	2.73	2.76	2.50	1.97	1.33
Π-subchannel II	2.73	2.76	3.00	3.64	4.43
Σ-subchannel III	3.96	3.92	3.76	3.30	2.61
Π-subchannel III	3.96	3.92	4.08	4.44	4.85
Π-subchannel IV	5.28	5.35	5.88	6.22	6.21

[a] Experimental data from Ref [34]; all values in eV.

is confined by a cylindrical repulsive potential. In addition, the $2s$ orbital is destabilized more intensely than the $2p_z$ orbital, thus reducing the $2s - 2p_z$ splitting.

5.3.2 Doublet Σ States

Several low-lying doublet Σ states of Be_2^+ and their response to the change of ω are depicted in Figure 5.2. The ground state of Be_2^+ is of $^2\Sigma_u^+$ symmetry, as reported by Fischer et al. [22] and Hogreve [23]. The predominant configuration of this state is $1\sigma_g^2 1\sigma_u^2 2\sigma_g^2 2\sigma_u^1$ throughout the entire range of the internuclear distance R. The presence of a confining potential increases both the well depth and the vibrational frequency, and shortens the equilibrium internuclear distance. These changes are expected, as the external potential enhances electron density within the space between nuclei, resulting in a strengthened bonding interaction.

The next $1\ ^2\Sigma_g^+$ state is characterized by a small local maximum at about 6.50 a.u. which is caused by the interaction between the $1\sigma_g^2 1\sigma_u^2 2\sigma_g^2 3\sigma_g^1$ and $1\sigma_g^2 1\sigma_u^2 2\sigma_g^1 2\sigma_u^2$ states [23]. At small R the former configuration is predominant while at $R > 8.00$ a.u. the latter becomes the most important contribution. As the confining potential is switched on, the local maximum moves towards larger values of R, and the $1\sigma_g^2 1\sigma_u^2 2\sigma_g^2 3\sigma_g^1$ state dominates over a larger range of R. This variation of configurations could be attributed to the lowering of $3\sigma_g$ MO which leads to a smaller $2\sigma_u \rightarrow 3\sigma_g$ excitation energy and increased accessibility of the $3\sigma_g$ MO. The larger contribution of the $3\sigma_g$ MO increases the energy difference of the $1\sigma_g^2 1\sigma_u^2 2\sigma_g^2 3\sigma_g^1$ and the $1\sigma_g^2 1\sigma_u^2 2\sigma_g^1 2\sigma_u^2$ potential energy curves by stabilizing the former configuration,

thus shifting the avoided crossing towards larger R.

The $2\ ^2\Sigma_g^+$ state in a field-free environment exhibits a broad potential minimum in the region around 5.10 a.u. Hogreve decided that the state is composed of the $1\sigma_g^2 1\sigma_u^2 1\pi_g^2 2\sigma_g^1$ configuration [23] while Wright et al. suggested that the state arises from the $1\sigma_g^2 1\sigma_u^2 2\sigma_g^1 2\sigma_u^2$ configuration with a strong mixing with the $1\sigma_g^2 1\sigma_u^2 2\sigma_g^2 3\sigma_g^1$ configuration. The present study supports the latter conclusion that $1\sigma_g^2 1\sigma_u^2 2\sigma_g^1 2\sigma_u^2$ is the predominant configuration at $R \approx r_e$ while at large R the state is determined by both the $1\sigma_g^2 1\sigma_u^2 2\sigma_g^2 3\sigma_g^1$ and $1\sigma_g^2 1\sigma_u^2 2\sigma_u^2 3\sigma_g^1$ configurations.

A drastic change of the PEC of the $2\ ^2\Sigma_g^+$ state was observed when the cylindrical harmonic potential is present. A potential hump appears at $R \approx 6.00$ a.u. which may be caused by an avoided crossing with a higher $^2\Sigma_g^+$ state. In addition, a second minimum (absent in the field-free case) is formed at about 8.00 a.u. when $\omega = 0.30$ a.u., possibly due to the enhanced bonding interaction of $3\sigma_g$ MO, via configuration mixing, at large R. Besides the altered shape of PEC, the major configuration of the state at the region close to r_e changes from $1\sigma_g^2 1\sigma_u^2 2\sigma_g^1 2\sigma_u^2$ to a doubly-excited $1\sigma_g^2 1\sigma_u^2 2\sigma_g^1 3\sigma_g^2$ in the presence of the external potential. The value of T_e drops from 3.89 eV to 3.23 eV when ω increases from 0.00 to 0.30 a.u., in consequence of the smaller splitting between $3\sigma_g$ and the valence $2\sigma_g$ and $2\sigma_u$ MOs that favours the $2\sigma_g^2 2\sigma_u^1 \rightarrow 2\sigma_g^1 3\sigma_g^2$ double excitation.

For $\omega = 0.00$ a.u., the states $2\ ^2\Sigma_u^+$ and $3\ ^2\Sigma_u^+$ are involved in an avoided crossing at about 5.7 a.u. which results in the metastability of the minimum of the $2\ ^2\Sigma_u^+$ state at 4.85 a.u. whose binding energy is less than 100 cm^{-1}, and in the minimum of the $3\ ^2\Sigma_u^+$ state. Very strong configuration interaction occurs for these states. For $R < 5.00$ a.u., the predominant configuration of the $2\ ^2\Sigma_u^+$ state is $1\sigma_g^2 1\sigma_u^2 2\sigma_g^1 2\sigma_u^1 3\sigma_g^1$ while the $3\ ^2\Sigma_u^+$ state is composed of a mixture of $1\sigma_g^2 1\sigma_u^2 2\sigma_g^2 3\sigma_u^1$ and $1\sigma_g^2 1\sigma_u^2 2\sigma_g^1 2\sigma_u^1 3\sigma_g^1$. When R exceeds the point of avoided crossing, these two states interchange the configurations. The $1\sigma_g^2 1\sigma_u^2 2\sigma_g^2 3\sigma_u^1$ configuration becomes the dominant one for the $2\ ^2\Sigma_u^+$ state, and the $3\ ^2\Sigma_u^+$ state possesses $1\sigma_g^2 1\sigma_u^2 2\sigma_g^1 2\sigma_u^1 3\sigma_g^1$ as the major component.

Both states become more strongly bound in the presence of the confining po-

tential, and the metastable minimum of the 2 $^2\Sigma_u^+$ state turns to a global minimum. Furthermore, the point of avoided crossing shifts towards larger values of R. These phenomena may be accounted for by considering that the antibonding $1\sigma_g^2 1\sigma_u^2 2\sigma_g^2 3\sigma_u^1$ structure is more destabilized by the applied potential than the bonding $1\sigma_g^2 1\sigma_u^2 2\sigma_g^1 2\sigma_u^1 3\sigma_g^1$ configuration. Hence, the repulsive PEC of $1\sigma_g^2 1\sigma_u^2 2\sigma_g^2 3\sigma_u^1$ configuration lifts in energy more rapidly and crosses the PEC of $1\sigma_g^2 1\sigma_u^2 2\sigma_g^1 2\sigma_u^1 3\sigma_g^1$ configuration at larger R. Meanwhile, as the $3\sigma_g$ MO is stabilized relative to the $2\sigma_u$ MO, the local minimum of 2 $^2\Sigma_u^+$ state, which is predominantly $1\sigma_g^2 1\sigma_u^2 2\sigma_g^1 2\sigma_u^1 3\sigma_g^1$, is significantly deepened, and becomes a global minimum for $\omega > 0.20$ a.u.

The 3 $^2\Sigma_g^+$ state is another state, besides the 2 $^2\Sigma_u^+$ state, that possesses a metastable minimum. The minimum is characterized by the $1\sigma_g^2 1\sigma_u^2 2\sigma_g^1 1\pi_u^2$ configuration. The state crosses with other higher Σ_g^+ states, yielding a local maximum at 4.85 a.u., which agrees well with the value reported by Wright et al. [24]. For $R > 5.00$ a.u. the state is dominated by a mixture of a strongly bonding $1\sigma_g^2 1\sigma_u^2 2\sigma_g^1 3\sigma_g^2$ and an antibonding $1\sigma_g^2 1\sigma_u^2 2\sigma_g^1 2\sigma_u^1 3\sigma_u^1$ configurations. The latter configuration is of increasing importance for larger R and eventually dominates the state and correlates to the dissociation products of Be ($1s^2 2s^2$) and Be^+ ($1s^2 2p_z^1$) (Σ-subchannel III).

In contrast to the 2 $^2\Sigma_u^+$ state, whose minimum becomes global and more strongly bound, the metastable minimum of the 3 $^2\Sigma_g^+$ state gradually disappears when ω increases, which suggests that the crossing between this state and other $^2\Sigma_g^+$ states at small R is eliminated by the potential. As shown in the study of Be atom [31], the triple degeneracy of 2p atomic orbitals is destroyed because of the symmetry of confining potential; the $2p_x$ and $2p_y$ orbitals lie at a higher energy than the $2p_z$ orbital. Accordingly, the dominant $1\sigma_g^2 1\sigma_u^2 2\sigma_g^1 1\pi_u^2$ configuration of the 3 $^2\Sigma_g^+$ state at $R = 3$ a.u. turns to be less stable compared to the repulsive $1\sigma_g^2 1\sigma_u^2 2\sigma_g^1 2\sigma_u^1 3\sigma_u^1$ configuration, and the local minimum vanishes. Surprisingly, a second minimum, lying 1000 cm^{-1} above the dissociation limit, starts to appear at about 6.00 a.u., possibly resulting from a new crossing between the 3 $^2\Sigma_g^+$ state and higher states. The new minimum arises from a strong mixing between the $1\sigma_g^2 1\sigma_u^2 2\sigma_g^1 3\sigma_g^2$ and

$1\sigma_g^2 1\sigma_u^2 2\sigma_g^1 2\sigma_u^1 3\sigma_u^1$ configurations, and the strongly bonding $1\sigma_g^2 1\sigma_u^2 2\sigma_g^1 3\sigma_g^2$ character contributes to the formation of the shallow minimum. At $R > 7.50$ a.u. the state turns to be repulsive again and is governed exclusively by the antibonding $1\sigma_g^2 1\sigma_u^2 2\sigma_g^1 2\sigma_u^1 3\sigma_u^1$ structure.

5.3.3 Doublet Π States

The first Π state, $1\ ^2\Pi_u$, is very strongly bound with the binding energy exceeding 3.30 eV; this may be attributed to a large number of bonding electrons [24]. The state arises from the $2\sigma_u \rightarrow 1\pi_u$ excitation, and the $1\sigma_g^2 1\sigma_u^2 2\sigma_g^2 1\pi_u^1$ configuration remains predominant throughout the entire range of R. The application of the confining potential shortens the bond length and increases the binding energy, as expected, due to the larger electron density between the two nuclei. However, no change of configurations is observed, and the state is still well described by the $1\sigma_g^2 1\sigma_u^2 2\sigma_g^2 1\pi_u^1$ configuration.

An interesting feature of the $1\ ^2\Pi_u$ state is the intersection with the ground-state $X\ ^2\Sigma_u^+$ PEC at 3.00 a.u. which provides a possible pathway of $^2\Pi_u \rightarrow\ ^2\Sigma_u^+$ predissociation. Hogreve showed that the predissociation can happen from the $v = 7$ vibrational level of the $1\ ^2\Pi_u$ state with extra energy of about 0.006 eV [23]. He also showed that this $^2\Pi_u - {}^2\Sigma_u^+$ intersection allows for the excitation of Be (^1S) to Be (^3P) via a rotational coupling in an inelastic scattering reaction of Be (^1S) and Be^+ (^2S). For $\omega > 0.00$ a.u., this intersection remains but it shifts to higher energy. In other words, the predissociation occurs less readily and higher energy is required in the inelastic scattering process in order to rotationally excite the ground-state of the Be^+ ion to its ^3P state. For instance, in the case of $\omega = 0.30$ a.u., the system can predissociate from the $v = 29$ vibrational level of the $1\ ^2\Pi_u$ state to the ground state with an excess energy of about 0.03 eV.

The $1\ ^2\Pi_g$ state lies about 2.3 eV above the $1\ ^2\Pi_u$ state. Because of the configuration mixing between $1\sigma_g^2 1\sigma_u^2 2\sigma_g^2 1\pi_g^1$ and $1\sigma_g^2 1\sigma_u^2 2\sigma_g^1 2\sigma_u^1 1\pi_u^1$ for $R \approx r_e$, the state has larger antibonding character (from the former configuration) and a smaller binding energy than the $1\ ^2\Pi_u$ state (1.10 eV *vs* 3.35 eV). The configuration mixing

in the region around r_e happens also when the external potential is applied. However, a new configuration, $1\sigma_g^2 1\sigma_u^2 2\sigma_g^1 3\sigma_u^1 1\pi_u^1$, appears to intervene, and becomes one of the major contributions at intermediate R. The increased contribution from the $1\sigma_g^2 1\sigma_u^2 2\sigma_g^1 3\sigma_u^1 1\pi_u^1$ configuration is not unexpected, since the exerted potential raises the energies of both $1\pi_g$ and $1\pi_u$ MOs while simultaneously lowering the energies of $3\sigma_g$ and $3\sigma_u$ MOs relative to the $2\sigma_u$ HOMO. This results in smaller $2\sigma_u \rightarrow 3\sigma_u$ excitation energy and larger contribution to the $1\ ^2\Pi_g$ state.

Both the $2\ ^2\Pi_g$ and $2\ ^2\Pi_u$ states have very complex PECs. They are members of channel III and are metastable with respect to the dissociation limit. In addition, they all possess multiple minima. For the $2\ ^2\Pi_g$ state, three local minima could be found at about 4.1, 5.0, and 9.0 a.u., whereas two minima, at 4.2 and 8.0 a.u. are found for the $2\ ^2\Pi_u$ state. This peculiar behaviour could result from the strong interaction with the high-lying $3\ ^2\Pi_g$ and $3\ ^2\Pi_u$ states that are correlated to the dissociation channel IV. An avoided crossing takes place between the $2\ ^2\Pi_g$ and $3\ ^2\Pi_g$ states at about 4.5 a.u. and leads to a small barrier on the $2\ ^2\Pi_g$ PEC, which lies 0.08 eV above the first minimum. At small R, the $2\ ^2\Pi_g$ state can be described by the $1\sigma_g^2 1\sigma_u^2 2\sigma_g^1 2\sigma_u^1 1\pi_u^1$ configuration, with a small admixture from the $1\sigma_g^2 1\sigma_u^2 2\sigma_g^2 1\pi_g^1$ configuration, while the $3\ ^2\Pi_g$ state comes almost entirely from the $1\sigma_g^2 1\sigma_u^2 2\sigma_g^1 2\sigma_u^1 1\pi_u^1$ configuration. When $R > 5.0$ a.u., however, an interchange of composition occurs in which the $1\sigma_g^2 1\sigma_u^2 2\sigma_g^1 2\sigma_u^1 1\pi_u^1$ configuration becomes predominant in the $2\ ^2\Pi_g$ state whereas the $3\ ^2\Pi_g$ state acquires a $1\sigma_g^2 1\sigma_u^2 2\sigma_g^2 1\pi_g^1$ character.

The changes of these states due to the influence of the confining potential are significant. Near equilibrium, the leading configuration $1\sigma_g^2 1\sigma_u^2 2\sigma_g^1 2\sigma_u^1 1\pi_u^1$ of the $3\ ^2\Pi_g$ state has a more diffuse electron density, and thus is more strongly destabilized by the cylindrical harmonic potential than the $1\sigma_g^2 1\sigma_u^2 2\sigma_g^2 1\pi_g^1$ configuration which is the major constituent of the $2\ ^2\Pi_g$ state. Hence, the splitting of the states at the point of avoided crossing becomes larger when the strength of applied potential increases from 0.00 to 0.30 a.u. and the maximum of the $2\ ^2\Pi_g$ state gradually disappears. Meanwhile, the PEC of $2\ ^2\Pi_g$ state becomes very irregular and a second maximum and minimum exist on the $2\ ^2\Pi_g$ and $3\ ^2\Pi_g$ states, respectively, at about

7.0 a.u., which are caused by a new avoided crossing.

Compared to the pair of 2 $^2\Pi_g$ and 3 $^2\Pi_g$ PECs, in which a serious mutual interference due to avoided crossings is observed, the PECs of 2 $^2\Pi_u$ and 3 $^2\Pi_u$ states are fairly well-separated. Both states are single-configurational at $R \approx r_e$; the 2 $^2\Pi_u$ state arises from the $2\sigma_g 2\sigma_u \rightarrow 3\sigma_g 1\pi_u$ double excitation and the 3 $^2\Pi_u$ state results from a high-energy $2\sigma_g \rightarrow 1\pi_g$ excitation. The 2 $^2\Pi_u$ state has energy very similar to the 2 $^2\Pi_g$ state because of the small energy gap between the $2\sigma_u$ and $3\sigma_g$ MOs. The potential hump of 2 $^2\Pi_u$ state at 5.4 a.u. is caused by the interaction with the 3 $^2\Pi_u$ state. In the region of $R > 5.4$ a.u., this avoided crossing switches the dominant configuration of the 2 $^2\Pi_u$ state to $1\sigma_g^2 1\sigma_u^2 2\sigma_g^1 2\sigma_u^1 1\pi_g^1$ and the 3 $^2\Pi_u$ state to $1\sigma_g^2 1\sigma_u^2 2\sigma_g^1 3\sigma_g^1 1\pi_u^1$.

In the presence of the cylindrical harmonic potential, the point of avoided crossing between the 2 $^2\Pi_u$ and 3 $^2\Pi_u$ states shifts to larger R. In addition, the inner minimum of the 2 $^2\Pi_u$ state becomes very strongly bound while the outer minimum disappears. Unlike the field-free case where there are three crossing points between the 2 $^2\Pi_{g,u}$ PECs, the entire 2 $^2\Pi_u$ PEC lies below that of the 2 $^2\Pi_g$ state when the system is confined. This behavior could be anticipated, since the 2 $^2\Pi_u$ state contains more electrons in bonding orbitals ($2\sigma_g^1 3\sigma_g^1 1\pi_u^1$) than the 2 $^2\Pi_g$ state ($2\sigma_g^2 1\pi_g^1$); furthermore, the $1\pi_g$ and $1\pi_u$ MOs are so destabilized that the $2\sigma_g 2\sigma_u \rightarrow 3\sigma_g 1\pi_u$ double excitation happens more readily than the $2\sigma_u \rightarrow 1\pi_g$ excitation. Therefore, the 2 $^2\Pi_u$ state becomes energetically more stable than the 2 $^2\Pi_g$ state in a confined environment.

5.3.4 Quartet States

Fischer et al. [22] and Wright et al. [24] computed the PECs for a number of quartet states of Be_2^+ using multi-reference CI method and extended basis sets. Spectroscopic constants as well as transition moments have been evaluated using the calculated PECs. In the present study, only three quartet states, 1 $^4\Sigma_u^+$, 1 $^4\Pi_g$ and 1 $^4\Pi_u$ were investigated since the other quartet states, except 1 $^4\Sigma_g^-$, are fairly high-lying (above the dissociation channel IV), and they, including 1 $^4\Sigma_g^-$, are all

correlated to channel V and channel VI [24] which are not discussed in the present work.

The lowest quartet state of Be_2^+ is 1 $^4\Sigma_u^+$ which lies about 3.3 eV above the ground state X $^2\Sigma_u^+$. This states has the same origin as the 2 $^2\Sigma_u^+$ and 3 $^2\Sigma_u^+$, i.e., it arises from the $2\sigma_g \rightarrow 3\sigma_g$ excitation. It is far more stable than the other two states because of the additional exchange interaction among the three unpaired electrons. On the other hand, the 1 $^4\Sigma_u^+$ state has a reduced bonding character compared to that of the ground state, as indicated by larger r_e, smaller D_e and ν_e; these effects may be attributed to the replacement of $2\sigma_g$ orbital by the less bonding $3\sigma_g$ orbital. As shown in Figure 4, the effects of confinement on this state are fairly typical: reduction of equilibrium bond distance is accompanied by an increase of binding energy and vibrational frequency. These can be attributed to the enhanced electron density between the two nuclei induced by the potential. Although the 1 $^4\Sigma_u^+$ state behaves differently from the 3 $^2\Sigma_u^+$ state in the variation of r_e with respect to ω, they, together with the 2 $^2\Sigma_u^+$ state, exhibit a decreased T_e in the presence of a confining potential. The changes of T_e for the 1 $^4\Sigma_u^+$ and 2 $^2\Sigma_u^+$ states are comparatively large ($\sim$ 27%) while that for the 3 $^2\Sigma_u^+$ is minimal ($\sim$ 3%) when the field strength goes up to $\omega = 0.30$ a.u. These results demonstrate that the $2\sigma_g - 3\sigma_g$ energy gap is reduced by the external potential which, due to its symmetry, selectively stabilizes the $3\sigma_g$ MO.

The 1 $^4\Pi_g$ state has a well-defined PEC which is slightly less bound than the 1 $^2\Pi_g$ state (0.90 eV vs 1.10 eV) despite the same dominating $1\sigma_g^2 1\sigma_u^2 2\sigma_g^1 2\sigma_u^1 1\pi_u^1$ configuration and dissociation channel. Interestingly, these two states cross at two positions: 3.5 a.u and 5.3 a.u. At $R \approx r_e$, the 1 $^4\Pi_g$ state lies 0.1 eV above the doublet counterpart but for $R > 5.3$ a.u. 1 $^4\Pi_g$ state becomes more stable. The intersection at 5.3 a.u. could be rationalized by the fact that the increased contribution of the antibonding $1\sigma_g^2 1\sigma_u^2 2\sigma_g^2 1\pi_g^1$ to the 1 $^2\Pi_g$ state weakens the attractive interaction at large R and makes it less stable relative to the 1 $^4\Pi_g$ state. On the other hand, the intersection at 3.5 a.u. is possibly caused by the exchange interaction of the 1 $^4\Pi_g$ state that partly overcomes the strong Coulomb repulsion at

small R, thus making the $1\ ^4\Pi_g$ state slightly more stable than the $1\ ^2\Pi_g$ state. For $\omega > 0.00$ a.u., both intersection points move towards larger R until $\omega = 0.30$ a.u. for which the outer intersection point disappears. For small and intermediate R, since the applied potential increases the electron density in the bonding region, the strengthened shielding effect on nuclei shrinks the internuclear distance. Simultaneously, however, the Coulomb repulsion between electrons is significantly increased. The $1\ ^2\Pi_g$ state is thus more destabilized than the $1\ ^4\Pi_g$ state where the Coulomb interaction is compensated by the exchange effect. In the large R region, the antibonding $1\sigma_g^2 1\sigma_u^2 2\sigma_g^2 1\pi_g^1$ and $1\sigma_g^2 1\sigma_u^2 2\sigma_g^1 3\sigma_u^1 1\pi_u^1$ configurations still dominate the $1\ ^2\Pi_g$ and $1\ ^4\Pi_g$ states, respectively. However, the stronger interaction between the $1\ ^2\Pi_g$ and $2\ ^2\Pi_g$ states provides additional stability to the $1\ ^2\Pi_g$ state, making it somewhat more stable than the $1\ ^4\Pi_g$ state.

For both zero- and nonzero-field situations, the $1\ ^4\Pi_u$ state has an interesting PEC that parallels the PEC of the $2\ ^2\Pi_u$ state, although they converge to two different limits (channels II and III, respectively). Both states originate from the configuration $1\sigma_g^2 1\sigma_u^2 2\sigma_g^1 3\sigma_g^1 1\pi_u^1$ which results from the $2\sigma_g 2\sigma_u \rightarrow 3\sigma_g 1\pi_u$ double excitation, and are metastable with respect to the dissociation products. The $1\ ^4\Pi_u$ state also experiences a change of configuration, from $1\sigma_g^2 1\sigma_u^2 2\sigma_g^1 3\sigma_g^1 1\pi_u^1$ to $1\sigma_g^2 1\sigma_u^2 2\sigma_g^1 2\sigma_u^1 1\pi_g^1$, at large R because of weak interaction with the $2\ ^4\Pi_g$ state, which is 2 eV above it. The interaction forms a hump at 5.0 a.u. and the antibonding character turns the PEC to be repulsive for $R > 5.0$ a.u. The stability of the $1\ ^4\Pi_u$ state relative to the $2\ ^2\Pi_u$ state could be attributed exclusively to the exchange interaction in the quartet state. The evolution of the $1\ ^4\Pi_u$ state PEC in a harmonic confining potential is similar to that of the $2\ ^2\Pi_u$ state, where the potential hump slowly disappears. This can be accounted for by the fact that the $1\sigma_g^2 1\sigma_u^2 2\sigma_g^1 3\sigma_g^1 1\pi_u^1$ configuration is stabilized by the reduced $2\sigma_u \rightarrow 3\sigma_g$ energy gap. The stronger bonding character from $3\sigma_g$ MO lowers the energy of the local minimum and leads to the shift of the point of avoided crossing towards larger R. For $\omega > 0.10$ a.u. the state becomes very strongly bound, and the minimum becomes global. As in the case without any external field, the $1\ ^4\Pi_u$ state at large R arises from the $2\sigma_g \rightarrow 1\pi_g$ excitation which

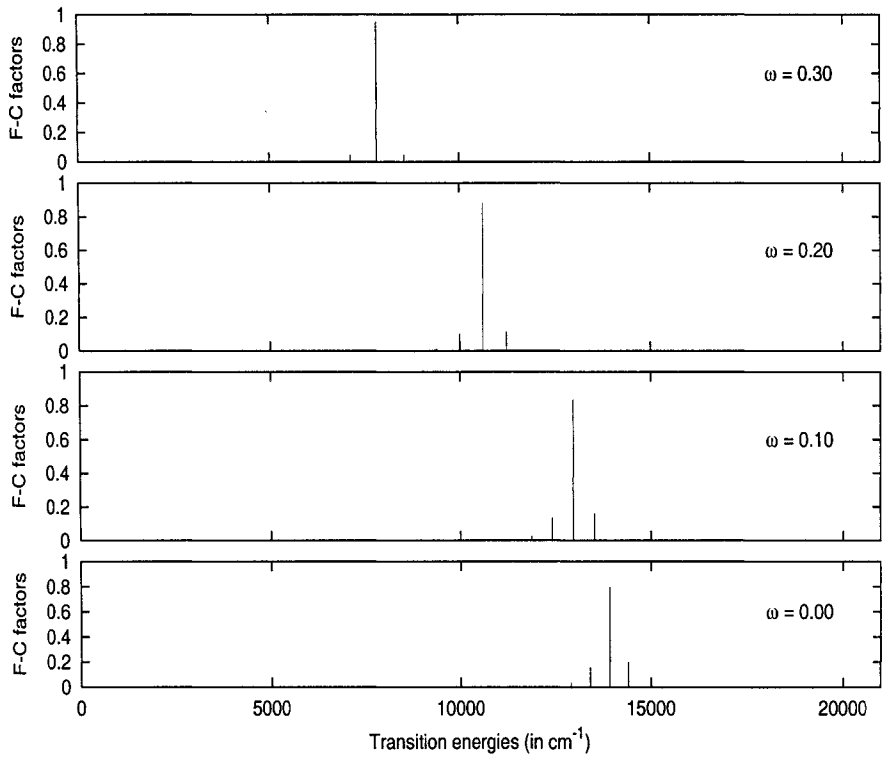

Figure 5.5: Franck-Condon factors for $X^2\Sigma_u^+ \leftrightarrow 1^2\Sigma_g^+$ transitions of Be_2^+.

is correlated to the Π-subchannel II.

5.3.5 Vibronic Spectra

The effects of confinement could be manifested not only in the changes of equilibrium internuclear distances and binding energies, but also in the electronic spectra of Be_2^+ confined in a potential. In order to elucidate the effects of confinement, the vibronic spectra of Be_2^+ due to the transitions $^2\Sigma_g^+ \leftrightarrow {}^2\Sigma_u^-$, $^2\Pi_u \leftrightarrow {}^2\Pi_g$, and $^2\Sigma_u^+ \leftrightarrow {}^2\Pi_g$ were calculated using LeRoy's program LEVEL [35], and the results were plotted in Figures 5.5-5.7. It was assumed that the transitions occur between the $v'' = 0$ level of the initial electronic state and the v' vibrational level of the final electronic state. The initial rotational state was fixed to be 1, i.e., $J'' = 1$, and only the P-branch, corresponding to $\Delta J = -1$, was included in each spectrum.

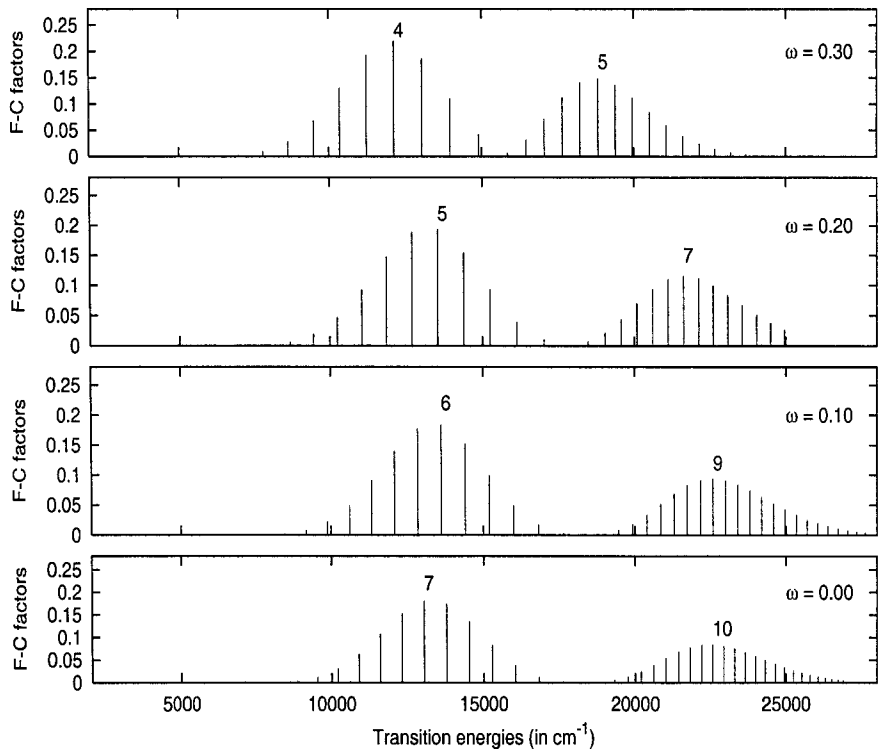

Figure 5.6: Franck-Condon factors for $1^2\Pi_g \leftrightarrow 1^2\Pi_u$ transitions of Be_2^+.

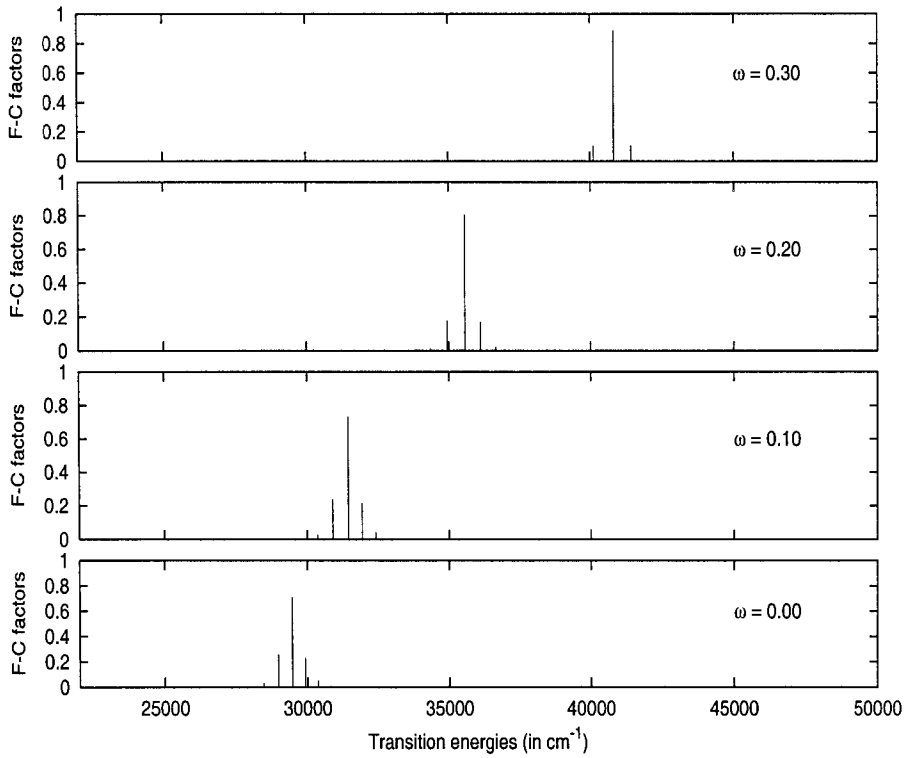

Figure 5.7: Franck-Condon factors for $X^2\Sigma_u^+ \leftrightarrow 1^2\Pi_g$ transitions of Be_2^+.

The states involved in these transitions result from the one-electron transitions $2\sigma_g \rightarrow 2\sigma_u/1\pi_u$ or $2\sigma_u \rightarrow 1\pi_g/1\pi_u/3\sigma_g$. The spectra exhibit very distinct features, and the differences between them may be rationalized in terms of the variations of the PECs of the electronic states involved. Both the $^2\Sigma_g^+ \leftrightarrow {}^2\Sigma_u^-$ and $^2\Pi_u \leftrightarrow {}^2\Pi_g$ spectra became red-shifted (with the former one more pronounced) when confining potential was present. On the other hand, the $^2\Sigma_u^+ \leftrightarrow {}^2\Pi_g$ spectrum was remarkably blue-shifted by the potential. These opposite shifts could be attributed to different relative changes of excitation energies, T_e, of these states (Tables 5.1 and 5.2). The reduction of T_e for the $1\,^2\Sigma_g^+$ state due to the confining potential induces a small red-shift ($\sim$ 7000 cm^{-1}, 0.8 eV) in its vibronic spectrum; nevertheless, the 40% increase in T_e for the $1\,^2\Pi_g$ state causes a considerable shift of the spectrum ($\sim$ 12000 cm^{-1}, 1.5 eV) towards high energies. On the other hand, the shift in the $^2\Pi_u \leftrightarrow {}^2\Pi_g$ spectrum is rather small, and this could be accounted for by the small change in the energy difference between the $1\,^2\Pi_g$ and $1\,^2\Pi_u$ states, which decreased from 2.31 eV (for $\omega = 0.00$ a.u.) to 1.99 eV (for $\omega = 0.30$ a.u.).

The spectra involving both the $^2\Sigma_g^+ \leftrightarrow {}^2\Sigma_u^-$ and $^2\Sigma_u^+ \leftrightarrow {}^2\Pi_g$ transitions show presence of intense $0-0$ transitions. The electronic states involved in these transitions possess very similar r_e, leading to excellent overlap of the $v = 0$ vibrational wavefunctions of the ground and excited electronic states. The disappearance of satellite peaks for $\omega > 0.10$ a.u. is related to the smaller difference in r_e, which is, at $\omega = 0.30$ a.u. about 0.06 a.u. for $^2\Sigma_g^+/^2\Sigma_u^+$ and 0.11 a.u. for $^2\Pi_g/^2\Sigma_u^+$.

The $^2\Pi_u \leftrightarrow {}^2\Pi_g$ vibronic spectrum, in contrast to the two previous spectra which are essentially featureless, is very rich in detail. The numbers shown on Figure 6 indicate the v' values of the final electronic state. These values (for both absorption and emission bands) decrease with increasing ω, suggesting that the difference in r_e is gradually reduced. This conclusion is also supported by results of the spectroscopic analysis for these states, that shows the reduction of the difference in r_e from 0.85 a.u., in the field-free case, to 0.59 a.u., for $\omega = 0.30$ a.u. In addition, the larger peak separations in the emission band, as compared to the absorption band, reveal that the $^2\Pi_u$ state is more strongly bound than the $^2\Pi_g$, as expected

given the bonding $1\sigma_g^2 1\sigma_u^2 2\sigma_g^2 1\pi_u^1$ character of the former state. Interestingly, the fact that the peak spacings for the absorption band increase faster than those for the emission band indicates that the confining potential affects the $^2\Pi_g$ state more than the $^2\Pi_u$ state; this observation again agrees with the greater changes in D_e and r_e for the $^2\Pi_g$ state relative to the $^2\Pi_u$ state.

5.4 Conclusion

The effects of external confining potential on the electronic states of the three-valence-electron Be_2^+ molecular ion have been investigated, and in total 15 states have been studied. In contrast to the two-electron hydrogen molecule, the multi-electron nature of Be_2^+ leads to a more complex bahaviour because of the Coulomb and exchange interactions among the valence electrons, as well as the core-valence correlation effects that might play an important role in the evolution of these electronic states subjected to the external potential.

Due to the geometrical constraints imposed by the cylindrical harmonic repulsive potential, the Σ- and Π-manifolds split at the dissociation limits, with the Π-channels being more destabilized. In addition, the Σ and Π electronic states behave in substantially different ways at $R < 10.00$ a.u. While the avoided crossing between the states 2 and 3 $^2\Sigma_u^+$ persists, an additional avoided crossing appears between 2 and 3 $^2\Sigma_g^+$ states, and it leads to metastable minima. On the other hand, the strong coupling of the $^2\Pi_g$ states that causes several local minima on the PEC of the 2 $^2\Pi_g$ state is, interestingly, slightly reduced by the confining potential. Moreover, the $^2\Pi_g$ and $^2\Pi_u$ states show the tendency of becoming degenerate at $R >$ 5.00 a.u. In contrast to the dramatic changes of the doublet counterparts, the quartet Σ and Π states demonstrate a typical response to the confining potential. The only significant variation is the disappearance of the barrier that occurs at 5 a.u. on the $^4\Pi_u$ state when the applied potential is stronger than 0.10 a.u.

Bibliography

[1] D. Yoshioka, *The Quantum Hall Effect*, Springer, New York, 2002.

[2] L. Jacak, P. Hawrylak, A. Wójs, *Quantum Dots*, Springer, New York, 1998.

[3] S. Schmitt-Rink, D. A. B. Miller, D. S. Chemla, *Phys. Rev. B.* **35**, 8113 (1987).

[4] E. Anisimovas, A. Matulis, *J. Phys.: Condens. Matter* **10**, 601 (1998).

[5] W. D. Heiss, R. G. Nazmitdinov, *Phys. Rev. B* **55**, 13707 (1997).

[6] P. A. Maksym, H. Imamura, G. P. Mallon, H. Aoki, *J. Phys. D: Condens. Matter* **12**, R299 (2000).

[7] J. Laskin, T. Peres, C. Lifshitz, M. Saunders, R. J. Cross, A. Khong, *Chem. Phys. Lett.* **285**, 7 (1998).

[8] P. K. Chattaraj, U. Sarkar, *J. Phys. Chem. A* **107**, 4877 (2003).

[9] S. A. Cruz, J. Soullard, *Chem. Phys. Lett.* **391**, 138 (2004).

[10] A. Nossov, E. Haddad, F. Guenneau, A. Gédéon, *Phys. Chem. Chem. Phys.* **5**, 4473 (2003).

[11] V. Singh, S. N. Biswas, K. Datta, *Phys. Rev. D* **18**, 1901 (1978).

[12] J. Karwowski, L. Cyrnek, *Annalen der Physik* **13**, 181 (2004).

[13] D. Bielińska-Wąż, J. Karwowski, G. H. F. Diercksen, *J. Phys. B: At. Opt. Mol. Phys.* **34**, 1987 (2001).

[14] D. Bielińska-Wąż, G. H. F. Diercksen, M. Klobukowski, *Chem. Phys. Lett.* **349**, 215 (2001).

[15] T. Sako, G. H. F. Diercksen, *J. Phys. B: At. Opt. Mol. Phys.* **36**, 1433 (2003).

[16] T. Sako, G. H. F. Diercksen, *J. Phys. B: At. Opt. Mol. Phys.* **36**, 1681 (2003).

[17] T. Sako, I. Cernusak, G. H. F. Diercksen, *J. Phys. B: At. Opt. Mol. Phys.* **37**, 1091 (2004).

[18] K. P. Huber, G. Herzberg, *Molecular Structure and Molecular Spectra*, Vol. IV, Van Nostrand Reinhold, New York, 1979.

[19] V. E. Bondybey, *Chem. Phys. Lett.* **109**, 436 (1984).

[20] R. O. Jones, *Adv. Chem. Phys.* **67**, 413 (1987).

[21] S. N. Khanna, F. Reuse, J. Buttet, *Phys. Rev. Lett.* **61**, 535 (1988).

[22] I. Fischer, V. E. Bondybey, P. Rosmus, H. J. Werner, *Chem. Phys.* **151**, 295 (1991).

[23] H. Hogreve, *Chem. Phys. Lett.* **187**, 479 (1991).

[24] B. Meng, B. J. Bruna, J. S. Wright, *Mol. Phys.* **79**, 1305 (1993).

[25] D. Tomanek, S. Mukherjee, K. H. Bennemann, *Phys. Rev. B* **28**, 665 (1983).

[26] C. W. Bauschlicher Jr., M. Rosi, *Chem. Phys. Lett.* **159**, 485 (1989).

[27] G. H. Lushington, P. J. Bruna, F. Grein, *Int. J. Quantum Chem.* **63**, 511 (1997).

[28] P. J. Bruna, F. Grein, *Mol. Phys.* **100**, 1681 (2002).

[29] K. Gottfried, T. M. Yan, *Quantum Mechanics: Fundamentals*, 2nd ed., Springer, New York (2004).

[30] T. H. Dunning, Jr. *J. Chem. Phys.* **90**, 1007 (1989).

[31] J. M. H. Lo, M. Klobukowski, *Mol. Phys.* **102**, 2511 (2004).

[32] M. W. Schmidt, K. K. Baldridge, J. A. Boatz, S. T. Elbert, M. S. Gordon, J. H. Jensen, S. Koseki, N. Matsunaga, K. A. Nguyen, S. J. Su, T. L. Windus, M. Dupuis, J. A. Montgomery, *J. Comput. Chem.* **14**, 1347 (1993).

[33] J. Ivanic, K. Ruedenberg, *Theoret. Chem. Acc.* **106**, 339 (2001).

[34] C. Moore, *Atomic Energy Levels*, US Government Printing Office, Washington DC, 1971.

[35] R. J. LeRoy, *Level 7.5: A Computer Program for Solving the Radial Schrödinger Equation for Bound and Quasibound Levels*, University of Waterloo Chemical Physics Research Report CP-655 (2002).

Chapter 6

Structure and Spectra of a Confined HeH Molecule

Both Chapters 6 and 7 are concerned primarily with the interactions of weakly-bound molecular species and the environment. In particular, the autoionization of noble-gas hydrides induced by the confining electrostatic potential is investigated. The studies of HeH molecule are described in this chapter, and the next chapter deals with the heavier NeH molecule.

6.1 Introduction

Confining potentials are frequently used to model the effects of environmental factors on properties of atoms and molecules, as for example the influence of plasma [1, 2], external magnetic fields [3], and surfaces [4, 5]. A good review of the subject has been written by Jaskólski [6] and recently by Karwowski [7]. The influence of confining potentials on properties of atoms has been analyzed extensively by several authors [8, 9, 10], and several studies on confined molecules have also been published. One should mention a detailed study of the H_2 molecule confined by a spherical harmonic potential [11] and another one on H_3^+ and H_2 in cylindrical confinements [12]. Effects of a cylindrical confining potential on the excited states of the H_2 molecule were studied [13] and detailed studies of the Li_2 in anisotropic harmonic potentials are available [14].

In the present work the influence of cylindrical harmonic confinement on the HeH

molecule has been investigated. HeH is one of the smallest diatomic molecules that has been the subject of theoretical studies in past several decades. Early molecular orbital studies predicted that HeH should possess a repulsive ground state but bound excited states [15]. Subsequent multi-reference configuration interaction calculations by Theodorakopoulos et al. also yielded the same conclusion [16]. However, no experimental evidence was available for the existence of bound excited electronic states of HeH until the detection of $B^2\Pi \rightarrow X^2\Sigma^+$ fluorescence of HeH via the reactive collision of excited H_2 and He [17] in 1985. Following this observation, several studies were devoted to the measurement and analysis of bound-free radiative decay and predissociation of these states [18, 19, 20, 21]. Up to now, about 14 states, corresponding to $n \leq 4$, have been fully characterized [22, 23, 24, 25], and many high-lying states ($11 \leq n \leq 34$) have been detected employing the field ionization technique [26]. In addition, a series of bound states (for $n = 5$) was located by the scattering R-matrix method [27].

Despite its simplicity, HeH molecule possesses unique properties in powerful UV lasers [28]. Noble gas hydrides belong to the family of Rydberg (or excimer) molecules characterized by their unstable ground state and bound excited states [29]. The stability of the excited states of HeH has been ascribed to the polarization of He by the H^+ core when the H(1s) electron is excited. The resulting system can thus be regarded as a pair of HeH^+ ion and an electron; the Coulombic interaction between the pair is rather weak, and the Rydberg electron is sensitive to any kind of external perturbation. Therefore, the effects of spatial confinement should be evident even when a relatively weak perturbation is applied.

Two particular effects were investigated in the present work. The first one is the influence of the confining potentials on the shapes of the potential energy curves, i.e., the vibronic spectra. To obtain a better understanding of this effect the ground and first few singlet excited states of HeH were calculated for several values of the potential strength ω, and wavefunction analysis in terms of orbital response to the external potentials was performed. The second effect is the ionization process induced by confinement. The values of the parameters defining the strength of con-

finement, under which the molecule in a given electronic state becomes ionized due to the confinement, were determined. These values are closely related to the intensity of external magnetic field that causes the field-induced ionization of magnetized molecules in the interstellar space.

The final problem addressed in this work is the applicability of the perturbation theory to the studies on the influence of confinement on molecular properties. While all the calculations have been performed using variational self-consistent-field (SCF) Roothaan-Hartree-Fock configuration interaction (CI) method, the analysis of results shows that the harmonic confining potentials can be treated as a perturbation to the HeH molecule, and a much simpler perturbation theory is adequate for the description of the effects of confinement.

6.2 Perturbation Theory of The Effects of Confinement

The Hamiltonian of a confined N-electron diatomic molecule is taken as

$$\hat{H}_\omega(\boldsymbol{r}, R) = \hat{H}_0(\boldsymbol{r}, R) + \mathcal{W}_\omega(\boldsymbol{r}), \tag{6.1}$$

where

$$\hat{H}_0(\boldsymbol{r}, R) = \hat{T}(\boldsymbol{r}) + \hat{V}_{en}(\boldsymbol{r}, R) + \hat{G}(\boldsymbol{r}) + \hat{V}_{nn}(R), \tag{6.2}$$

is the Born-Oppenheimer Hamiltonian of the free system, $\hat{T}(\boldsymbol{r})$, $\hat{V}_{en}(\boldsymbol{r}, R)$, $\hat{G}(\boldsymbol{r})$, and $\hat{V}_{nn}(R)$ represent, respectively, the operators describing the kinetic energy, the nuclear attraction potential, the electron and nuclear repulsion potentials; $\boldsymbol{r} \equiv \{\boldsymbol{r}_1, \boldsymbol{r}_2, \ldots, \boldsymbol{r}_N\}$ stands for the electron coordinates and R denotes the internuclear distance. The N-electron confining potential $\mathcal{W}_\omega(\boldsymbol{r})$ is defined as a sum of one-electron contributions:

$$\mathcal{W}_\omega(\boldsymbol{r}) = \sum_{i=1}^{N} W_\omega(\boldsymbol{r}_i), \tag{6.3}$$

where $\boldsymbol{r}_i = \{x_i, y_i, z_i\}$. In this work it is assumed that the molecular axis overlaps with the z-axis of the coordinate system, and that the confining potential is in the form of the cylindrical oscillator potential, i.e

$$W_\omega(\boldsymbol{r}_i) = \frac{\omega^2}{2}(x_i^2 + y_i^2), \tag{6.4}$$

The confinement expressed in terms of x^2+y^2 may model an external magnetic field. The Hamiltonian of an electron in a uniform magnetic field is:

$$\hat{H} = \frac{1}{2\mu}\left(\hat{\boldsymbol{p}} - \frac{e}{c}\hat{\boldsymbol{A}}\right)^2 + \hat{V}(\boldsymbol{r}) - \frac{e}{\mu c}(\hat{\boldsymbol{S}}\cdot\boldsymbol{B}) \tag{6.5}$$

The magnetic field $\boldsymbol{B}$ and the vector potential $\hat{\boldsymbol{A}}$ are related via:

$$\hat{\boldsymbol{A}} = \tfrac{1}{2}\left[\boldsymbol{B}\times\hat{\boldsymbol{r}}\right]. \tag{6.6}$$

If $\boldsymbol{B}=(0,0,B)$ then the following Coulomb gauge can be defined:

$$\hat{\boldsymbol{A}} = \tfrac{1}{2}B(-\hat{y},\hat{x},0), \quad \hat{A}^2 = \tfrac{1}{4}B^2(\hat{x}^2+\hat{y}^2). \tag{6.7}$$

Since

$$\left(\hat{\boldsymbol{p}} - \frac{e}{c}\hat{\boldsymbol{A}}\right)^2 = \hat{p}^2 + \frac{e^2}{c^2}\hat{A}^2 - \frac{eB}{c}\left(\hat{x}\hat{p}_y - \hat{y}\hat{p}_x\right), \tag{6.8}$$

substituting equation 6.7 into equation 6.8 yields

$$\hat{H} = \frac{\hat{p}^2}{2\mu} + \frac{\mu\omega^2}{2}\left(\hat{x}^2+\hat{y}^2\right) - \omega\left(\hat{L}_z + 2\hat{S}_z\right) + \hat{V}(\hat{\boldsymbol{r}}), \tag{6.9}$$

where

$$\omega = \frac{eB}{2\mu c}. \tag{6.10}$$

If $\hat{V}$ is axially symmetric with respect to the z-axis, then $\hat{H}$ commutes with $\hat{L}_z$ and the two operators share a common set of eigenfunctions. Let

$$\hat{H}\Psi_{mm_s} = E\Psi_{mm_s}, \quad \hat{L}_z\Psi_{mm_s} = m\Psi_{mm_s}, \quad \hat{S}_z\Psi_{mm_s} = m_s\Psi_{mm_s}. \tag{6.11}$$

Then

$$\left[\frac{\hat{p}^2}{2\mu} + \hat{V}(\boldsymbol{r}) + \frac{\mu\omega^2}{2}\left(\hat{x}^2+\hat{y}^2\right)\right]\Psi_{mm_s} = \epsilon\Psi_{mm_s}, \tag{6.12}$$

where

$$\epsilon = E + \omega(m+2m_s). \tag{6.13}$$

The final relationship in eq. (6.13) shows that the energies calculated using the harmonic confinement model and those obtained by solving the Schrödinger equation using the Hamiltonian of eq. (6.9) are related by an additional term which depends

on ω, m and m_s. Interestingly, this term is independent of R, and induces solely the vertical shift of the potential energy curves. Accordingly, the present confinement model is able to provide the details of the fine structure of potential energy curves and their evolution in parallel magnetic fields.

The energy of the electronic states of a confined HeH molecule containing three electrons increases faster with the increasing strength of the confinement than the ground state energy of the positive two-electron ion HeH^+. Therefore there exists a critical confinement parameter ω_c for each electronic state beyond which the energy of the neutral molecule is larger than that of the ion. For confinements stronger than the critical confinement, the corresponding electron is bound by the confining potential rather than by the nuclei and its energy spectrum is mainly determined by the form of the confinement. This behaviour of the energies is related to the phenomenon of *autoionization of atoms by pressure* [30] and was discovered already in the 1930s [31]. The theory developed in the present paper applies to the bound states only. Therefore the range of valid confinement parameters is determined by the inequality

$$0 < \omega < \omega_c. \tag{6.14}$$

As will be shown in the next section, in the cases considered here the critical confinement parameter ω_c is much smaller than 1. In addition, the strengths of magnetic fields met in nature rarely exceed a fraction of atomic unit ($\sim 10^5$ T). For such cases, when $\omega \ll 1$, the effects of confinement may be studied using the perturbation theory.

The Schrödinger equation describing the confined molecule may be written as

$$\left[\hat{H}_0(\boldsymbol{r}, R) + \omega^2 \hat{H}'(\boldsymbol{r})\right] \Psi^n_\omega(\boldsymbol{r}, R) = E^n_\omega(R) \Psi^n_\omega(\boldsymbol{r}, R), \tag{6.15}$$

where

$$\hat{H}'(\boldsymbol{r}) = \frac{1}{2} \sum_{i=1}^{N} \left(x_i^2 + y_i^2\right). \tag{6.16}$$

The zeroth-order Hamiltonian ($\omega = 0$) defined in eq. (6.2) satisfies the Schrödinger equation

$$\hat{H}_0(\boldsymbol{r}, R) \Psi^n_0(\boldsymbol{r}, R) = E^n_0(R) \Psi^n_0(\boldsymbol{r}, R). \tag{6.17}$$

The perturbation expansion in ω can be written as

$$E_\omega^n(R) = E_0^n(R) + E_I^n(R)\omega^2 + E_{II}^n(R)\omega^4 + \ldots, \tag{6.18}$$

where the first-order correction coefficient is given by

$$E_I^n(R) = \langle \Psi_0^n | \hat{H}' | \Psi_0^n \rangle = \frac{1}{2} \sum_{i=1}^{N} \langle \Psi_0^n | x_i^2 + y_i^2 | \Psi_0^n \rangle. \tag{6.19}$$

Note that H' may alternatively be expressed in terms of the quadrupole moment operator

$$H' = \frac{1}{6}\left(Q_{xx} + Q_{yy}\right) + \frac{1}{3} r^2, \tag{6.20}$$

where $Q_{xx} = \sum_{i=1}^{N} \left(3x_i^2 - r_i^2\right)$ and $Q_{yy} = \sum_{i=1}^{N} \left(3y_i^2 - r_i^2\right)$ are two components of the quadrupole moment tensor. Consequently, the first-order perturbational treatment of the confinement effects can be related to the quadrupole moment of the confined molecule via:

$$E_I^n(R) = \frac{1}{6} \langle \Psi_0^n | Q_{xx} + Q_{yy} | \Psi_0^n \rangle + \frac{1}{3} \sum_{i=1}^{N} \langle \Psi_0^n | r_i^2 | \Psi_0^n \rangle. \tag{6.21}$$

6.3 Computational Method

The electronic Schrödinger equation for the n-th electronic state

$$\hat{H}_\omega(\boldsymbol{r}, R) \Psi_\omega^n(\boldsymbol{r}, R) = E_\omega^n \Psi_\omega^n(\boldsymbol{r}, R) \tag{6.22}$$

was solved using full configuration interaction (FCI) method implemented in the systems of programs OpenMol [32] and GAMESS-US [33, 34]. In all the calculations several Gaussian basis sets were adopted. Two basis sets, He-21 and He-34, have been used for He. The first one is derived from the Römlet's $7s2p1d$ basis set [35], contracted to $5s2p1d$, plus a set of $2s1p$ diffuse functions (α = 0.08 and 0.02 for s and 0.08 for p), while the second one is constructed from H-21 with additional $1p2d$ polarization functions [36].

In order to describe the Rydberg character of the first several low-lying excited states of HeH, three basis sets of hydrogen, H-18, H-36 and H-55, with different sizes

of the polarization and diffuse spaces have been utilized [36]. The smallest one, H-18, is the Huzinaga's $(6s)/[4s]$ basis set [37] augmented by $2s4p$ diffuse set whose exponents are optimized for the proper description of the long-range interaction of the excited states of H_2 [35]. Both the H-36 and H-55 share the same $(13s7p)$ set grouped into a (3,2,1,1,1,1,1,1,1,1/1,1,1,1,1,1,1) contraction. The former one possesses an extra d-function, leading to a $10s7p1d$ basis set, while in the latter one a group of $1s1p4d$ diffuse functions is added, giving rise to a $11s8p4d$ basis set.

Potential energy curves $E^n_\omega(R)$, where n is the index of excited states, of the HeH molecule and the ground-state potential energy curve of HeH^+ for various values of the confinement parameters ω, were calculated. In order to check the applicability of the perturbational approach to studies on the influence of confinement on the potential energy curves, a k-th order polynomial approximation of the energy for the n-th state was constructed:

$$\tilde{E}^n_k(\omega, R) = \sum_{i=1}^{k} C^n_i(R)\omega^{2i} \tag{6.23}$$

A quadratic approximation ($k = 1$) corresponds to the first-order perturbation expansion. The fourth-order one ($k = 2$) corresponds to the perturbation expansion up to second order. Coefficients C^n_k of the approximations are estimated using the results for several values of ω: $\omega = 0.0, 0.05$ for $k = 1$ and $\omega = 0.0, 0.05, 0.10$ for $k = 2$.

6.4 Results and Discussion

6.4.1 Basis Sets

Four different combinations of He and H basis sets, *vis.* He-21/H-18, He-21/H-36, He-21/H-55, and He-34/H-55, have been tested in order to determine the suitable basis set for the studies of confined HeH molecule. The calculated spectroscopic constants for the first six excited electronic states of HeH are shown in Table 6.1. In Table 6.2 are also included the spectroscopic constants for the cation HeH^+ deduced using various combinations of He and H basis sets. In general, a very good agreement with the available experimental and theoretical data was achieved. The estimated

Table 6.1: Spectroscopic constants of HeH without confinement (r_e in atomic units, ν_e and $\nu_e x_e$ in cm^{-1}, D_e in eV)

State	Reference	r_e	ν_e	$\nu_e x_e$	D_e
A $^2\Sigma^+$	He-21/H-18	1.4077	3670	255	2.53
	He-21/H-36	1.4118	3699	196	2.54
	He-21/H-55	1.4149	3722	183	2.54
	He-34/H-55	1.4120	3726	182	2.54
	[27]	1.4040	3512		
	[38]	1.4115	3662		2.48
	[39]	1.43	3701		
	[22]	1.4003	3718	161	
B $^2\Pi$	He-21/H-18	1.4634	3364	199	2.21
	He-21/H-36	1.4629	3330	205	2.18
	He-21/H-55	1.4652	3367	201	2.19
	He-34/H-55	1.4622	3372	199	2.20
	[27]	1.4571	3158		
	[38]	1.4629	3302		2.20
C $^2\Sigma^+$	He-21/H-18	1.5413	2928	210	1.64
	He-21/H-36	1.5409	2930	190	1.61
	He-21/H-55	1.5417	3007	199	1.61
	He-34/H-55	1.5370	2957	211	1.61
	[27]	1.5255	2788		
	[38]	1.5428	2872		1.65
	[39]	1.57	2896		
	[22]	1.5324	2902	141	
D $^2\Sigma^+$	He-21/H-18	1.4545	3418	196	2.18
	He-21/H-36	1.4479	3467	289	2.16
	He-21/H-55	1.4584	3402	202	2.15
	He-34/H-55	1.4555	3405	201	2.16
	[27]	1.4504	3187		
	[38]	1.4508	3383		2.14
E $^2\Pi$	He-21/H-18	1.4719	3296	204	2.09
	He-21/H-36	1.4725	3258	193	2.08
	He-21/H-55	1.4736	3297	207	2.07
	He-34/H-55	1.4708	3299	207	2.08
	[27]	1.4655	3083		
	[38]	1.4718	3233		2.09
F $^2\Sigma^+$	He-21/H-18	1.5518	3013	209	1.46
	He-21/H-36	1.4696	3276	303	2.03
	He-21/H-55	1.4801	3246	209	2.05
	He-34/H-55	1.4771	3252	208	2.06
	[27]	1.4693	3057		

Table 6.2: Spectroscopic constants of HeH^+ without confinement (r_e in atomic units, ν_e and $\nu_e x_e$ in cm^{-1})

State	Reference	r_e	ν_e	$\nu_e x_e$
HeH^+ $^1\Sigma^+$	He-21/H-36	1.4770	3177	141
	He-21/H-36	1.4694	3275	149
	He-21/H-55	1.4765	3201	145
	He-34/H-55	1.4732	3206	146
	[15]	1.444	3379	314
	[40]	1.4632	$3233^{(a)}$	$617^{(a)}$
	[41]	1.4632	$3220^{(a)}$	$166^{(a)}$

(a) Calculated by fitting Wolniewicz's and Kolos' *ab initio* potential energy curves to Dunham's 4-th order polynomial.

r_e values deviate from the best values by at most 0.01 Å, while the calculated ν_e agree with the experimental values with the average discrepancy of about 3%.

Despite the overall good performance of these four combinations of basis sets, several differences between the basis sets have been observed. A fairly big discrepancy was seen for both the r_e and ν_e values of the F $^2\Sigma^+$ state obtained using He-21/H-18 basis sets. This is not unexpected since H-18 lacks d-type primitives which are essential for accurately describing the $3d$ character of the F state. Inclusion of an additional d-type primitive and extra s- and p-type diffuse functions (basis H-36) slightly changed the equilibrium bond lengths and harmonic frequencies for A to E states, but greatly improved the r_e for the F state. Further expanding the d-space (basis H-55) led to the elongation of r_e and significant variation of ν_e for all states. The effects of increasing the diffuse space of He basis set have also been investigated (basis He-34). The resulting ν_e values remained approximately unaffected but r_e were decreased by about 0.003 Å.

Since the low-lying excited states of HeH arise from the excitation of H $1s$ electron, the estimated excitation energies of H atom using H-18, H-36 and H-55 basis sets can serve as an excellent indication of their qualities in the molecular studies of the Rydberg HeH molecules. Schreiner has performed a series of atomic calculations on hydrogen with these basis sets, and the results revealed that H-36 is among

the best basis set which yielded the excitation energies up to $n = 4$, except for $3d$-orbitals, with the averaged error of 6 μHartree [36].

In consequence, H-36 basis set was utilized in the subsequent full CI calculations of the low-lying electronic states of HeH in the presence of a harmonic confining potential. In order to enhance the flexibility of the basis set combination He-21/H-36 in the description of distorted electron density, an additional set of $1s1p1d$ Gaussian-type functions was added in the middle of the He-H bond; exponents of these functions were equal to $\omega/2$. The use of such auxiliary basis functions has been justified in the calculations of a confined two-electron system [8], helium atom [10], and lithium molecule [14]. In the present study, potential energy curves of the ground and low-lying excited states of HeH molecules were calculated for the confinement parameter ranging from 0.0 to 0.4 au. However, the discussion would be focused only on small values of ω (i.e., $\omega < 0.20$ au) due to the field-induced ionization, which will be discussed in the following section.

6.4.2 Potential Energy Curves of HeH

Figure 6.1 depicts the potential energy curves of the ground and several low-lying excited states of HeH. On the same diagram the ground state potential of HeH^+ is also included for comparison. As shown, except for the ground state which is repulsive and only shows a van der Waals minimum at about 7.00 a.u., the excited states of HeH are all characterized by a deep potential well which is similar to the ground state potential of the molecular ion. An exception is the C $^2\Sigma^+$ state potential where a barrier, which lies 0.6 eV above the dissociation limit, is present at about 4.00 au due to the interaction between the Rydberg electron and the He core electrons [16]. It has been predicted that the F $^2\Sigma^+$ state potential energy curve of NeH also contains an energy barrier at 4.5 au [16] which is smaller than the one for the C state. However, an analogous feature is absent in HeH which could indicate weaker interaction between core and Rydberg electrons.

The excited states of HeH considered in the present work can essentially be described by a single reference configuration resulting from the excitation of the

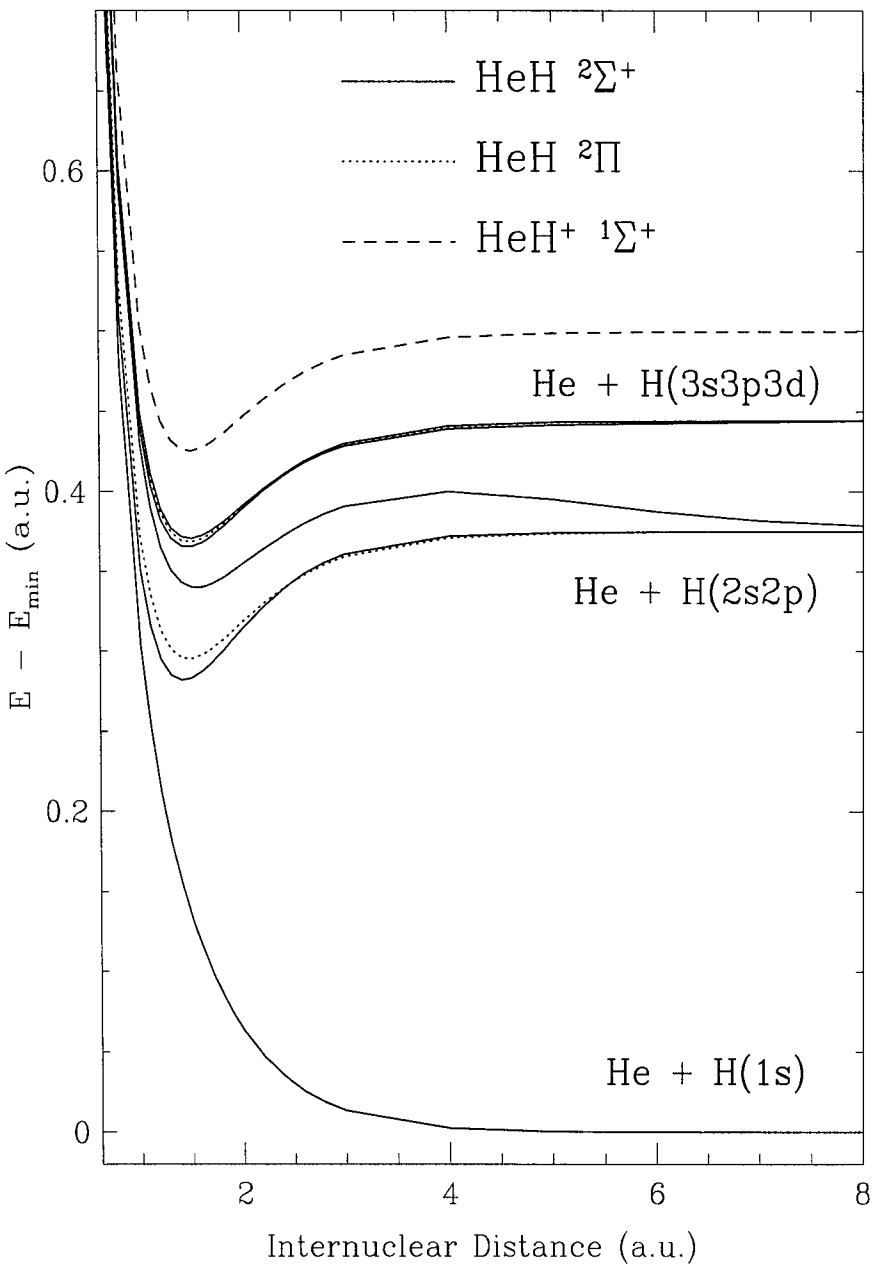

Figure 6.1: Potential energy curves of selected low-lying electronic states of HeH and the ground state of HeH^+.

H-atom $1s$ electron to the Rydberg orbitals. Unlike the case of NeH where a strong configuration mixing is observed between the $^2\Sigma^+$ states, Petsalakis et al. found that the non-adiabatic coupling matrix elements between the A and C states are rather small [42]. The A state is dominated by the He + H($2s$) configuration while the C state acquires mainly the H($2p$) character for the whole range of R, and they both lead to the same dissociation limit of He + H($2s2p$).

The B state, which has the dominant H($2p$) character, is also correlated to the dissociation products of He and excited H($n = 2$) atoms. This state lies very closely to the A state potential energy curve yet is fairly well separated from that of the C state. This behavior can be attributed to the fact that the π molecular orbitals resulting from the hydrogen $2p_x$ and $2p_y$ atomic orbitals are less destabilized by the Coulombic interaction with the He core electron density compared to the σ orbital which is formed from the hydrogen $2p_z$ atomic orbital. As a result, the latter state potential energy curve is up-shifted for small and intermediate values of R. As $R \rightarrow \infty$, these two states gradually become degenerate, leading to the same asymptotic limit of He + H($n = 2$).

The potential energy curves of the X to F states of HeH have been computed for a number of different values of the confinement parameter ω between 0.00 and 0.40 au in order to investigate the effects of the harmonic confining potential on both the spectroscopic and electronic properties of HeH molecule. Figures 6.2-6.4 show the A, B and C states of HeH for ω smaller than 0.15 a.u. while Figure 6.5 illustrates the ground state potential energy curves of HeH^+ for the same range of ω. As shown, these states behave in substantially different ways under the influence of an external potential. The potential energy curves of both the B state of HeH and the ground state of HeH^+ retain the same shapes for $\omega \leq 0.15$ au; these states are only shifted to higher energies by the confining potential and become slightly more bound. These observations can be accounted for by the fact that the harmonic potential, which increases the electron density between nuclei through Coulomb interaction, does not significantly enhance the π-type bonding in HeH. Instead, the Rydberg H($2p$) orbital will become distorted so that the B state is destabilized.

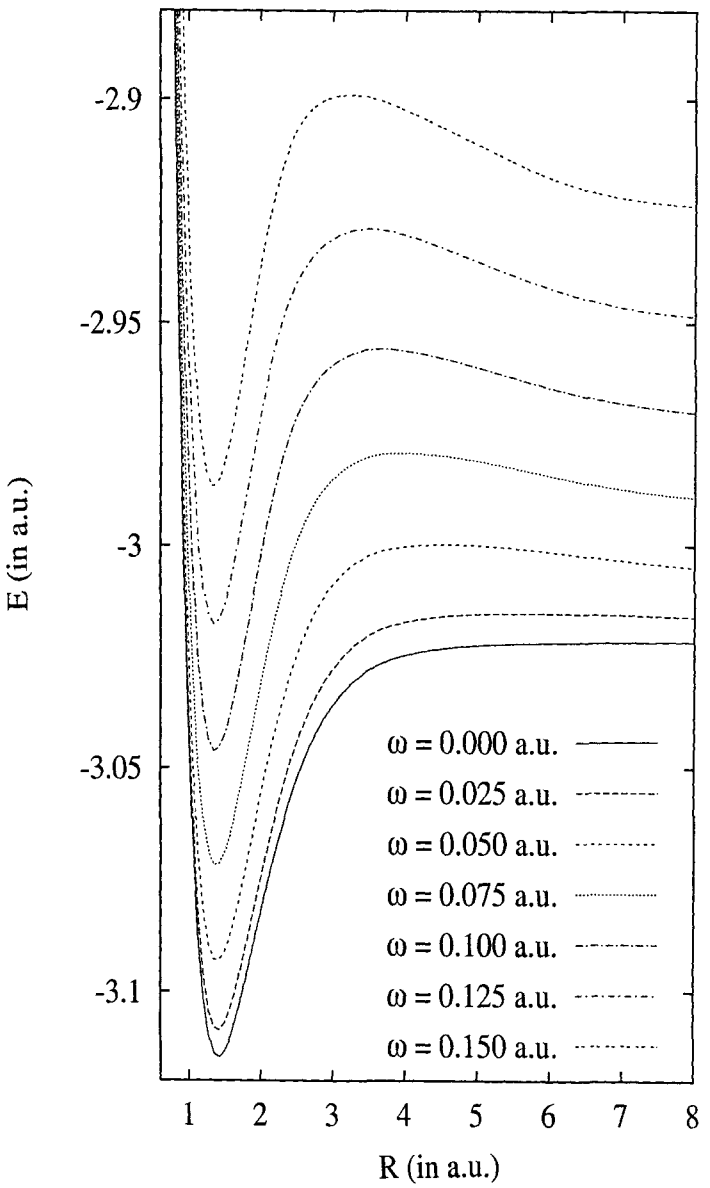

Figure 6.2: Potential energy curves of the A $^2\Sigma^+$ state of HeH in confinement.

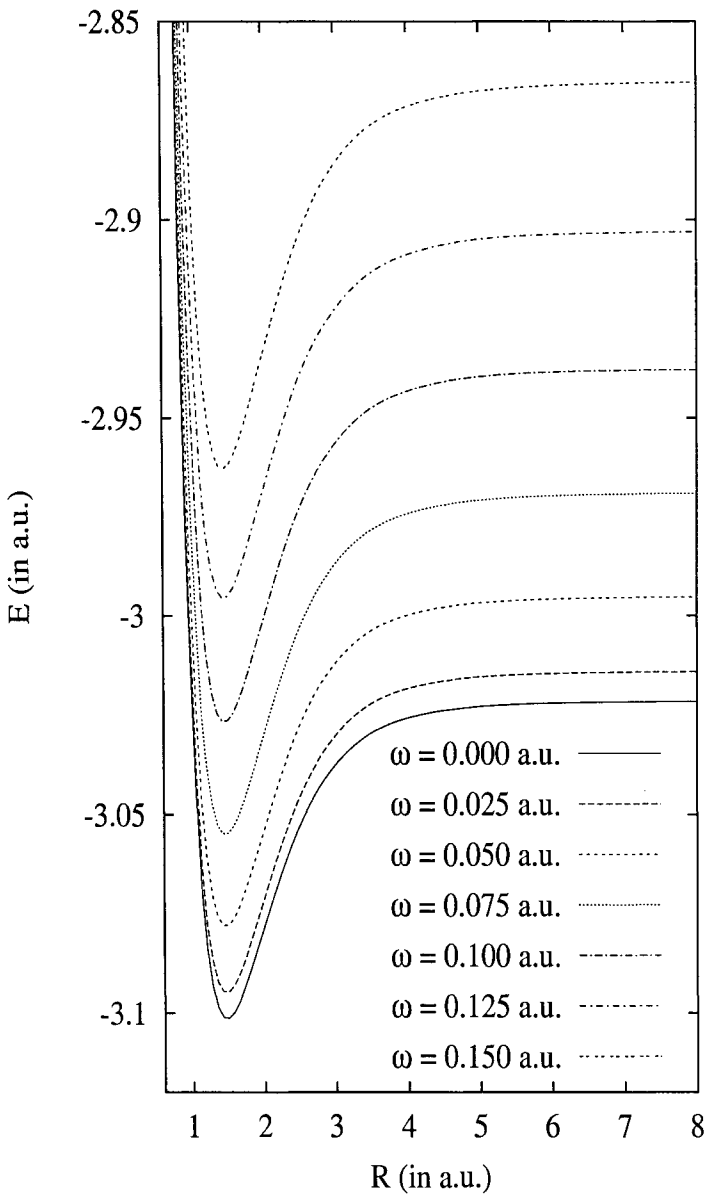

Figure 6.3: Potential energy curves of the B $^2\Pi$ state of HeH in confinement.

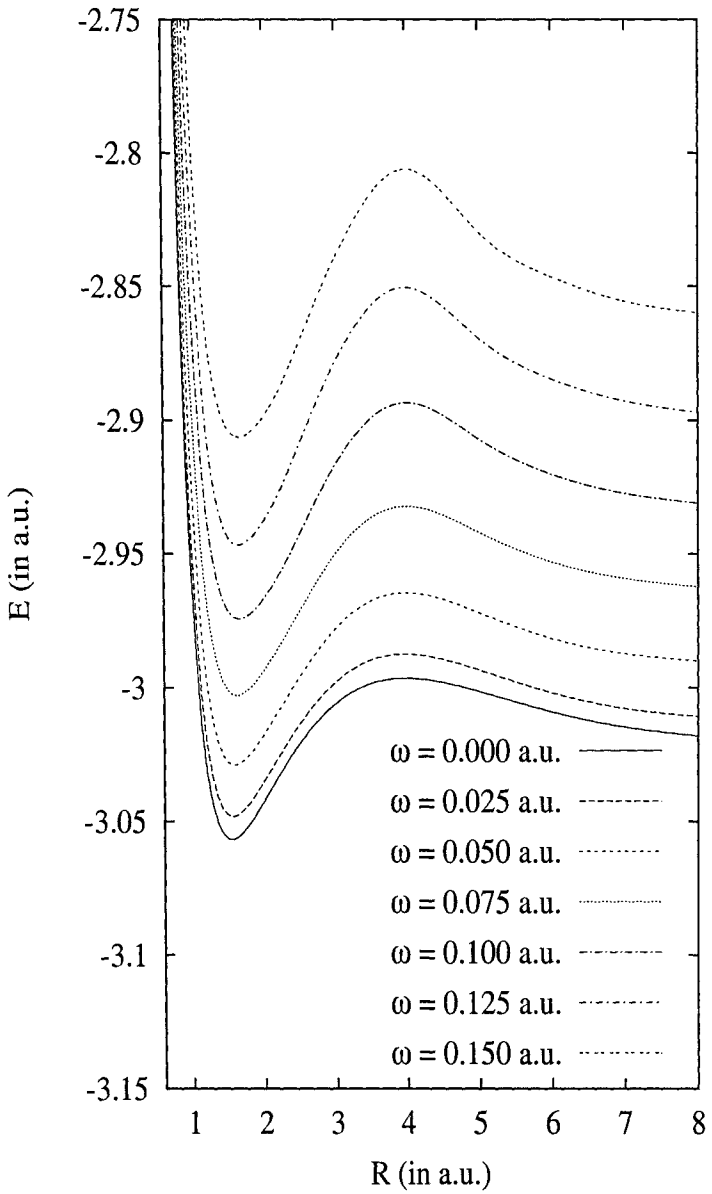

Figure 6.4: Potential energy curves of the C $^2\Sigma^+$ state of HeH in confinement.

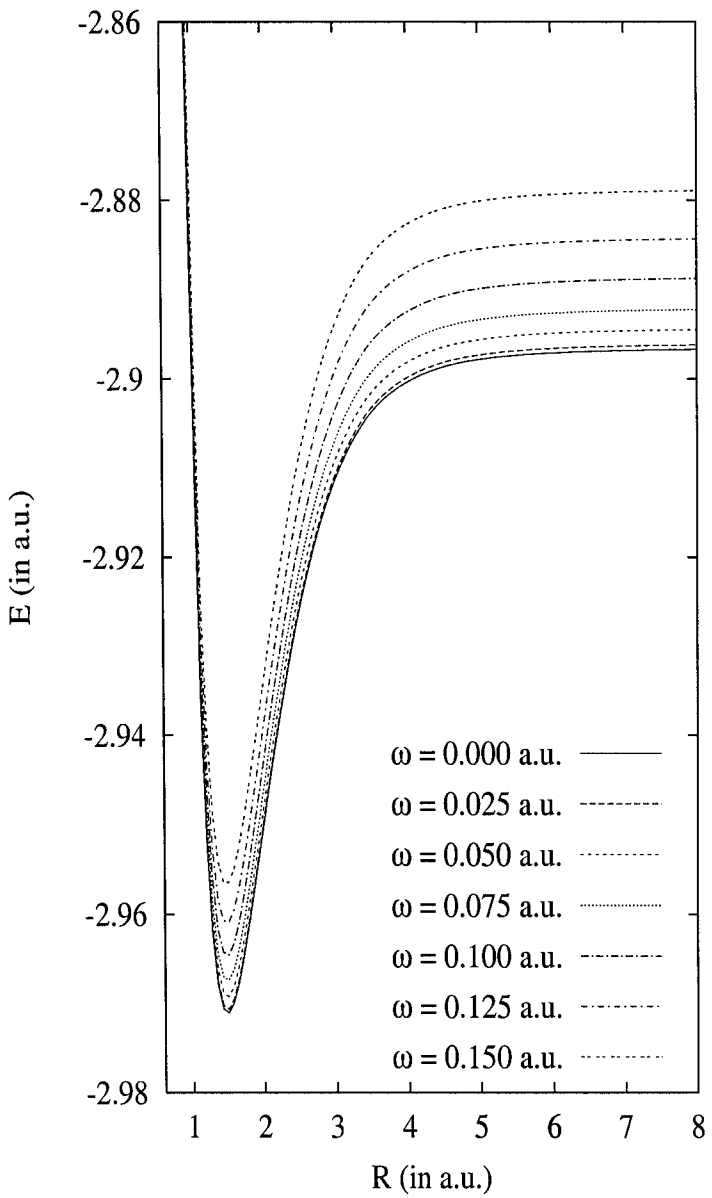

Figure 6.5: Potential energy curves of the X $^1\Sigma^+$ state of HeH^+ in confinement.

On the other hand, the $^2\Sigma^+$ state potential energy curves of HeH are strongly affected when the applied potential is present. The characteristic local barrier on the C state potential remains for $\omega > 0.00$, but its height increases with ω. For instance, the local maximum lies about 0.58 eV above the limit of He + H($2p$) when $\omega = 0.00$; this barrier increases, for $\omega = 0.15$ au, to 1.46 eV which is comparable to the binding energy (i.e., 1.61 eV) of the unconfined C state. Simultaneously, the binding energy with respect to the dissociation products increases from 1.01 eV to 1.26 eV because of the greater σ-bonding electron density.

Two interesting and unexpected changes occur on the A state potential energy curve due to the confining potential. The first one is the presence of a potential barrier at 3.00 au when HeH is confined by a cylindrical harmonic potential. A similar situation has also been observed in NeH molecule [43]. The emerging potential maximum is possibly the consequence of an avoided crossing between the A and C $^2\Sigma^+$ at the point where these two states interchange their configurations. At small R, the A state still possesses mainly the hydrogen $2s$ character as the free-field counterpart. However, the dominant configuration of the state in the long range region turns to be He + H($2p_z$). Previous studies have demonstrated that the orbital degeneracy of a hydrogen atom embedded in a prolate-type potential will be partially removed, with the p_z component being more stabilized with respect to s and other p-components [8]. Accordingly, the dissociation channel of He + H($n = 2$) splits, giving rise to three sub-channels when a cylindrical confining potential is applied to HeH. The avoided crossing can thus allow the A and C states to exchange the configurations and dissociate to the proper limits.

The second feature of the A state potential energy curve is reduction of the binding energy with increasing ω. The binding energy in the case of $\omega = 0.15$ au is 1.70 eV while in the unconfined case it is equal to 2.53 eV. This change can be rationalized in terms of the avoided crossing: the larger shift of the H($2s$) potential compared to that of H($2p_z$) potential causes the diminishing energy gap between these two states, and thus the binding energy of the A state potential energy curve.

In spite of the complicated changes of shapes of the potential energy curves of

different states of HeH, the variation of r_e, the equilibrium bond distances, is rather small, as shown in Figure 6.6. For $\omega \leq 0.10$ au the averaged deviation of r_e for these states is less than 3%. This behavior is different from the case of a confined H_2 molecule where the confinement led to a considerable reduction of the bond length [44]. An intuitive explanation of this difference is fairly simple. The cylindrical confinement moves the electronic charge closer to the molecular bond. In the ground state of strongly bound molecules such as H_2 and H_2^+, the electronic cloud is compact and the compression along the molecular axis results in an increase of the electron density in the space between the nuclei and, consequently, to a decrease of r_e. In a Rydberg molecule, however, the valence electronic cloud is diffuse. Therefore, the compression of electron cloud does not induce a considerable increment of electron density in the internuclear region, and, in effect, the internuclear distance does not change very much.

6.4.3 Transition Dipole Moments and Oscillator Strengths

It has been shown, from the molecular orbital analysis, that the application of a confining potential alters the configurations of both A and C states by introducing an avoided crossing at 2.5 to 3.0 au. This configuration interaction leads to the changes of r_e and the binding energy of these states. In addition, this configuration mixing influences the intensities of the electronic transitions involving the A and C states. In order to examine the variation of the transition intensities with respect to ω, the transition dipole moments for the transitions between X, A, B, and C states and the associated oscillator strengths (or f-values) were calculated.

The electronic transition dipole moment for an n-electron system can be defined in two ways [45]: the dipole length approximation

$$\langle \psi_f | \vec{\mu} | \psi_i \rangle = \int_\tau \psi_f^*(\vec{r}) \left(e \sum_{k=1}^{n} \vec{r}_k \right) \psi_i(\vec{r}) d\tau, \tag{6.24}$$

or the dipole velocity approximation

$$\langle \psi_f | \vec{\mu} | \psi_i \rangle = \frac{h}{4\pi^2 m_e \omega_{if}} \int_\tau \psi_f^*(\vec{r}) \nabla \psi_i(\vec{r}) d\tau. \tag{6.25}$$

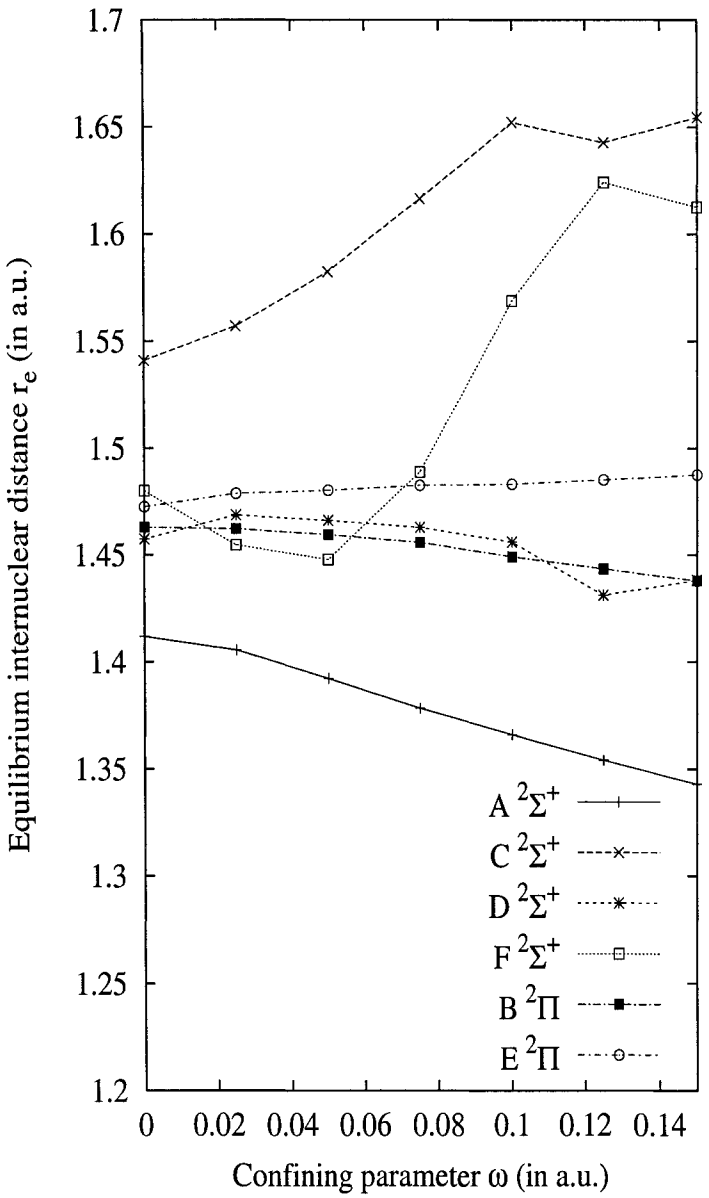

Figure 6.6: Plot of equilibrium internuclear distances versus the confining parameters.

In these expressions ψ_i and ψ_f represent, respectively, the initial and final states of the transition, and ω_{if} is the frequency of the radiation. The dimensionless oscillator strengths can be calculated from the following equation:

$$f_{i\to f} = \frac{8\pi^2 m_e}{3he^2}\omega_{if}|\langle\psi_f|\vec{\mu}|\psi_i\rangle|^2. \tag{6.26}$$

This quantity constitutes the measure of the possibility of an electronic transition. Hence, the comparison of the f-values of different transitions can provide the information regarding their intensity ratio, population densities, and lifetimes.

Chandrasekhar [46] proved that eqs. (6.24) and (6.25) will yield different values of dipole transition moments if an approximate wavefunction is used. Therefore, a test has been performed in which eqs. (6.24) and (6.25) were used, respectively, with the full CI wavefunction computed in the present study. It is seen that both formulas give the dipole transition moments (and, in turn, the oscillator strength) which differ by only 1 to 2 % for $^2\Sigma^+$ states. However, a larger difference of about 10 % is found for $^2\Pi$ states, which is possibly due to the deficiency in the basis sets describing the π-electron density.

In spite of the less satisfactory agreement for the $^2\Pi$ states, the data from both calculations support the conclusion of the wavefunction analysis that the A and C states undergo the interchange of configurations when HeH molecule is confined. In the case of $\omega = 0.0$ au the A $\rightarrow$ B transition moment is greater than that of the B $\rightarrow$ C transition for the range of R (see figure 6.7). The B state can be characterized as $2p$ state; therefore, it is expected that the A state, which is essentially the $2s$ state, should lead to a large dipole transition moment. The increasing B $\rightarrow$ C dipole transition moment at large R results from the enhanced $2s$ character of the C state, which has the dominant $2p$ configuration at intermediate R, when approaching the asymptotic limit where the $2s$ and $2p$ orbitals become degenerate.

Nevertheless, the A $\rightarrow$ B dipole transition moment curve drops very rapidly when a confining potential is present, which suggests that the A state loses a significant amount of $2s$ character due to the confinement. Meanwhile, a crossing exists between the A $\rightarrow$ B and B $\rightarrow$ C transition moment curves and it shifts to a smaller R with increasing ω. These phenomena indicate an important interaction between the A

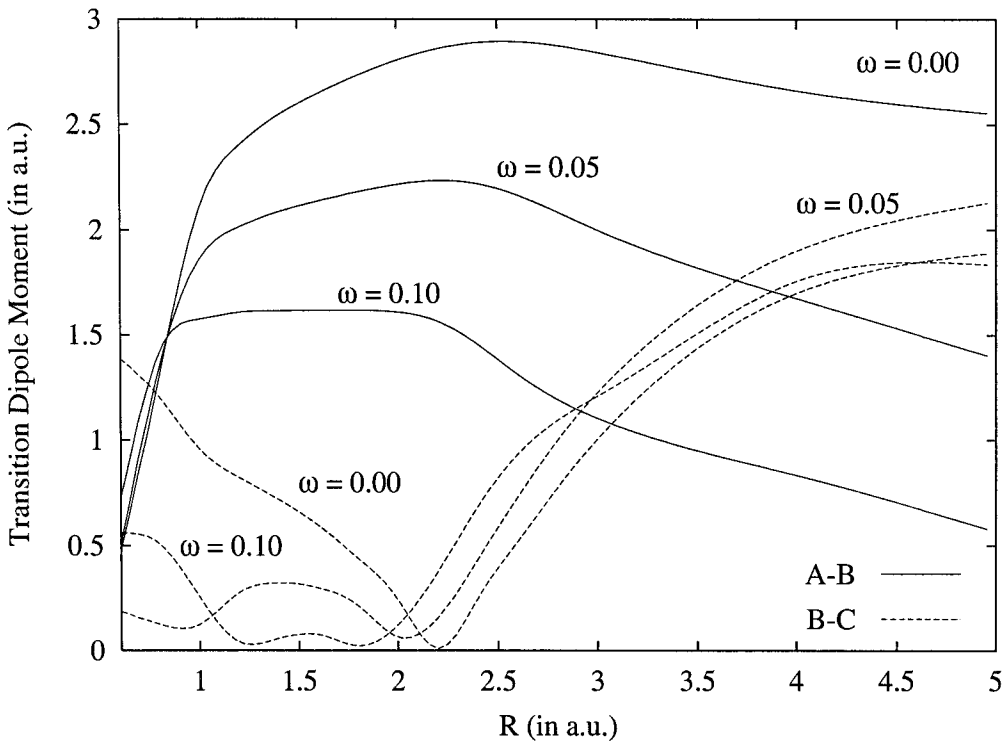

Figure 6.7: Transition dipole moments (in atomic units) of HeH as a function of R. Solid-lines: A-B transitions. Dashed-lines: B-C transitions.

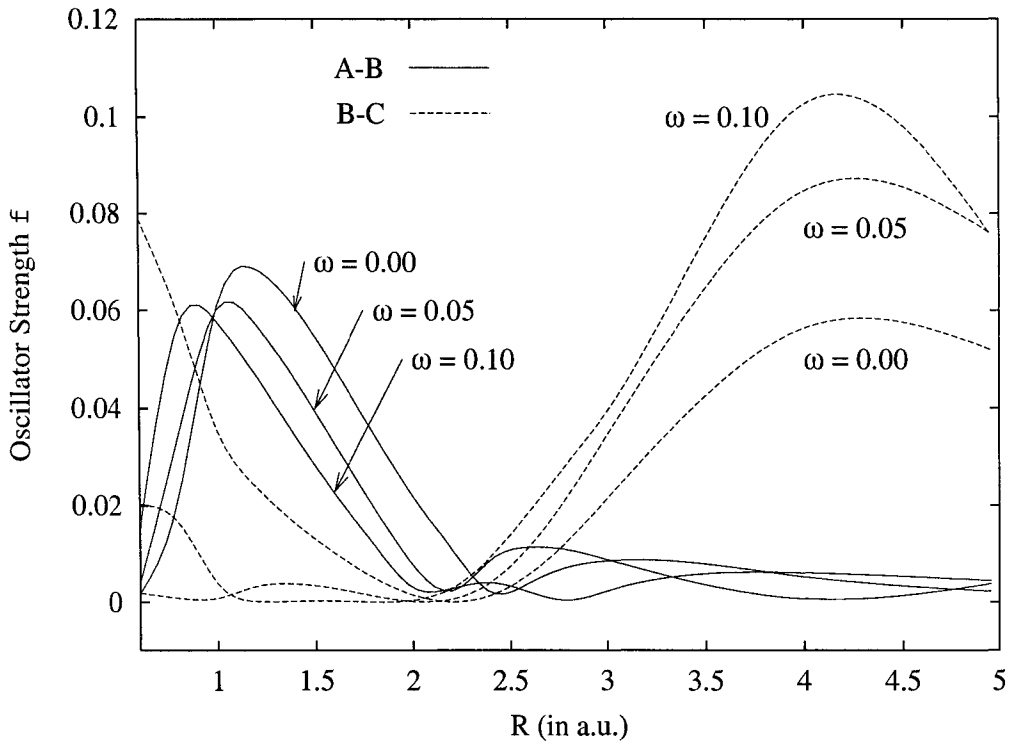

Figure 6.8: Oscillator strength of HeH as a function of R. Solid-lines: A-B transitions. Dashed-lines: B-C transitions.

and C state at which the C state attains the hydrogen $2s$ character. Interestingly, the increased $2s$ character of the C state does not affect the B $\rightarrow$ C dipole transition moment very much at large R, although its magnitude becomes larger than that of the A $\rightarrow$ B transition moment.

Because of the configuration mixing of the A and C states, a prominent change in the peak intensities of the electronic spectrum is anticipated. Figure 6.8 shows the calculated oscillator strengths for both the A $\rightarrow$ B and B $\rightarrow$ C transitions with respect to R and ω. Clearly, the oscillator strength, and thus the transition intensity, for the B $\rightarrow$ C transition significantly increases with ω at large R, which may be attributed to the greater $2s$ character of the C state. On the other hand, the maximum for the A $\rightarrow$ B transition decreases, which corresponds to the diminishing

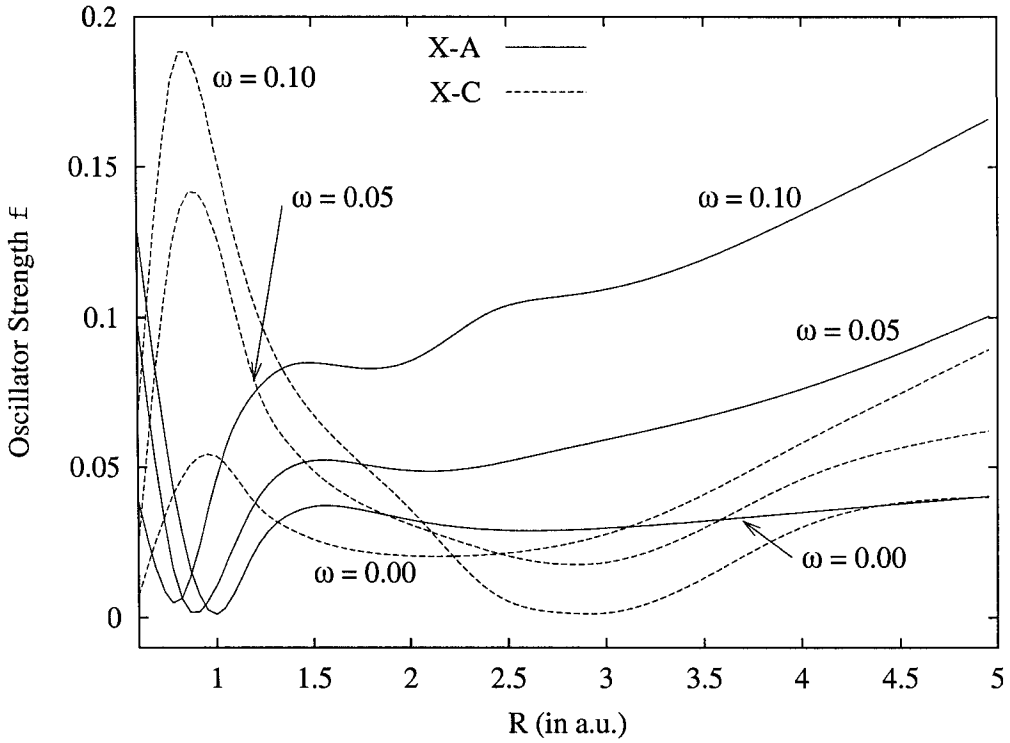

Figure 6.9: Oscillator strength of HeH as a function of R. Solid-lines: X-A transitions. Dashed-lines: X-C transitions.

$2s$ character of the A state.

For comparison purposes, the oscillator strengths for the X $\rightarrow$ A and X $\rightarrow$ C transitions were also computed and displayed in Figure 6.9. Since the ground state of HeH is composed of the ground-state He($1s^2$) and H($1s$), the evolution of the transition probabilities, which are proportional to the oscillator strengths, for the X $\rightarrow$ A and X $\rightarrow$ C transitions should be opposite to that for the A $\rightarrow$ B and A $\rightarrow$ C transitions. As expected, the oscillator strength for the X $\rightarrow$ A transition increases at large R for $\omega > 0.0$ since the increased $2p$ character of the A state brings about a stronger transition to the X state. Conversely, the $2s$ character on the C state reduces the X $\rightarrow$ C transition quite appreciably. A surprising feature is noticed at the small R region where the transition probability for the X $\rightarrow$ C sharply increases

Table 6.3: Critical confinement ω_c for different electronic states of HeH

State	ω_c / eV
A $^2\Sigma^+$	0.178
B $^2\Pi$	0.155
C $^2\Sigma^+$	0.111
D $^2\Sigma^+$	0.067
E $^2\Pi$	0.055
F $^2\Sigma^+$	0.042

at $R = 1.0$ au. This observation indicates that at small R regime the $2p_z$ orbitals are more destabilized and lie in a higher energy than the $2s$-orbital, in contrast to the situation in the intermediate R regime where the $2p_z$ orbital is more stable than the $2s$ orbital in the presence of a cylindrical confining potential.

6.4.4 Critical Confinement and Perturbational Analysis

When an atom or molecule is excited into an energy level which lies above its first ionization limit, the system will become unstable, and a spontaneous ionization will occur in which an electron will be ejected. This process is referred to as the autoionization, or field-induced ionization [47]. As the valence electrons of Rydberg molecules are only weakly bound to the parent ion core, it is expected that they could be easily expelled by an external potential.

To determine the strength of confinement at which an electronic state of HeH undergoes the autoionization, the following quantities:

$$\Delta E^n(\omega) = E^n_{HeH}(\omega; r_e) - E^1_{HeH^+}(\omega; r_e), \tag{6.27}$$

were computed where n is the index of the excited state, i.e., A ($n = 1$), B ($n = 2$) and so on. The critical confinement is defined by the value of ω at which $\Delta E^n = 0$. The results are plotted in Figure 6.10 and summarized in Table 6.3. As might be expected, the higher the excitation, i.e., larger n, the smaller the confinement parameter ω_c because of the more diffuse nature of the valence electron density. It is interesting to note that ω_c obtained in the present study for HeH are larger than the corresponding values for the analogous NeH molecule [43]. This observation reveals

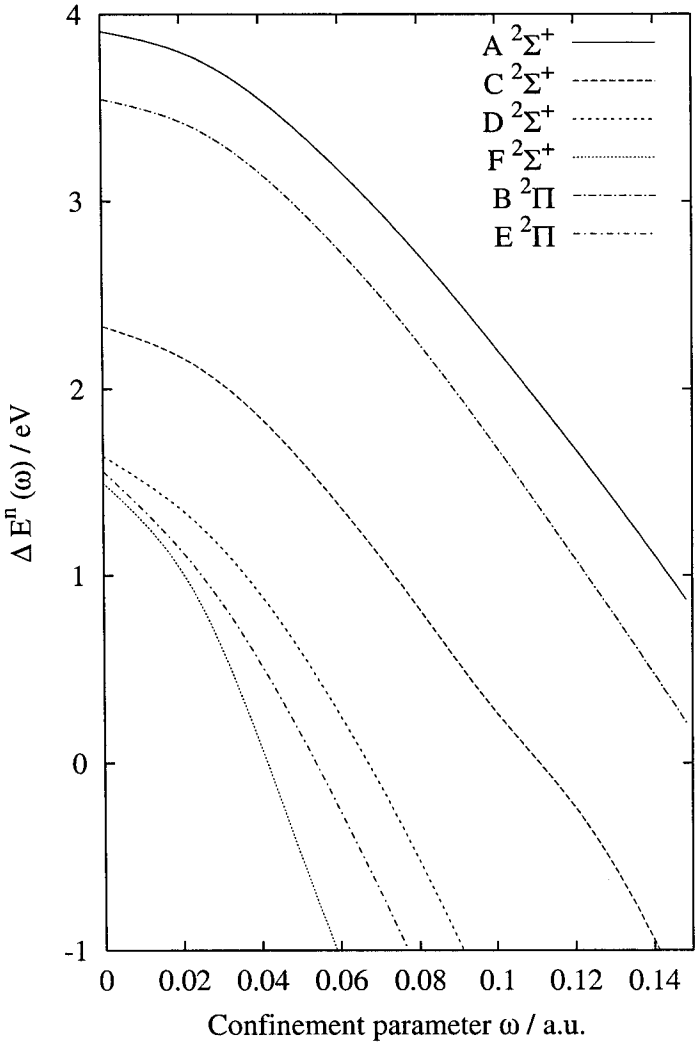

Figure 6.10: Plot of $\Delta E^n(\omega)$ (Eq. 24) versus ω for different electronic states of HeH.

that the Rydberg electron in HeH is in fact more strongly bound by the HeH^+ core than the one in NeH molecule; this is consistent with the earlier finding that the H($2p$) Rydberg orbital of HeH, estimated by the location of the potential barrier of the C state potential, is slightly smaller than that of NeH. These two phenomena can all be accounted for by the weaker attraction between the NeH^+ core and the Rydberg electron due to the screening effect of the Ne electron cloud. The less-effective shielding in HeH results in a stronger binding of the Rydberg electron and a smaller Rydberg orbital.

As illustrated by Figure 6.10, the critical confinement parameters under which the electronic states of HeH remain bound are rather small, not exceeding 0.2 au Therefore, the classical perturbation theory would be sufficient to describe the ω-dependence of the spectroscopic properties of the low-lying states of HeH.

The calculated potential energy curves for X to C states have been fitted to the first- and second-order polynomials in terms of ω^2, respectively, derived from eq. (6.23), and the coefficients C_i^n were determined for different values of R. For the first-order approximation only C_1^n was calculated while for the second-order approximation both C_1^n and C_2^n were computed. The term C_0^n corresponds to the energy of unconfined HeH molecule in the state n. Figures 6.11-6.14 present the the first-order and second-order approximations to the first four electronic states of HeH, and figure 6.15 illustrates the dependence of the perturbation coefficients on R.

It is quite obvious that the first-order approximation is not sufficient when ω exceeds 0.05 au, although it is still accurate enough for smaller values of ω. The interpolated energies are too large, which may be attributed to over-estimation of the perturbation from the confining potential. To achieve a better agreement with the exact energies, the second-order correction is necessary; this point is well illustrated in Figures 6.11-6.14. For the ground state of HeH, an excellent agreement between the exact and interpolated energy values is observed. The discrepancy is in general in the order of 10^{-5} au. The performance of the perturbation treatment becomes poor for higher excited states. For instance, the error for the A state is about 0.001

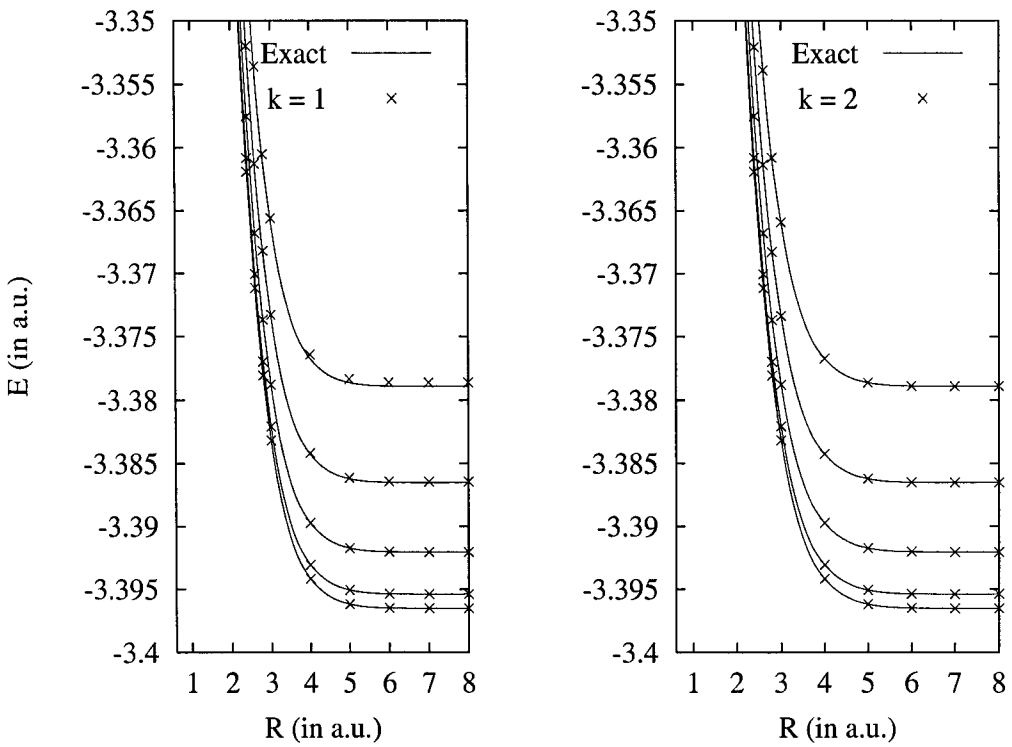

Figure 6.11: Potential energy curves of the ground X $^2\Sigma^+$ state of a confined HeH molecule (solid lines) and their approximations (crosses) resulting from the first-order (left, $k = 1$) and second-order (right, $k = 2$) interpolation. The consecutive curves correspond to the increment of 0.025 au in ω.

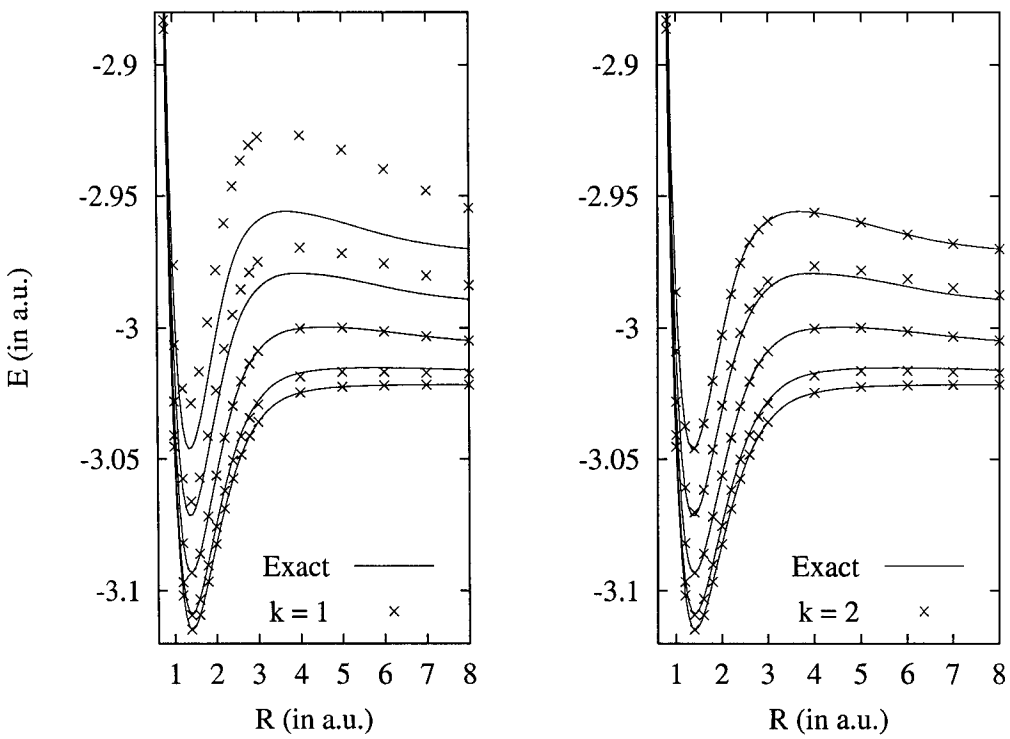

Figure 6.12: Potential energy curves of the ground A $^2\Sigma^+$ state of a confined HeH molecule (solid lines) and their approximations (crosses) resulting from the first-order (left, $k = 1$) and second-order (right, $k = 2$) interpolation. The consecutive curves correspond to the increment of 0.025 au in ω.

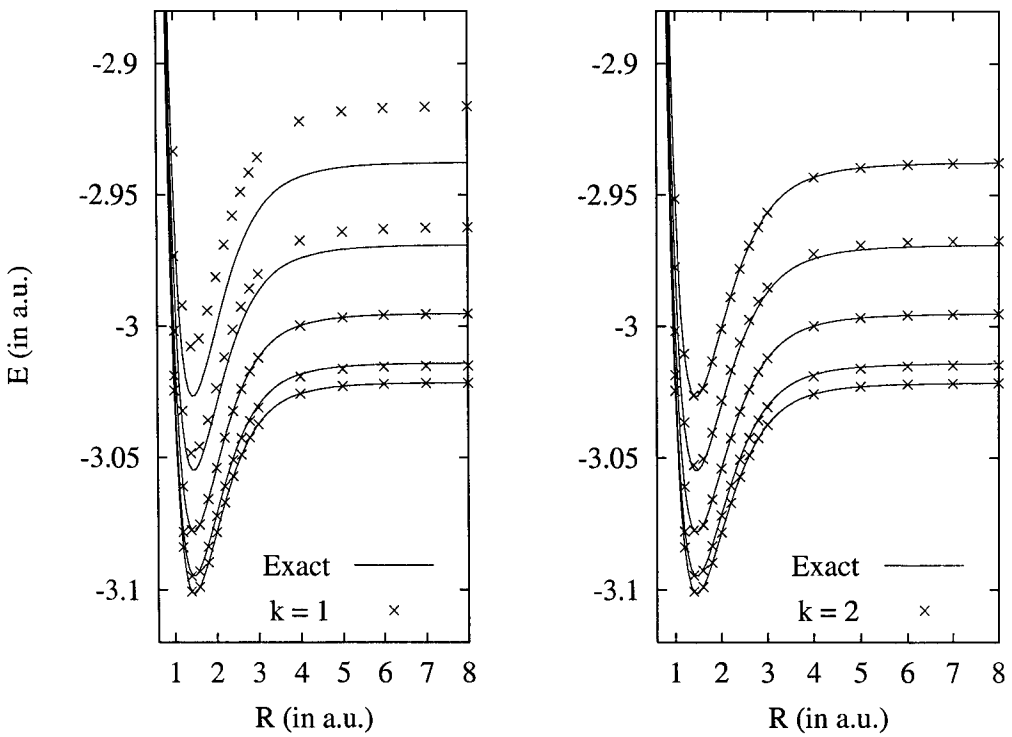

Figure 6.13: Potential energy curves of the ground B $^2\Pi$ state of a confined HeH molecule (solid lines) and their approximations (crosses) resulting from the first-order (left, $k = 1$) and second-order (right, $k = 2$) interpolation. The consecutive curves correspond to the increment of 0.025 au in ω.

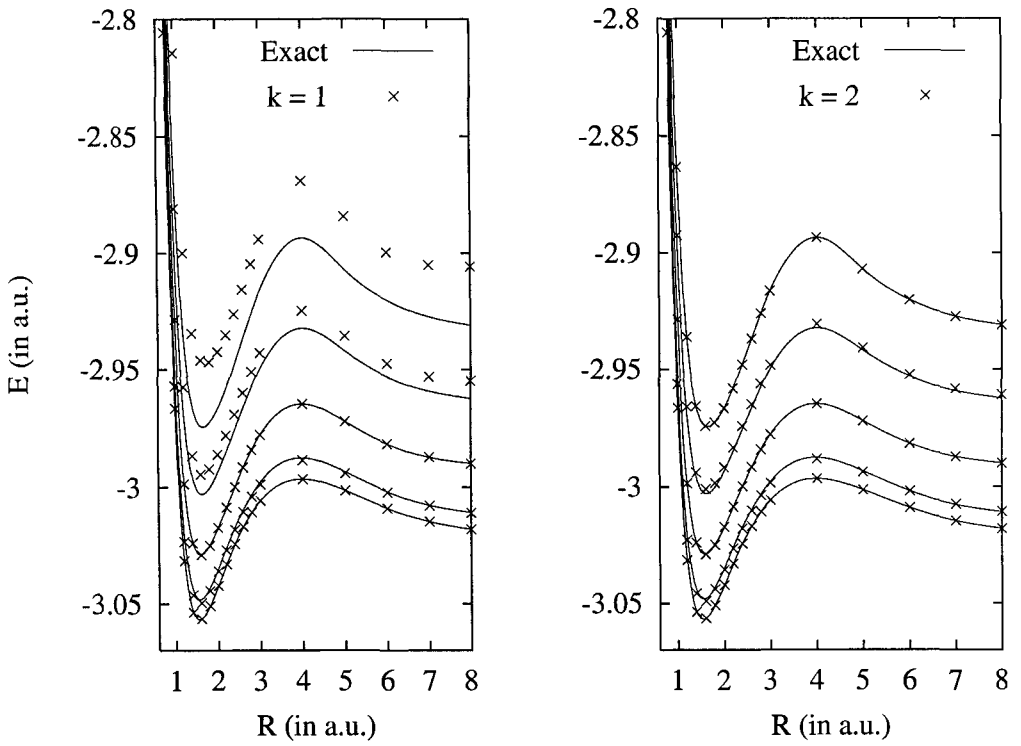

Figure 6.14: Potential energy curves of the ground C $^2\Sigma^+$ state of a confined HeH molecule (solid lines) and their approximations (crosses) resulting from the first-order (left, $k = 1$) and second-order (right, $k = 2$) interpolation. The consecutive curves correspond to the increment of 0.025 au in ω.

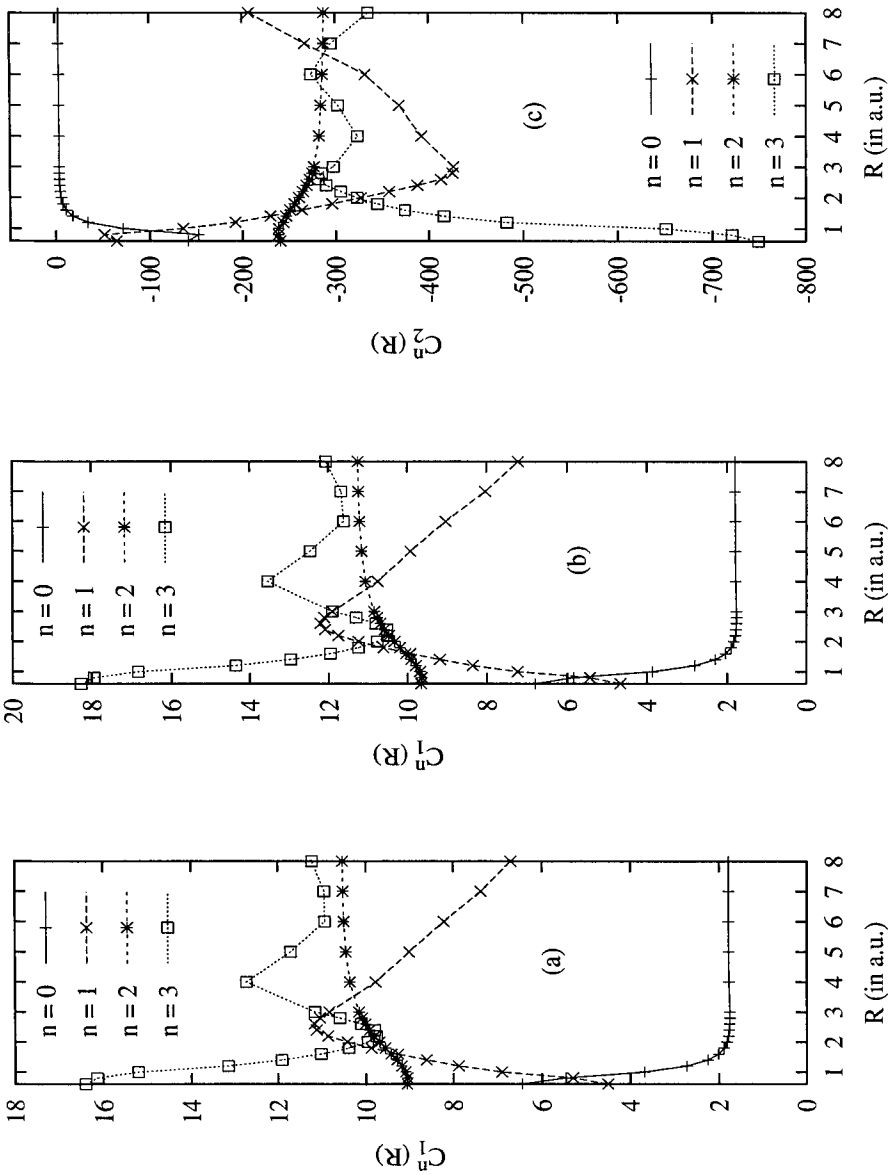

Figure 6.15: Coefficients $C_i^n(R)$ (equation 23) of the approximations for the X, A, B and C (corresponding to $n = 1, 2, 3$ and 4 respectively) states of confined HeH molecules. (a) Coefficients for the first-order approximation. (b-c) Coefficients for the second-order approximation.

au, which is 100 times bigger than that for the ground state. This is not surprising as those states are strongly perturbed via the avoided crossing caused by the confining potential.

6.5 Final Remarks

A Rydberg molecule HeH confined by a cylindrical harmonic potential has been investigated. It has been found that this molecule behaves differently from the strongly-bound diatomic molecules. The effects of the confining potentials on the molecular properties of HeH have been studied. The confinement does not dramatically vary the bond lengths for the low-lying electronic states of HeH, although the bond lengths could be either stretched or compressed. Besides, the states are not necessarily more strongly bound by the potential. It has been shown that some of the states become less bound when the potential is applied. While the X and B states retain their configurations for the whole range of R, there exists a new avoided crossing between the A and C states where they interchange the dominant configurations. This configuration mixing is manifested in the variations of the dipole transition moments and the oscillator strengths of the electronic transitions involving these states.

It is predicted that this system will be easily ionized by even modestly strong applied potential. For higher excited states weaker potentials are required to trigger the process of autoionization. Because of the relatively small valid confinement parameters (i.e. for $\omega < \omega_c$), perturbation theory may be applied to the studies of the confinement effects. The first-order correction is insufficient for correctly describing the changes in the potential energy curves of the confined HeH molecule. The second- or higher-order correction is definitely important in improving the accuracy. The present study shows that for $\omega \leq 0.12$ au the second-order perturbation theory is an excellent alternative for calculating reliable potential energy curves of the low-lying excited states of Rydberg HeH molecule.

Bibliography

[1] P. K. Mukherjee, J. Karwowski, G. H. F. Diercksen, *Chem. Phys. Lett.* **363**, 323 (2002).

[2] D. Bielińska-Wąż, J. Karwowski, B. Saha, P. K. Mukherjee, *Phys. Rev. E* **68**, 016404 1-6 (2003).

[3] U. Kappes, P. Schmelcher, *Phys. Rev. A* **51**, 4542 (1995).

[4] F. Rosei, R. Rosei, *Surf. Science* **500**, 395 (2002).

[5] F. Rosei, M. Schunack, P. Jiang, A. Gourdon, E. Lægsgaard, I. Stensgaard, C. Joachim, F. Besenbacher, *Science* **296**, 328 (2002).

[6] M. Jaskólski, *Phys. Rep.* **271**, 1 (1996).

[7] J. Karwowski, *J. Mol. Struct.: THEOCHEM* **727**, 1 (2005).

[8] D. Bielińska-Wąż, J. Karwowski, G. H. F. Diercksen, *J. Phys. B: At. Mol. Opt. Phys.* **34**, 1987 (2001).

[9] T. Sako, G. H. F. Diercksen, *J. Phys. B: At. Mol. Opt. Phys.* **36**, 1433 (2003).

[10] T. Sako, G. H. F. Diercksen, *J. Phys. B: At. Mol. Opt. Phys.* **36**, 1681 (2003).

[11] D. Bielińska-Wąż, G. H. F. Diercksen, M. Klobukowski, *Chem. Phys. Lett.* **349**, 215 (2001).

[12] D. Lai, E. E. Salpeter, S. L. Shapiro, *Phys. Rev. A* **45**, 4832 (1992).

[13] J. M. H. Lo, M. Klobukowski, and G. H. F. Diercksen, *Adv. Quantum Chem.*, **48**, 59 (2005).

[14] T. Sako, I. Černušák, G. H. F. Diercksen, *J. Phys. B: At. Mol. Opt. Phys.* **37**, 1091 (2004).

[15] H. H. Michels, F. E. Harris, *J. Chem. Phys.* **39**, 1464 (1963).

[16] G. Theodorakopoulos, S. C. Farantos, R. J. Buenker, S. D. Peyerimhoff, *J. Phys. B: At. Mol. Phys.* **17**, 1453 (1984).

[17] T. Möller, M. Beland, G. Zimmerer, *Phys. Rev. Lett.* **55**, 2145 (1985).

[18] T. Möller, M. Beland, G. Zimmerer, *Chem. Phys. Lett.* **136**, 551 (1987).

[19] C. Kubach, V. Sidis, D. Fussen, J. van der Zande, *Chem. Phys.* **117**, 439 (1987).

[20] W. Ketterle, *Phys. Rev. Lett.* **62**, 1480 (1989).

[21] D. W. Tokaryk, R. L. Brooks, J. L. Hunt, *Phys. Rev. A* **40**, 6113 (1989).

[22] W. Ketterle, A. Dodhy, H. Walther, *J. Chem. Phys.* **89**, 3442 (1988).

[23] W. Ketterle, *J. Chem. Phys.* **93**, 3752 (1990).

[24] W. Ketterle, *J. Chem. Phys.* **93**, 3760 (1990).

[25] W. Ketterle, *J. Chem. Phys.* **93**, 6929 (1990).

[26] W. Ketterle, H. P. Messmer, H. Walther, *Phys. Rev. A* **40**, 7434 (1989).

[27] B. K. Sarpal, S. E. Branchett, J. Tennyson, L. A. Morgan, *J. Phys. B: At. Mol. Opt. Phys.* **24**, 3685 (1991).

[28] C. K. Rhodes, *Topics in Applied Physics. Excimer Lasers*, 2nd ed., Springer, Berlin, 1984.

[29] G. Herzberg, *Annu. Rev. Phys. Chem.* **38**, 27 (1987).

[30] J. P. Connerade, V. H. Dolmatov, P. A. Lakshmi, *J. Phys. B: At. Mol. Opt. Phys.* **33**, 251 (2000).

[31] A. Sommerfeld, H. Welker, *Ann. Phys., Lpz.* **32**, 56 (1938).

[32] G. H. F. Diercksen, G. Hall, *Comput. Phys.* **8**, 215 (1994).

[33] M. W. Schmidt, K. K. Baldridge, J. A. Boatz, S. T. Elbert, M. S. Gordon, J. J. Jensen, S. Koseki, N. Matsunaga, K. A. Nguyen, S. Su, T. L. Windus, M. Dupuis, J. A. Montgomery, *J. Comp. Chem.* **14**, 1347 (1993).

[34] J. Ivanic, K. Ruedenberg, *Theoret. Chem. Acc.* **106**, 339 (2001).

[35] J. Römelt, S. D. Peyerimhoff, R. J. Buenker, *Chem. Phys.* **34**, 403 (1978).

[36] E. W. S. Schreiner, *Ph.D. Thesis*, Technische Universität München (1996).

[37] S. Huzinaga, *J. Chem. Phys.* **42**, 1293 (1965).

[38] G. Theodorakopoulos, I. D. Petsalakis, C. A. Nicolaides, R. J. Buenker, *J. Phys. B: At. Mol. Phys.* **20**, 2339 (1987).

[39] W. Ketterle, H. Figger, H. Walther, *Phys. Rev. Lett.* **55**, 2941 (1985).

[40] L. Wolniewicz, *J. Chem. Phys.* **43**, 1087 (1965).

[41] W. Kolos, J. M. Peek, *Chem. Phys.* **12**, 381 (1976).

[42] I. D. Petsalakis, G. Theodorakopoulos, C. A. Nicolaides, R. J. Buenker, *J. Phys. B: At. Mol. Opt. Phys.* **20**, 5959 (1987).

[43] J. M. H. Lo, M. Klobukowski, D. Bielińska-Wąż, G. H. F. Diercksen, E. W. S. Schreiner, *J. Phys. B: At. Mol. Opt. Phys.* **38**, 1143 (2005).

[44] T. Detmer, P. Schmelcher, F. K. Diakonos, L. S. Cederbaum, *Phys. Rev. A* **56**, 1825 (1997).

[45] D. R. Bates, *J. Chem. Phys.* **19**, 1122 (1951).

[46] S. Chandrasekhar, *Astrophys. J. 102*, 223 (1945).

[47] A. Thorne, U. Litzén, S. Johansson, *Spectrophysics: Principles and Applications*, Springer, New York, 1999.

Chapter 7

Effects of Confinement on the Rydberg Molecule NeH

In the present chapter[1], the main focus is switched to a heavier noble-gas compound, NeH. As in the previous chapter, the influences due to the applied potential to a various structural and spectroscopic properties are explored and discussed using both variational CI and perturbative techniques.

7.1 Introduction

In recent decades excimers (molecules with repulsive or very unstable ground state but stable excited states) have become one of the major areas of research in laser physics and spectroscopy [1]. In cases when the excited states are Rydberg states, the excimers are also known as Rydberg molecules [2]. Rydberg molecules are characterized by the Rydberg electron, which is far from the ion core, and a small ionization potential. Due to the large orbital radius of the Rydberg electron, its interaction with the parent core could be regarded as approximately Coulombic. The presence of the Rydberg electron gives rise to a series of lines in atomic and molecular spectra which can be described using the quantum defect theory [3].

The first Rydberg molecule, He_2, was discovered and investigated by Goldstein [4] and Curtis [5] in 1913, and in the following years many Rydberg molecules were found and analyzed [6]. Among them, the noble-gas hydrides (NgH) have attracted

[1] A version of this chapter was published in *J. Phys. B: At. Mol. Opt. Phys.* **38**, 1143 (2005).

significant attention from both theoreticians and experimentalists. Since the early work on HeH by Michels and Harris [7], Miller, Schaefer and Slocomb [8, 9], and by Das and Wahl [10], many studies have been focused on the spectroscopic observations of the electronic transitions of NgH (e.g. Refs. [11, 12, 13, 14]) and the theoretical computations of accurate potential energy curves (PECs) of the electronic states of these systems (see Refs. [15, 16, 17, 18, 19]). It is known that all these molecules possess a van der Waals minimum in the ground electronic and a series of Rydberg bound excited states. As the Rydberg electron does not interact strongly with the ion core, the potential energy curves of these states closely resemble those of the corresponding molecular ions. An interesting feature of these NgH Rydberg molecules appears in their bound-bound and bound-free fluorescence spectra. The A $^2\Sigma^+$ state of HeH and ArH was found to decay preferably by predissociation via nonadiabatic radial coupling with the ground state at small internuclear distances while a continuous A $^2\Sigma^+ \rightarrow$ X $^2\Sigma^+$ emission spectrum could be observed for NeH and KrH [20] although line-broadening due to a small rate of predissociation was still detectable [21].

A number of experimental techniques have been developed to generate atoms and molecules in Rydberg states and to determine their properties (see, for example, Refs. [22, 23, 24, 25]). Field-ionization [26] is an efficient method for detecting Rydberg molecules and measuring their energy levels. Relying on the fact that the Rydberg electron with high principal quantum number possesses a very small ionization potential, a tunable pulsed field is applied to the system and used to determine the threshold amplitude, that corresponds to the ionization potential, at which the Rydberg electron is ejected [6]. By carefully adjusting the pulsed field, microwave transitions between fine-structure states could also be detected [27]. However, a serious technical problem arises because the electronic and spectroscopic properties of these systems are vulnerable to the variation of fields; a fast increase of field may give rise to the diabatic effects in which these systems transverse between states via the avoided crossing [28]. Therefore, a detailed understanding of the electronic structures and behavior of Rydberg molecules with respect to the external

fields is desirable.

Field modulation of molecular properties has been a subject of extensive studies since the early stage of quantum physics. Hydrogen atom in electric and magnetic field is a typical example, demonstrating the influence of external fields on the spectroscopic properties of atomic systems. Following the rapid advancement of solid-state physics and laser technology, the concept of field-induced confinement has been applied to the creation of quantum dots [29], nano-scaled semi-conducting materials [30] and opto-electronic devices [31]. Meanwhile, theories have also been established to understand and explain, from the theoretical viewpoint, the experimental observations of the special properties exhibited by these systems (for a recent review, see Ref. [32]).

Due to the diffuse distribution of the excited valence electron, the Rydberg molecules, as compared to other ground-state systems, will be very sensitive to the existence of external potentials and to their slight variations. Therefore, it is intriguing to explore the Rydberg molecules confined by an external potential and understand how they respond to the application of both weak and strong potentials. In the present work, the influence of spatial confinement on NeH molecule was studied, in which a weak harmonic potential was adopted and treated as a perturbation. The potential energy curves of the ground and the three lowest excited states of NeH were calculated, and the geometric parameters and vibrational constants were determined. Additionally, the process of field-induced ionization of the system at different electronic states was investigated and the threshold field strengths for autoionization were extrapolated.

7.2 Computational Methodology

The basic ideas of the formulation of the model of confinement have been introduced and discussed in Chapter 2. In this work, the potential is again assumed taking the form of a cylindrical harmonic potential defined as eqs. (2.23) and (2.24). The present work can be treated as a model study in which the electron density, $\rho(\vec{r})$, of the molecular system is modified due to the external potential. The choice of

the harmonic-type model potential seems suitable, since such potentials have been found of great use in condensed-matter physics and nanotechnology. For instance, the lateral potential of a small, two-dimensional quantum dot, when the scattering states are neglected, can be adequately represented by a parabolic well [31]. This model potential can also explain the unexpected independence of the excitation energy and the number of particles in a quantum dot [35]. On the other hand, the harmonic oscillator potential can be used as an approximate model for the studies of charged particles and molecules in parallel magnetic fields [36], and has recently been utilized in the studies of magnetized molecular hydrogen [37].

The calculations of the potential energy curves of four electronic states of NeH were performed using multi-reference configuration interaction (MRCI) method implemented in the object-oriented OPENMOL program [38] for values of ω ranging from 0.00 to 0.12 a.u. In all the calculations, Dunning's cc-pVTZ basis set for neon [39] and a (13s7p1d) basis set, denoted by H-36, contracted to (10s7p1d) for hydrogen atom [40] were used. In order to appropriately describe the distortion of electron density by the harmonic potential, a set of auxiliary basis functions with exponents of $\omega/2$ was added at the midpoint position between the nuclei [41]. These so-called confinement basis functions are the eigenfunctions of the harmonic oscillator with strength ω.

7.3 Results and Discussion

7.3.1 Basis set

One of the characteristics of the Rydberg molecules is the valence electron that moves in an orbit with a large dimension. Consequently, the interaction between the Rydberg electron and the molecular core is purely electrostatic, and long-range interaction becomes significant. Accurate calculations of the interaction of the Rydberg electron require basis sets with diffuse exponents that are able to properly describe electrons in the high-lying states and with large angular momentum. The H-36 basis set has been tested in atomic calculation of hydrogen atom, and it yielded superior excitation energies for 2s, 2p, 3s, 3p and 4s states [40] with the average error

of only 0.2 microhartrees. Baer et al. have pointed out that the correlation effect between the Rydberg electron and the molecular core is very small and the excited states could be well described by a single configuration [42]. Previous calculations [16, 43, 44] and the present study also support the single dominant reference configuration. Hence, the main contribution to the electron correlation arises from the core electrons in the parent ion, and correlation-consistent type basis sets such as cc-pVTZ should enable the recovery of most of the correlation energy. As the primary goal of the present work is to investigate the ground and first three excited states, which are correlated only to 1s, 2s and 2p atomic orbitals of hydrogen, the H-36 basis set is suitable and provides excellent description of the states in the presence of a confining potential.

In order to reduce the extremely large number of configurations that could arise in extensive CI calculations, in the MRCI calculations the reference space is truncated by selecting only the configurations for which the coefficient in the wavefunction, c_i, is greater than 0.1, i.e., $|c_i| > 0.1$. This leads to the reference space with less than eleven configurations and about 300000 determinants in the subsequent CI calculations. The core 1s orbital of Ne was kept frozen. Spectroscopic parameters for the ground and excited states of NeH for $\omega = 0.00$ are presented in Table 7.1, and the potential energy curves are shown on Figure 7.1. The calculated values show good agreement with the data reported by Baer et al. [42] and Bondybey et al. [43], except for the C $^2\Pi$ state where the r_e value from Bondybey et al. is 0.1 a.u. longer than the value obtained in this work. The discrepancies in r_e, ν_e and D_e are acceptable, although the computed $\nu_e x_e$ are systematically about 26 $\sim$ 36% larger than the ones from Ref. [42]. Accordingly, the truncated MRCI method is still able to yield potential energy curves with good accuracy for the study of influence of confinement.

7.3.2 Structural Alterations in Confinement

Similarly to the cases of other noble-gas hydrides [15, 18], the low-lying excited states of NeH strongly resemble the ground-state potential energy curve of NeH^+,

Table 7.1: Spectroscopic constants of NeH and NeH^+ without confinement. (r_e in atomic units, D_e in eV, and ν_e and $\nu_e x_e$ in cm^{-1})

State	Reference	r_e	ν_e	$\nu_e x_e$	D_e
A $^2\Sigma^+$	This work	1.8894	2869	136.7	2.03
	[42]	1.9067	2855	108.4	2.04
	[43]	1.8822	2801		1.53
	[16]	1.9332	2727		2.01
B $^2\Pi$	This work	1.8681	2952	167.8	1.86
	[42]	1.8671	2883	124.0	1.84
	[43]	1.8671	2913		1.50
	[16]	1.9162	2792		1.79
C $^2\Sigma^+$	This work	1.9392	2780	129.0	1.50
	[42]	1.9464	2646	95.6	1.37
	[43]	2.0579	2737		1.51
	[16]	1.9842	2596		1.79
NeH^+ X $^1\Sigma^+$	This work	1.8628	2953	135.8	2.37
	[43]	1.8689	2917		2.10
	[45]$^{(a)}$	1.876	2910	105.9	2.33
	[45]$^{(b)}$	1.882	2894	116.9	2.27
	[45]$^{(c)}$	1.876	2892	114.5	2.29
	Expt$^{(d)}$	1.8727	2904	113.4	2.28

$^{(a-c)}$ CCSD(T) + BSSE with cc-pVTZ, aug-cc-pVTZ, and aug-cc-pVQZ basis sets respectively. $^{(d)}$ Refs [46] and [47].

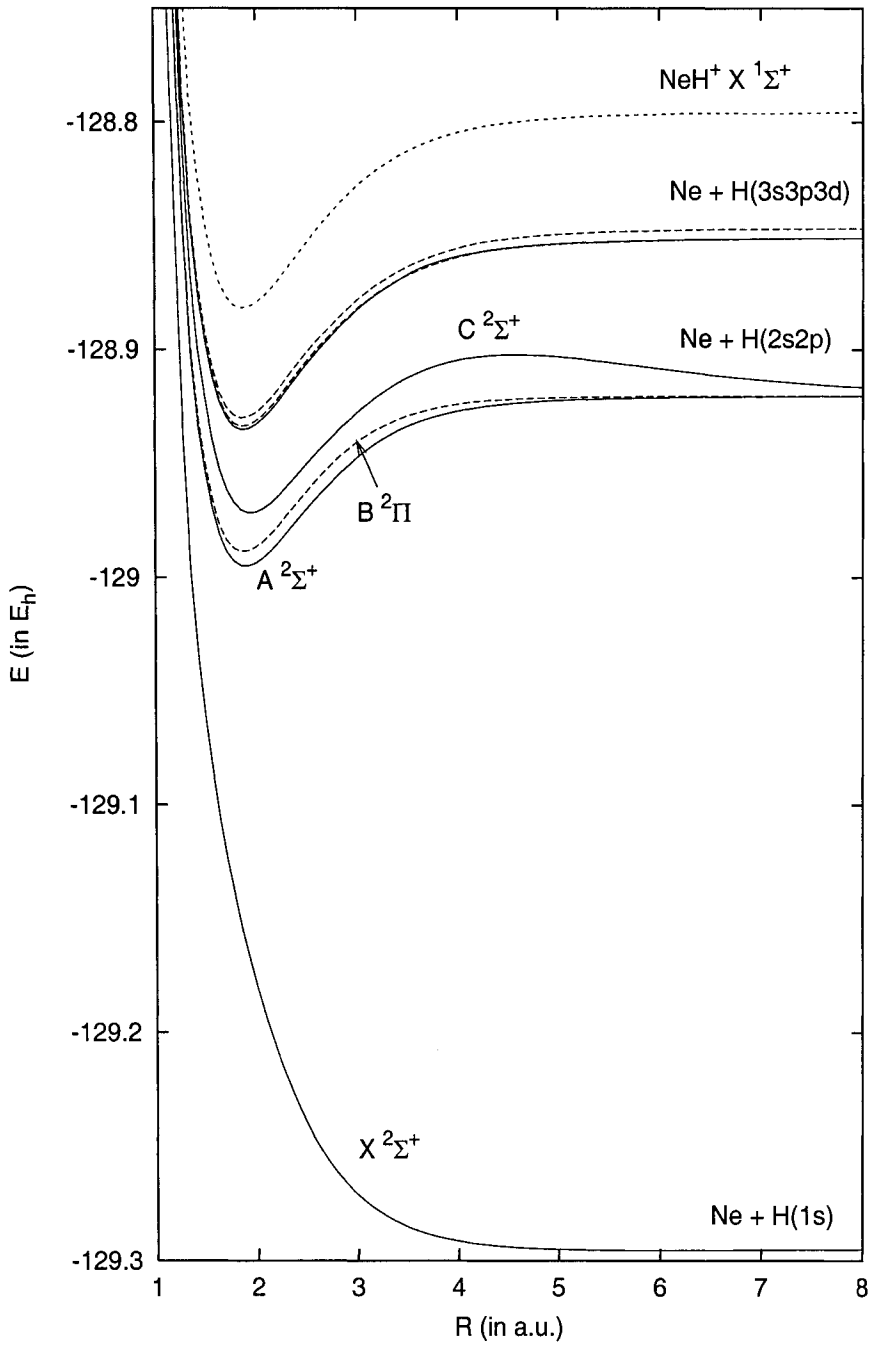

Figure 7.1: Potential energy curves of selected low-lying states of NeH and the ground state of NeH^+. ($\omega = 0.00$ a.u.)

which constitutes the parent ion core of the Rydberg states of NeH. However, the C $^2\Sigma^+$ potential energy curve shows a local maximum at about 4.00 a.u., which is possibly caused by the interaction of the Rydberg electron (n=2) of the hydrogen atom with the neon core. A counterpart has also been found in HeH where its C $^2\Sigma^+$ potential energy curve possesses a small barrier at 3.8 a.u. [40]. Theodorakopoulos et al. showed that the large radial coupling between the A $^2\Sigma^+$ and C $^2\Sigma^+$ states gives rise to the exchange of configurations between the states at intermediate R [16]. At small R, the A $^2\Sigma^+$ state is characterized by the hydrogen 2p function while the C $^2\Sigma^+$ state is dominated by the Rydberg character of hydrogen's 2s orbital. When R increases, the A $^2\Sigma^+$ acquires more of the hydrogen 2s character. On the other hand, the C $^2\Sigma^+$ state could be described by the hydrogen 2p function, with an admixture of ionic ($Ne^+ + H^-$) character that gradually vanishes at very large R.

The effects of cylindrical confining potential on the ground and Rydberg states of NeH are diverse. Figures 7.2-7.5 depict the variations of potential energy curves for the X $^2\Sigma^+$, A $^2\Sigma^+$, B $^2\Pi$ and C $^2\Sigma^+$ states under the influence of external confinement. Calculations of molecular H_2 and Li_2 revealed that spherical and prolate-type confining harmonic-oscillator potentials always restrict electron density within the internuclear space, thus yielding a stronger bonding interaction, larger binding energy, and shorter bond distances [33, 34]. In the case of cylindrical-type confinement, however, the above-mentioned conclusions are not necessarily appropriate. For instance, as shown in Figure 7.6, the A $^2\Sigma^+$ state is the only one that has a decreased r_e and a larger ν_e in the presence of confining potential, which could be ascribed to the enriched electron density in the internuclear region that consequently strengthens the bonding interaction. On the other hand, the B $^2\Pi$ and C $^2\Sigma^+$ states exhibit the opposite trend with a stretched bond distances and reduced vibrational constants.

The different geometric variations of the states could be attributed to the changes of the electronic structures and the electron density distributions of the molecular orbitals due to the confining potential. For all the four states investigated here the

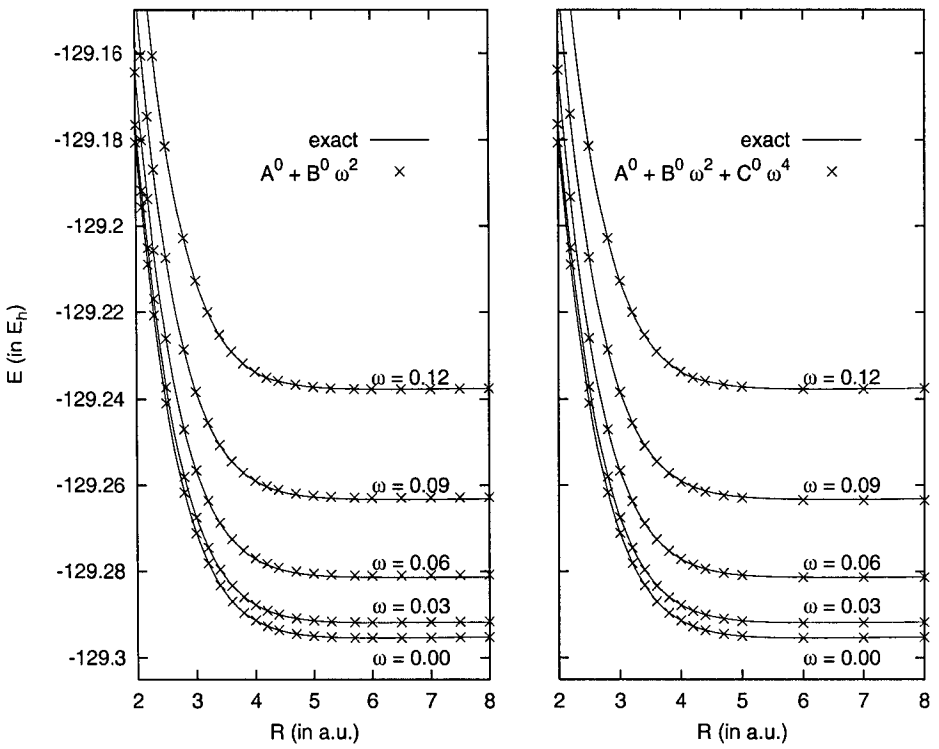

Figure 7.2: Potential energy curves of X $^2\Sigma^+$ state in confinement. Exact results from MRCI and approximate results from perturbation theory (first and second-order, respectively).

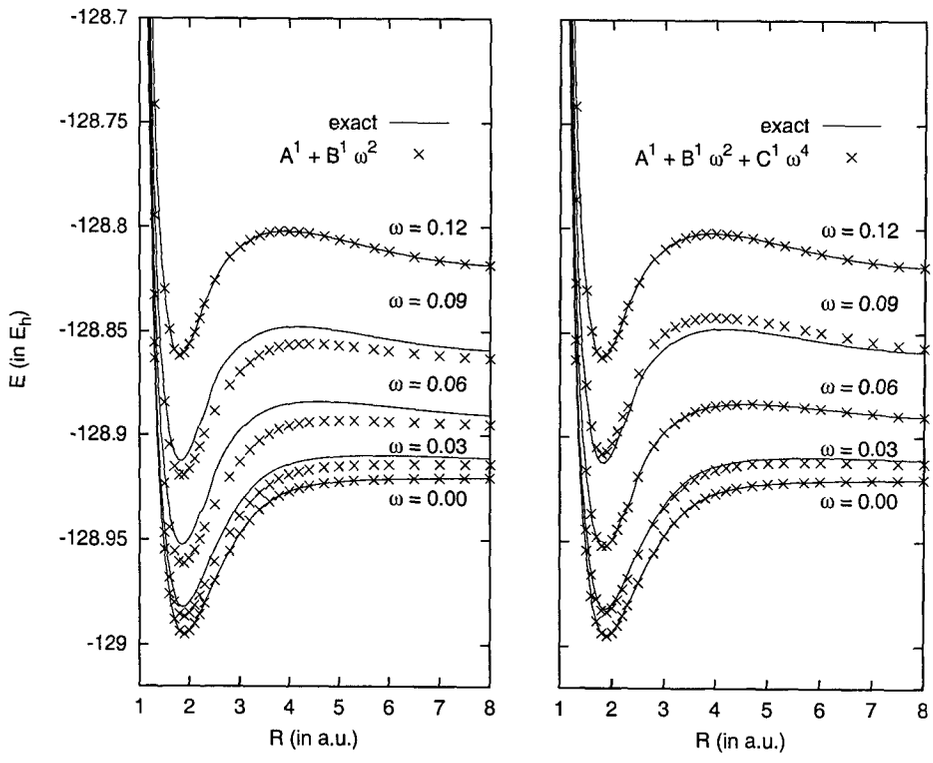

Figure 7.3: Potential energy curves of A $^2\Sigma^+$ state in confinement. Exact results from MRCI and approximate results from perturbation theory (first and second-order, respectively).

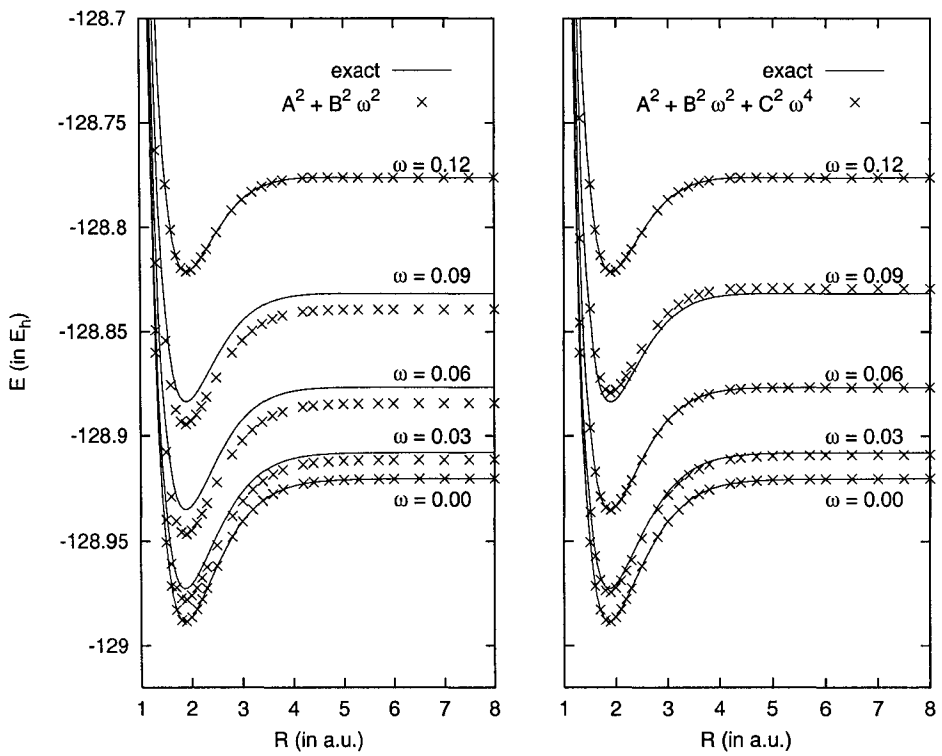

Figure 7.4: Potential energy curves of B $^2\Pi$ state in confinement. Exact results from MRCI and approximate results from perturbation theory (first and second-order, respectively).

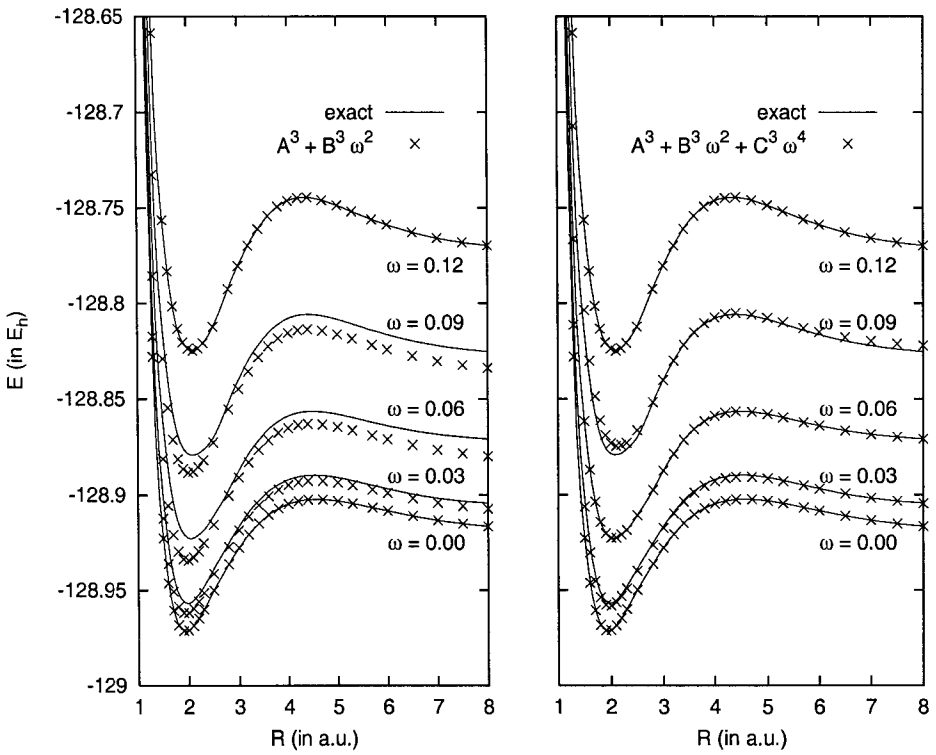

Figure 7.5: Potential energy curves of C $^2\Sigma^+$ state in confinement. Exact results from MRCI and approximate results from perturbation theory (first and second-order, respectively).

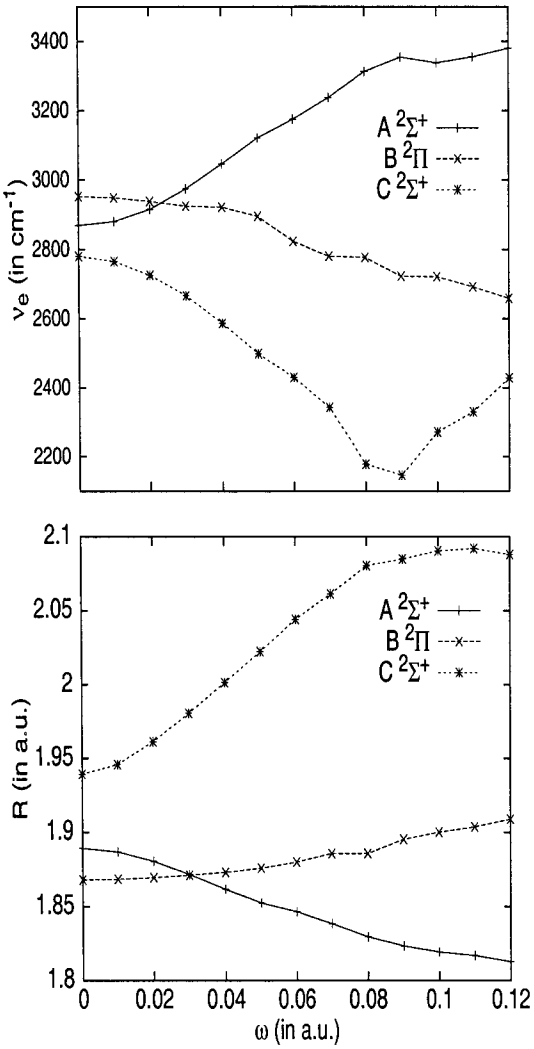

Figure 7.6: Plots of equilibrium bond distances and vibrational frequencies versus the strengths of confinement for the first three low-lying electronic states of NeH.

asymptotes are correlated to the ground state of neon and various states of hydrogen. Diercksen et al. have shown that orbitals of atoms and molecules reorder according to the strengths and types of the applied potentials [48]. Prolate-type confining potentials split the triply-degenerate 2p orbitals, giving rise to the $2p_z < 2s < (2p_x, 2p_y)$ ordering of orbital energies. Because of the additional relative stability of $2p_z$ atomic orbitals, the dissociation limits associated with the A $^2\Sigma^+$, B $^2\Pi$ and C $^2\Sigma^+$ states change. The asymptote for the A $^2\Sigma^+$ state, which corresponds to Ne and H($2p_z$), is lowered while that for the B $^2\Pi$ state, leading to Ne and H($2p_x$,$2p_y$), is shifted upward. These findings agree with the predicted ordering of 2s and 2p atomic orbitals embedded in prolate-type confining potentials.

Although there exists no avoided crossing between the low-lying $^2\Sigma^+$ states in the case of $\omega = 0.00$ a.u., for $\omega > 0.05$ a.u. an explicit avoided crossing of the A and C $^2\Sigma^+$ states starts to appear at $R = 3.00$ a.u., indicating a stronger interaction between the states due to the external potential. In addition, the applied potential suppresses the hydrogen 2p character in the A $^2\Sigma^+$ state while greatly enhancing it in the C $^2\Sigma^+$ state. Through the avoided crossing these states exchange their characteristics: the A $^2\Sigma^+$ state acquires more hydrogen 2p character and the hydrogen 2s orbital becomes dominant for the C $^2\Sigma^+$ state. The new avoided crossing also leads to the formation of a local maximum in the A $^2\Sigma^+$ state, lying about 0.4 eV above the dissociation limit when $\omega = 0.12$ a.u., since the relative stability of $2p_z$ with respect to other 2p orbitals brings about the downward shift of the potential energy curve. Furthermore, this avoided crossing causes the reduction of the binding energy for this state, with D_e changing from 2.0 eV ($\omega = 0.00$ a.u.) to 1.6 eV ($\omega = 0.12$ a.u.).

The B $^2\Pi$ state exhibits a monotonically increasing r_e and decreasing ν_e for $\omega > 0.00$ a.u., even if the changes in r_e and ν_e are small (2% and 10% respectively). The relatively small variations might possibly result from the insignificant change of the shapes of $2p_x$ and $2p_y$ atomic orbitals, whose lobes along x- and y-directions are squeezed, thus enhancing the orbital overlap with the closed-shell neon at slightly larger R. The binding energy also exhibits a decreasing trend, indicating that the

bonding interaction is weakened by the confining potential.

Despite the prominent effects of the confining potential on the A $^2\Sigma^+$ potential energy curve, the potential energy curve of the C $^2\Sigma^+$ state remains essentially the same regardless of the strength of the applied potential. The only significant changes are observed in the barrier of the local maximum at the internuclear distance of about 4 a.u. and the potential minimum at small R. The increasing r_e is apparently a consequence of the additional avoided crossing with the A $^2\Sigma^+$ state that shifts the potential well towards a larger R. Interestingly, the position and height of the energy barrier provide information about the orbital extent of the Rydberg electron and its interaction with the Ne core [49]. The maximum moves towards smaller R when $\omega > 0.00$ a.u., suggesting that the orbital of the Rydberg electron is compressed by the external potential. This is not unexpected, because the potential is repulsive to electrons therefore contracting and deforming the orbitals. Apart from the reduced size of orbital, the Rydberg electron experiences a stronger interaction with the Ne core when the molecule is confined. As illustrated by Figure 7.5, the potential hump is enlarged by approximately 50% when ω is increased to 0.12 a.u. This strengthened interaction is attributable to the larger confined electron density, which shields the Ne core, that gives rise to a stronger Coulomb repulsion.

Additional insights into the effect of confinement on the wavefunction at different internuclear distances may be obtained by analyzing contributions from dominant configurations. Figures 7.7 and 7.8 show the values of $|c|^2$ for three configurations that correspond to the excitations $H(1s^1) \rightarrow H(2s^1)$, $H(1s^1) \rightarrow H(2p_z^1)$, and $Ne(2p_z^2)H(1s^1) \rightarrow Ne(2p_z^1)H(1s^2)$ (the latter is called ionic in the following discussion). In the region of small R (i.e., $R < 2.0$ a.u.) the A $^2\Sigma^+$ state (Figure 7.7) is dominated by the Rydberg H(2p) character while the C $^2\Sigma^+$ state (Figure 7.8) is essentially of the Rydberg H(2s) character for all values of ω. These results are consistent with the X $^2\Sigma^+$ - A $^2\Sigma^+$ coupling matrix element calculations performed by Theodorakopoulus et al. [16], in which the small X-A coupling matrix elements of NeH compared to those for HeH are due to the Rydberg H(2p) character of the A $^2\Sigma^+$ state.

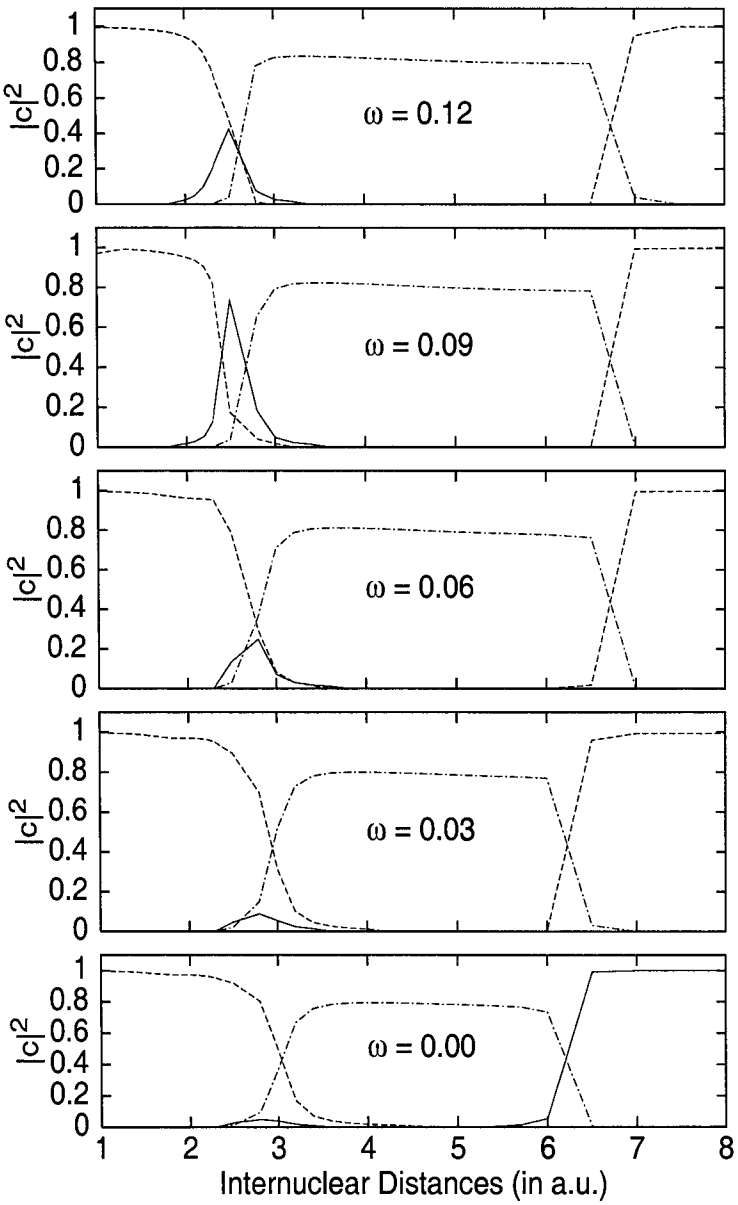

Figure 7.7: Decomposition of the A $^2\Sigma^+$ state wavefunction. Solid lines: Ne(ground-state) + H(2s); dashed lines: Ne(ground-state) + H($2p_z$); dotted-dashed lines: ionic Ne^+ and H^- resulting from the excitation of Ne(2p) $\rightarrow$ H(1s).

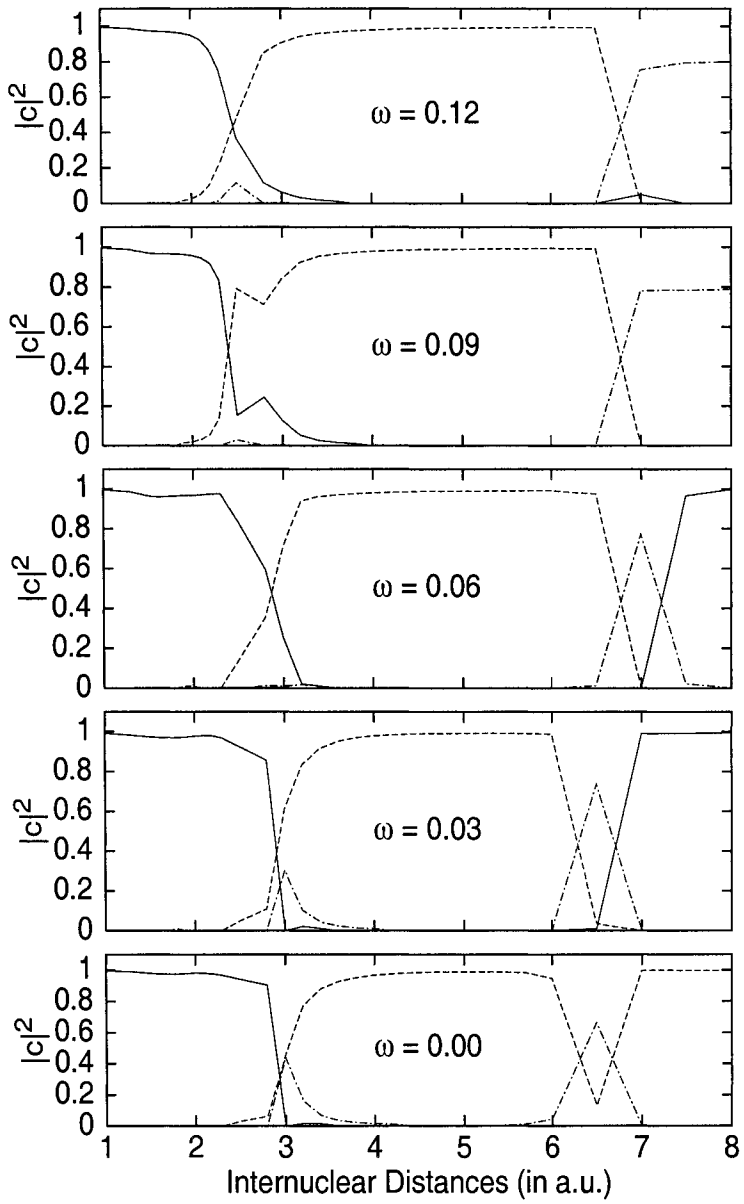

Figure 7.8: Decomposition of the C $^2\Sigma^+$ state wavefunction. Solid lines: Ne(ground-state) + H(2s); dashed lines: Ne(ground-state) + H($2p_z$); dotted-dashed lines: ionic Ne^+ and H^- resulting from the excitation of Ne(2p) $\rightarrow$ H(1s).

At the point of avoided crossing, a sharp interchange of configurations is observed where the C $^2\Sigma^+$ state acquires the H($2p_z$) character from the A $^2\Sigma^+$ state, and this configuration becomes dominant for the range of intermediate R. Meanwhile, the small contribution from the ionic configuration appears in the C $^2\Sigma^+$ state wavefunction but it declines gradually for $R > 3.5$ a.u. This may be attributed to the additional crossing of the C $^2\Sigma^+$ state and the $Ne^+ + H^-$ ionic potential. On the other hand, the avoided crossing causes the increase in the H(2s) character of the A $^2\Sigma^+$ state, but, surprisingly, this character vanishes rapidly. Instead, the ionic configuration arises, possibly due to the crossing with the ionic potential, and dominates the state. Interestingly, the H(2s) character in the A $^2\Sigma^+$ state wavefunction at small R increases with ω, which can be accounted for in terms of the extent of the A $^2\Sigma^+$ - C $^2\Sigma^+$ avoided crossing. The stronger interaction between these states for $\omega \approx 0.09$ a.u. gives rise to the larger contribution of the H(2s) configuration to the A $^2\Sigma^+$ state.

The situation at large R (i.e., $R > 6$ a.u.) is more complicated. The reordering of 2p orbitals induced by the confining potential suggests the differentiation of asymptotic limits of the A, B, and C states. This change is observed in the A $^2\Sigma^+$ state where the dissociation channel switches from H(2s) (free-space) to H($2p_z$) ($\omega = 0.12$ a.u.). Similar change of dissociation limit is noticed in the C $^2\Sigma^+$ state where the asymptote correlates to Ne(ground-state) + H(2s) when an external potential is present. Nevertheless, it is also found that the contribution of the ionic configuration increases with ω, which outweighs the H(2s) character in the region of $6.0 < R < 8.0$ a.u. when $\omega > 0.06$ a.u. Calculations for $R > 10.00$ a.u. reveal that the ionic character diminishes gradually and the H(2s) character appears again, leading to the limit of Ne(ground-state) and H(2s); furthermore, the point where the H(2s) character reappears is dependent on ω. This intrusion of ionic character in the C $^2\Sigma^+$ potential energy curve indicates a possible existence of a strong configuration interaction between the C $^2\Sigma^+$ state and the ionic potential which is caused by the destabilization of the C $^2\Sigma^+$ state. The upshift of the C $^2\Sigma^+$ potential energy curve with respect to the ionic potential results in the shift of this additional

avoided crossing toward larger R.

7.3.3 Perturbational Approach to The Studies of The Effects of Confining Potential

In all the calculations performed in the present work, the values of ω remain very small, i.e., $\omega << 1$. In addition, as may be seen in Figures 7.2-7.5 and 7.9, the influence of confinement on the properties of potential energy curves of the low-lying electronic states of NeH is rather small. It is therefore interesting to explore whether the effect of confinement may be treated via perturbation theory, while maintaining the full variational flexibility of the MRCI approach for the treatment of the electron correlation [50].

According to the definition in eq. (2.24), the confining potential that appears in eq. (2.1) can be rewritten as

$$\mathcal{W}(\vec{r}) = \omega^2 \sum_{i=1}^{N} \frac{1}{2}\left(x_i^2 + y_i^2\right) \equiv \omega^2 \mathcal{W}'(\vec{r}), \tag{7.1}$$

leading to the following form of eq. (2.1):

$$\mathcal{H}(\vec{r};\vec{R}) = \mathcal{H}^{(0)}(\vec{r};\vec{R}) + \omega^2 \mathcal{W}'(\vec{r}). \tag{7.2}$$

The perturbation approach to the confinement effects was introduced in Chapter 6. Here, a more detailed exposition of the method is presented. Using the Rayleigh-Schrödinger perturbation theory, it is assumed that the unperturbed Hamiltonian $\mathcal{H}^{(0)}(\vec{r};\vec{R})$ satisfies the Schrödinger equation:

$$\mathcal{H}^{(0)}(\vec{r};\vec{R})\Psi_n^{(0)}(\vec{r};\vec{R}) = E_n^{(0)}(\vec{R})\Psi_n^{(0)}(\vec{r};\vec{R}) \tag{7.3}$$

where n labels electronic states (i.e., n = 0, 1, 2, 3 for the states X $^2\Sigma^+$, A $^2\Sigma^+$, B $^2\Pi$, and C $^2\Sigma^+$, respectively) and the superscript represents the order of correction. The corrected total energy can be expanded in a power series of the perturbation parameter ω^2:

$$E_n(\vec{R}) = E_n^{(0)}(\vec{R}) + \omega^2 E_n^{(1)}(\vec{R}) + \omega^4 E_n^{(2)}(\vec{R}) + \cdots, \tag{7.4}$$

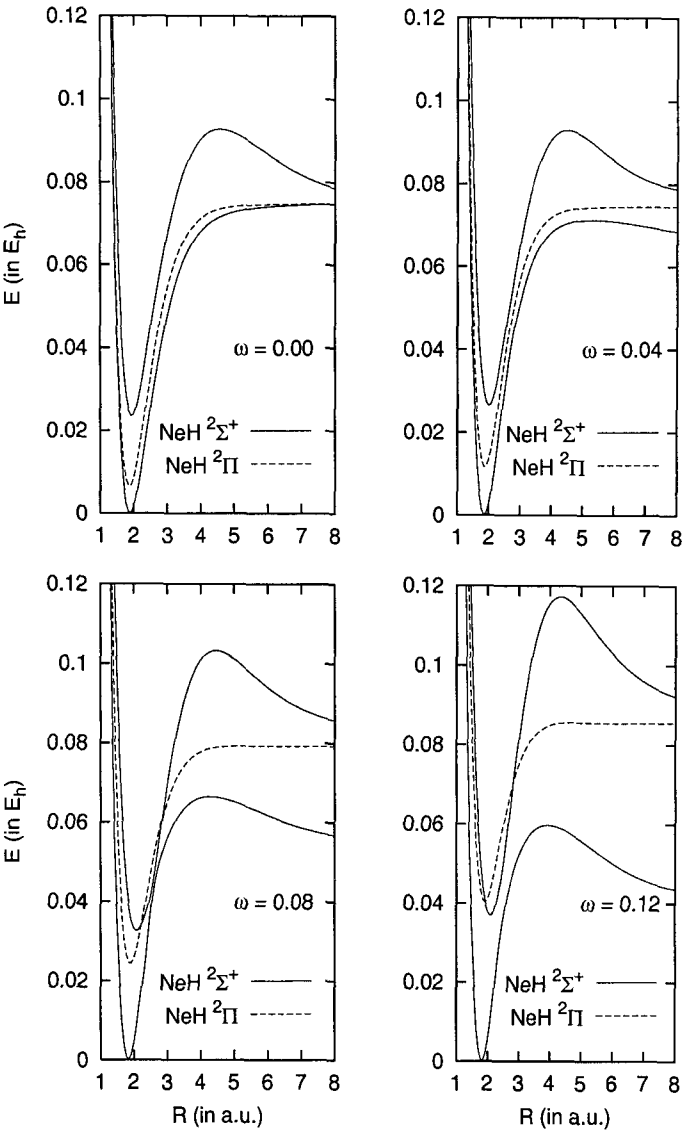

Figure 7.9: Potential energy curves of $^2\Sigma^+$ and $^2\Pi$ states in confinement. Energy is rescaled with E_{min} of the A $^2\Sigma^+$ state as the reference.

where the first and second-order energy corrections are

$$E_n^{(1)}(\vec{R}) = \langle \Psi_n^{(0)}(\vec{r};\vec{R})|\mathcal{W}'(\vec{r})|\Psi_n^{(0)}(\vec{r};\vec{R})\rangle \quad (7.5)$$
$$E_n^{(2)}(\vec{R}) = \langle \Psi_n^{(0)}(\vec{r};\vec{R})|\mathcal{W}'(\vec{r})|\Psi_n^{(1)}(\vec{r};\vec{R})\rangle.$$

To investigate the accuracy of the energies from perturbation theory, two polynomial approximations to the energy $E^n(\vec{R})$ in eq. (7.4) were used:

$$E_n(\vec{R}) = A^n(\vec{R}) + B^n(\vec{R})\omega^2 \quad (7.6)$$
$$E_n(\vec{R}) = A^n(\vec{R}) + B^n(\vec{R})\omega^2 + C^n(\vec{R})\omega^4. \quad (7.7)$$

The first term $A^n(\vec{R})$ in these equations is the unperturbed energy corresponding to $\omega = 0.00$. The coefficients $B^n(\vec{R})$ and $C^n(\vec{R})$ are determined by requiring that eqs. (7.6) and (7.7) are fitted exactly with the MRCI potential energy curves for $\omega = 0.12$ a.u. and both $\omega = 0.06$ a.u. and $\omega = 0.12$ a.u., respectively. Results are displayed in Figures 7.2-7.5, in which the solid lines are the MRCI potential energy curves ("exact") and the points marked with $\times$ represent the approximate energy values computed using eqs. (7.6) and (7.7). The values of $B^n(\vec{R})$ and $C^n(\vec{R})$ are also plotted in Figure 7.10. Evidently, eq. (7.7) leads to results superior to those obtained with eq. (7.6), and the correction up to second-order is necessary to provide the energy values comparable to the MRCI results. For the X $^2\Pi$ state both approximate polynomials work equally well as the potential energy curve does not vary much when the confining potential is applied. For the other excited states, however, eq. (7.7) yields potential energy curves that indisputably match the exact potential energy curves better than those predicted using eq. (7.6). Parameters from eq. (7.6) systematically over-estimate the perturbation, resulting in potential energy curves that are lower in energy than the exact ones. The addition of the second-order term (i.e., C^n's) greatly improves the results but the perturbation effect becomes slightly under-estimated when $\omega \approx 0.09$ a.u. As the A and C $^2\Sigma^+$ states are involved in the avoided crossing for $0.05 < \omega < 0.10$ a.u., the perturbation treatment leads to very large errors in the approximate potential energy curves.

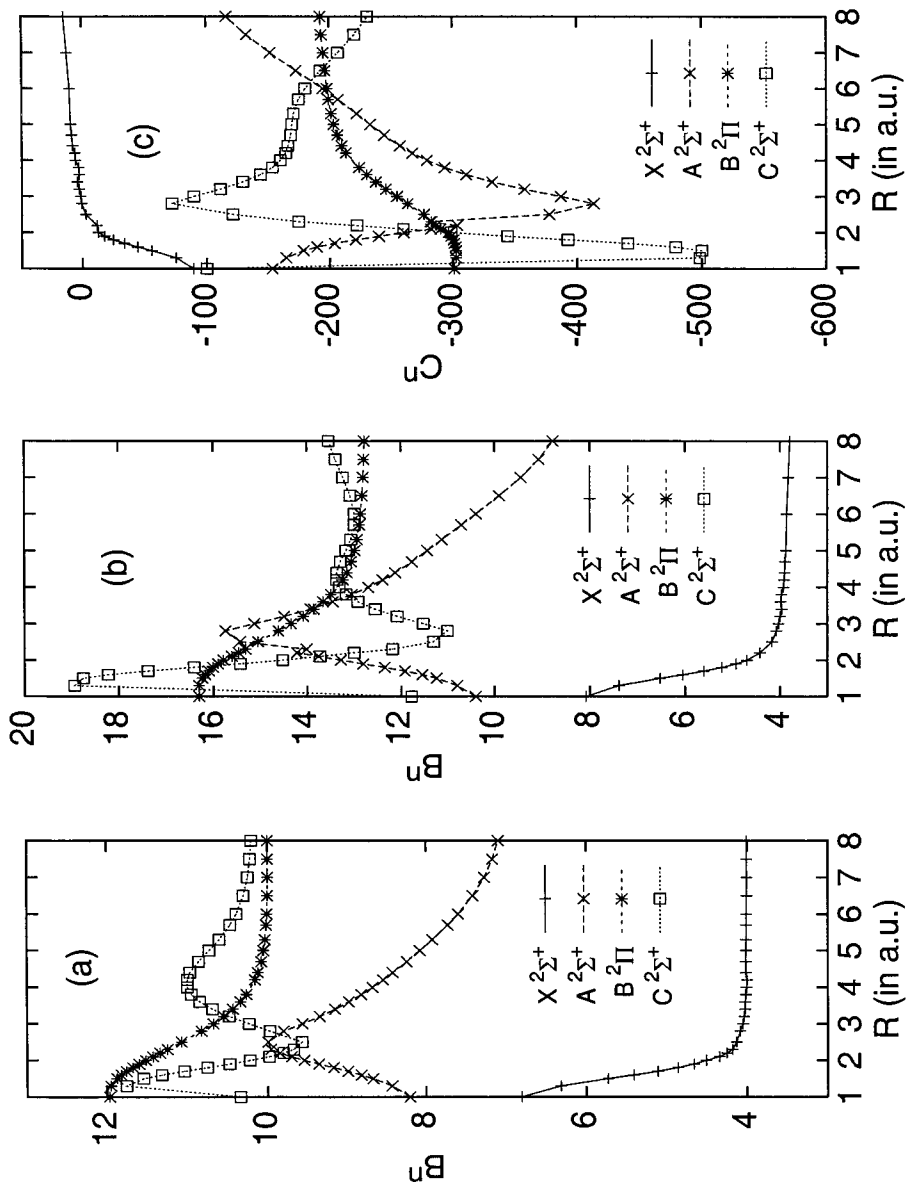

Figure 7.10: Coefficients of the approximate polynomials for different electronic states of NeH: (a) for Eq. (10), (b)-(c) for Eq. (11).

Table 7.2: Critical strength of confinement leading to autoionization (ω_c in atomic units).

State	ω_c
A $^2\Sigma^+$	0.144
B $^2\Pi$	0.106
C $^2\Sigma^+$	0.107

7.3.4 Autoionization Process

When enough energy is provided, an atomic system in its ground-state configuration could be excited to a bound excited state whose energy is above the first ionization limit and is embedded in the continuum. In this case, there exists a very high probability that the excited atom undergoes the process of autoionization and ejects an electron [51]. Similar process could also occur in molecular species. Since the electrons in Rydberg states interact less strongly with the parent core, they are very susceptible to the influence of external potentials and the autoionization process, or field-induced ionization, should happen more readily in Rydberg molecules.

The present study provides data to estimate the critical strengths of potential, ω_c, at which NeH in different electronic excited states becomes less stable relative to the electronic ground state of the NeH^+ ion. The energy differences E_{min} (NeH^+) - E_{min} (NeH) for the A $^2\Sigma^+$, B $^2\Pi$ and C $^2\Sigma^+$ states and the ground-state NeH^+ are calculated for $\omega < 0.12$ a.u. and the results are plotted in Figure 7.11. The critical strength of potential ω_c could be estimated as the value of ω corresponding to the vanishing energy difference. The values of estimated ω_c are tabulated in Table 7.2. Interestingly, the ω_c associated with the B $^2\Pi$ state is smaller than that of the C $^2\Sigma^+$ state, indicating that the B $^2\Pi$ state, compared to the C $^2\Sigma^+$ state, is destabilized by the confining potential more rapidly. The same conclusion could also be drawn from Figure 9, which shows that the B $^2\Pi$ state lies above the C $^2\Sigma^+$ state at $R \sim r_e$ for $\omega > 0.10$ a.u.

For all the three excited states the values of ω_c are smaller than 0.15 a.u. Previous calculations on molecular hydrogen [37] and beryllium dimer [52] yielded values of

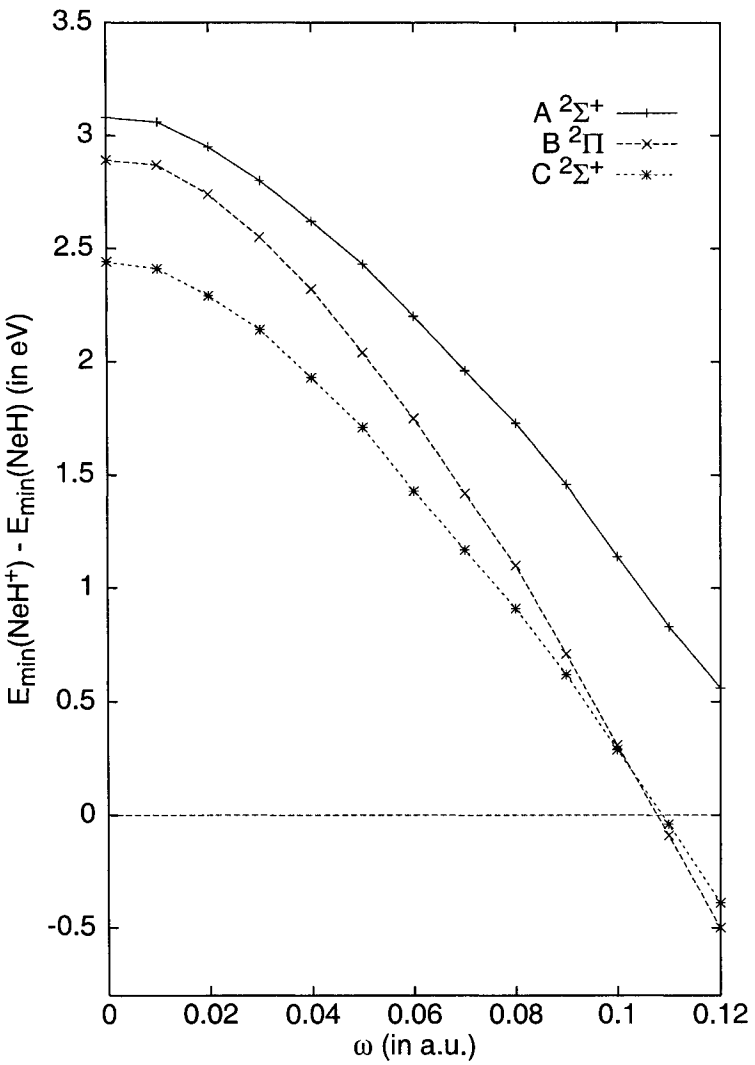

Figure 7.11: Plot of $E_{min}(NeH^+)$ - $E_{min}(NeH)$ for various values of ω. Energies are zero-point-energy corrected.

ω_c that are larger than 0.20 a.u. The results from the present study support the proposed idea that the Rydberg molecules, in contrast to strongly bound species, could undergo the autoionization process more readily.

7.4 Conclusion

Studies of the behavior of the Rydberg molecule NeH have been carried out using MRCI method. The ground and first three low-lying electronic states of NeH, subject to the influence of a cylindrical harmonic potential, have been computed. While the A $^2\Sigma^+$ and C $^2\Sigma^+$ experience rather substantial changes due to the presence of a confining potential, neither the X $^2\Sigma^+$ nor B $^2\Pi$ respond very strongly to the applied potential. A new potential maximum appears on the A $^2\Sigma^+$ potential energy curve at the intermediate values of R. In addition, the results show that an avoided crossing exists between the A and C $^2\Sigma^+$ states.

Suitability of the perturbation approach to the study of confinement effects has been studied, and it has been demonstrated that perturbational treatment up to the second-order correction could successfully yield the potential energy curves comparable to those obtained from the MRCI calculations. The errors for $\omega \approx 0.09$ a.u. may be attributed to the possible strong diabatic coupling between the A and C $^2\Sigma^+$ states.

Under the influence of confinement, the autoionization process of Rydberg NeH molecule could be facilitated, and the first three excited states would undergo field-induced autoionization for $\omega < 0.15$ a.u., which is definitely smaller than the values estimated previously for strongly bound diatomic molecules such as H_2 and Be_2^+.

Bibliography

[1] K. Kuchitsu, *Dynamics of Excited Molecules*, Elsevier, New York, 1994.

[2] G. Herzberg, *Annu. Rev. Phys. Chem.* **38**, 27 (1987).

[3] M. Seaton, *Rep. Prog. Phys.* **46**, 167 (1983).

[4] F. Goldstein, *Verh. Dtsch. Phys. Ges.* **15**, 402 (1913).

[5] W. E. Curtis, *Proc. R. Soc. London Ser. A* **89**, 146 (1913).

[6] R. F. Stebbings, F. B. Dunning, *Rydberg States of Atoms and Molecules*, Cambridge University Press, London, 1983.

[7] H. H. Michels, F. E. Harris, *J. Chem. Phys.* **39**, 1464 (1963).

[8] W. H. Miller, H. F. Schaefer III, *J. Chem. Phys.* **53**, 1421 (1970).

[9] C. A. Slocomb, W. H. Miller, H. F. Schaefer III, *J. Chem. Phys.* **55**, 926 (1971).

[10] G. Das, A. C. Wahl, *Phys. Rev. A* **4**, 825 (1971).

[11] J. W. C. Johns, *J. Molec. Spectrosc.* **36**, 488 (1970).

[12] W. Ketterle, H. Figger, H. Walther, *Phys. Rev. Lett.* **55**, 2941 (1985).

[13] I. Dabrowski, G. Herzberg, B. P. Hurley, R. H. Lipson, M. Vervloet, D. C. Wang, *Mol. Phys.* **63**, 269 (1987).

[14] R. H. Lipson, *Chem. Phys. Lett.* **129**, 82 (1986).

[15] G. Theodorakopoulos, I. D. Petsalakis, C. A. Nicolaides, R. J. Buenker, *J. Phys. B: At. Opt. Mol. Phys.* **20**, 2339 (1987).

[16] G. Theodorakopoulos, I. D. Petsalakis, R. J. Buenker, *J. Phys. B: At. Opt. Mol. Phys.* **20**, 5335 (1987).

[17] G. Theodorakopoulos, I. D. Petsalakis, *Chem. Phys. Lett.* **149**, 196 (1988).

[18] G. Theodorakopoulos, I. D. Petsalakis, R. J. Buenker, *Mol. Phys.* **71**, 1055 (1990).

[19] I. D. Petsalakis, G. Theodorakopoulos, S. Consta, *Mol. Phys.* **75**, 805 (1992).

[20] I. D. Petsalakis, G. Theodorakopoulos, R. J. Buenker, *Phys. Rev. A* **38**, 4004 (1988).

[21] T. Möller, M. Beland, G. Zimmerer, *Chem. Phys. Lett.* **136**, 551 (1987).

[22] P. Devynck, W. G. Graham, J. R. Peterson, *J. Chem. Phys.* **91**, 6880 (1989).

[23] S. F. Selgren, D. E. Hipp, G. I. Gellene, *J. Chem. Phys.* **88**, 3116 (1988).

[24] H. Beyer, K. Kollath, *J. Phys. B* **10**, L5 (1977).

[25] C. Fabre, S. Haroche, P. Goy, *Phys. Rev. A* **18**, 229 (1978).

[26] C. Fabre, P. Goy, S. Haroche, *J. Phys. B* **10**, L183 (1977).

[27] T. F. Gallagher, R. M. Hill, S. A. Edelstein, *Phys. Rev. A* **14**, 744 (1976).

[28] T. H. Jeys, G. W. Foltz, K. A. Smith, E. J. Beiting, F. G. Kellert, F. B. Dunning, R. F. Stebbings, *Phys. Rev. Lett.* **44**, 398 (1980).

[29] M. A. Reed, R. T. Bate, K. Bradshaw, W. M. Duncan, W. M. Frensley, J. W. Lee, H. D. Smith, *J. Vacuum Sci. Technol. B* **4**, 358 (1986).

[30] T. Fukui, S. Ando, Y. Tokura, *Appl. Phys. Lett.* **58**, 2018 (1991).

[31] L. Jacak, P. Hawrylak, A. Wójs, *Quantum Dots*, Springer, New York, 1998.

[32] W. Jaskolski, *Phys. Rep.* **271**, 1 (1996).

[33] D. Bielińska-Wąż, G. H. F. Diercksen, M. Klobukowski, *Chem. Phys. Lett.* **349**, 215 (2001).

[34] T. Sako, I. Cernusak, G. H. F. Diercksen, *J. Phys. B: At. Mol. Opt. Phys.* **37**, 1091 (2004).

[35] D. Pfannkuche, V. Gudmundsson, P. Hawrylak, R. R. Gerhards, *Solid State Electronics* **37**, 1221 (1994).

[36] K. Gottfried, T. M. Yan, *Quantum Mechanics: Fundamentals*, 2nd edition, Springer, New York, 2004.

[37] J. M. H. Lo, M. Klobukowski, G. H. F. Diercksen, *Adv. Quantum Chem.* **48**, 59 (2005).

[38] G. H. F. Diercksen, G. Hall, *Comput. Phys.* **8**, 215 (1994).

[39] T. H. Dunning, Jr. *J. Chem. Phys.* **90**, 1007 (1989).

[40] E. W. S. Schreiner, *Ph.D. Thesis*, Technische Universität München, 1996.

[41] D. Bielińska-Wąż, J. Karwowski, G. H. F. Diercksen, *J. Phys. B: At. Mol. Opt. Phys.* **34**, 1987 (2001).

[42] S. Baer, D. G. Fleming, J. J. Sloan, D. J. Arseneau, M. Kolbuszewski, J. Wright, M. Senba, J. J. Pan, R. Snooks, *J. Chem. Phys.* **101**, 1202 (1994).

[43] V. Bondybey, P. K. Pearson, H. F. Schaefer III, *J. Chem. Phys.* **57**, 1123 (1972).

[44] H. Partridge, D. W. Schwenke, C. W. Bauschlicher, Jr., *J. Chem. Phys.* **99**, 9776 (1993).

[45] P. Pendergast, J. M. Heck, E. F. Hayes, *Int. J. Quantum Chem.* **49**, 495 (1994).

[46] R. S. Ram, P. F. Bernath, J. W. Brault, *J. Mol. Spectrosc.* **113**, 451 (1985).

[47] J. Lorenzen, H. Hotop, M. W. Ruf, H. Morgner, *Z. Phys. A* **297**, 19 (1980).

[48] T. Sako, G. H. F. Diercksen, *J. Phys. B: At. Mol. Opt. Phys.* **36**, 1681 (2003).

[49] S. L. Guberman, W. A. Goddard III, *Phys. Rev. A* **12**, 1203 (1975).

[50] D. Bielińska-Wąż, J. M. H. Lo, M. Klobukowski, G. H. F. Diercksen, and E. W. S. Schreiner, submitted for publication.

[51] A. Thorne, U. Litzén, S. Johansson, *Spectrophysics: Principles and Applications*, Springer, New York, 1999.

[52] J. M. H. Lo, M. Klobukowski, *Mol. Phys.* **102**, 2511 (2004).

Chapter 8

Relativistic Calculations on The Ground and Excited States of AgH and AuH in Cylindrical Harmonic Confinement

This chapter[1] focuses on the preliminary investigation of the interaction between the confinement effects, electron correlation and relativity, and their mutual dependence in the electronic structure calculations for field-captured heavy element-containing compounds in which all these effects have to be considered simultaneously.

8.1 Introduction

Calculations of molecular properties of compounds containing heavy transition-metal elements is one of the most challenging issues in computational quantum chemistry. On one hand, these calculations can provide information related to the development and applications of transition metal compounds in the areas such as materials science and catalysis [1]. On the other hand, the accuracy of the calculations involving heavy transition metals is very sensitive to the methods employed. Since there are a large number of electrons and possible electronic states which are quasi-degenerate, sophisticated methods including the extensive treatment of

[1] A version of this chapter was submitted to *Phys. Chem. Chem. Phys.*

electron correlation effects are mandatory. In addition, the large relativistic effects experienced by both core and valence electrons often lead to failures of the conventional non-relativistic quantum chemistry methods.

There are several promising approaches of incorporating the relativistic effects in quantum chemical calculations. The simplest one involves the use of pseudopotentials that greatly reduce the number of electrons explicitly considered in the computations by removing the chemical unreactive core electrons and replacing with an averaged potential operator [2]. Since the generation of pseudopotential parameters depends on the reference orbitals and energies from all-electron calculations, a relativistic pseudopotential can then be produced by utilizing the reference from the Dirac-Hartree-Fock (DHF) atomic calculation [3]. A proper all-electron approach is to perform the molecular calculations using directly the Dirac-Coulomb Hamiltonian. However, it suffers from a deficiency that the two-electron interaction term is not Lorentz-invariant. This problem can be partially solved by introducing the frequency-independent Breit operator to the two-electron Coulomb term [4], leading to a so-called Dirac-Coulomb-Breit (DCB) Hamiltonian. The resulting DHF equation is very complicated and the four-component wavefunctions are very difficult to interpret. Therefore, several schemes have been proposed to decouple the large component (which corresponds to the electronic solution) and the small component (which corresponds to the positronic solution) of the DHF solutions (for example, ref. [5, 6, 7, 8]).

Among these two-component methods, the Douglas-Kroll (DK) transformation [9], further developed by Heß and coworkers [10], is the one most successfully applied in relativistic molecular calculations. This method stems from the free-particle Foldy-Wouthuysen transformation where a unitary transformation is carried out on the Dirac Hamiltonian in the external field. It follows that subsequent unitary transformations are to be performed in order to eliminate the odd terms of arbitrary orders in the external potential to avoid the problem of singularity. The DKn (where n is the order of transformations) method has been tested on a number of atomic and molecular calculations of heavy metal compounds and satisfactory results have been

obtained [11, 12, 13]. In consequence, in the present study of coinage metal hydrides, the third-order Douglas-Kroll transformation was chosen to recover the relativistic energy contributions. The spin-orbit effect was included in a perturbative fashion using the full one- and two-electron Breit-Pauli Hamiltonian [14].

Two coinage metal hydrides, AgH and AuH, were investigated in the present study. These two molecules have been often studied in quantum chemistry because of the profound effects of relativity. For instance, the strong relativistic effect experienced by the $6s$ electrons of Au atom causes the anomalously high first ionization potential and the unusual order of the low-lying excited states [15]. Both non-relativistic and relativistic molecular calculations on these compounds, using extended all-electron basis sets and effective potentials, have been performed (for a summary, see ref [16]). Nevertheless, the majority of these studies was focused only on the ground state properties, such as r_e, ω_e and D_e, and only a few was devoted to the excited states (for example, ref. [17, 18]).

In the present study the ground and excited state properties of AgH and AuH confined in a cylindrical harmonic potential were computed. Studies of confinement effects have become a major research topic [19], and confining potentials have been shown to be very useful models in the studies of plasma [20], external magnetic field [21], and quantum dots [22]. The model of harmonic confining potential has been recently applied to several molecular systems [23, 24, 25], and the basic understanding of the confinement effects in terms of orbital response has been obtained. Therefore, the aim of the present work was to investigate the combined effects of external confinement and relativity on the molecular properties, in particular the spin-orbit coupling constants, of AgH and AuH.

8.2 Computational Details

An excellent review of the Douglas-Kroll (or Douglas-Kroll-Heß) transformation could be found on the series of publications by Heß et al. [26, 27] and Hirao et al. [28, 29]. In the present work, no transformation on the two-electron operators was considered, and the instantaneous non-relativistic Coulomb two-electron operator

was used instead

$$\mathcal{H}(\mathbf{r}_i, \mathbf{r}_j) = \sum_{i<j}^{N} \frac{e^2}{r_{ij}}. \tag{8.1}$$

However, it is believed that the influence will be minimal [30].

The confining potential used in the present study is a parabolic, electrostatic repulsion operator acting solely on electrons. It is defined, for an N-electron system, as a sum of one-electron terms:

$$\mathcal{W}(\mathbf{r}) = \sum_{i=1}^{N} w(\mathbf{r}_i) \tag{8.2}$$

in which $\mathbf{r}_i$ is the coordinates of the i-th electron. The potential has the axial symmetry with the principal axis overlapped the molecular axis of AgH and AuH molecules, and the center of the potential located at the origin of the coordinate system. Therefore, the resulting confining potential can thus be represented by

$$\mathcal{W}(\mathbf{r}) = \sum_{i=1}^{N} \frac{1}{2} \left[\omega_x^2 x_i^2 + \omega_y^2 y_i^2\right] = \sum_{i=1}^{N} \frac{1}{2} \omega^2 \mathbf{r}_i^2. \tag{8.3}$$

and the total spin-free Hamiltonian is given by adding eqs. (8.1) and (8.3) to the DK3 Hamiltonian.

To deal with the electron correlation effects, the recently developed spin-orbit second-order quasi-degenerate perturbation theory (SO-MCQDPT2) [31] was employed. This method makes use of the orbitals generated in the complete active space self-consistent field (CASSCF) calculations to obtain the zeroth-order states for the spin-free Hamiltonian. The spin-orbit coupling is calculated using the full microscopic Breit-Pauli spin-orbit Hamiltonian [32] which gives rise to the off-diagonal coupling terms between the zeroth-order states in the effective Hamiltonian. Subsequently, the second-order perturbation is performed on both the spin-free and spin-orbit parts, and the resulting spin-mixed states (in terms of linear combination of the zeroth-order states) are produced via the diagonalization of the perturbed Hamiltonian [33]. This approach ensures the inclusion of the scalar relativistic effects from the spin-free wavefunctions obtained from the Douglas-Kroll Hamiltonian, and the proper treatment of the avoided crossing between states of the same symmetry [31].

All-electron basis sets were used for Ag, Au, and H in all calculations. The primitive basis set for Ag is the $24s17p12d4f3g$ set developed by Witek et al. [34], with exponents optimized at the second-order Douglas-Kroll and averaged coupled-pair functional levels for the balance description of the ^2S, ^2D and ^2P states. This basis set is contracted to $13s10p8d4f3g$ by contracting the tightest $14s10p6d$ to $3s3p2d$. In the present work, the three g-functions were dropped, yielding the final $13s10p8d4f$ basis set. For Au, the first-order polarized $21s17p11d9f$ basis set of Sadlej was used [35]. This basis set was designed for the relativistic calculations of molecular electric properties in the Douglas-Kroll no-pair approximation. The set of $13s10p7d$ with the largest exponents are contracted to $5s4p3d$, leaving all the other s, p and d primitives uncontracted. For the f-functions they are contracted in the 3,2,2,2 pattern. These contraction schemes lead to the contracted $13s11p7d4f$ Gaussian basis set. In both cases, the Dunning's cc-pVQZ basis set was used for H [36]. Spherical harmonic Gaussians were used in all calculations.

The orbitals required in the SO-MCQDPT2 calculations for AgH and AuH were generated using the CASSCF method, with the active space for both AgH and AuH consisting of ten orbitals: $1s$ for H, $4d$, $5s$ and $5p$ for Ag and $5d$, $6s$ and $6p$ for Au; 12 electrons were explicitly correlated. In order to perform the spin-orbit calculations, one common set of molecular orbitals was used to describe all the zeroth-order states. This set of orbitals was obtained from a state-averaged CASSCF over the lowest 18 electronic states which correlate to the first four dissociation channels. In the subsequent perturbation calculations, 18 core orbitals, corresponding to $1s2s2p3s3p3d4s4p$ orbitals, were frozen for AgH while 34 core orbitals composed of [Kr]$4d4f5s5p$ orbitals were uncorrelated for AuH. To eliminate the intruder states in the effective Hamiltonian, the intruder state avoidance (ISA) scheme [37] was used in which the energy denominators around the poles are shifted. The parameters of 0.02 for the spin-free terms and 0.1 for the spin-orbit terms were used as suggested by Witek et al.

The spectroscopic parameters for different electronic states of AgH and AuH were calculated based on the computed SO-MCQDPT2 potential energy curves

employing the Dunham's 4-th order polynomial [38]. All the CASSCF and SO-MCQDPT2 calculations were performed using the *ab initio* quantum chemical program GAMESS-US [39] which has been modified to include the features for the calculations of confinement effects.

8.3 Results and Discussion

8.3.1 AgH Molecule

In the SO-MCQDPT2 calculations of AgH in C_{2v} point group symmetry, 18 states (eight A_1, two A_2, four B_1, and four B_2) have been calculated, corresponding to the following twelve electronic states for diatomics in $C_{\infty v}$ symmetry: four $^1\Sigma^+$, one $^1\Delta$, two $^1\Pi$, two $^3\Sigma^+$, one $^3\Delta$, and two $^3\Pi$. These states, except for the 4 $^1\Sigma^+$ which correlates to the asymptote of $Ag(^2S, 6s)$ + $H(^2S)$, arise from the $Ag(^2S)$ + $H(^2S)$, $Ag(^2P)$ + $H(^2S)$, and $Ag(^2D)$ + $H(^2S)$ atomic states and comprise the first three dissociation channels. The estimated excitation energies for $Ag(^2S) \rightarrow Ag(^2P)$ and $Ag(^2S) \rightarrow Ag(^2D)$ are 3.794 eV and 4.051 eV, respectively, which agree fairly well with the values of 3.740 eV and 3.971 eV recently measured by Fourier-transform spectrometry [40]. The systematically over-estimated excitation energies could be a consequence of using the CASSCF orbitals optimized for both the ground and excited states of AgH.

The spectroscopic constants for these states are summarized in Tables 8.1 and 8.2. As indicated, in general the performance of the SO-MCQDPT2 is not excellent. For the ground and first several low-lying states the agreement with the available experimental data is acceptable. However, it becomes very poor for higher excited states; for example, the discrepancy in r_e is 0.2 Å for the 3 $^1\Sigma^+$ state. This is not quite unexpected, since the orbitals utilized in the SO-MCQDPT2 calculations for different states were optimized at CASSCF level for states of Σ, Π and Δ symmetries and of different spins. Consequently, these orbitals might not be able to describe the rather high-lying states. Nevertheless, these state-averaged CASSCF orbitals were used in order to provide qualitatively correct zeroth-order states for the subsequent spin-orbit calculations with the purpose of understanding the general confinement

Table 8.1: Spectroscopic constants of the singlet states of AgH (r_e in Å, ν_e and B_e in cm^{-1}, T_e in eV). Experimental data from ref. [41, 42, 43].

State		r_e	ν_e	B_e	T_e
$1\ ^1\Sigma^+$	This work	1.5635	2024	6.906	0.00
	[18]	1.620	1901	6.43	0.00
	[34]	1.564	2073	6.904	0.00
	Experiment	1.618	1760	6.449	0.00
$2\ ^1\Sigma^+$	This work	1.7503	1166	5.511	4.03
	[18]	1.604	1807	6.56	3.64
	[34]	1.717	1422	5.730	3.99
	Experiment	1.665	1664	6.265	3.71
$3\ ^1\Sigma^+$	This work	2.0669	1126	3.952	6.73
	[18]	2.201	925	3.48	6.87
	[34]	2.093	1026	3.856	6.72
	Experiment	1.862	1220	4.87	5.52
$4\ ^1\Sigma^+$	This work	1.7035	2682	5.817	7.80
	[34]	4.596	433	0.7995	7.22
$1\ ^1\Delta$	This work	1.7743	1303	5.362	6.31
	[18]	1.790	1310	5.27	5.90
$1\ ^1\Pi$	This work	1.5763	1654	6.794	6.19
	[18]	1.842	1240	4.98	5.65
	Experiment	1.61	1589	6.54	5.11
$2\ ^1\Pi$	This work	1.8119	1271	5.142	6.32
	[18]	1.643	1720	6.25	5.87
	Experiment	1.80	845	5.23	5.79

Table 8.2: Spectroscopic constants of the triplet states of AgH (r_e in Å, ν_e and B_e in cm^{-1}, T_e in eV). Experimental data from ref. [41, 42, 43].

State		r_e	ν_e	B_e	T_e
$2\ ^3\Sigma^+$	This work	1.9511	1326	4.435	6.17
	[18]	1.953	1516	4.42	6.26
$1\ ^3\Delta$	This work	1.7726	1327	5.372	6.20
	[18]	1.795	1276	5.24	5.78
	Experiment	1.875		4.81	
$1\ ^3\Pi$	This work	1.5994	1530	6.599	5.59
	[18]	1.582	1751	6.75	5.38
	[34]	1.594	1620	6.644	5.49
	Experiment	1.64	1450	6.3	5.17
$2\ ^3\Pi$	This work	1.7954	1397	5.237	6.07
	[18]	1.814	1329	5.13	5.39
	[34]	1.845	1198	4.960	6.01
	Experiment	1.85		4.95	

effects on the spectral and structural properties of coinage metal hydrides.

The ground state $^1\Sigma^+$ of AgH is characterized exclusively by the σ_g configuration composed of Ag $5s$ and H $1s$ orbitals. The calculated bond length r_e is 1.5635 Å which is about 0.05 Å shorter than the experimental value; correspondingly, the vibrational frequency is over-estimated by 300 cm^{-1}. These deviations could be due to the deficiency of the MP2 method in recovering the dynamic correlation effects. Applying the same basis set, geometry optimizations for the ground state of AgH have been performed using RHF, MP2 and DFT methods. The results (Table 8.3) illustrate that the relativistic MP2 predicts the bond lengths generally shorter than the experiment by 0.04 to 0.05 Å, but the relativistic B3LYP yields the values in an excellent agreement. The extension of MP2 to include multi-configuration references slightly contracts the bond distance by 0.006 Å. The previous studies by Witek et al. using the multi-reference MP2 with $18s8p5d2f$ basis set predicted $r_e = 1.620$ Å [18]. Therefore, the under-estimated r_e in the present work could result from the smaller s-space in the basis set, as well as the absence of g-type functions, that could not adequately describe the relativistic effects on the s-orbitals in Ag and their interaction with H (^2S).

Table 8.3: Structural parameters for the ground state of AgH (r_e in Å, ν_e in cm^{-1}) using the Witek's basis set. Experimental data from ref. [43].

Method	r_e	ν_e
NR RHF	1.7872	1460
RESC RHF	1.6999	1603
DK1 RHF	1.6901	1619
DK2 RHF	1.6998	1603
DK3 RHF	1.6995	1604
NR MP2	1.6647	1661
RESC MP2	1.5788	1876
DK1 MP2	1.5693	1901
DK2 MP2	1.5788	1875
DK3 MP2	1.5785	1876
NR B3LYP	1.7042	1567
RESC B3LYP	1.6254	1750
DK1 B3LYP	1.6163	1772
DK2 B3LYP	1.6253	1750
DK3 B3LYP	1.6249	1751
This work	1.5635	2024
Experiment	1.618	1760

The first triplet $^3\Sigma^+$ state also dissociates to the ground state Ag(^2S) and H(^2S). Although a metastable minimum was found at 1.5 Å at the CASSCF level, the SO-MCQDPT2 calculations predicted a repulsive potential with a turning point at about 2 Å, as depicted in Figure 8.1. This state possesses the Ag $5p_z$ character at small R but acquires more $5s$ character when approaching the asymptotic limit. The same configuration also gives rise to the 2 $^1\Sigma^+$ state which has attracted much attention from the spectroscopists because of the peculiar 2 $^1\Sigma^+ \rightarrow$ 1 $^1\Sigma^+$ emission spectra [41]. The Birge-Sponer plot indicated a strong perturbation which results in a plateau on the potential curve. Learner suggested that this unusual shape was due to the avoided crossing with the 3 $^1\Sigma^+$ state [44] but Witek et al. proved that the perturbation comes from the electrostatic interaction of the charge transfer between Ag $5s$ and H $1s$ orbitals [34]. The present study supports Witek's idea; the 2 $^1\Sigma^+$ state at the intermediate R is dominated by the ionic Ag^+H^- character. In contrast to the ground state, whose r_e is under-estimated, the computed bond length for the 2 $^1\Sigma^+$ is about 0.09 Å longer than the experimental value. Similar effect has also been observed by Witek et al. [18, 34]. This rather poor agreement could be attributed to the state averaging of the CASSCF orbitals. In spite of this discrepancy, the calculated potential curve is still in a qualitative correspondence with experiment.

The picture for the second and third dissociation channels is very complicated, as many excited states with T_e between 5.80 eV and 6.30 eV exist because of the near-degenerate electronic states arising from the Ag(^2D) and Ag(^2P) atomic configurations. Four Π states have been investigated in the present work and they exhibit very interesting characteristics. The two $^3\Pi$ states lie below the corresponding $^1\Pi$ states but they correlate to the different dissociation limits. The 1 $^1\Pi$ and 1 $^3\Pi$ states belong to the second dissociation channel leading to the Ag(^2P) + H(^2S) while the 2 $^1\Pi$ and 2 $^3\Pi$ states have the asymptotic limit of Ag(^2D) + H(^2S). The spectroscopic parameters determined from the computed potential curves for these states agree very well with the experiment, the largest discrepancies in r_e being 0.05 Å and in ν_e being 200 cm^{-1}. Avoided crossings were found between these states at

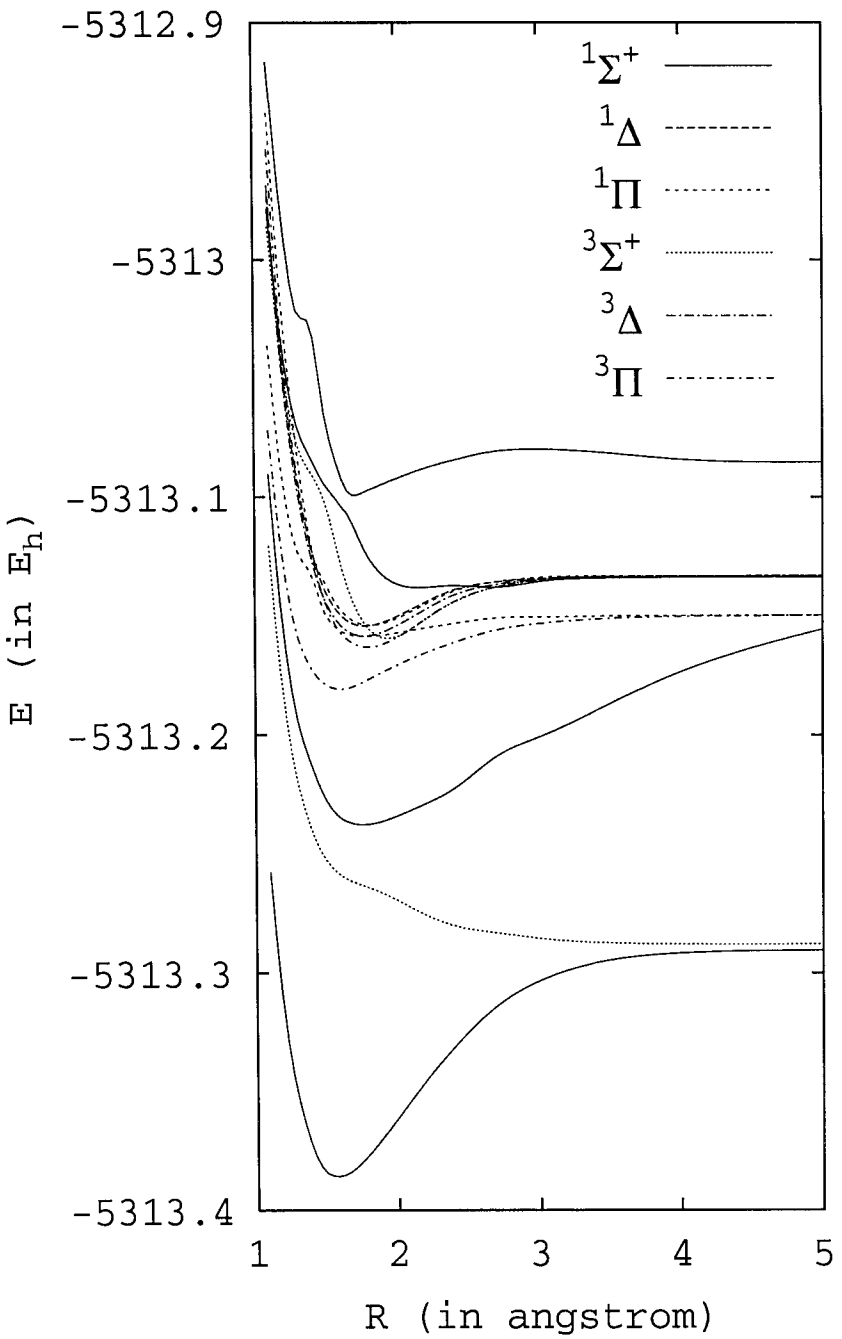

Figure 8.1: Relativistic spin-free MCQDPT2 potential energy curves for the selected low-lying states of AgH in free space.

small R. At the equilibrium region, the 1 $^1\Pi$ and 1 $^3\Pi$ states are characterized by the configuration arising from the $4d_{xz} \rightarrow 5s$ excitation of Ag, while the 2 $^1\Pi$ and 2 $^3\Pi$ states are dominated by the Ag($5p$) character. When R increases, these states interchange their configurations; the contribution of Ag ($5p$) to the 1 $^1\Pi$ and 1 $^3\Pi$ states raises rapidly at large R, while the leading configurations of the 2 $^1\Pi$ and 2 $^3\Pi$ become the Rydberg Ag($4d$). Witek et al. found an explicit crossing between the $^3\Pi$ potential curves at 1.5 Å [18]. However, this avoided crossing was not observed in a recent multi-reference configuration-interaction calculation by Li et al. [45]. The present results agree with the latter study, and the avoided crossing was found at 2.0 Å. On the other hand, an avoided crossing was observed at 1.5 Å between the two $^1\Pi$ state potential curves, which was also identified by Witek et al. [18].

Both the $^1\Delta$ and $^3\Delta$ states originate from the $4d_{xy} \rightarrow 5s$ excitation of Ag, and the Ag($4d$) character remains dominant for the whole range of R. These states, similar to the $^1\Pi$ and $^3\Pi$ states, are only weakly bound, and their binding energies are only 0.58 eV and 0.67 eV, respectively, approximately a quarter of that for the ground state. The unusually small binding energies can be accounted for by the ineffective overlap of the Ag $4d$ orbitals and the H $1s$ orbital. The relatively poor bonding interaction can also explain the larger r_e of these states compared to the ground state.

The 2 $^3\Sigma^+$ state, resulting from the $4d_{z^2} \rightarrow 5s$ excitation of Ag, lies 6.17 eV above the ground state. Because of slightly better overlap between the Ag $4d_{z^2}$ and H $1s$ orbitals, this state possesses larger r_e (1.9511 Å) and binding energy (0.70 eV) than the 2 $^1\Pi$ and 2 $^3\Pi$ states. There is a noticeable irregularity on the potential curve at 1.5 Å which could possibly be caused by the avoided crossing with higher $^3\Sigma^+$ states.

The 3 and 4 $^1\Sigma^+$ states have also been studied in the present work. However, the strong interaction between these states gives rise to the potential curves that are difficult to interpret. Two minima were found for the 3 $^1\Sigma^+$ at 2.0 and 2.7 Å respectively, with the barrier between them is only 66 cm^{-1}; this feature was not observed in the previous calculations [18, 34, 45]. The 4 $^1\Sigma^+$ state comes from the

excitation of an electron from $5s$ to $6s$ orbital of Ag. Due to the diffuse nature of the Rydberg Ag $6s$ orbital, this state is very strongly perturbed by other $^1\Sigma^+$ states and several points of avoided crossing have been located. Witek et al. discovered that there is a second, flat minimum at 4.50 Å with a very large binding energy (about 1.25 eV) [34]. This minimum is absent in the present SO-MCQDPT2 calculations. As the basis set for Ag is not designed for properly describing the Rydberg character of AgH, the accuracy of the potential curve of 4 $^1\Sigma^+$ is questionable. Therefore, this state would be ignored in the subsequent discussion concerning the spin-orbit and confinement effects.

8.3.2 AuH Molecule

The potential energy curves for a number of low-lying states of AuH were calculated using SO-MCQDPT2 method in C_{2v} symmetry, and they are shown in Figure 8.2. Twelve electronic states were investigated which correspond to the following eight states in diatomics: two of $^1\Sigma^+$, two of $^3\Sigma^+$, and one for each of $^1\Pi$, $^3\Pi$, $^1\Delta$ and $^3\Delta$. Spectroscopic parameters were obtained based on the calculated potentials, and they are listed in Table 8.4. The data from Witek et al. [34] and Heß et al. [17], together with available experimental values, are also included for comparison. In general, the results of the present work agree fairly well with the available experimental and computed values, with the largest error found for the 2 $^1\Sigma^+$ state, where the calculated r_e is about 0.09 Å shorter.

Only two dissociation channels were studied for AuH: Au(^2S) + H(^2S) and Au(^2D) + H(^2S). Contrary to the situation of AgH where the excited Ag(^2P) lies about 0.2 eV below Ag(^2D), the first excited state of Au is ^2D, with excitation energy is 1.74 eV [17]. The atomic calculation of Au using the Sadlej's basis set at SO-MCQDPT2 level yielded the excitation energy of 1.69 eV which differs from the experiment by only 0.05 eV. However, the value estimated in the molecular calculations of AuH at $R = 5$ Å was about 2.1 eV, closer to experiment than the value of 2.4 eV, deduced from the work of Witek *et al* [18].

The calculated r_e for the ground state of AuH using relativistic SO-MCQDPT2

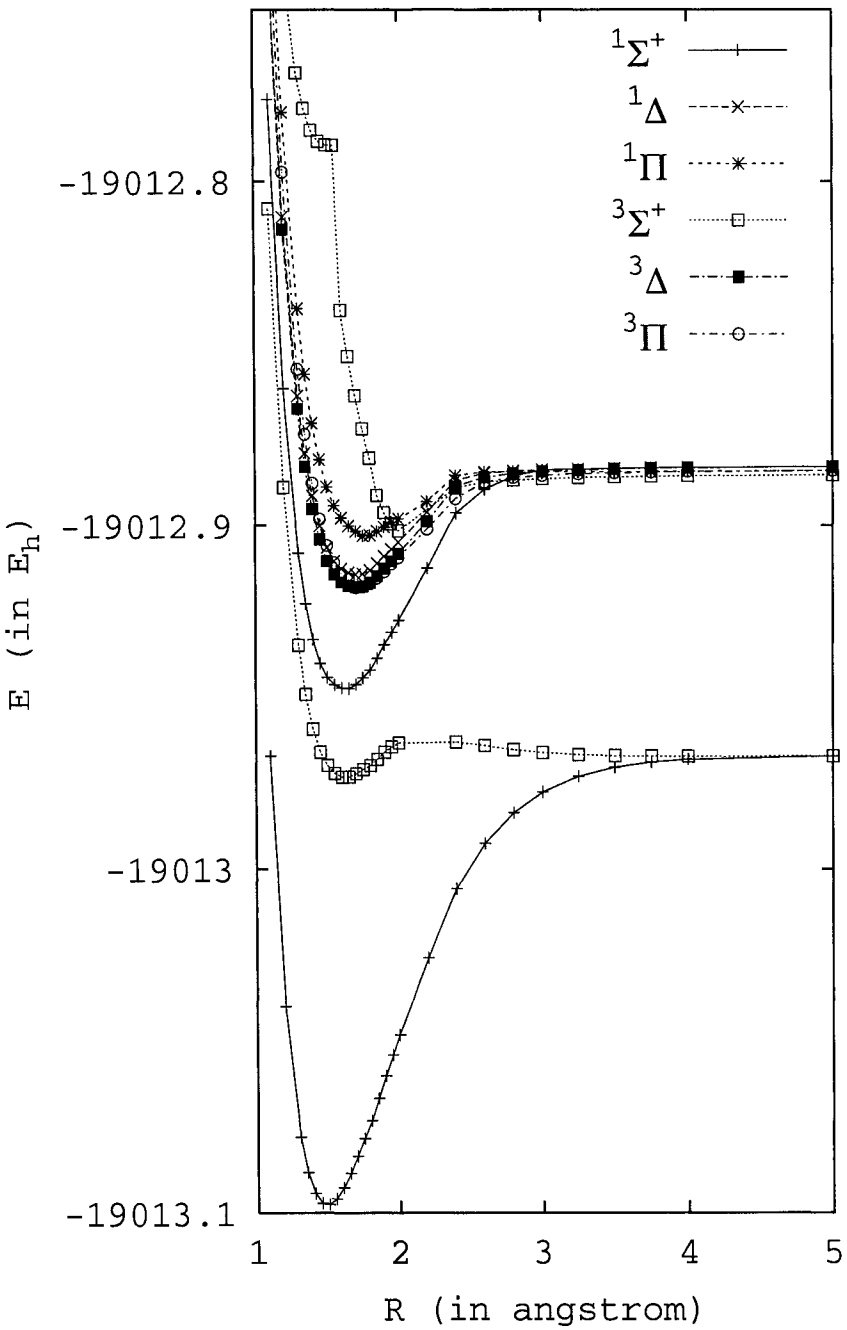

Figure 8.2: Relativistic spin-free MCQDPT2 potential energy curves for the selected low-lying states of AuH in free space.

Table 8.4: Spectroscopic constants of the selected states of AuH (r_e in Å, ν_e and B_e in cm^{-1}, T_e in eV). Experimental data from ref. [43].

State		r_e	ν_e	B_e	T_e
$1\ ^1\Sigma^+$	This work	1.4942	2480	7.53	0.00
	[34]	1.493	2414	7.54	0.00
	[17]	1.52	2381	7.36	0.00
	Experiment	1.5238	2305	7.24	0.00
$2\ ^1\Sigma^+$	This work	1.5864	2118	6.68	3.71
	[34]	1.572	2198	6.80	3.27
	[17]	1.60	2029	6.62	3.31
	Experiment	1.673	1670	6.01	3.43
$1\ ^1\Delta$	This work	1.7116	1335	5.74	4.77
	[34]	1.662	1658	6.09	4.65
	[17]	1.64	1827	6.28	4.01
$1\ ^1\Pi$	This work	1.7704	1784	5.36	5.10
	[34]	1.747	1342	5.51	5.12
	[17]	1.73	1492	5.63	4.37
$1\ ^3\Sigma^+$	This work	1.6224	1737	6.39	3.30
	[34]	1.654	1715	6.14	3.31
	[17]	1.63	1755	6.35	2.75
$2\ ^3\Sigma^+$	This work	2.0312	1568	4.07	5.12
	[34]	2.100	1693	3.81	6.82
$1\ ^3\Delta$	This work	1.7042	1339	5.79	4.67
	[34]	1.656	1688	6.13	4.53
	[17]	1.66	1503	6.16	3.91
$1\ ^3\Pi$	This work	1.7234	1402	5.66	4.71
	[34]	1.700	1598	5.81	4.64
	[17]	1.72	1221	5.72	3.90
	Experiment	1.695	1545	5.85	4.78

Table 8.5: Structural parameters for the ground state of AuH (r_e in Å, ν_e in cm^{-1}) using the Sadlej's basis set. Experimental data from ref. [43].

Method	r_e	ν_e
RESC RHF	1.5583	2050
DK1 RHF	1.5156	2261
DK2 RHF	1.5502	2086
DK3 RHF	1.5479	2097
RESC MP2	1.4723	2507
DK1 MP2	1.4467	2687
DK2 MP2	1.4673	2541
DK3 MP2	1.4659	2551
RESC B3LYP	1.5253	2235
DK1 B3LYP	1.4958	2397
DK2 B3LYP	1.5197	2264
DK3 B3LYP	1.5181	2273
This work	1.4942	2480
Experiment	1.5238	2305

method is about 0.03 Å shorter than the experimental value. It is known that both relativistic and electron correlation effects are important for heavy transition metal compounds, in particular for gold compounds. However, as shown in the case of AgH, MP2 predicts a too strong binding and thus too small r_e. The multi-configuration MP2 improves r_e by better describing the non-dynamical correlation, but its performance is slightly inferior to the relativistic DFT methods (see Table 8.5).

At large R, the ground state is correctly described by the Au($6s$) and H($1s$) character which constitutes the first dissociation channel. At small R regime, however, the ionic configuration is dominant. A partial charge transfer was observed between Au and H, which is caused by the avoided crossing between the ionic and covalent potential curves [46]. The Mulliken population analysis performed with the CASSCF wavefunction yielded -0.3 charge on H, which is consistent with the values reported by McLean (-0.42) [47] and Heß et al. (-0.27) [17]. The too large binding energy is attributable to the over-evaluation of the stabilization of the Au^+H^- configuration at the equilibrium region due to the relativistic contraction of Au $6s$

orbital [48].

The first $^3\Sigma^+$ is an interesting state of AuH: its non-relativistic potential energy curve is purely repulsive but the relativistic counterpart shows a minimum at about 1.6 Å and a hump at 2.0 Å. Heß et al. explained the change in terms of the reordering of the Au $5d_\sigma$ and H $1s_\sigma$ orbitals with varying R as a consequence of avoided crossing between the ionic and covalent configurations [17]. In the present work, a minimum was found that is 0.17 eV below the dissociation limit. This observation agrees with the conclusion of Heß et al. but contradicts the finding of Witek et al. where they located a metastable minimum lying 0.44 eV above the asymptote. In spite of this inconsistency, their computed r_e and ν_e agree very well with the values determined in the present calculations.

The second dissociation channel consists of six electronic states: $2\ ^{1,3}\Sigma^+$, $1\ ^{1,3}\Pi$ and $1\ ^{1,3}\Delta$. Except for the $2\ ^1\Sigma^+$ which possesses a relatively deep potential curve, all the other states are only weakly bound with respect to the dissociation products of Au(^2D) + H(^2S). Similarly to the second and third dissociation channels of AgH, this phenomenon can be understood in terms of the destabilization of Au $5d$ orbitals that weakens the overlap with the H $1s$ orbital, and thus the bonding interaction.

The $2\ ^1\Sigma^+$ state, at the equilibrium bond distance, is only 0.40 eV higher than the $1\ ^3\Sigma^+$ state, and their r_e values are very similar. These two states share the same ionic configuration arising from the Au($5d$) $\rightarrow$ H($1s$) excitation at small R. The difference in T_e thus indicates the stabilization of the triplet state over the singlet state due to relativistic effect. At larger R, the covalent contribution of Au($5d6s^2$) + H($1s$) rises rapidly, leading to the correct dissociation limit of Au(^2D) + H(^2S).

Unlike the other Σ^+ states, which are characterized by the ionic Au^+H^- configuration at small R, the $2\ ^3\Sigma^+$ state is described by the covalent character for the whole range of R. At very small R, this state acquires the Rydberg Au $7s$ character which changes to the Au $6s$ character when it interacts with the $3\ ^3\Sigma^+$ state at about 1.5 Å. The very shallow minimum is formed possibly due to the crossing with the ionic Au^+H^- potential. Another avoided crossing appears at large R

which enhances the contribution of the Au $5d_\sigma$ configuration that originated from the $5d_{z^2} \rightarrow 6s$ excitation.

All of the 1 $^{1,3}\Pi$ and 1 $^{1,3}\Delta$ states exhibit ionic character at the region around r_e, and are dominated by the covalent Au(^2D) + H(^2S) configuration at the long range region. The ionic configurations for the Π and Σ states originate from the excitations of, respectively, $5d_\pi$ and $5d_\delta$ orbitals to the $6s$ orbital of Au. Therefore, their equilibrium bond distances, excitation energies and binding energies are very similar. Due to the expanded, via the secondary relativistic effect, $5d$-shell of Au, the Coulomb interaction in these states is relatively weak which, in consequence, stretches r_e and reduces the binding energies.

8.3.3 Spin-Orbit Coupling

The potential energy curves for the ground and excited states of AgH and AuH, calculated including the spin-orbit coupling interaction, are plotted in Figures 8.3 and 8.4 respectively. Spectroscopic parameters were extracted using these potentials, and are compared with the available experimental data in Tables 8.6 and 8.7.

When the spin-orbit coupling is included in the calculations, the $\Lambda - S$ scheme for the state symmetry assignment is no longer valid, and the $\omega - \omega$ scheme has been used. According to the double group analysis, the following relativistic state symmetries will be obtained from the non-relativistic classifications of diatomic electronic states: 0^+ from $^1\Sigma^+$ and $^3\Pi$; 0^- from $^3\Sigma^+$ and $^3\Pi$; 1 from $^{1,3}\Pi$ and $^{1,3}\Delta$; 2 from $^3\Pi$ and $^{1,3}\Delta$ and 3 from $^3\Delta$ [49]. Accordingly, 22 relativistic states will be generated from the 12 electronic states of AgH while 15 relativistic states are derived from the 8 electronic states of AuH.

The first three dissociation channels for the excited states of AgH in the spin-free calculations split into five channels due to the spin-orbit coupling. While the first channel does not split because of the non-degenerate Ag($^2S_{1/2}$) state, the other two give rise to Ag($^2P_{1/2}$) + H($^2S_{1/2}$) and Ag($^2P_{3/2}$) + H($^2S_{1/2}$), and Ag($^2D_{5/2}$) + H($^2S_{1/2}$) and Ag($^2D_{3/2}$) + H($^2S_{1/2}$), respectively. The energy differences between these limits allow for the measurement of the fine structure splitting. The estimated

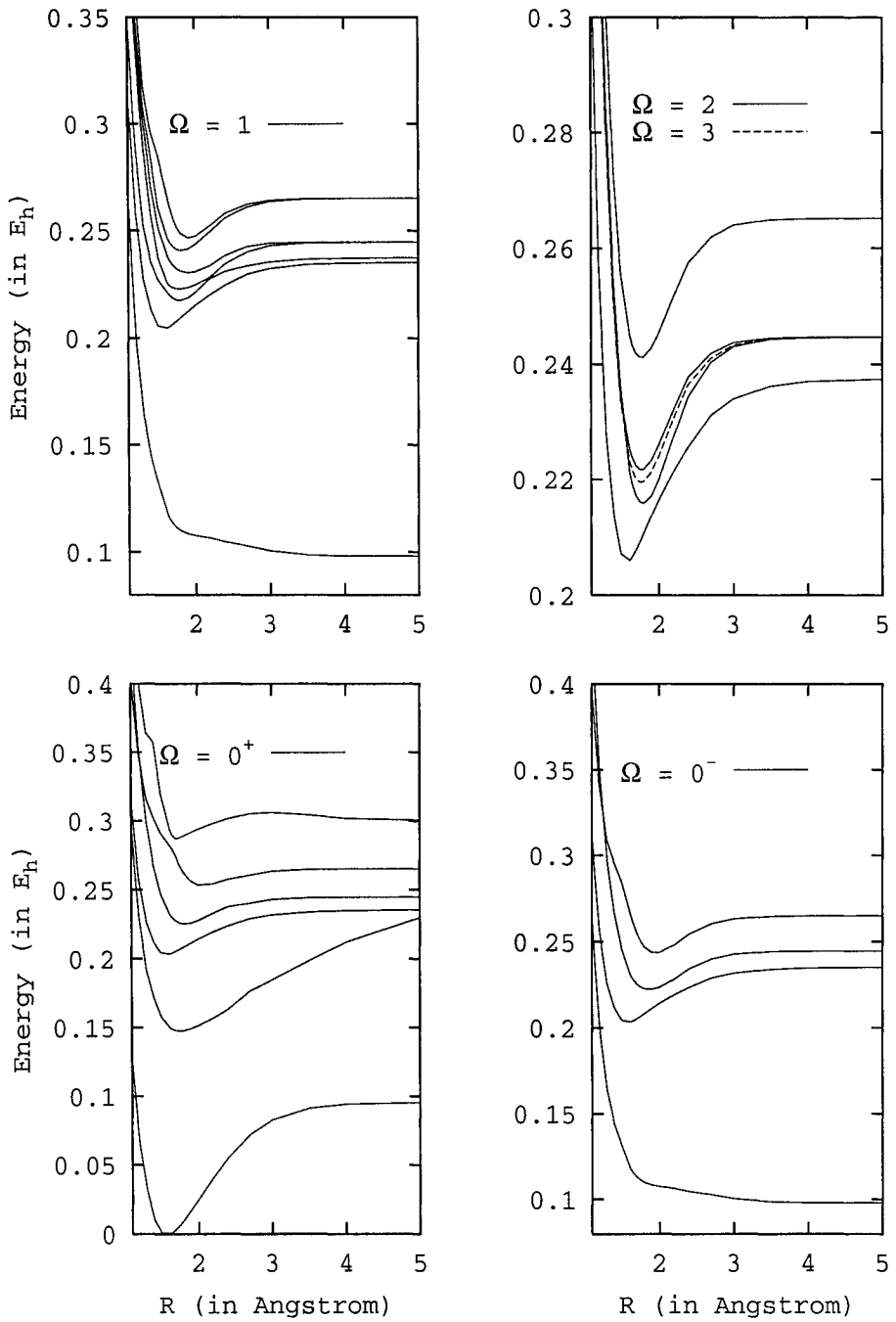

Figure 8.3: Relativistic spin-orbit MCQDPT2 potential energy curves for the selected low-lying states of AgH in free space. Energies are plotted with respect to E_{min} of the 0^+(I) state.

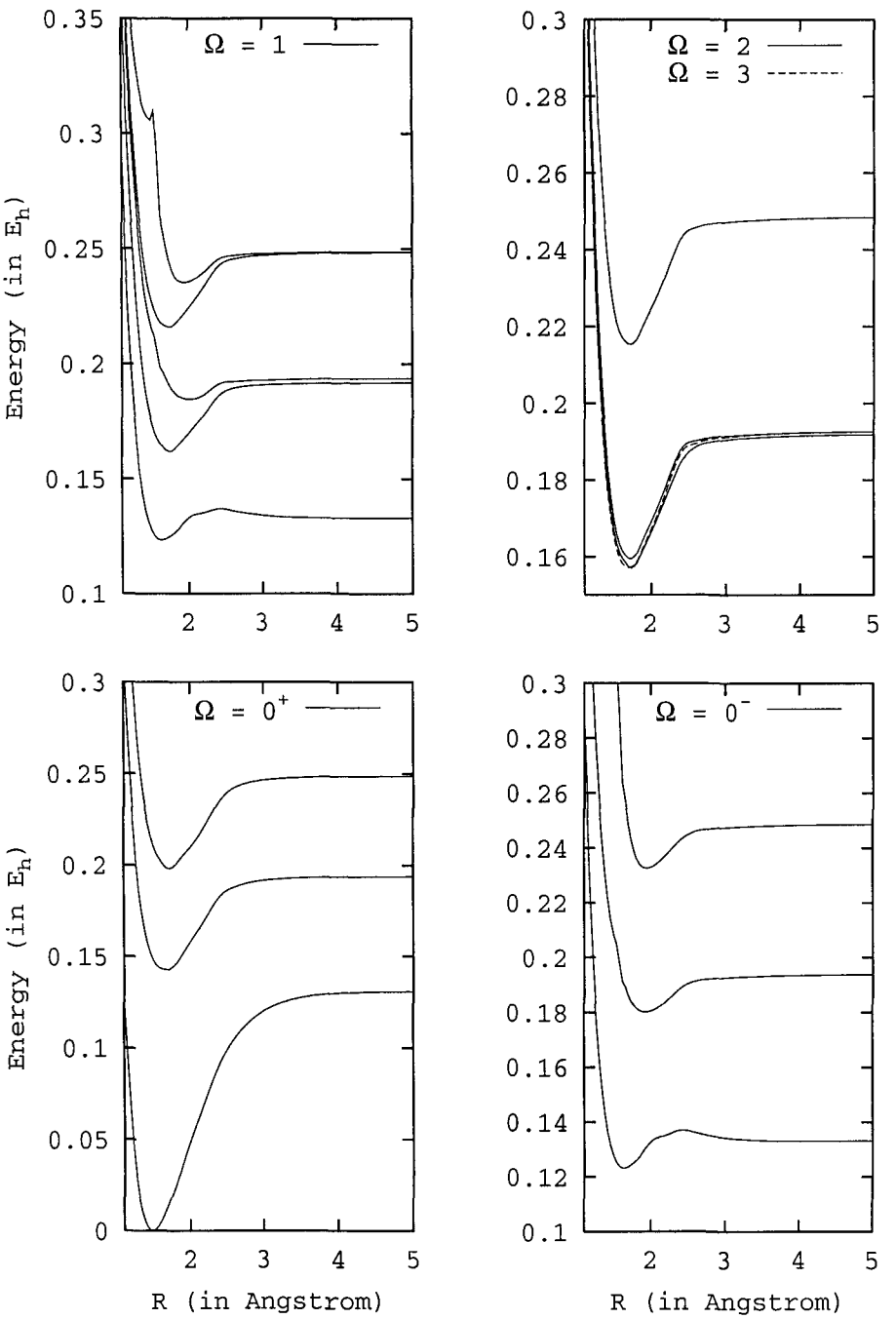

Figure 8.4: Relativistic spin-orbit MCQDPT2 potential energy curves for the selected low-lying states of AuH in free space. Energies are plotted with respect to E_{min} of the 0^+(I) state.

Table 8.6: Spectroscopic constants of the spin-orbit states of AgH (r_e in Å, ν_e and B_e in cm^{-1}, T_e in eV). Experimental data from ref. [43].

State		r_e	ν_e	B_e	T_e
0^+(I)	calc.	1.5614	2078	6,92	0.00
	expt.	1.618	1760	6.45	0.00
0^+(II)	calc.	1.7549	1194	5.48	4.03
	expt.	1.665	1490	6.09	3.71
0^+(III)	calc.	1.5745	1661	6.81	5.54
	expt.	1.64	1450	6.3	5.17
0^+(IV)	calc.	1.8284	1251	5.05	6.14
	expt.	1.86	1089	4.87	5.52
0^+(V)	calc.	2.0669	1126	3.95	6.89
	expt.	2.10		3.83	
0^+(VI)	calc.	1.7134	2575	5.75	7.82
0^-(II)	calc.	1.5717	1673	6.83	5.54
	expt.	1.64	1450	6.3	5.17
0^-(III)	calc.	1.8645	1138	4.86	6.06
0^-(IV)	calc.	1.9511	1326	4.44	6.64
1(II)	calc.	1.5763	1654	6.79	5.58
	expt.	1.61	1589	6.54	5.11
1(III)	calc.	1.7956	1321	5.24	5.93
	expt.	1.875		4.81	
1(IV)	calc.	1.7822	882	5.32	6.08
	expt.	1.85		4.95	
1(V)	calc.	1.9116	907	4.62	6.28
	expt.	1.80	845	5.23	5.79
1(VI)	calc.	1.8120	1282	5.14	6.56
	expt.	1.82		5.10	
1(VII)	calc.	1.9181	1382	4.59	6.72
2(I)	calc.	1.5785	1650	6.78	5.61
	expt.	1.64	1450	6.3	5.17
2(II)	calc.	1.7917	1379	5.26	5.89
2(III)	calc.	1.7726	1327	5.37	6.05
2(IV)	calc.	1.7746	1330	5.36	6.58
3(I)	calc.	1.7709	1337	5.38	5.99

Table 8.7: Spectroscopic constants of the spin-orbit states of AuH (r_e in Å, ν_e and B_e in cm^{-1}, T_e in eV). Experimental data from ref. [43].

State		r_e	ν_e	B_e	T_e
0^+(I)	calc.	1.4827	2504	7.65	0.00
	expt.	1.524	2305	7.24	0.00
0^+(II)	calc.	1.6692	1621	6.03	3.88
	expt.	1.673	1670	6.01	3.43
0^+(III)	calc.	1.7165	2008	5.71	5.40
	expt.	1.695	1545	5.85	4.78
0^-(I)	calc.	1.6324	1573	6.31	3.34
0^-(II)	calc.	1.9327	784	4.50	4.91
0^-(III)	calc.	1.9436	1244	4.45	6.34
	expt.	1.68	1229	5.96	5.32
1(I)	calc.	1.6304	1579	6.32	3.34
1(II)	calc.	1.7453	2074	5.52	4.41
1(III)	calc.	2.0386	715	4.05	5.03
1(IV)	calc.	1.7376	1619	5.57	5.88
	expt.	1.728	1076	5.63	5.32
1(V)	calc.	1.9388	1186	4.47	6.41
2(I)	calc.	1.7327	2052	5.60	4.28
2(II)	calc.	1.7237	1754	5.66	4.34
2(III)	calc.	1.7228	1633	5.66	5.86
	expt.	1.745	1020	5.52	5.30
3(I)	calc.	1.7032	1335	5.80	4.28

Ag($^2S_{1/2}$ - $^2P_{1/2}$) and Ag($^2D_{5/2}$ - $^2D_{3/2}$) splittings are 3.73 eV and 0.56 eV which agree with the experimental values within 2% of error [40]. However, the value for the Ag($^2P_{1/2}$ - $^2P_{3/2}$) splitting determined by this method is only 0.06 eV which is 48 % smaller than the experimental data (0.1142 eV). Atomic SO-MCQDPT2 calculations of Ag employing the same basis set increased the spin-orbit splitting to 0.1061 eV, but the discrepancy is still remarkably large ($\sim$ 10 %). There are two possible reasons to account for the observed large error in the spin-orbit splitting for the P term. On one hand, the imbalanced spin-orbit interaction and electron correlations treatment of the atomic Ag p-orbitals during the state-averaged MCSCF calculations causes the spin-polarization [2] that stabilizes the $P_{3/2}$ component more than the $P_{1/2}$ component, leading to the reduced Ag($^2P_{1/2}$ - $^2P_{3/2}$) splitting. On the other hand, in the computer code implementation, the neglect of the screening effect by the contracted Ag $5s$ orbital provides extra contribution to the core-valence correlation on the $5p_{3/2}$ orbital which diminishes the spin-orbit splitting of the P state [29].

The potential energy curves including spin-orbit for the excited states of AgH are very similar to the corresponding spin-free potentials. For the 0^+ and 0^- states the values of r_e differ by about 0.05 Å, and ν_e by 100 to 200 cm^{-1}. The rather small changes are due to the large separation of the $^1\Sigma^+$, $^3\Sigma^+$ and $^3\Pi$ states which results in a weak coupling. Nonetheless, a complicated situation occurs in the 1 states, where a prominent avoided crossing due to spin-orbit coupling exists between the 1(III) and 1(IV) states. These two states originate from the non-relativistic 1 $^1\Pi$ and 2 $^3\Pi$ states which cross at 2.1 Å due to spin selection rule. At the point of avoided crossing, a state mixing of $^1\Pi$ and $^3\Pi$ states was detected. For small R the 1(III) state is well described by $^1\Pi$ while the 1(IV) state is dominated by $^3\Pi$; for large R, however, these contributions interchange, and the $^3\Pi$ configuration becomes the major one for the 1(III) state yet the 1(IV) possesses the singlet π character. In addition to the 1(III) and 1(IV) states, the higher 1 states are also mixtures of the closely spaced $^{1,3}\Pi$ and $^{1,3}\Delta$. Their equilibrium bond lengths and vibrational constants are largely dependent of the dominant configurations of these states in

the region. An exception is the 1(V) state, which can be classified as the 2 $^1\Pi$ state, whose r_e is shifted by 0.1 Å due to the interaction with the $^3\Sigma^+$ states.

An interesting feature was found between the 2(III) and 3(I) states where the 3(I) potential curve lies only 450 cm^{-1} below that for the 2(III) state at r_e. Both states arise from the 1 $^3\Delta$ state which has the inverted splitting due to the spin-orbit effect. The calculated spin-orbit coupling constant for the $^3\Delta$ state is 2520 cm^{-1} at r_e. However, the strong second-order coupling with the $^1\Delta$ state, which comprises the 2(IV) state, lowers the $\Omega = 2$ component of the $^3\Delta$ state by 1776 cm^{-1}. This perturbation, together with the coupling with the $^3\Pi$ state, significantly lowers the 2(III) state and reduces the energy separation between the 2(III) and 3(I) states.

The influence of spin-orbit interaction on the spectroscopic parameters and electronic structure of AuH molecule is more pronounced compared to AgH. This strong effect is clearly manifested in the order of electronic states of Au and in their fine structure splitting constants. Contrary to the case of Ag where the ^2P states are slightly lower in energy than the ^2D states, the ^2D and ^2P states of Au are well separated, and the ^2D states are in fact lower than the ^2P states by 3.20 eV [43], when averaged over all the fine structure components. This is a direct consequence of the relativistic contraction of Au $6s$ orbital which favors the $5d \rightarrow 6s$ over the $6s \rightarrow 6p$ excitations. In addition to the different ordering of atomic states, the $^2D_{5/2}$ - $^2D_{3/2}$ splitting is three times larger than the corresponding value in Ag. The computed value in the present work is 1.494 eV which shows a very good agreement with the experiment (1.522 eV); however, the calculated $^2S_{1/2}$ - $^2D_{5/2}$ splitting is 1.712 eV which is 51 % larger than the value deduced by Ehrhardt and Davis [50]. Because the spin-polarization effect is small for d-shell orbitals, the over-estimated $^2S_{1/2}$ - $^2D_{5/2}$ gap could possibly be due to the excessive stabilization of the $6s$-orbital by the use of the atomic charge of 79 for Au, instead of an effective nuclear charge.

The first relativistic 0^+(I) state of AuH, which is derived from the 1 $^1\Sigma^+$ state, was not much affected when spin-orbit coupling was considered because of the wide separation from other 0^+ states. Meanwhile, the 3(I) state resembles the parent $^3\Delta$ state in terms of r_e and ν_e since only one 3 state was calculated. A small increase

in the binding energy for the 0^+(I) state was observed; this effect is expected since the spin-orbit coupling induces the decrease of the overlap-related kinetic energy at r_e [51]. A similar effect was also seen in the 3(I) state, whose binding energy was also increased by 0.06 eV, compared to that for the $^3\Pi$ state.

In general, the effect of spin-orbit interaction on r_e for these states is small, except for the 0^-(II) and 1(III) states where the bond lengths were stretched by 0.21 Å and 0.30 Å, respectively. While vibrational constants are normally increased due to the relativistic effects, the calculated values of ν_e for some states of AuH decreased when spin-orbit interaction was added. Furthermore, the magnitude of changes in ν_e was large, ranging from 200 cm^{-1} to 600 cm^{-1}. It was also observed that the states arising from the second dissociation channel, i.e., Au(^2D) + H(^2S), were more susceptible to the influence of the spin-orbit interaction. In contrast to AgH, the relativistic states of AuH with $\Omega = 1$ or 2 contain large contributions from $^{1,3}\Pi$ and $^{1,3}\Delta$ states. The off-diagonal spin-orbit coupling constants between the Π and Δ states, and Δ and Δ states are, as measured at the SO-MCQDPT2 level, approximately 3000 cm^{-1} and 5000 cm^{-1}, respectively. Therefore, their potential curves are strongly distorted from the corresponding non-relativistic potentials, giving rise to relatively large and irregular changes in r_e and ν_e.

The effects of spin-orbit interaction on the 2 states are unique: their bond lengths were stretched by 0.01 to 0.02 Å but the vibrational constants were raised by 400 to 600 cm^{-1}. The 2(I) state is characterized almost exclusively by the $^3\Pi$ state while the 2(II) and 2(III) states are composed of the $^1\Delta$ and $^3\Delta$ states. These states possess very strong ionic character of Au^+H^- arising from the charge transfer from Au $5d$ orbitals to H $1s$ orbital at r_e. Hence, the spin-orbit coupling destabilizes these states and lifts their potential curves at the region around r_e. Simultaneously, the covalent $1s_H 5d_\sigma 6s_\sigma^2$ character, that intervenes and leads these states to the correct dissociation limit of Au(^2D) + H(^2S), is stabilized at large R. In consequence, the resulting potential curves for these states are deepened and shifted towards larger R.

8.3.4 Effects of Confinement

In order to investigate the combined effects of relativity and external confining potentials on the structural and electronic properties of AgH and AuH, the SO-MCQDPT2 calculations incorporating eq. 3 have been performed. Several values of the confinement parameters ω were used: 0.025, 0.050, 0.075 and 0.100 au, and both spin-free and spin-orbit potential energy curves for the low-lying excited states of these molecules were computed. In order to better describe the electron density distorted by the harmonic electrostatic potential, a set of $1s1p1d$ basis functions with the exponent of $\omega/2$ were utilized and located at mid-bond position. Previous studies have demonstrated that the use of these so-called confinement functions can yield more realistic molecular orbitals and energy levels [52].

Generally, the electron density, enhanced between the nuclei due to confining potential, leads to a stronger bonding interaction, a shorter bond length, and a larger vibrational constant. However, the situation becomes more complicated in AgH where a serious mixing of configurations occurred when the confining potential was applied, as illustrated in Tables 8.8 and 8.9. The ground state of AgH, which is essentially formed by the covalent interaction of Ag $5s$ and H $1s$ orbitals, is mixed with the Ag $4d_{z^2}$ configuration. In consequence, the bonding orbital is elongated, giving rise to an increased r_e and a smaller ν_e. The $1\ ^3\Sigma^+$ state remains unbound regardless the strengths of the applied potential. However, a small plateau starts to appear at about 2.0 Å, which is possibly due to the confinement-induced, increased relative stability of Ag $5p_z$ orbital over the Ag $5s$ orbital: the more stable Ag $5p_z$ character lowers the $1\ ^3\Sigma^+$ potential at small R. An evidence for the downshift of the $1\ ^3\Sigma^+$ potential is also found in its T_e, measured at the r_e of the ground state of AgH, which decreases from 3.47 eV for $\omega = 0.00$ to 3.04 eV for $\omega = 0.10$ au. Figure 8.5 shows that under the influence of the harmonic confining potential, the second and third dissociation channels gradually merge and split into several new channels. This phenomenon is ascribed to the complex multiplet splitting of quasi-degenerate Ag(^2P) and Ag(^2D) states. The axially symmetrical geometry of the applied potential removes the degeneracy within the d-shell and p-shell; in confine-

Table 8.8: Spectroscopic constants of the singlet states of AgH with confinement. (r_e in Å, ν_e in cm^{-1}, T_e in eV)

State		$\omega = 0.000$	$\omega = 0.025$	$\omega = 0.050$	$\omega = 0.075$	$\omega = 0.100$
$1\ ^1\Sigma^+$	r_e	1.5635	1.5596	1.5680	1.5825	1.5904
	ν_e	2024	2237	1939	1968	1923
	T_e	0.00	0.00	0.00	0.00	0.00
$2\ ^1\Sigma^+$	r_e	1.7503	1.7599	1.7329	1.7201	1.6884
	ν_e	1166	1298	1269	1266	1546
	T_e	4.03	4.01	3.94	3.89	3.85
$3\ ^1\Sigma^+$	r_e	2.0669	2.1416	2.1334	2.1284	2.1237
	ν_e	1126	814	824	861	870
	T_e	6.73	6.76	6.77	6.80	6.87
$4\ ^1\Sigma^+$	r_e	1.7035	1.6407	1.6522	1.6468	1.8590
	ν_e	2682	2917	898	1378	1383
	T_e	7.80	8.09	8.50	8.95	9.05
$1\ ^1\Delta$	r_e	1.7743	1.7717	1.7669	1.7600	1.7495
	ν_e	1303	1316	1339	1369	1436
	T_e	6.31	6.34	6.33	6.36	6.40
$1\ ^1\Pi$	r_e	1.5763	1.7125	1.7672	1.7890	1.7856
	ν_e	841	911	1151	1308	1419
	T_e	6.19	6.14	6.28	6.37	6.45
$2\ ^1\Pi$	r_e	1.8119	1.8464	1.8440	1.8126	1.7829
	ν_e	1271	1136	894	753	750
	T_e	6.32	6.47	6.58	6.81	7.15

Table 8.9: Spectroscopic constants of the triplet states of AgH in confinement. (r_e in Å, ν_e in cm^{-1}, T_e in eV)

State		$\omega = 0.000$	$\omega = 0.025$	$\omega = 0.050$	$\omega = 0.075$	$\omega = 0.100$
$2\ ^3\Sigma^+$	r_e	1.9511	2.0420	2.0199	2.0088	1.9919
	ν_e	1326	1022	1160	1203	1250
	T_e	6.17	6.46	6.48	6.52	6.60
$1\ ^3\Delta$	r_e	1.7726	1.7690	1.7651	1.7595	1.7513
	ν_e	1327	1346	1367	1394	1462
	T_e	6.20	6.22	6.21	6.22	6.25
$1\ ^3\Pi$	r_e	1.5994	1.5490	1.4957	1.5673	1.7736
	ν_e	1530	2101	3521	1721	1513
	T_e	5.59	5.62	5.79	6.10	6.15
$2\ ^3\Pi$	r_e	1.7954	1.7918	1.7890	1.6932	1.5914
	ν_e	1397	1395	1430	2298	2497
	T_e	6.07	6.09	6.09	6.17	6.45

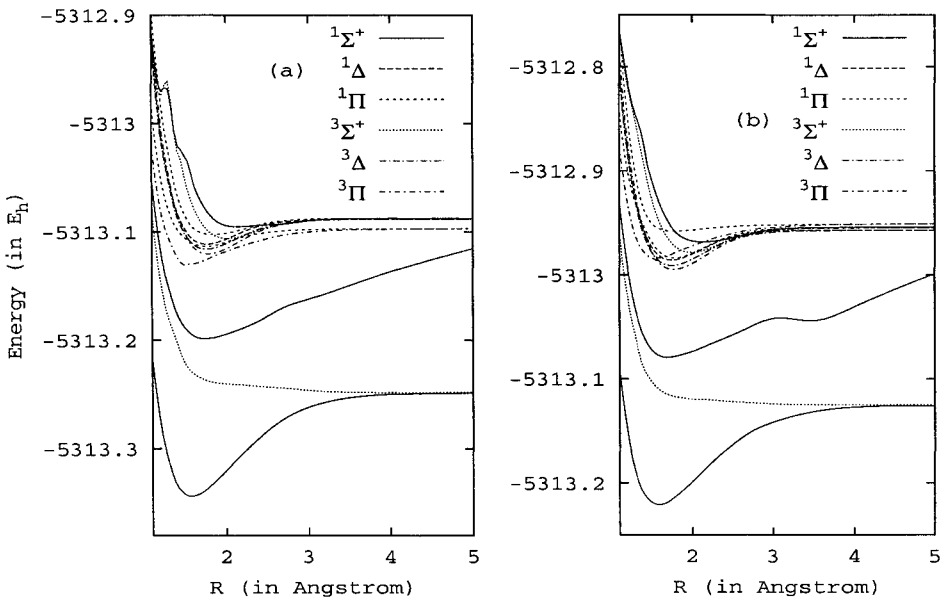

Figure 8.5: Relativistic spin-free potential energy curves for the selected low-lying states of confined AgH molecule. (a) $\omega = 0.050$ au (b) $\omega = 0.100$ au

ment of cylindrical symmetry, the subshells that spread along the molecular bond axis are more stabilized compared to the ones perpendicular to the axis. Therefore, the p-shell is split into two subsets $\{p_z\}$ and $\{p_x, p_y\}$ while the d-shell is split into $\{d_{xy}, d_{x^2-y^2}\}$, $\{d_{z^2}\}$, and $\{d_{yz}, d_{xz}\}$, with the energy of the last two sets being very similar. The resulting new atomic energy levels of Ag lead to a very complicated excited state potentials of AgH which are difficult to interpret.

A marked change for the confined AgH molecule is that the $1\ ^1\Sigma^+$ potential curve departs from the second and third channels with increasing ω, which is reflected in its T_e decreasing from 4.03 eV to 3.85 eV when ω increases to 0.10 au. On the other hand, a local minimum appears at 3.5 Å which is formed due to the lowering of the ionic Ag^+H^- potential at intermediate R. The depth of this minimum is about 465 cm^{-1}, which may allow to accommodate a single vibrational level.

Both the $^{1,3}\Delta$ states respond to the confining potential in a typical way: their equilibrium bond distances turn shorter for a stronger applied potential. As these states are formed by the $4d_\delta \rightarrow 5s$ excitation of Ag, this behavior can be understood in terms of the distorted $4d_\delta$ orbitals along the molecular axis that favors the bonding interaction with the H $1s$ orbital. The change of r_e is accompanied by the increasing ν_e, which implies stronger bonding and thus steeper potential curves for the Δ states.

The picture for the Π states is intricate, as r_e and ν_e of these states do not vary monotonically in the presence of the confining potential. The $1\ ^{1,3}\Pi$ states are first compressed when a small potential is exerted; when the strength of potential exceeds 0.05 au their bonds start to stretch very rapidly. However, the opposite trend is observed for the $2\ ^1\Pi$ state, while the $2\ ^3\Pi$ state exhibits the same behavior as the Δ states. These unusual variations can be rationalized in terms of orbital responses to the external confinement. As the $^{1,3}\Pi$ states arise from the $4d_\pi \rightarrow 5s$ excitation of Ag, the deformation of the $4d_\pi$ orbitals of Ag due to the cylindrical confining potential enhances their π-interaction with the H $1s$ orbital, thus strengthening the Π states and reducing r_e. On the other hand, the centripetal compression on the $5p_\pi$ orbitals of Ag leads to the angular distortion of the orbital towards the molecular axis and the increase in r_e of the $2\ ^{1,3}\Pi$ states which are dominated by the $Ag(5p_z)$

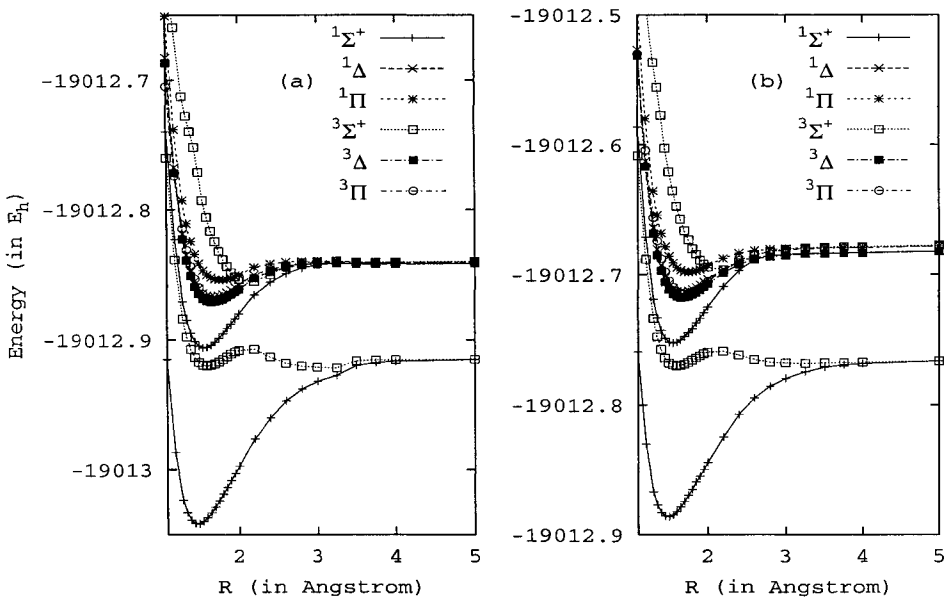

Figure 8.6: Relativistic spin-free potential energy curves for the selected low-lying states of confined AuH molecule. (a) $\omega = 0.050$ au (b) $\omega = 0.100$ au

+ H($1s$) bonding character. For $\omega > 0.05$ au the avoided crossing between the $^1\Pi$ states vanishes, while a new avoided crossing appears between the $^3\Pi$ states, and these state interactions result in the marked distortion of the potential curves, and hence r_e and ν_e, of these states.

The effects of spatial confinement on AuH, in contrast to the case of AgH, are rather simple, as illustrated in Figure 8.6. Again, the dissociation channel leading to the asymptotes of Ag(^2D) + H(^2S) splits into two small channels corresponding to the $\{d_{xy}, d_{x^2-y^2}\}$ and $\{d_{z^2}, d_{yz}, d_{xz}\}$ sets. The d-shell splitting for AuH is slightly smaller than that of AgH because of the more diffuse character of the $5d$ orbitals compared to the more contracted $4d$ counterparts in Ag. Another difference between these two systems is that the entanglement of the second and third channels of AgH, induced by the confining potential, is not found in AuH. The states that constitute the second channel remain fairly separated even at $\omega = 0.10$ au. In addition, an interesting feature is observed solely in AuH: the excitation energies T_e for different low-lying states of AuH are hardly affected by the confining potential, the biggest

change in T_e being 0.17 eV for the 2 $^1\Sigma^+$ state.

The ground state geometry of AuH does not change significantly when the confining potential is applied. The variation in r_e is negligibly small, within 0.01 Å. However, its binding energy is increased by almost 1 eV, which suggests that, in confinement, the stability of the ionic Au^+H^- configuration is greater than that of the covalent $Ag(6s) + H(1s)$ configuration. This difference also causes the reduction in T_e of the 2 $^1\Sigma^+$ and 1 $^3\Sigma^+$ states, which are described by the excited Ag^+H^- arising from Ag $5d \rightarrow 6s$ excitation. The amplified Coulomb attraction results in the shorter bond lengths for these states.

Additional interaction is found at intermediate R, for $\omega < 0.05$ au, where both the 1 $^1\Sigma^+$ and 1 $^3\Sigma^+$ are strongly mixed, leading to a wiggle on both potential curves. This configuration interaction induces not only the irregularity of the potential curves, but also the shift of r_e towards smaller R. The mixing of states diminishes when ω increases further until 0.10 au at which the second minimum on the 1 $^3\Sigma^+$ potential energy curve disappears, and the global minimum starts to increase.

Although they are formed via the charge transfer process from Ag $5d$ orbitals to H $1s$ orbital, the $^{1,3}\Delta$ and $^{1,3}\Pi$ states exhibit slightly different behavior in confinement. The changes in the spectroscopic parameters of the Δ states caused by the applied potential are as expected: the equilibrium bond lengths shrink and the vibrational frequencies increase with increasing ω. The change of r_e for the Π states also follows the anticipated trend; however, the variations in ν_e for these two states are entirely opposite (Table 8.10). The anomaly for the $^1\Pi$ state is a consequence of a possible avoided crossing with higher $^1\Pi$ states that also produces a small potential barrier on the potential curve at about 3.0 Å.

The relativistic spin-orbit states of the confined AgH and AuH inherit the characteristics of the $\Lambda - S$ states from which they are derived. Figures 8.7 and 8.8 display the resulting Ω states of AgH at $\omega = 0.050$ au and 0.100 a.u respectively. The corresponding plots for AuH are depicted on figures 8.9 and 8.10. The spectroscopic parameters deduced from these states are summarized in Tables 8.11 to

Table 8.10: Spectroscopic constants of the selected states of AuH in confinement. (r_e in Å, ν_e in cm^{-1}, T_e in eV)

State		$\omega = 0.000$	$\omega = 0.025$	$\omega = 0.050$	$\omega = 0.075$	$\omega = 0.100$
$1\ ^1\Sigma^+$	r_e	1.4942	1.4790	1.4783	1.4806	1.4849
	ν_e	2480	2512	2479	2425	2354
	T_e	0.00	0.00	0.00	0.00	0.00
$2\ ^1\Sigma^+$	r_e	1.5864	1.5861	1.5615	1.5595	1.5411
	ν_e	2118	2191	2069	2112	2083
	T_e	3.71	3.81	3.69	3.67	3.64
$1\ ^1\Delta$	r_e	1.7116	1.6785	1.6676	1.6722	1.6641
	ν_e	1335	1471	1461	1545	1512
	T_e	4.77	4.72	4.76	4.74	4.70
$1\ ^1\Pi$	r_e	1.7704	1.7922	1.7555	1.7534	1.7466
	ν_e	1784	885	948	1252	1254
	T_e	5.10	5.05	5.12	5.11	5.12
$1\ ^3\Sigma^+$	r_e	1.6224	1.6027	1.5912	1.6025	1.6117
	ν_e	1737	1682	1695	1842	1697
	T_e	3.30	3.33	3.32	3.25	3.16
$2\ ^3\Sigma^+$	r_e	2.0312	2.1456	2.1252	2.1375	2.1377
	ν_e	1568	1185	1262	1399	1321
	T_e	5.12	5.02	5.07	5.08	5.15
$1\ ^3\Delta$	r_e	1.7042	1.6739	1.6609	1.6673	1.6599
	ν_e	1339	1550	1512	1576	1563
	T_e	4.67	4.62	4.65	4.62	4.58
$1\ ^3\Pi$	r_e	1.7234	1.7210	1.7105	1.7113	1.6987
	ν_e	1402	1721	1667	1651	1569
	T_e	4.71	4.65	4.69	4.68	4.67

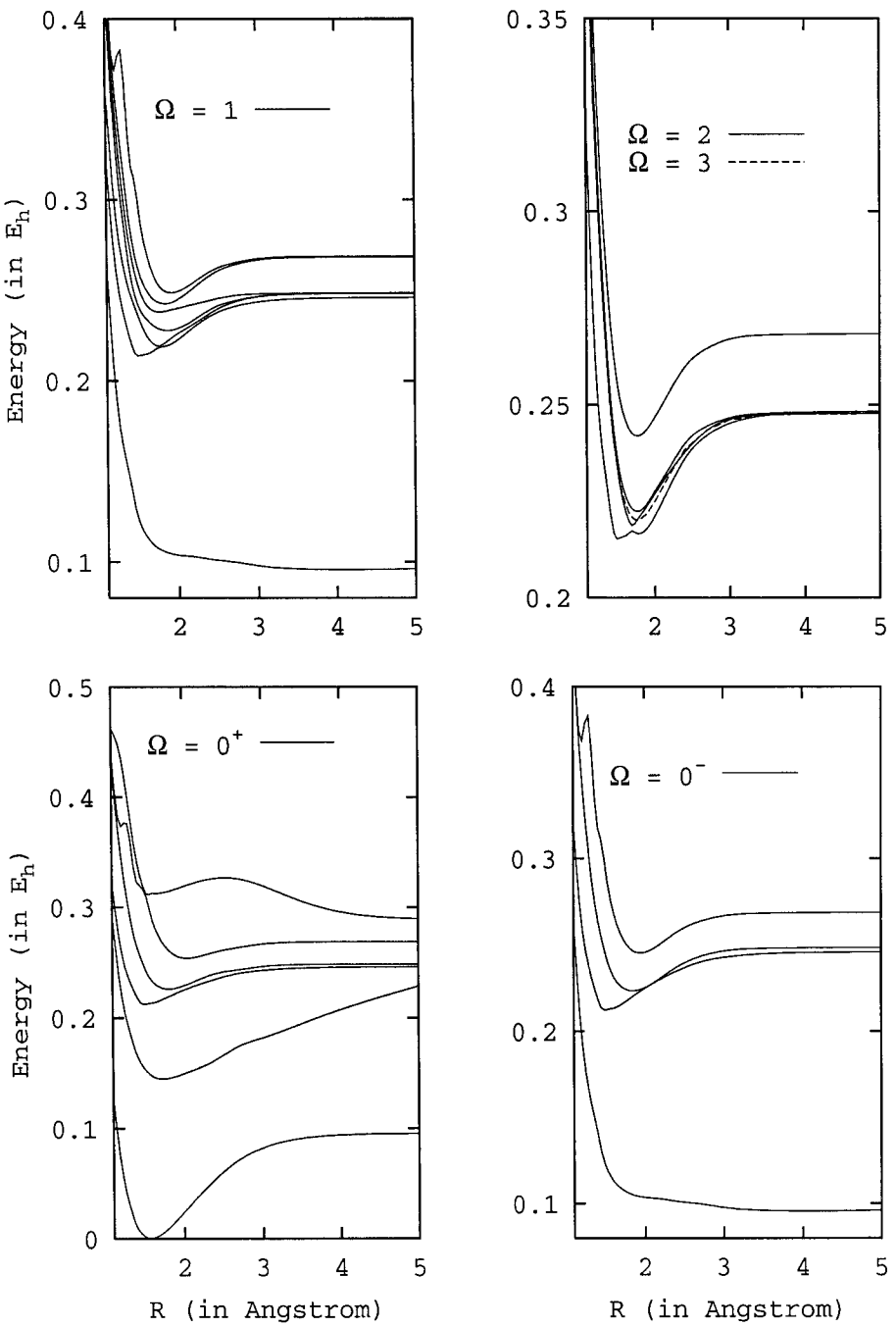

Figure 8.7: Relativistic spin-orbit states of AgH in confinement for $\omega = 0.050$ au Energies are plotted with respect to E_{min} of the 0^+(I) state.

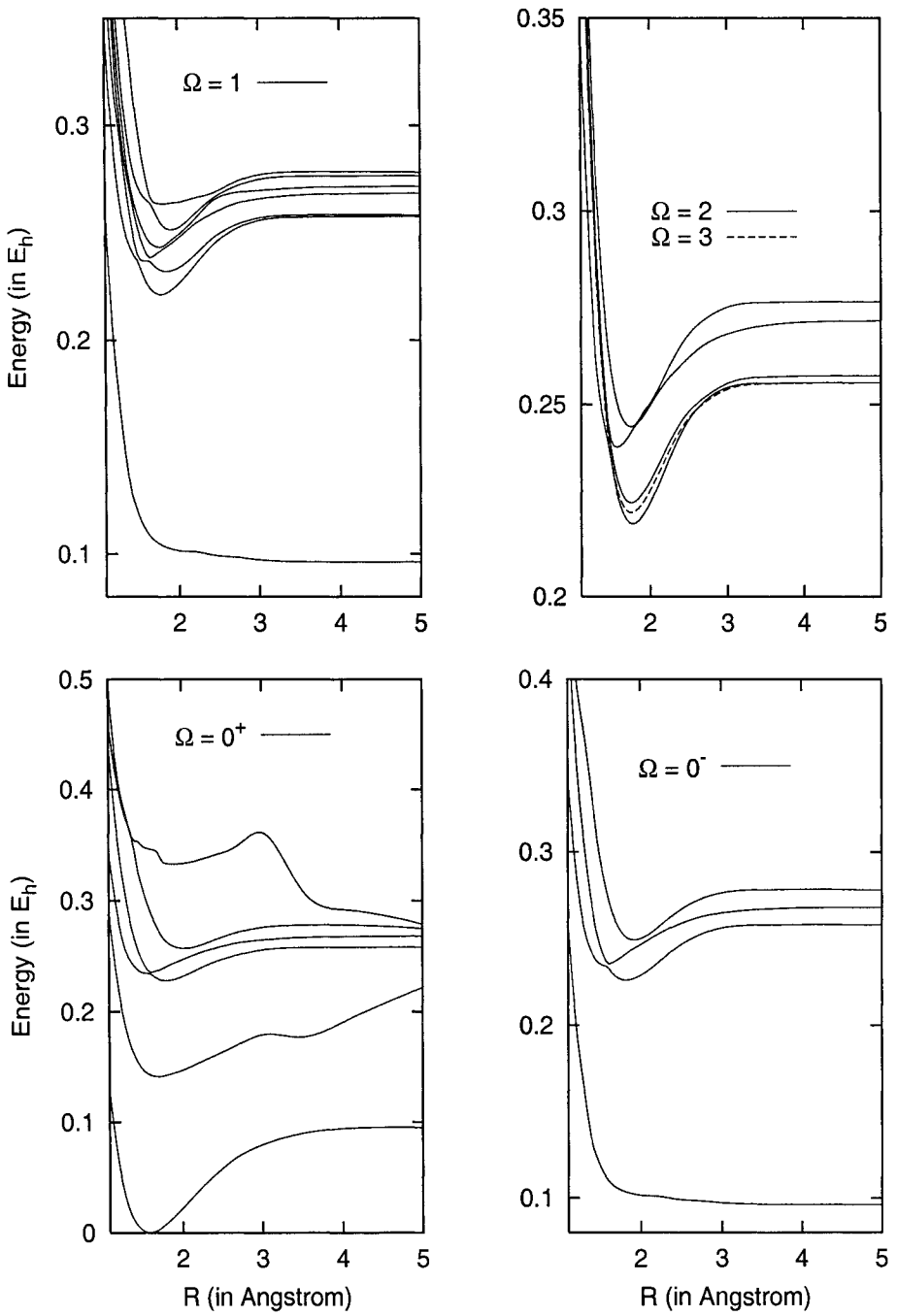

Figure 8.8: Relativistic spin-orbit states of AgH in confinement for $\omega = 0.100$ au Energies are plotted with respect to E_{min} of the 0^+(I) state.

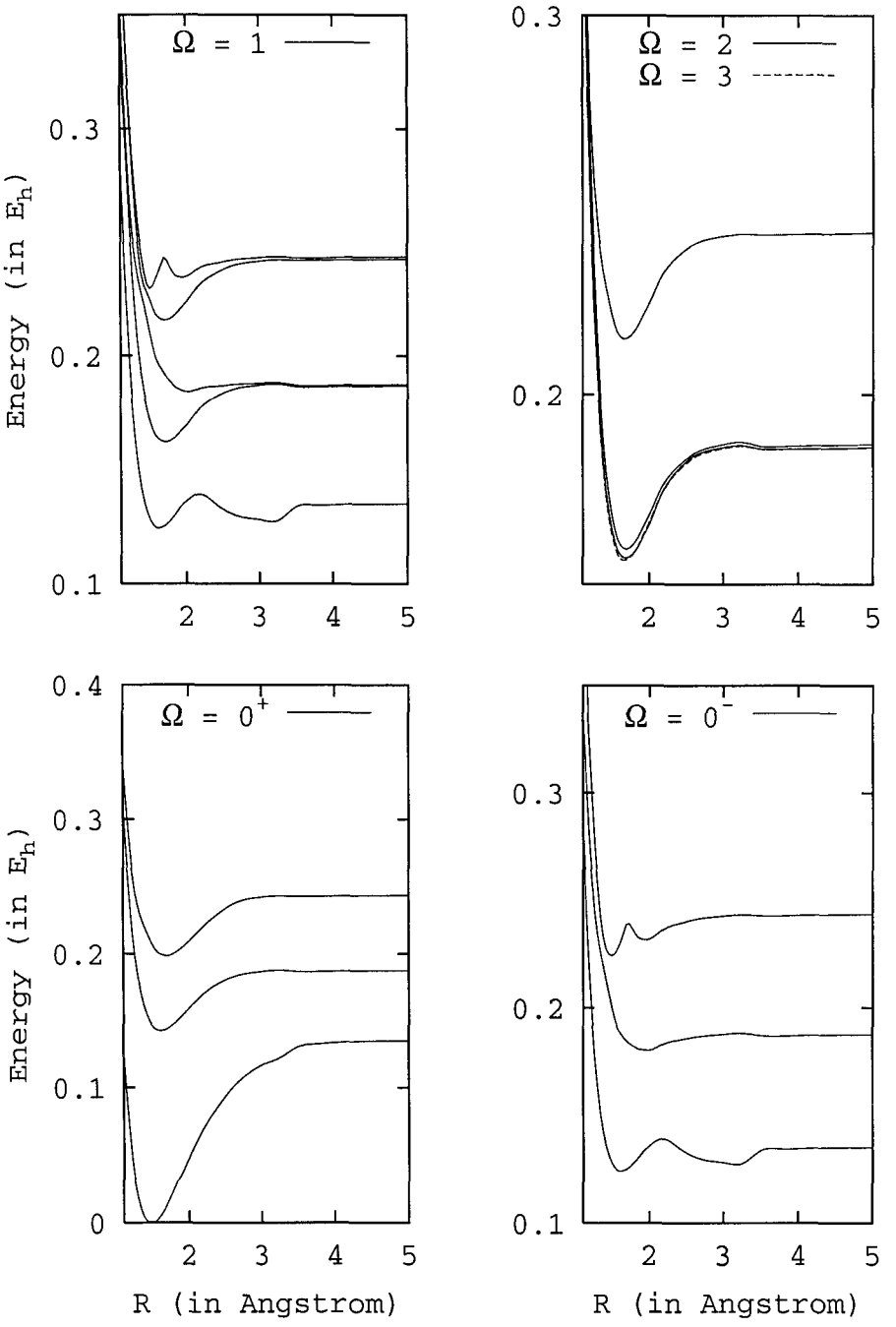

Figure 8.9: Relativistic spin-orbit states of AuH in confinement for $\omega = 0.050$ au Energies are plotted with respect to E_{min} of the 0^+(I) state.

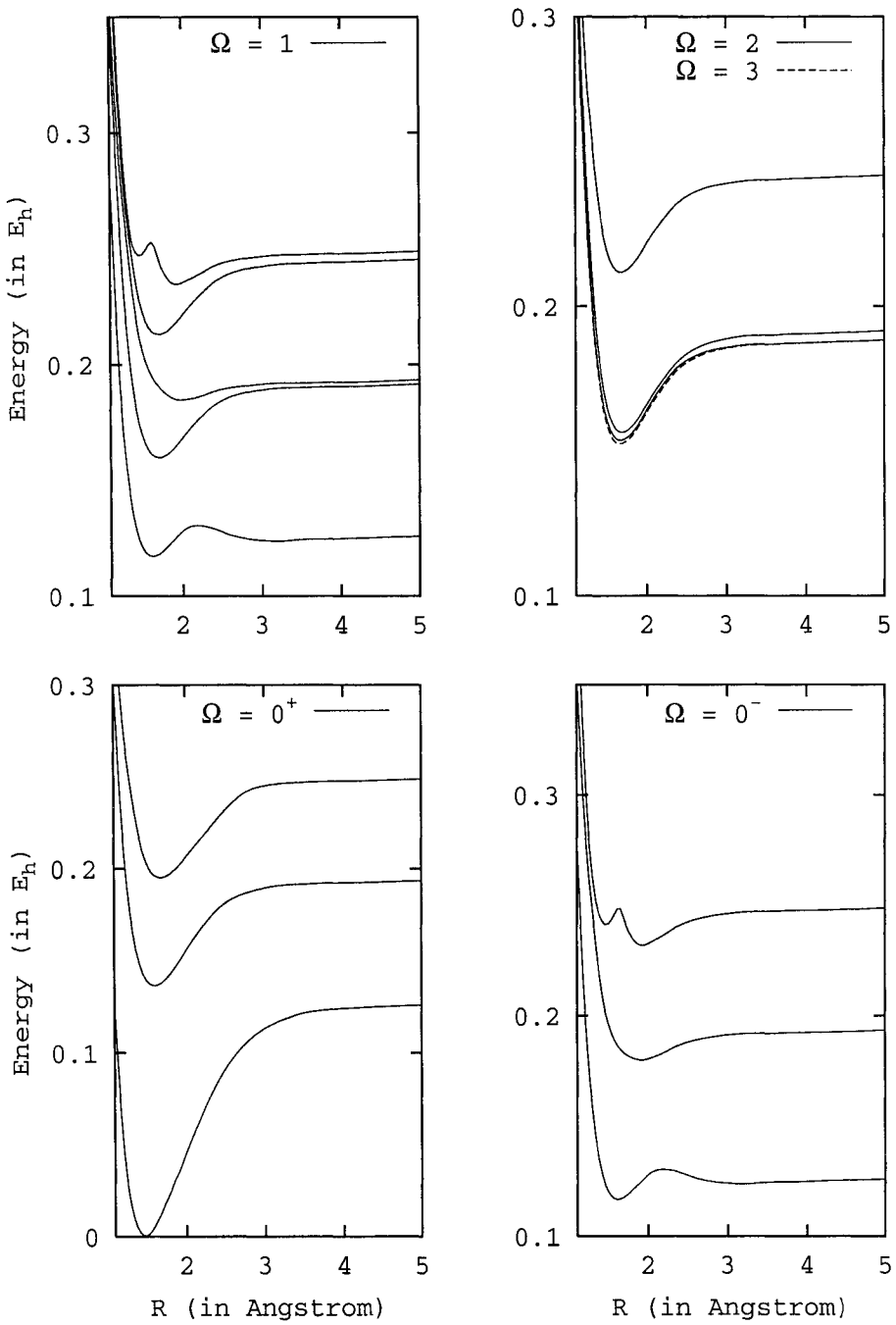

Figure 8.10: Relativistic spin-orbit states of AuH in confinement for $\omega = 0.100$ au Energies are plotted with respect to E_{min} of the 0^+(I) state.

8.14. Similarly to the spin-free case, the spin-orbit states for AgH are in general more complicated than those of AuH. When the confining potential is applied, only the states that originated from the first two $^1\Sigma^+$ and 1 $^3\Sigma^+$ states are essentially unaffected. For $\Omega = 0^+$, 0^-, 1 and 2, the applied potential causes a numerous new avoided crossings because of the close proximity of the parent Π and Δ states. Consequently, the r_e and ν_e values for different Ω states, determined for different values of ω, do not evolve in the same way as their parent spin-free states, and fluctuations of these quantities are observed.

Since only the first two dissociation channels were studied, the resulting spin-orbit state diagram for AuH is much simpler than that of AgH. These states, because of their rather large separations, do not interfere with each other strongly, and thus the changes of r_e and ν_e with respect to ω correlate nicely to the corresponding $\Lambda - S$ states. Even so, there are still several intriguing features that have been observed in the Ω states of the confined AuH. Due to the wiggling potential curves the 0 and 1 components of the 1 $^3\Sigma^+$ state, i.e., 0^-(I) and 1(I) states, also exhibit this character at large R. Through the spin-orbit interaction, the potential energy curves for the higher 0^- and 1 states are slightly distorted and a small potential hump is formed on the potential curves of these states. Another noticeable new feature is the double-minimum potential for the Ω states derived from the 2 $^3\Sigma^+$ state. For small values of ω, a new global minimum is formed at about 1.5 Å via the avoided crossing of the 1(V) and 1(IV) states, the latter being the 1 component of the $^3\Delta$ and $^1\Pi$ states. This minimum shifts up in energy relative to the outer minimum when ω increases. For ω exceeding 0.050 au the outer minimum becomes the global minimum again while the inner one starts disappearing. There is no counterpart in the spin-free potentials, and this feature can be considered entirely due to spin-orbit interaction.

An interesting effect of confinement is the variation of spin-orbit coupling constants with respect to the strength of the confining potential. Since the magnitude of spin-orbit coupling between two electronic states is closely related to their electronic structure, the application of an external potential to a molecular system,

Table 8.11: Spectroscopic constants of the spin-orbit 0 states of AgH in confinement. (r_e in Å, ν_e in cm^{-1}, T_e in eV)

State		$\omega = 0.000$	$\omega = 0.025$	$\omega = 0.050$	$\omega = 0.075$	$\omega = 0.100$
0^+(I)	r_e	1.5614	1.5582	1.5679	1.5825	1.5903
	ν_e	2078	2095	1940	1968	1923
	T_e	0.00	0.00	0.00	0.00	0.00
0^+(II)	r_e	1.7549	1.7496	1.7308	1.7182	1.6874
	ν_e	1194	1544	1281	1277	1554
	T_e	4.03	4.00	3.94	3.89	3.84
0^+(III)	r_e	1.5745	1.5481	1.5094	1.5671	1.7983
	ν_e	1661	2108	2041	1662	1385
	T_e	5.54	5.59	5.78	6.05	6.21
0^+(IV)	r_e	1.8284	1.8247	1.8174	1.7527	1.6194
	ν_e	1251	1250	1282	2698	2935
	T_e	6.14	6.15	6.14	6.18	6.41
0^+(V)	r_e	2.0669	2.0563	2.0491	2.0485	2.0285
	ν_e	1126	1146	1150	1223	1151
	T_e	6.89	6.90	6.90	6.94	7.00
0^+(VI)	r_e	1.7134	1.6449	1.6371	1.6469	1.8595
	ν_e	2575	2643	1324	1379	1368
	T_e	7.82	8.12	8.50	8.95	9.05
0^-(II)	r_e	1.5717	1.5607	1.5079	1.5685	1.8210
	ν_e	1673	1862	2062	1658	1299
	T_e	5.54	5.60	5.78	6.05	6.15
0^-(III)	r_e	1.8645	1.8583	1.8507	1.7362	1.6162
	ν_e	1138	1153	1178	2649	2797
	T_e	6.06	6.08	6.08	6.16	6.41
0^-(IV)	r_e	1.9511	1.9529	1.9477	1.9414	1.9244
	ν_e	1326	1309	1350	1388	1426
	T_e	6.64	6.66	6.67	6.71	6.78

Table 8.12: Spectroscopic constants of the spin-orbit 1,2, and 3 states of AgH in confinement. (r_e in Å, ν_e in cm^{-1}, T_e in eV)

State		$\omega = 0.000$	$\omega = 0.025$	$\omega = 0.050$	$\omega = 0.075$	$\omega = 0.100$
1(II)	r_e	1.5763	1.5641	1.5120	1.7868	1.7769
	ν_e	1654	1857	1976	1386	1468
	T_e	5.58	5.63	5,82	5.97	6.02
1(III)	r_e	1.7956	1.7953	1.7509	1.6380	1.8494
	ν_e	1321	1347	2030	2470	1143
	T_e	5.93	5.95	5.96	6.13	6.31
1(IV)	r_e	1.7822	1.8098	1.8672	1.7927	1.6613
	ν_e	882	851	1042	1928	2570
	T_e	608	6.13	6.19	6.27	6.48
1(V)	r_e	1.9116	1.8827	1.7657	1.7653	1.7582
	ν_e	907	876	1108	1323	1604
	T_e	6.28	6.33	6.47	6.56	6.61
1(VI)	r_e	1.8120	1.8122	1.8400	1.9242	1.9055
	ν_e	1282	1293	1254	1291	1454
	T_e	6.56	6.58	6.59	6.73	6.83
1(VII)	r_e	1.9181	1.9207	1.9146	1.8804	1.7911
	ν_e	1382	1371	1380	1208	821
	T_e	6.72	6.74	6.76	6.85	7.16
2(I)	r_e	1.5785	1.5520	1.5527	1.7792	1.7703
	ν_e	1650	1931	1477	1426	1510
	T_e	5,61	5.67	5.86	5.91	5.95
2(II)	r_e	1.7917	1.7903	1.7018	1.7609	1.7520
	ν_e	1379	1386	2236	1385	1456
	T_e	5.89	5.90	5.95	6.06	6.10
2(III)	r_e	1.7726	1.7710	1.7644	1.6300	1.5712
	ν_e	1327	1334	1459	2500	1770
	T_e	6.05	6.05	6.05	6.17	6.50
2(IV)	r_e	1.7746	1.7730	1.7688	1.7627	1.7526
	ν_e	1330	1338	1360	1388	1491
	T_e	6.58	6.58	6.58	6.60	6.64
3(I)	r_e	1.7709	1.7659	1.7655	1.7599	1.7516
	ν_e	1337	1343	1365	1392	1460
	T_e	5.99	6.00	5.99	6.00	6.03

Table 8.13: Spectroscopic constants of the spin-orbit 0 states of AuH in confinement. (r_e in Å, ν_e in cm^{-1}, T_e in eV)

State		$\omega = 0.000$	$\omega = 0.025$	$\omega = 0.050$	$\omega = 0.075$	$\omega = 0.100$
0^+(I)	r_e	1.4827	1.4482	1.4765	1.4775	1.4793
	ν_e	2504	3671	2451	2571	2592
	T_e	0.00	0.00	0.00	0.00	0.00
0^+(II)	r_e	1.6692	1.6219	1.6078	1.6086	1.6042
	ν_e	1621	1793	1678	1823	1860
	T_e	3.88	3.93	3.89	3.81	3.71
0^+(III)	r_e	1.7165	1.6907	1.6907	1.6904	1.6752
	ν_e	2008	1575	1540	1716	1641
	T_e	5.40	5.43	5.41	5.35	5.30
0^-(I)	r_e	1.6324	1.6169	1.6064	1.6142	1.6173
	ν_e	1573	1645	1603	1590	1676
	T_e	3.34	3.43	3.39	3.30	3.17
0^-(II)	r_e	1.9327	2.0171	2.0549	1.9361	1.9149
	ν_e	784	1169	884	1087	1077
	T_e	4.91	4.87	4.91	4.89	4.89
0^-(III)	r_e	1.9436	1.4908	1.4862	1.9362	1.9299
	ν_e	1244	3275	2799	1509	1592
	T_e	6.34	6.02	6.11	6.30	6.30

Table 8.14: Spectroscopic constants of the spin-orbit 1,2 and 3 states of AuH in confinement. (r_e in Å, ν_e in cm^{-1}, T_e in eV)

State		$\omega = 0.000$	$\omega = 0.025$	$\omega = 0.050$	$\omega = 0.075$	$\omega = 0.100$
1(I)	r_e	1.6304	1.6153	1.6041	1.6121	1.6156
	ν_e	1579	1654	1619	1596	1681
	T_e	3.34	3.33	3.40	3.31	3.18
1(II)	r_e	1.7453	1.7256	1.7101	1.7090	1.6976
	ν_e	2074	1465	1557	1552	1522
	T_e	4.41	4.42	4.42	4.38	4.34
1(III)	r_e	2.0386	2.0496	2.0324	2.0003	1.9670
	ν_e	715	1202	1066	828	1144
	T_e	5.03	4.97	5.02	5.01	5.02
1(IV)	r_e	1.7376	1.7097	1.6986	1.7011	1.6955
	ν_e	1619	1458	1459	1529	1374
	T_e	5.88	5.88	5.88	5.83	5.79
1(V)	r_e	1.9388	1.5330	1.4983	1.9295	1.9237
	ν_e	1186	4103	3459	1457	1462
	T_e	6.41	6.12	6.26	6.37	6.38
2(I)	r_e	1.7327	1.7003	1.6813	1.6814	1.6676
	ν_e	2052	1369	1457	1544	1515
	T_e	4.28	4.29	4.28	4.23	4.18
2(II)	r_e	1.7237	1.6938	1.6846	1.6884	1.6859
	ν_e	1754	1490	1519	1636	1575
	T_e	4.34	4.35	4.34	4.29	4.25
2(III)	r_e	1.7228	1.6879	1.6702	1.6750	1.6697
	ν_e	1633	1417	1463	1543	1535
	T_e	5.86	5.86	5.85	5.80	5.76
3(I)	r_e	1.7032	1.6742	1.6616	1.6680	1.6595
	ν_e	1335	1480	1500	1591	1576
	T_e	4.28	4.28	4.26	4.20	4.14

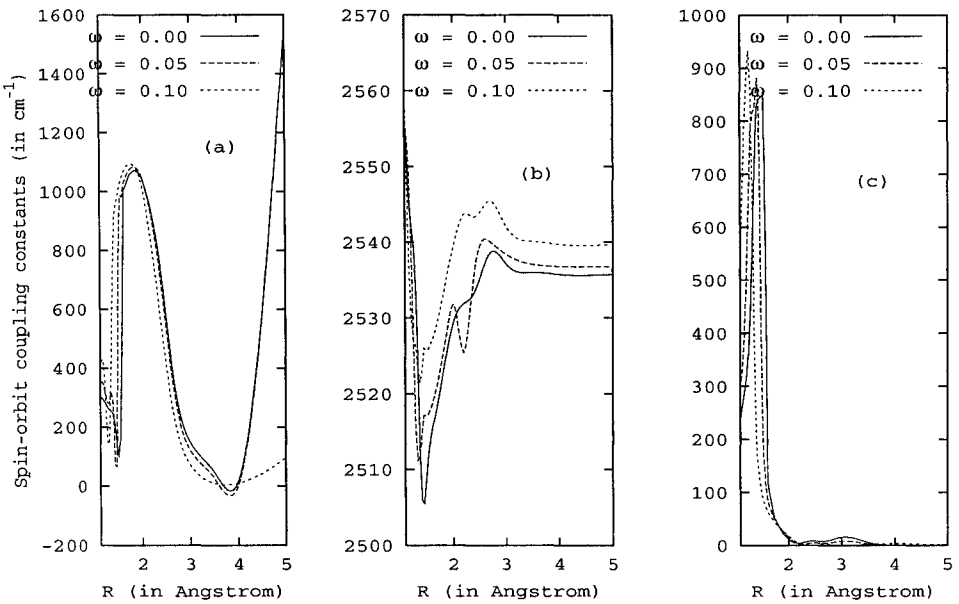

Figure 8.11: Spin-orbit coupling constants for selected states of AgH in confinement. (a) 2 $^3\Sigma^+$ and 1 $^3\Pi$ states; (b) 1 $^3\Delta$ and 1 $^3\Delta$; (c) 1 $^1\Pi$ and 2 $^3\Pi$ states.

which alters the wavefunction composition of the different electronic states, should give rise to the changes of the spin-orbit coupling constants. To demonstrate this, the calculated diagonal and off-diagonal spin-orbit coupling constants for some of the excited states of AgH and AuH are plotted in Figures 8.11 and 8.12, respectively. Surprisingly, the effects of confinement on the magnitude of spin-orbit interaction is fairly small. Generally, the confining potential increases the coupling constants, but their variations with respect to the internuclear distances remain very similar compared to the unconfined cases.

More detailed information regarding the spin-orbit interaction can be extracted from these plots. For instance, the Figures 8.11(b) and 8.12(b) illustrate the computed diagonal spin-orbit coupling constants for the $^3\Delta$ state at various R. Since the $^3\Delta$ state transforms into A_1 and A_2 irreducible representations in C_{2v} symmetry, this $^3\Delta$ spin-orbit coupling constant will be dependent on both the interaction between different components of the d-shell and, in turn, the splitting of the $4d$-shell and $5d$-shell of AgH and AuH, respectively, due to the presence of the confining poten-

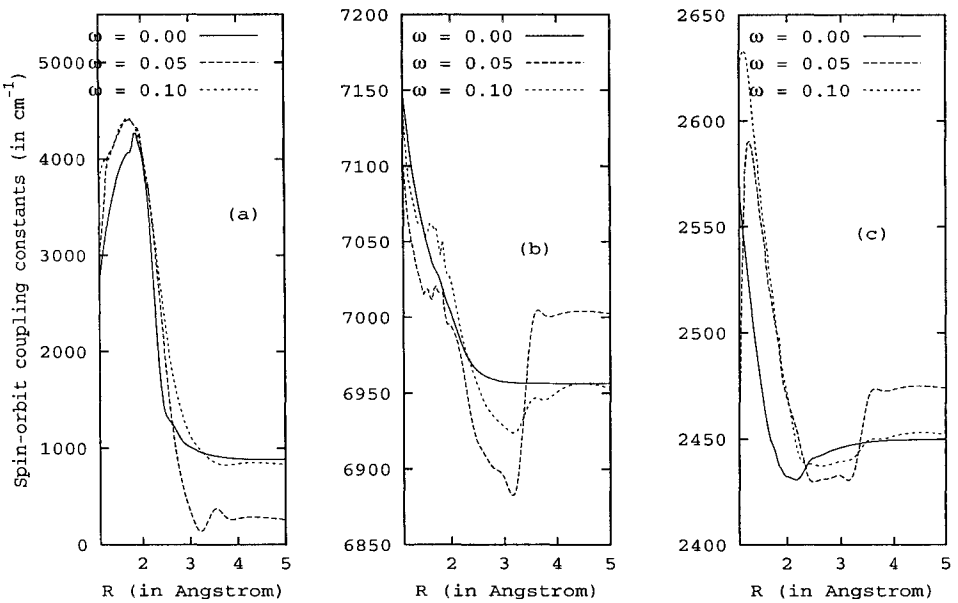

Figure 8.12: Spin-orbit coupling constants for selected states of AuH in confinement. (a) 1 $^3\Sigma^+$ and 1 $^3\Pi$ states; (b) 1 $^3\Delta$ and 1 $^3\Delta$; (c) 1 $^1\Pi$ and 1 $^3\Delta$ states.

tial. As seen, the coupling constants increase with ω; this observation is consistent with the molecular calculations showing that the confining potential increases the fine structure splittings of $^2D_{5/2}$ - $^2D_{3/2}$ of Ag and Au.

The second-order spin-orbit interactions on AgH, as revealed by Figures 8.11(a) and 8.11(c), are not significant. The applied potential only increases the coupling constants by about 100 cm^{-1}. The larger coupling constants result from the smaller energy separation between these state potential curves that gives rise to a larger second-order perturbation contribution. A noticeable drop of the coupling constant in Figure 8.11(a) can be accounted for by strong interaction between the two $^3\Pi$ states for the confined AgH molecule. The enhanced p character in the 1 $^3\Pi$ state sharply reduces the spin-orbit interaction with the 2 $^1\Sigma^+$ which is also dominated by the Ag $5p$ character at large R.

On the other hand, the influence of the second-order spin-orbit coupling on AuH is more pronounced; in some cases, the coupling constants are of the same order of magnitude as the binding energies of certain Ω states. Moreover, fluctuations in the

variations of the coupling constants with respect to ω are observed, especially for $\omega \approx 0.05$ au, indicating possibly the insufficient treatment of the double perturbation from both the confinement effects and the spin-orbit interaction. The sudden decline of the coupling constant for $\omega = 0.05$ au in Figure 8.12(a) is likely caused by the configuration mixing of the $1\ ^3\Sigma^+$ state, in which the additional anti-bonding character diminishes the spin-orbit interaction with the $1\ ^3\Pi$ state. The $1\ ^1\Pi$ and $1\ ^3\Delta$ states are the major components of both the 1(III) and 1(IV) spin-orbit states. For small values of ω, a significant mixing of these states with the higher 1 states leads to the irregular shapes of these potential curves at intermediate R, and is responsible for the abnormal increment in the $^1\Pi$-$^3\Delta$ spin-orbit coupling constant (Figure 8.12(c)).

8.4 Conclusions

In the studies of combined effects of relativity, electron correlation, and confinement, the potential energy curves for the low-lying excited states of coinage metal hydrides AgH and AuH were calculated employing the second-order spin-orbit quasi-degenerate perturbation theory with the third-order Douglas-Kroll Hamiltonian. It was found that, with the application of the confining potential, the spin-free channels connected to the excited dissociation products of these molecular systems split due to the symmetry restriction imposed by the cylindrical geometry of the applied potential on the p-shells and d-shells of Ag and Au atoms. While the ^2P states of these atoms divide into two subsets, $\{p_z\}$ and $\{p_x, p_y\}$, the ^2D states partition into three subsets, $\{d_{z^2}\}$, $\{d_{x^2-y^2}, d_{xy}\}$ and $\{d_{xz}, d_{yz}\}$, the first two being very close in energy. An unusual feature discovered in AgH is that the second and third dissociation channels merge and redistribute when ω increases, which could possibly result from the complex re-ordering of the atomic orbitals of the confined Ag atom. The responses of different electronic states of AgH and AuH to the confining potential are not always typical; several abnormal changes in r_e, ν_e and binding energies have been noticed and are accounted for by the induced avoided crossing between the excited states.

The Ω state potential curves of these molecules have also been calculated for a several values of ω. More complicated pictures have been obtained because of the significant configuration mixing among the states possessing the same Ω components. As a result, the changes of the deduced spectroscopic parameters for these states are not in parallel to the trends observed for the spin-free counterparts. Both diagonal and off-diagonal spin-orbit coupling constants for different states of AgH and AuH molecules have been computed. It was found that the dependence of the spin-orbit coupling constants on the strengths of the confining potential is very small. Instead, the configuration mixing in the excited state wavefunctions plays a more important role in determining the resultant magnitude of the spin-orbit interactions.

Bibliography

[1] N. N. Greenwood and A. Earnshaw, *Chemistry of the Elements*, 2nd edition, Butterworth Heinemann, New York, 2002.

[2] L. Szasz, *Pseudopotential Theory of Atoms and Molecules*, Wiley, New York, 1985.

[3] O. Gropen, *The Relativistic Effective Core Potential Method*, Chapter 3 in: S. Wilson (editor), *Methods in Computational Chemistry, Vol 2*, Plenum, New York, 1988.

[4] G. Breit, *Phys. Rev.* **34**, 553 (1929).

[5] L. L. Foldy and S. A. Wouthuysen, *Phys. Rev.* **78**, 29 (1950).

[6] R. D. Cowan and D. C. Griffin, *J. Opt. Soc. A.* **66**, 1010 (1976).

[7] J. Sucher, *Phys. Rev. A* **22**, 348 (1980).

[8] E. van Lenthe, E. J. Baerends, and J. G. Snijders, *J. Chem. Phys.* **99**, 4597 (1993).

[9] M. Douglas and N. M. Kroll, *Ann. Phys. (N. Y.)* **82**, 89 (1974).

[10] B. A. Heß, *Phys. Rev. A* **33**, 3742 (1986).

[11] T. Nakajima and K. Hirao, *Chem. Phys. Lett.* **329**, 511 (2000).

[12] J. Paulovic, T. Nakajima, K. Hirao, and L. Seijo, *J. Chem. Phys.* **117**, 3597 (2002).

[13] A. Wolf, M. Reiher, and B. A. Heß, *J. Chem. Phys.* **120**, 8624 (2004).

[14] H. A. Bethe and E. E. Salpeter, *Quantum Mechanics of One and Two-electron Atoms*, Plenum, New York, 1977.

[15] P. Pyykkö and J. P. Desclaux, *Acc. Chem. Res.* **12**, 276 (1979).

[16] P. Pyykkö, *Angew. Chem. Int. Ed.* **43**, 4412 (2004).

[17] G. Jensen and B. A. Heß, *Z. Phys. D: At. Mol. Clusters* **13**, 363 (1989).

[18] H. A. Witek, T. Nakajima, and K. Hirao, *J. Chem. Phys.* **113**, 8015 (2000).

[19] W. Jaskólski, *Phys. Rep.* **271**, 1 (1996).

[20] D. Bielińska-Wąż, J. Karwowski, B. Saha, and P. K. Mukherjee, *Phys. Rev. E* **68**, 1 (2003).

[21] U. Kappes and P. Schmelcher, *Phys. Rev. A* **51**, 4542 (1995).

[22] D. Bielińska-Wąż, J. Karwowski, and G. H. F. Diercksen, *J. Phys. B: At. Mol. Opt. Phys.* **34**, 1987 (2001).

[23] T. Sako, I. Černušák, and G. H. F. Diercksen, *J. Phys. B: At. Mol. Opt. Phys.* **37**, 1091 (2004).

[24] D. Bielińska-Wąż, G. H. F. Diercksen, and M. Klobukowski, *Chem. Phys. Lett.* **349**, 215 (2001).

[25] J. M. H. Lo and M. Klobukowski, *Mol. Phys.* **102**, 2511 (2004).

[26] B. A. Heß, *Phys. Rev. A* **39**, 6016 (1989).

[27] A. Wolf, M. Reiher, and B. A. Heß, *J. Chem. Phys.* **117**, 9215 (2002).

[28] T. Nakajima and K. Hirao, *J. Chem. Phys.* **113**, 7786 (2000).

[29] T. Nakajima, T. Yanai, and K. Hirao, *J. Comput. Chem.* **23**, 847 (2002).

[30] R. Samzow, B. A. Heß, and G. Jensen, *J. Chem. Phys.* **96**, 1227 (1992).

[31] H. Nakano, *J. Chem. Phys.* **99**, 7983 (1993).

[32] T. R. Furlani and H. F. King, *J. Chem. Phys.* **82**, 5577 (1985).

[33] D. G. Fedorov and J. P. Finley, *Phys. Rev. A* **64**, 042502 (2001).

[34] H. A. Witek, D. G. Fedorov, K. Hirao, A. Viel, and P.-O. Widmark, *J. Chem. Phys.* **116**, 8396 (2002).

[35] V. Kellö and A. J. Sadlej, *Theor. Chim. Acta.* **94**, 93 (1996).

[36] T. H. Dunning, *J. Chem. Phys.* **90**, 1007 (1989).

[37] H. A. Witek, J. P. Finley, Y. K. Choe, and K. Hirao, *J. Comput. Chem.* **23**, 957 (2002).

[38] J. L. Dunham, *Phys. Rev.* **41**, 721 (1932).

[39] M. W. Schmidt, K. K. Baldridge, J. A. Boatz, S. T. Elbert, M. S. Gordon, J. J. Jensen, S. Koseki, N. Matsunaga, K. A. Nguyen, S. Su, T. L. Windus, M. Dupuis, and J. A. Montgomery, *J. Comput. Chem.* **14**, 1347 (1993).

[40] J. C. Pickering and V. Zilio, *Eur. Phys. J. D* **13**, 181 (2001).

[41] E. Bengtsson and E. Olsson, *Z. Phys.* **72**, 163 (1931).

[42] U. Ringström and N. Åslund, *Ark. Fys.* **32**, 19 (1966).

[43] K. P. Huber and G. Herzberg, *Constants of Diatomic Molecules*, Van Nostrand, New York, 1979.

[44] R. C. M. Learner, *Proc. R. Soc. London. Ser. A* **269**, 327 (1962).

[45] Y. Li, H. P. Libermann, R. J. Buenker, and L. Pichl, *Chem. Phys. Lett.* **389**, 101 (2004).

[46] P. J. Hay, W. R. Wadt, L. R. Kahn, and F. W. Bobrowicz, *J. Chem. Phys.* **69**, 984 (1978).

[47] A. D. McLean, *J. Chem. Phys.* **79**, 3392 (1983).

[48] P. Schwerdtfeger, M. Dolg, W. H. E. Schwarz, G. A. Bowmaker, and P. D. W. Boyd, *J. Chem. Phys.* **91**, 1762 (1989).

[49] K. Balasubramanian, *Relativistic Effects in Chemistry. Part A*, Wiley-Interscience, New York, 1997; Chapter 5.

[50] J. C. Ehrhardt and S. P. Davis, *J. Opt. Soc. Am.* **61**, 1342 (1971).

[51] P. Pyykkö, *Chem. Rev.* **88**, 563 (1988).

[52] T. Sako and G. H. F. Diercksen, *J. Phys. B: At. Mol. Opt. Phys.* **36**, 1681 (2003).

Chapter 9

Computational Studies of One-Electron Properties of Confined LiH Molecule

The main objective of Chapter 9 is to investigate a variety of one-electron properties of polar LiH molecule in the presence of a confining potential, and to try to reveal the principles with which these electric and optical properties can be manipulated by the strength and geometry of the applied electrostatic potential.

9.1 Introduction

The studies of systems confined by various forms of external potentials has commenced as of the beginning of quantum mechanics. Following the early work of Fock [1] on the confinement by magnetic fields, the concept of confinement has been utilized in several branches of science such as nuclear physics [2], condensed-matter physics [3], and surface chemistry [4]. The breakthrough in semi-conductors and nanotechnology in the past two decades, where artificial atoms and molecules [5] can be constructed in experiments, provides a platform for verifying the validity of the developed confinement models and stimulates the advancement of the theory of confinement.

Recently, Diercksen and co-workers have extensively investigated the spectral and structural properties of quantum dots and closely related confined atoms using

three-dimensional harmonic oscillator potentials of spherical, elliptical, prolate, and oblate symmetries [6, 7, 8]. Meanwhile, similar studies have been performed on molecular systems such as H_2 [9], Li_2 [10], and NeH [11]. These works concluded that the changes of geometries and spectral properties of the confined systems, caused by the spatial restriction imposed by the symmetry and strength of the confining potentials on the electronic wavefunctions, results in the lifted orbital degeneracy, the shifts of equilibrium bond distances, and existence of new points of avoided crossing.

Due to the fact that the distorted electron density of a molecule gives rise to the variations of the electronic and magnetic properties of the molecule, the measurement of these quantities and comparison with the values for the reference system in free space can serve as a probe to provide the structural information of the environment. An excellent example demonstrating the usefulness of this concept is provided by the TDHF and CASPT2 studies of auride ion by Sadlej et al. [12] who successfully accounted for the lack of colour of the tetramethylammonium auride crystal using the Helium cluster confinement model.

As the simplest neutral heterodiatomic molecule, LiH has been the subject for numerous benchmarking theoretical studies due to the small number of electrons that makes the calculations employing highly sophisticated methods and extended basis sets feasible. Hence, in the present study, the electric dipoles, dipole polarizabilities, and electric field gradients of the LiH molecule embedded in an axially symmetrical harmonic oscillator potential were calculated. The electric dipole moments and dipole polarizabilities for the ground X $^1\Sigma^+$ and A $^1\Sigma^+$ states, as well as the dissociative a $^3\Sigma^+$ state, were computed for several values of the confinement parameter ω. However, the electric field gradient (EFG) components were calculated only for the X and A $^1\Sigma^+$ states. The dependence of these quantities on the internuclear distances was also investigated.

9.2 Computational Details

The confining potential $W(\mathbf{r}_i)$ adopts the form of an isotropic two-dimensional harmonic oscillator centered at the origin of the coordinate system as used in the previous parts of the present work, i.e.,

$$W(\mathbf{r}_i) = \frac{1}{2}\omega^2 \mathbf{r}_i^2 = \frac{1}{2}\omega^2 \left(x_i^2 + y_i^2\right) \tag{9.1}$$

It is assumed, in all the calculations, that the principal axis of the cylindrical harmonic oscillator, i.e., the z-axis, overlaps with the molecular axis of LiH. The confining parameter ω defines the strength of the applied harmonic oscillator potential.

The dipole moments, polarizabilities and EFGs of the ground and first two excited states of LiH were calculated using the full second-order configuration interaction (FSOCI) method implemented in the program GAMESS-US [13, 14]. The zeroth-order configurations were generated by CASSCF with the active space composed of the $1s$, $2s$ and $2p$ orbitals of Li and the $1s$ orbital of H. All the electrons were correlated. In the subsequent SOCI calculations, with the same CASSCF active space except that the 1σ MO was frozen, all possible configurations were generated by the single and double excitations from the CASSCF reference functions. The Davidson correction [15] was added to include the estimated quadruple-excitation contributions. This CASSCF/SOCI technique has been extensively used in the molecular calculations involving heavy metal atoms (for example, Refs. [16, 17, 18, 19]), and very satisfactory performance was observed when compared to the multi-reference CI method.

The accuracy of the calculations of dipole moments and polarizabilities is strongly dependent on the quality of the basis sets in terms of the size of valence space and the diffuseness of the orbital exponents [20]. Therefore, two fairly large basis sets were employed in the present calculations. The basis set of Jaszuński and Roos [21] for H, derived from the Huzinaga's $10s$ basis set [22], was used and augmented by an additional $2s6p3d$ set and contracted in a (411111111/111111/111) scheme. A diffuse p function of exponent 0.01 was added to this basis set, leading to the resulting $9s7p3d$ set. Its performance has been verified in the calculations of the

static polarizability and hyperpolarizability of H_2 molecule, and an excellent agreement was found with the accurate results from Kolos and Wolniewicz [23] who used explicitly correlated wavefunctions.

The basis set for Li is the $(10s6p4d)/[5s3p2d]$ set of Sadlej [24] optimized for the calculations of molecular electric properties. An extra $1s1p1d$ set of exponents with values 0.03, 0.03 and 0.02, respectively, was added, giving rise to a $6s4p3d$ basis. At the midpoint position between the Li and H nuclei, a set of confining functions consisting of $4s4p4d$ Gaussian primitives was added in order to properly describe the distorted electron density at this region due to the harmonic oscillator potential [6]. Their exponents, i.e., 0.025, 0.050, 0.075 and 0.100, were determined by the expression $\omega/2$ where ω are the confinement parameters adopted in the present calculations.

Unlike the electric dipole moments and electric field gradients, which were evaluated directly from the electron densities derived from the CASSCF/SOCI wavefunctions, the components of the dipole polarizabilities were calculated using the energy-based finite field method developed from the many-body perturbation theory [25]. Kurtz, Stewart and Dieter have shown that the numerical accuracy of the finite field method is sensitive to the precision in the energy calculations [26]. Therefore, a very high convergence criterion, 10^{-20} a.u., was selected in all the energy evaluations. A small electric field, 0.001 a.u., as suggested by Kurtz et al. [26], was used so as to avoid the unnecessary significant configurational changes of LiH.

9.3 Results and Discussion

9.3.1 Dipole Moments

Initially, the potential energy curves for the first several low-lying states of LiH were calculated to confirm the performance of the method and basis sets. Figure 9.1 contains the plots for LiH molecule in both free space (9.1(a)) and in a cylindrical confining potential of ω 0.100 a.u. (9.1(b)). As can be seen from Table 9.1, the calculated binding energies and excitation energies of free LiH are in very good agreement with the experimental values. In spite of the fact that the estimated

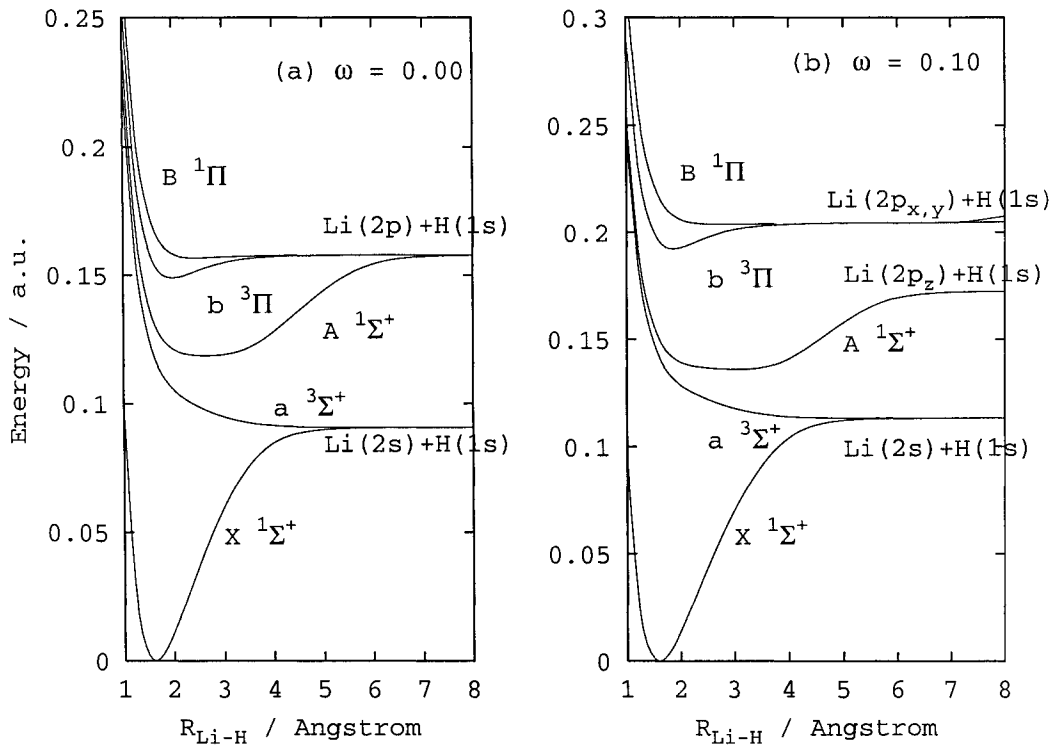

Figure 9.1: CASSCF/SOCI potential energy curves for several low-lying electronic states of LiH (a) for the zero field ($\omega = 0.00$ a.u.), and (b) for $\omega = 0.10$ a.u. Energies are plotted with respect to the potential minimum of the ground X $^1\Sigma^+$ state.

Table 9.1: Calculated excitation energies T_e (in cm^{-1}) and binding energies D_e (in eV) of LiH in free space

Parameter	State	Calc.	Expt. [27]
D_e	X $^1\Sigma^+$	2.4692	2.5154
	A $^1\Sigma^+$	1.0619	1.0765
	B $^1\Pi$	0.0314	0.035
T_e	X $\rightarrow$ A	26031	26510
	X $\rightarrow$ B	34371	34912
	A $\rightarrow$ B	8339	8402

equilibrium distance of the ground-state LiH (1.6102 Å) is slightly longer than the measured value of 1.5949 Å [28], the CASSCF/SOCI method, in general, is able to provide reliable wavefunctions and energies for the subsequent calculations of various one-electron properties of LiH.

There are several remarkable changes of the potential curves when the confining potential is applied. Compared to field-free situation (Figure 9.1(a)), the binding energies for the X state increases while that for the A state declines. Meanwhile, the dissociation channel that leads to the asymptotic products of Li(^2P) + H(^2S) split into two branches; the lower branch is in σ symmetry and connects with the $2p_z$ configuration of Li while the upper branch is in exclusively π symmetry, giving rise to the Li($2p_x$) and Li($2p_y$) products. These phenomena can be attributed to the geometric constraint imposed by the confining potential as the axially symmetric potential lifts the triple degeneracy of the p-shell and brings about two subsets: $\{p_x, p_y\}$ and $\{p_z\}$, the latter one being more stabilized and lower in energy [29]. As a consequence, the reformation of the second dissociation channel upshifts the two Π states and greatly increases their T_e values. In addition, the relative stability of $2p_z$ orbital with respect to $2p_x$ and $2p_y$ orbitals leads to variation of the configuration of the A state which is manifested in its electric properties.

Electric dipole moments for the first three electronic states of LiH were computed based on the SOCI wavefunctions for a range of internuclear distances. The calculated dipole moments for the X state for several values of ω are depicted in Figure 9.2. Since the Li atom in LiH molecule was defined at the positive z-axis, the positive values of the dipole moment indicates the accumulation of electron density on the more electronegative H atom. The large magnitude of the electic dipole moments reveals the strong ionic character of the ground state of LiH molecule, which results from the partial charge transfer from Li to H. The CASSCF/SOCI dipole moment at the experimental equilibrium distance of 1.5957 Å is 5.897 Debye which agrees very well (within 0.3%) with the experimental value of 5.882 Debye [30]. The dipole moment reaches a maximum at $R \approx 2.7$ Å where the ground state potential energy curve crosses the Li^+H^- ionic potential curve [31]. For larger R the electric

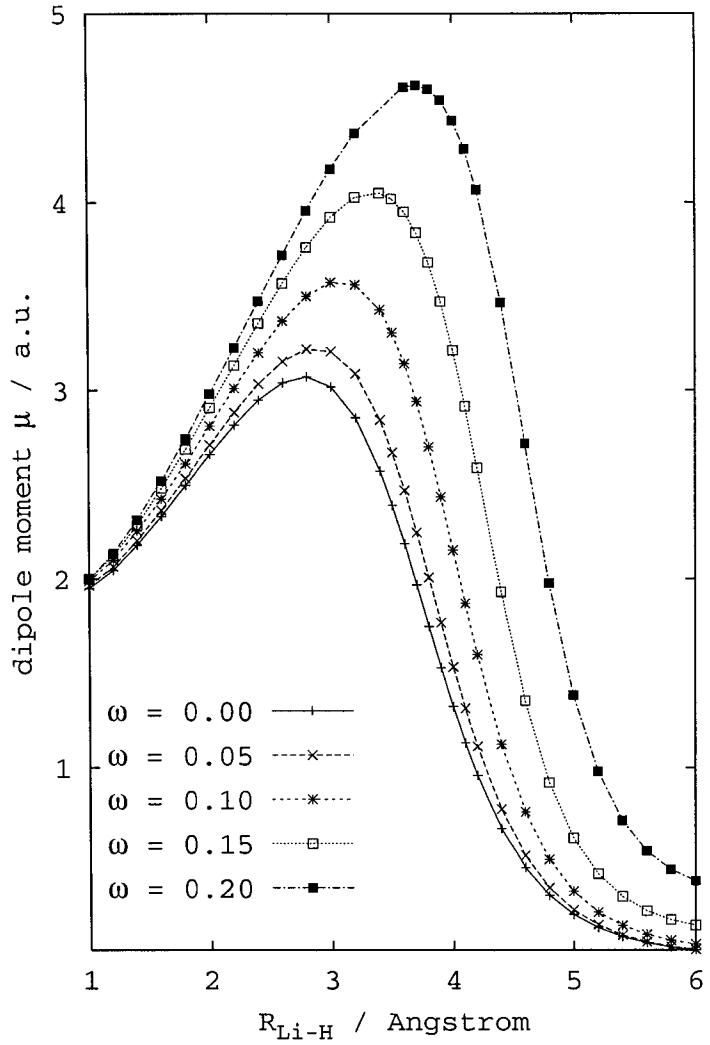

Figure 9.2: Electric dipole moments for the X $^1\Sigma^+$ state of LiH.

dipole moment gradually vanishes because of the increasing covalent bond character that leads the X state to the correct dissociation limit of the ground-state Li and H atoms.

Compared to that of the ground state configuration, the dipole moments for the a $^3\Sigma^+$ and A $^1\Sigma^+$ states exhibit substantially different behaviour for the whole range of R. At small internuclear distances, both a and A states possess negative dipole moments, contrary to the positive dipole moment for the X state. Despite the significant ionic character, the excited $1\sigma^2 2\sigma 3\sigma$ configuration, resulting from the electron promotion $2\sigma \rightarrow 3\sigma$, induces a polarized electron density residing on Li atom, and thus reverses the dipole orientation. Similarly to the ground state scenario, the dipole moment for the a $^3\Sigma^+$ state converges to 0 when $R \rightarrow \infty$ due to the increasing covalent character.

The R dependence of the dipole moment for the A $^1\Sigma^+$ state, however, is more complex. As shown in Figure 9.3, the dipole moment increases rapidly when R increases from 1.0 Å, until its maximum value appears at 4.8 Å. This observation is consistent with the MCSCF studies of Docken and Hinze in which the ionic potential intersects the A state potential at 8.0 a.u. [31]. Similarly to the X and a states, the configuration mixing with the covalent Li($2p_z$) + H($1s$) configuration diminishes the dipole moment for the A state at larger R and yields an anticipated zero dipole moment at the asymptotic limit.

The confinement effects on the electric dipole moments of these states are fairly distinct, as illustrated in figures 9.2 and 9.3. A more profound effect is found on the X state in which the magnitude of the dipole moment is increased by 50% for $\omega = 0.20$ a.u. Meanwhile, the internuclear distance r_{max}, at which the dipole moment reaches its maximum, is shifted to larger values of R. On the other hand, the extreme values of the dipole moments for the a and A states are not prominently affected by the presence of confining potential; in both cases, the values are only slightly increased by 0.3 a.u. The plot of the dipole moment for the A state is also shifted towards larger values of R as in the X state. This shift could be accounted for by the fact that the cylindrical confining potential upshifts both the covalent

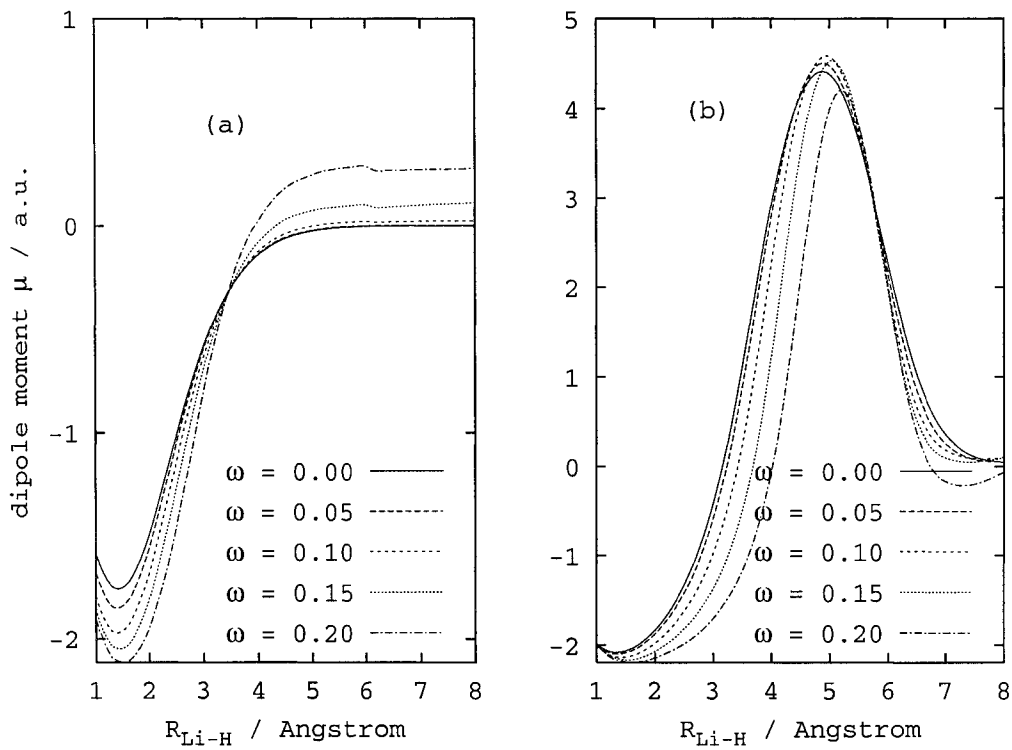

Figure 9.3: Electric dipole moments for LiH. (a) a $^3\Sigma^+$ state; (b) A $^1\Sigma^+$ state.

and ionic potentials of LiH in terms of energy, but to a lesser extent for the latter one. Accordingly, the X and A state potentials cross the ionic potential at larger internuclear distances and lead to the shifts of maximum dipole moments toward larger R. The stability of the ionic character can also explain the larger dipole moments for the confined LiH molecule.

9.3.2 Dipole Polarizabilities

The dipole polarizabilities of LiH for the X, a and A states, computed by the finite field method at the CASSCF/SOCI level, are plotted in Figure 9.4 as a function of internuclear distances. Recently these values have been calculated by Mérawa, Bégué and Dargelos [32] using the time-dependent gauge invariant (TDGI) approach and the CCSD(T) method. Their values are, although slightly smaller, in good agreement with the results obtained in the present work. These deviations can be attributed to the differences between the TDGI and the energy-based finite field methods where the latter one is very sensitive to the accuracy of the computed energies of LiH in the static electric fields. The smaller polarization and diffuse sets in the Sadlej's $5s3p2d$ basis compared to Jeung's $7s5p3d1f$ basis set [33] and the confinement functions at the mid-bond position may also contribute to the larger dipole polarizability, although the actual basis set dependence is not certain [34].

Despite the systematically larger magnitude, the characteristics of the dipole polarizability components for the X and A states are the same as the ones predicted by Mérawa et al. The α_{xx} components for both states are small compared to the α_{zz} counterparts because of the dominant σ-type bonding character. A maximum is noticed at 4.0 Å for α_{zz} for the X state which is due, as suggested by Kołos and Wolniewicz [23], to the dipole-induced dipole interaction. A similar feature is also found for the A state where the maximum of α_{zz} occurs at about 5.8 Å. Interestingly, the A state exhibits a minimum at R where the maximum α_{zz} for the X state is present, which is caused by the largest negative contribution of the X state to the polarizability for the A state [32].

At very large internuclear distances, the α_{xx} and α_{zz} components of the polariz-

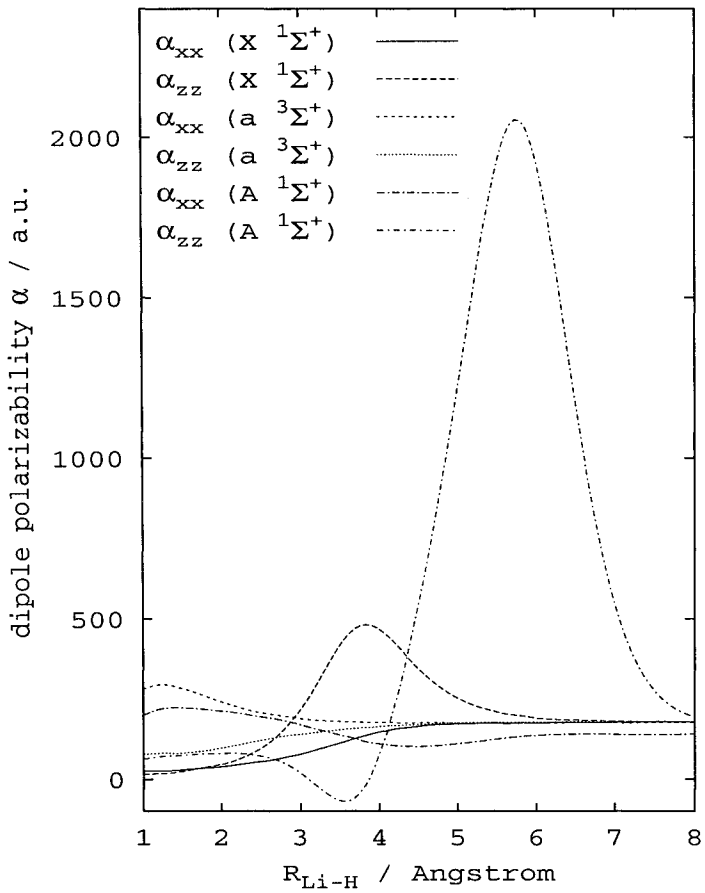

Figure 9.4: Dipole polarizability components of the X $^1\Sigma^+$, a $^3\Sigma^+$ and A $^1\Sigma^+$ states of LiH molecule in free space.

abilities for these three states converge to two distinct values corresponding to the sum of the atomic polarizabilities of H(^2S) and Li(^2S), for the X and a states, and H(^2S) and Li(^2P), for the A state. The finite field calculations yielded the limiting values of, respectively, 177.5 a.u. and 140.5 a.u. which are larger, in particular the latter one, than the TDGI and CCSD(T) values deduced by Mérawa et al. [32].

Due to the cylindrical symmetry of the confining potential, it is anticipated that the effects of spatial confinement on the xx and zz components of the dipole polarizabilities of LiH molecule would be different, and the anisotropy $\Delta\alpha = \alpha_{zz} - \alpha_{xx}$ should be increased. These are justified by the plots in Figure 9.5, in which the α_{xx} (the top panel) and α_{zz} (the bottom panel) for the X, a and A states demonstrate completely different responses to the presence of the confining potential. As expected, the α_{xx} components are suppressed because of the radial compression of the electron density. The α_{zz} components, however, are dramatically increased by the confining potential as the z-axis is the only unconfined degree of freedom that allows for the distortion of electron density when a weak electric field is applied.

The enhancement of α_{zz} is more pronounced for the X state due to the larger contribution from the A state by the induced configuration mixing of the $2s$ and $2p_z$ orbitals of Li. Furthermore, its maximum is shifted toward larger R, in contrast to the case of the A state, where the maximum appears at approximately the same internuclear distance regardless the strength of the confining potential. One intriguing feature concerning the evolution of the α_{zz} for the a $^3\Sigma^+$ state is noteworthy. An isosbestic point is found at 2.60 Å, indicating a switch of configurations of the state. The reduction of α_{zz} at $R < 2.60$ Å is caused by the strong electrostatic interaction of the ionic configuration. For the value of R greater than 2.60 Å, the inclusion of covalent $2s$ and $2p_z$ character relaxes the Coulomb attraction along the molecular axis and thus increases the dipole polarizability α_{zz}.

9.3.3 Electric Field Gradients

As a measure of the second derivatives of the external electric potential arising from the surrounding nuclei and electrons, the electric field gradients (EFGs) at the

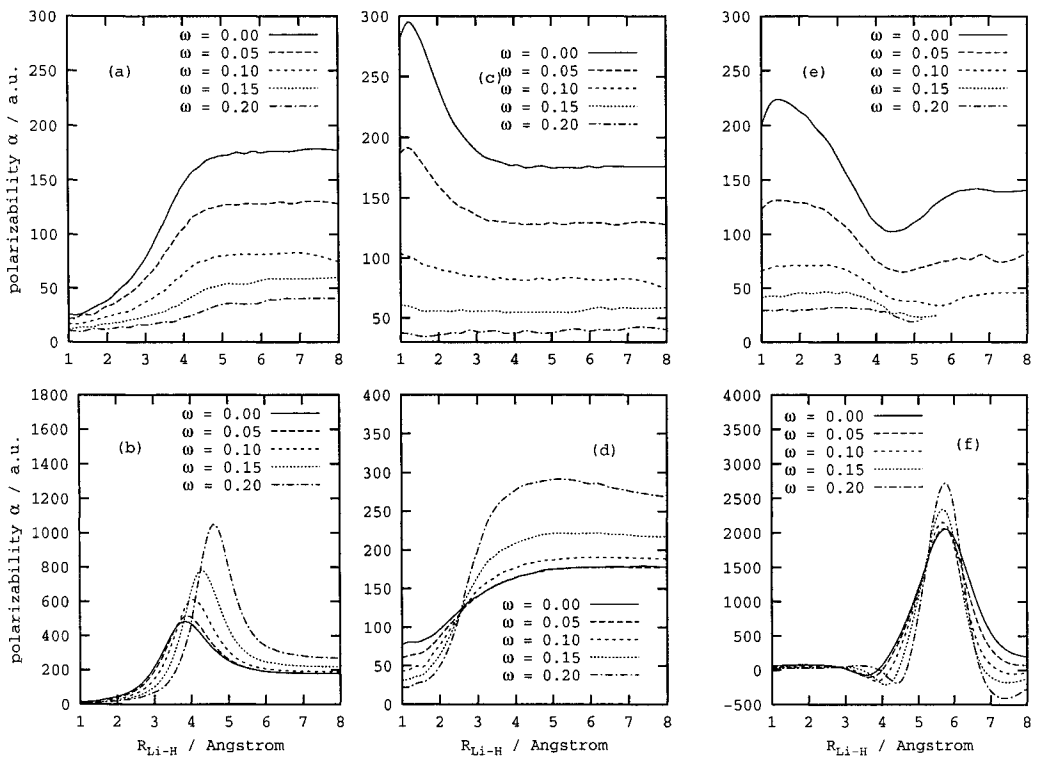

Figure 9.5: Responses of dipole polarizabilities α of LiH molecule to the confining potential. (a) α_{xx} of X $^1\Sigma^+$ state; (b) α_{zz} of X $^1\Sigma^+$ state; (c) α_{xx} of a $^3\Sigma^+$ state; (d) α_{zz} of a $^3\Sigma^+$ state; (e) α_{xx} of A $^1\Sigma^+$ state; (f) α_{zz} of A $^1\Sigma^+$ state.

Table 9.2: Electric field gradients (in a.u.) of the ground state LiH at 1.60 Å.

	Li			H		
ω	V_{xx}	V_{yy}	V_{zz}	V_{xx}	V_{yy}	V_{zz}
0.00	-0.021841	-0.021841	0.043681	0.026709	0.026709	-0.053417
0.05	-0.023369	-0.023369	0.046739	0.025898	0.025898	-0.051796
0.10	-0.027167	-0.027167	0.054333	0.023594	0.023594	-0.047188
0.15	-0.032142	-0.032142	0.064284	0.020051	0.020051	-0.040102
0.20	-0.037648	-0.037648	0.075296	0.015537	0.015537	-0.031073

nuclei of a molecule are expected to be vulnerable to the applied confining potential because of the induced distortion of the electron density of the entire molecule.

The computed EFGs at Li and H nuclei at $R = 1.60$ Å for several values of ω are listed in Table 9.2. Due to the linear symmetry of the molecule and the traceless property of the EFG tensor, $V_{xx} + V_{yy} + V_{zz} = 0$ and $V_{xx} = V_{yy}$. The details of the charge distribution around the nucleus of interest can therefore be determined solely by V_{zz}. As seen in Table 9.2, the magnitudes of V_{zz} for both Li and H are small, indicating the ionic character of ground state LiH as inferred from the enormous electric dipole moment. The closed-shell $Li^+(1s^2)$ and $H^-(1s^2)$ do not contribute to the EFG because of the spherical symmetry [35]. Yet, the non-zero EFGs of Li and H reveal that the polarization of the electron distribution by the bonding electrons of 2σ molecular orbital located in the region between the two nuclei, and that the spherical symmetry is not perfect in a molecular environment.

The variations of EFGs of Li and H due to the confinement effects, although not very remarkable in magnitude, are very informative concerning the changes of the electron distribution caused by the external harmonic potential. Two opposite trends are observed for the EFGs of Li and H. The V_{zz} of H is reduced by 60% when the confinement parameter ω is increased from zero to 0.20 a.u. Simultaneously, the V_{zz} of Li is incremented by 70%. The vanishing EFGs of H is apparently consistent with the conclusion from the wavefunction analysis that the ionic Li^+H^- character becomes more dominant in the ground state of confined LiH molecule. The larger extent of charge transfer to H results in the closed s-shell $1s^2$ configuration which

always has zero contribution to the EFG.

The situation of Li is more complicated, and two effects play the role in determining the V_{zz}. On one hand, the transfer of electron density towards H turns the electronic configuration of Li to be more $1s^2$-like, and decreases the EFG. On the other hand, the confining potential enhances the hybridization of the 2σ molecular orbital with the Li $2p_z$ atomic orbital, which modifies the valence electron density of Li and provides a positive contribution to the EFG. Because of the $1/r^3$ dependence of V_{zz}, the former effect is less important, and the deformation of the valence electron distribution predominates the change of EFG, leading to the net increase of V_{zz} in the presence of the confining potential.

9.4 Conclusions

In the present work, several of one-electron properties for the ground and first two excited states of LiH molecule, as well as their responses to the application of a harmonic confining potential of cylindrical symmetry were studied. It was observed that the ground state dipole moment is significantly increased by the confining potential due to enhanced ionic character. The effects are less profound in the excited states, but the configuration interactions prompted by the external potential result in subtle changes of the R-dependence of the dipole moments in these states.

The influence of the confining potential on the components of dipole polarizabilities of LiH, compared to the dipole moments, is more drastic. The geometric restriction imposed by the cylindrical potential gives rise to the anisotropic behavior of the axial and equatorial components of the polarizability tensor of the confined LiH. The compressed electron density in the equatorial directions results in the diminishing α_{xx} and α_{yy}; the α_{zz}, however, is more enhanced by the polarization of the 2σ molecular orbital.

The EFGs of LiH molecule are also affected by the alteration of its electronic configuration. The more important ionic character causes the reduction of the EFG of H as it possesses a larger extent of the closed-shell configuration. On the other hand, the confining potential induces the lowering of the Li $2p_z$ orbital and its mixing

with the 2σ molecular orbital, which brings forth the positive contribution to the EFG of Li.

Bibliography

[1] V. Fock, *Z. Phys.* **47**, 446 (1928).

[2] B. Povh, K. Rith, C. Scholz, F. Zetsche, *Particles and Nuclei: An Introduction to the Physical Concepts*, 3rd ed., Springer, New York, 2002.

[3] J. S. Blakemore, *Solid State Physics*, 2nd ed., Cambridge University Press, New York, 1998.

[4] G. A. Somorjai, *Chemistry in Two Dimensions: Surfaces*, Cornell University Press, London, 1981.

[5] R. C. Ashoori, *Nature* **379**, 413 (1996).

[6] D. Bielińska-Wąż, J. Karwowski, G. H. F. Diercksen, *J. Phys. B: At. Mol. Opt. Phys.* **34**, 1987 (2001).

[7] T. Sako, G. H. F. Diercksen, *J. Phys. B: At. Mol. Opt. Phys.* **36**, 1433 (2003).

[8] T. Sako, G. H. F. Diercksen, *J. Phys. B: At. Mol. Opt. Phys.* **36**, 1681 (2003).

[9] D. Bielińska-Wąż, G. H. F. Diercksen, M. Klobukowski, *Chem. Phys. Lett.* **349**, 215 (2001).

[10] T. Sako, I. Cernusak, G. H. F. Diercksen, *J. Phys. B: At. Opt. Mol. Phys.* **37**, 1091 (2004).

[11] J. M. H. Lo, M. Klobukowski, D. Bielińska-Wąż, G. H. F. Diercksen, E. Schreiner, *J. Phys. B: At. Opt. Mol. Phys.* **38**, 1143 (2005).

[12] D. Kedziera, A. Avramopoulos, M. G. Papadopoulos, A. J. Sadlej, *Phys. Chem. Chem. Phys.* **5**, 1096 (2003).

[13] M. W. Schmidt, K. K. Bridridge, J. A. Boatz, S. T. Elbert, M. S. Gordon, J. J. Jensen, S. Koseki, N. Matsunaga, K. A. Nguyen, S. Su, T. L. Windus, M. Dupuis, J. A. Montgomery, *J. Comput. Chem.* **14**, 1347 (1993).

[14] J. Ivanic, K. Ruedenberg, *Theoret. Chem. Acc.* **106**, 339 (2001).

[15] S. R. Langhoff, E. R. Davidson, *Int. J. Quantum Chem.* **8**, 61 (1974).

[16] K. K. Das, K. Balasubramanian, *J. Phys. Chem.* **95**, 42 (1991).

[17] H. Xu, K. Balasubramanian, *J. Mol. Spectrosc.* **171**, 555 (1995).

[18] L. Latifzadeh, K. Balasubramanian, *Chem. Phys. Lett.* **257**, 257 (1996).

[19] K. Balasubramanian, *J. Chem. Phys.* **112**, 7425 (2000).

[20] H. J. Werner, W. Meyer, *Phys. Rev. A* **13**, 13 (1976).

[21] M. Jaszuński, B. Roos, *Mol. Phys.* **52**, 1209 (1984).

[22] S. Huzinaga, *J. Chem. Phys.* **42**, 1293 (1965).

[23] W. Kołos, L. Wolniewicz, *J. Chem. Phys.* **46**, 1426 (1967).

[24] I. Černušák, V. Kellö, A. J. Sadlej, *Collect Czach. Chem. Commun.* **68**, 211 (2003).

[25] R. J. Bartlett, G. D. Purvis III, *Phys. Rev. A* **20**, 1313 (1979).

[26] H. A. Kurtz, J. J. P. Stewart, K. M. Dieter, *J. Comput. Chem.* **11**, 82 (1990).

[27] R. Velasco, *Can. J. Phys.* **35**, 1204 (1957).

[28] C. Yamada, E. Hirota, *J. Chem. Phys.* **88**, 6702 (1988).

[29] J. M. H. Lo, M. Klobukowski, *Mol. Phys.* **102**, 2511 (2004).

[30] L. Wharton, L. P. Gold, W. Klemperer, *J. Chem. Phys.* **37**, 2149 (1962).

[31] K. K. Docken, J. Hinze, *J. Chem. Phys.* **57**, 4928 (1972).

[32] M. Mérawa, D. Bégué, A. Dargelos, *J. Phys. Chem. A* **107**, 9628 (2003).

[33] R. Poteau, F. Spiegelmann, *J. Mol. Spectrosc.* **171**, 299 (1995).

[34] C. E. Dykstra, *Ab Initio Calculation of the Structures and Properties of Molecules*, Elsevier, New York, 1988.

[35] C. H. Townes, A. L. Schawlow, *Microwave Spectroscopy*, McGraw-Hill, New York, 1955.

Chapter 10

Final Remarks

10.1 Summary of the Thesis

This thesis presents the development of the model of confinement effects using a harmonic-type electrostatic potentials and its applications in the studies of electronic, structural, and spectral properties of a variety of diatomic molecules ranging from the simplest hydrogen molecule to the heavy coinage-metal hydrides such as AgH and AuH.

In this project, several classes of diatomic molecules have been used as probes of the influence of the axial parabolic potential on the chemical properties of the confined systems. The reason of choosing the diatomic molecules, as discussed in the previous chapters, is the fact that this arrangement assures the balanced Coulombic interaction between the confined linear diatomic molecule and the applied potential, with the molecule oriented so that its axis and the axis of the confining potential are collinear.

The series of studies started with the hydrogen molecule, which, because of its simplicity, allows for both the calculations employing highly sophisticated methods and very detailed wavefunction analysis, from which orbital responses to the confining potential can be understood. Then, the studies switched to an interesting system, Be_2, and its ions, whose HOMOs and LUMOs are nearly degenerate. Based on the understanding of the confinement effects on the hydrogenic atomic orbitals, it is anticipated that the orbital degeneracy in Be_2 molecule will be removed by the

cylindrical confining potential, and very interesting phenomena such as the changes of dissociation channels, the switch of ground-state symmetry, and induced ionization would likely be observed. To further explore the phenomenon of field-induced ionization due to the applied potential, the ionization of the valence electrons of the Rydberg noble-gas hydrides, which are only weakly bound, in the presence of the confining potential, was studies in details.

The interaction between the external confining potential and relativity, and their combined effects on many-electron molecular systems are not clearly understood because of the difficulties in terms of both experiment and computation. In order to shed light on this area, heavy coinage-metal hydrides, AgH and AuH, were chosen, whose relativistic properties are well known. In particular, the confinement effects on the spin-orbit coupling interaction were analyzed. Finally, a polar diatomic LiH molecule was selected as a candidate in the study of confinement effects on the dipole-induced electric and optical properties. This project aimed at the understanding of the influence of the distorted electron density due to the applied electrostatic potential on the measured polarizability of materials, and how this influence could be used in the design of new electronic materials with desirable non-linear optical properties.

Despite the popularity in the computational modeling of the electronic structures of multi-electron quantum dots and artificial atoms and molecules [1, 2, 3, 4, 5, 6, 7, 8], the applications of harmonic oscillator potential in the investigations of spatial confinement effects on molecular systems are still fairly limited. Hence, the present project should be considered as one of the first relatively systematic and comprehensive analyses in this area.

There are a number of interesting features of the model of harmonic-type confining potential that have been observed in the studies of confined molecules. As in the case of artificial atoms embedded in a magnetic field, the parabolic confinement with circular symmetry serves as a excellent model for the study of molecules in strong magnetic field. The analysis of the hydrogen molecule confined by a cylindrical two-dimension harmonic potential revealed that the results exhibit qualitative

and semi-quantitative agreement with those predicted for a magnetized hydrogen molecule on the surface of a neutron star by Detmer and co-workers using the numerical Hartree-Fock method [9, 10, 11, 12]. As shown in Chapter 3, the Hamiltonian used in the model of parabolic confinement is indeed closely related to that for a quantum system in a magnetic field; small modification may be performed in the confinement model so that it can be extended to the studies of magnetized objects.

Due to the geometry of the confining potential, the differentiation of orbitals which are degenerate in the field-free environment is achieved. Except for the s-orbitals which are spherically symmetric, the components of p and d-shell orbitals split according to the orientation of the applied harmonic potential. The induced reordering of atomic and molecular orbitals results in unusual changes in the physical and chemical properties of the confined systems. For example, the ground-state symmetry of Be_2^- molecular ion switches from $^2\Pi_u$ to $^2\Sigma_g^+$ because of the destabilization of the Π orbitals. In addition to the change of the molecular state symmetry, the presence of confining potentials causes the redistribution of dissociation channels and the existence of unprecedent avoided crossings between potential energy curves.

The effects of spatial confinement on the properties of Rydberg molecules have been investigated for two noble-gas compounds: HeH and NeH. Particular attention has been paid to the process of field-induced autoionization of the weakly-bound valence electrons of these systems. It was observed that this process can be facilitated by even a relatively weak confining potentials, and that the heavier the noble-gas element, the smaller the critical strength of the potential would be required. As an alternative theoretical treatment, the perturbative approach has been tested for these systems. Satisfactory results have been found; apparently, the perturbation theory up to the second-order would be sufficient for the studies of the low-lying excited states of Rydberg molecules in confinement.

The influence of the external harmonic oscillator was studied not only in the light main-group diatomic molecules but also in the transition-metal diatomics. The combined effects of relativity, electron correlation, and spatial confinement have been studied in the SO-MCQDPT2 calculations of the potential energy curves of the low-

lying electronic states of AgH and AuH. Like the previous examples, the presence of the confining potential alters the electronic configurations of these systems, giving rise to changes in various geometric and energetic parameters. Surprisingly, the influence is not as significant as could be seen in lighter species. In particular, only a very weak dependence of the spin-orbit coupling constants upon the strength of the confining potential is noticed.

Finally, the variations of electric properties of small molecules enclosed in a harmonic potential have been examined, as this may lead to a better understanding of the field modulation of molecular properties in nanomaterial electronics. For this purpose, dipole moments, dipole polarizabilities, and electric field gradients of several low-lying electronic states of LiH molecules confined by a parabolic potential were computed and their relation to the strength of the potential were analyzed. It has been found that the anisotropic spatial constraints can selectively enhance or suppress these electric properties in different orientations. This may allow for the fine-tuning of the molecular properties that suit the needs in the development of nanoscaled opto-electronic materials.

10.2 Future Work

The investigations of the model employed in this work are by no means complete, and further development is necessary. Among the required tasks, the derivation of analytic gradients is the most important as the current implementation allows only for the evaluation of single-point energies, and no geometry optimization is yet available. This restriction limited the present project to diatomic molecules whose potential energy curves could be mapped in a rather straightforward way. In order to perform geometry optimization, one has to utilize less accurate numerical techniques such as finite-difference methods.

An interesting project involving the confining potential is to investigate if the two-dimensional harmonic oscillator potential could be useful in the modeling of chemical reactions inside a confinement. To achieve this task, some preliminary calculations of collinear hydrogen exchange reactions have been performed using

both the current model and a helium nanotube.

An interesting future project would involve the modification of the present formalism so that it could be utilized in the studies of the effects of magnetic fields on molecular properties. As pointed out by Detmer et al. [9], the computations for molecules in magnetic field are very complicated, and so far most of the research has been focused on H_2^+ and H_2 only. Based on the comparison and analysis carried out in Chapter 3, the current model of confinement, with a small modification, offers a promising potential as an alternative method of looking into the magnetic effects on multi-electron molecules. As only small computer resources are required for the calculations including the confinement effects, the harmonic confining potential model would be an excellent means for the computational studies of the exotic molecular species in the outer space where magnetic field is a crucial factor determining their molecular properties.

Bibliography

[1] M. Macucci, K. Hess, G. J. Iafrate, *Phys. Rev. B* **48**, 17354 (1993).

[2] S. Tarucha, D. G. Austing, T. Honda, R. J. van der Haage, L. P. Kouwenhoven, *Phys. Rev. Lett.* **77**, 3613 (1996).

[3] D. G. Austing, Y. Tokura, T. Honda, S. Tarucha, M. Danoesastro, J. Janssen, T. H. Oosterkamp, L. P. Kouwenhoven, *Jpn. J. Appl. Phys., Part 1* **38**, 372 (1999).

[4] A. Sinha, R. Roychoudhury, *Int. J. Quantum Chem.* **73**, 497 (1999).

[5] J. Cioslowski, K. Pernal, *J. Chem. Phys.* **113**, 8434 (2000).

[6] C. Yannouleas, U. Landman, *Int. J. Quantum Chem.* **90**, 699 (2002).

[7] S. M. Reimann, M. Manninen, *Rev. Mod. Phys.* **74**, 1283 (2002).

[8] S. Dickmann, P. Hawrylak, *JEPT Lett.* **77**, 30 (2003).

[9] T. Detmer, P. Schmelcher, F. K. Diakonos, L. S. Cederbaum, *Phys. Rev. A* **56**, 1825 (1997).

[10] T. Detmer, P. Schmelcher, L. S. Cederbaum, *Phys. Rev. A* **57**, 1767 (1998).

[11] P. Schmelcher, T. Detmer, L. S. Cederbaum, *Phys. Rev. A* **61**, 043411 (2000).

[12] P. Schmelcher, T. Detmer, L. S. Cederbaum, *Phys. Rev. A* **64**, 023410 (2001).

Appendix A

Non-Crossing Rules

A.1 Introduction

The Born-Oppenheimer approximation [1] is among one of the best known and most widely used approximations in molecular physics and chemistry. This approximation is of great importance in the studies of chemical reaction dynamics in which the potential energy hypersurface of the system is required. This energy surface is usually constructed from the *ab initio* calculations of the involved atoms and molecules with the invocation of the Born-Oppenheimer approximation. By using it, the nuclear and electronic coordinates can be separated, and thus energies for different nuclear configurations can be computed and linked together to form the complete energy surface. However, recent studies have revealed that this approximation is not always valid; under certain circumstances the nuclear and electronic motions are not entirely uncoupled, and the simultaneous treatment of both the nuclear and electronic motions is mandatory. One typical example of such violation of the Born-Oppenheimer approximation is the conical intersection between electronic states of polyatomic molecules. For good reviews on the topic of conical intersections and vibronic coupling, see ref. [2, 3].

In most of the cases, the breakdown of Born-Oppenheimer approximation and the existence of conical intersection are not serious problems for diatomic molecules, especially for their ground-state potential energy curves. The situation, however, changes when one goes to studying the excited states of the diatomic molecules

where the energies of these states now become close to each other. In such scenario, it is possible to encounter a situation in which two states have same energy accidentally. The Born-Oppenheimer approximation guarantees the non-crossing property of different electronic states of the same spin and spatial symmetry according to the perturbation theory. Unfortunately, this analysis fails when there is another source of coupling, different from the spatial symmetry of the electronic states, coming into play.

Such situation has been observed in the cases of the E, F, G, and K $^1\Sigma_g^+$ states of cylindrically confined hydrogen molecule as described in Chapter 3. The figures

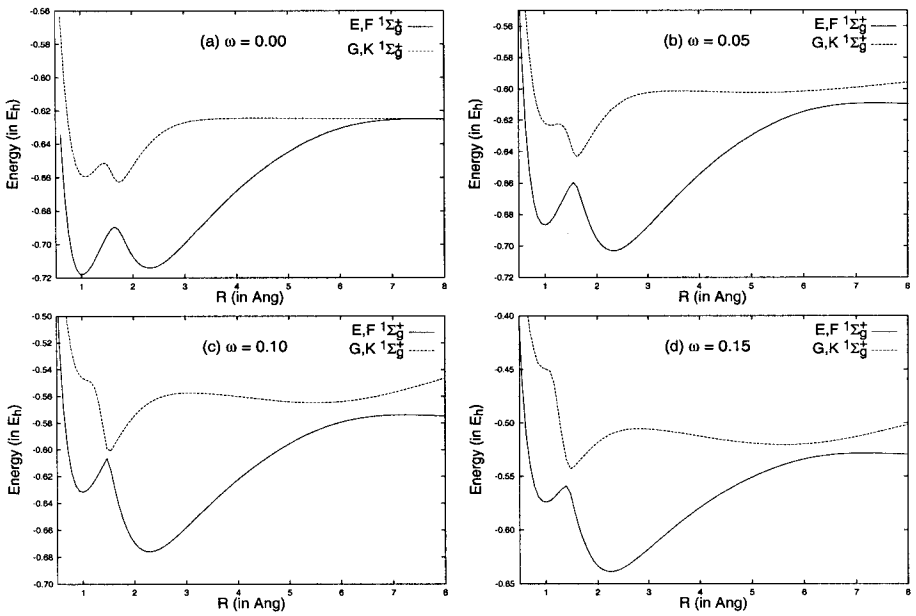

Figure A.1: The E,F and G,K States of H_2 in confinement.

A.1 show the potential energy curves of the E,F and G,K states of the hydrogen molecule confined by the harmonic potential of several different strengths ω. An avoided crossing is present between these states in the free space, which has been attributed to the interchange of the ionic $|1\sigma_u^2\rangle$ and covalent $|1\sigma_g 2\sigma_g\rangle$ configurations. At large internuclear distances, these states converge to the same dissociation limit of H($1s$) and H($n = 2$). When the confining potential is turned on, an ad-

ditional avoided crossing starts to appear at about 6 to 7 Å which is caused by the splitting of the second dissociation channel. These states have to undergo the second configuration interaction such that they could dissociate to the appropriate asymptotes. Surprisingly, it is found that the energy difference between the E,F and G,K states at the first avoided crossing dimishes with increasing ω, until at ω = 0.09 a.u. where the E,F and G,K states are only separated by about 500 cm^{-1} (as shown in figure A.2). Obviously, the strength of the applied potential ω has an

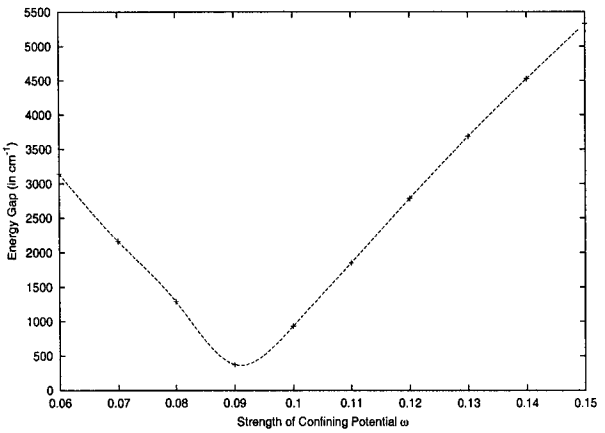

Figure A.2: Energy gap at the point of avoided crossing between the E,F and G,K $^1\Sigma_g^+$ states of H_2.

important role in the formation of the avoided crossings for confined molecules, and the Born-Oppenheimer approximation and degenerate perturbation theory are not sufficient to explain this phenomenon.

In the following sections, the derivation of the non-crossing rule from the traditional perturbation theory will be presented, and some of the breakdowns of this rule will be discussed.

A.2 Quasi-Degenerate Perturbation Theory

The treatment of quasi-degenerate energy levels using the perturbation theory can be found in many standard quantum mechanics textbooks. The derivation shown

below follows the approach of Bransden and Joachain [4].

Consider a two-level system in which the energy levels are not truly degenerate, but are separated by a small energy 2ϵ. Then,

$$E_1^{(0)} = E^{(0)} - \epsilon \tag{A.1}$$

$$E_2^{(0)} = E^{(0)} + \epsilon \tag{A.2}$$

where $E^{(0)}$ is the zeroth-order reference energy. Using the approach of the degenerate perturbation theory, the perturbed wavefunction can be expressed as a linear combination of the unperturbed wavefunctions:

$$\psi_r = \sum_k a_{rk}\psi_k^{(0)} = a_{r1}\psi_1^{(0)} + a_{r2}\psi_2^{(0)} + \sum_{k\neq 1,2} a_{rk}\psi_k^{(0)}. \tag{A.3}$$

Substituting ψ_r into the Schrödinger equation

$$\left(\mathcal{H}_0 + \lambda\mathcal{H}'\right)\psi_r = E_r\psi_r, \tag{A.4}$$

where $\mathcal{H}$ and $\mathcal{H}'$ are the unperturbed and perturbing Hamiltonians respectively, yields the following expression

$$\sum_k a_{rk}E_k^{(0)}\psi_k^{(0)} + \lambda\sum_k a_{rk}\mathcal{H}'\psi_k^{(0)} = E_r\sum_k a_{rk}\psi_k^{(0)}. \tag{A.5}$$

Recall that $\mathcal{H}\psi_k^{(0)} = E_k^{(0)}\psi_k^{(0)}$. In Dirac notation, left-multiplying eq. (A.5) by $\langle\psi_l^{(0)}|$ yields

$$\sum_k a_{rk}E_k^{(0)}\langle\psi_l^{(0)}|\psi_k^{(0)}\rangle + \lambda\sum_k a_{rk}\langle\psi_l^{(0)}|\mathcal{H}'|\psi_k^{(0)}\rangle = E_r\sum_k a_{rk}\langle\psi_l^{(0)}|\psi_k^{(0)}\rangle. \tag{A.6}$$

This expression will be simplified when assuming that $\langle\psi_l^{(0)}|\psi_k^{(0)}\rangle = 0$ for $l \neq k$:

$$a_{rl}E_l^{(0)} - a_{rl}E_r = -\lambda\sum_k a_{rk}\langle\psi_l^{(0)}|\mathcal{H}'|\psi_k^{(0)}\rangle. \tag{A.7}$$

When $l = 1$:

$$a_{r1}E_1^{(0)} - a_{r1}E_r = -\lambda a_{r1}\langle\psi_1^{(0)}|\mathcal{H}'|\psi_1^{(0)}\rangle - \lambda a_{r2}\langle\psi_1^{(0)}|\mathcal{H}'|\psi_2^{(0)}\rangle - \lambda\sum_{k\neq 1,2} a_{rk}\langle\psi_1^{(0)}|\mathcal{H}'|\psi_k^{(0)}\rangle. \tag{A.8}$$

For clarity, the notation $H'_{lk} = \langle \psi_l^{(0)} | \mathcal{H}' | \psi_k^{(0)} \rangle$ is used. Hence, the above expression can be rewritten as:

$$a_{r1} E_1^{(0)} - a_{r1} E_r = -\lambda a_{r1} H'_{11} - \lambda a_{r2} H'_{12} - \lambda \sum_{k \neq 1,2} a_{rk} H'_{1k} \tag{A.9}$$

$$a_{r1} \left(E_1^{(0)} + \lambda H'_{11} - E_r \right) + \lambda a_{r2} H'_{12} = -\lambda \sum_{k \neq 1,2} a_{rk} H'_{1k}. \tag{A.10}$$

Similarly, the expression for $l = 2$ can be worked out:

$$a_{r2} \left(E_2^{(0)} + \lambda H'_{22} - E_r \right) + \lambda a_{r1} H'_{21} = -\lambda \sum_{k \neq 1,2} a_{rk} H'_{1k}. \tag{A.11}$$

Because the coupling between these two states is small, it is anticipated that the terms on the right-hand side of eqs. (A.10) and (A.11) will be negligible. Therefore, these equations can be expressed as a matrix equation:

$$\begin{pmatrix} E_1^{(0)} + \lambda H'_{11} - E_r & \lambda H'_{12} \\ \lambda H'_{21} & E_2^{(0)} + \lambda H'_{22} - E_r \end{pmatrix} \begin{pmatrix} a_{r1} \\ a_{r2} \end{pmatrix} = \begin{pmatrix} 0 \\ 0 \end{pmatrix}. \tag{A.12}$$

This homogeneous matrix equation can be solved easily, and the energies E_r are given by:

$$\begin{aligned} E_r &= \frac{1}{2} \left\{ E_1^{(0)} + E_2^{(0)} + \lambda \left(H'_{11} + H'_{22} \right) \right\} \\ &\pm \frac{1}{2} \left\{ \left[E_1^{(0)} - E_2^{(0)} + \lambda \left(H'_{11} - H'_{22} \right) \right]^2 + 4\lambda^2 \left| H'_{12} \right|^2 \right\}^{1/2}. \end{aligned} \tag{A.13}$$

A.3 Non-Crossing Rule

The eq. (A.13) gives the energies for a quasi-degenerate two-level systems. It is straightforward to determine the energy difference between the two energy levels:

$$\Delta E = \left\{ \left[E_1^{(0)} - E_2^{(0)} + \lambda \left(H'_{11} - H'_{22} \right) \right]^2 + 4\lambda^2 \left| H'_{12} \right|^2 \right\}^{1/2}. \tag{A.14}$$

Again, λ is set to be unity for clarity. This expression can be used to evaluate the energy difference between two Born-Oppenheimer potentials. When two states are well separated, they can be treated as if they were two isolated electronic states, and no perturbation technique is required. However, when they are approaching each

other, the perturbation starts to take place, and the perturbation theory should be used in order to determine the coupling between the two states. In this situation, eq. (A.14) can serve as the probe indicating how the potential energy curves of these states respond to the mutual perturbation.

When two potential energy curves cross, $\Delta E = 0$, and

$$\left\{\left[E_1^{(0)} - E_2^{(0)} + H'_{11} - H'_{22}\right]^2 + 4\left|H'_{12}\right|^2\right\}^{1/2} = 0. \tag{A.15}$$

Since both terms inside the square root are always positive, the only way to have eq. (A.15) fulfilled is that both terms vanish simultaneously. That is,

$$\begin{cases} E_1^{(0)} - E_2^{(0)} + H'_{11} - H'_{22} = 0 \\ H'_{12} = 0 \end{cases}. \tag{A.16}$$

Assume that the two states $|\psi_1\rangle$ and $|\psi_2\rangle$ are of the same symmetry and degenerate. Obviously, the first part of eq. (A.16) is fulfilled. However, the second one is not since $H'_{12} = 0$ only if $|\psi_1\rangle$ and $|\psi_2\rangle$ are in different spatial symmetries. Consequently, eq. (A.15) is not true for two states which have the same symmetry. In other words, for any two states possessing the same symmetry, they can never become degenerate in energies, and their potential energy curves cannot cross.

A.4 Violation of the Non-Crossing Rule

The above-mentioned argument has been mathematically illustrated by von Neumann and Wigner [5] several decades ago, and this rule has worked very nicely for diatomic systems. Unfortunately, this rule does not hold for polyatomic molecules as there are more than one degree of freedom, and conical intersections can be formed on their potential energy surfaces.

Over the years, many researchers have noticed that even in the cases of diatomic molecules, the non-crossing rule is not necessarily valid. Gershtein and Krivchenkov [6], Power [7], and Hatton, Lichten and Ostrove [8] have shown the violation of the non-crossing rule in one-electron diatomics. Recently, Shi and co-workers generalized the results from previous studies and presented a thorough analysis of the non-crossing rule in high-order multi-dimensional spaces [9].

In all these analyses, it is argued that an assumption in the treatment of von Neumann and Wigner that the Hamiltonian operator for a diatomic molecule be determined solely by a single parameter, say the internuclear distance, is not appropriate. Recall that in the Born-Oppenheimer approximation, the molecular Hamiltonian can be written in terms of the internuclear distance R, and can be expanded as a Taylor series in R_0:

$$\mathcal{H}(R_0 + \delta R) = \mathcal{H}(R_0) + \left.\frac{\partial \mathcal{H}}{\partial R}\right|_{R=R_0} \delta R. \tag{A.17}$$

The second term in the Taylor series can be treated as a perturbation, yielding the off-diagonal matrix element H'_{12} in eq. (A.12):

$$H'_{12} = \langle \psi_1 | \left.\frac{\partial \mathcal{H}}{\partial R}\right|_{R=R_0} |\psi_2\rangle \delta R. \tag{A.18}$$

As shown above, this off-diagonal matrix element will disappear when $|\psi_1\rangle$ and $|\psi_2\rangle$ are of different symmetry.

For a more general case in which $\mathcal{H}$ is dependent upon more than one parameter, the Taylor series expansion on $\mathcal{H}$ will generate

$$\mathcal{H}(R_0 + \delta R, Z_0 + \delta Z, \ldots) = \mathcal{H}(R_0, Z_0, \ldots) + \left.\frac{\partial \mathcal{H}}{\partial R}\right|_{R=R_0} \delta R + \left.\frac{\partial \mathcal{H}}{\partial Z}\right|_{Z=Z_0} \delta Z + \cdots, \tag{A.19}$$

which will give the following off-diagonal matrix element:

$$H'_{12} = \langle \psi_1 | \left.\frac{\partial \mathcal{H}}{\partial R}\right|_{R=R_0} \delta R + \left.\frac{\partial \mathcal{H}}{\partial Z}\right|_{Z=Z_0} \delta Z + \cdots |\psi_2\rangle. \tag{A.20}$$

Obviously, now H'_{12} depends on R, Z, and other parameters, and there will be a number of ways H'_{12} can vanish. In the case of polyatomic molecules, R and Z can correspond to different structural parameters such as bond lengths and bond angles. As a result, the non-crossing rule fails for polyatomic molecules whose potential energy surfaces are characterized by more than one parameter.

Even though the electronic Hamiltonian for a diatomic molecule possesses one parameter R according to the Born-Oppenheimer approximation, indeed the wavefunction $|\psi\rangle$ can be written in terms of other quantities such as the charge density

under prolate spheroidal coordinate transformation [10]. In such a case, some specific combinations of charges will lead to the so-called second-order crossings.

In the present project, the strength of the confining potential ω can be considered as a parameter that defines the molecular Hamiltonian of the confined diatomic molecule. Accordingly, it is expected that the wavefunctions and the associated potential energy curves for different electronic states of the confined molecule should be dependent on ω as well, although the analytical expressions of the wavefunctions and energies in terms of ω are not known. Consequently, the variation of the energy gap between the E,F and G,K potential energy curves at the inner avoided crossing can be ascribed to the second-order crossing induced by the presence of the applied harmonic potential.

A.5 Summary

As a closing remark of this chapter, the short list of five experimentally observable situations concering the crossing of potential energy surfaces is given below.

1. *No crossing*: The two Born-Oppenheimer potentials do not cross because of the well-separated energies.

2. *Non-conical crossing*: Two states of different symmetries can cross as long as both requirements in eq. (A.16) are satisfieded simultaneously.

3. *Conical crossing*: Due to accidental circumstances, both conditions in eq. (A.16) are fulfilled without the consideration of spatial symmetry. This case happens most often on polyatomic molecules.

4. *The Jahn-Teller effect*: Both conditions in eq. (A.16) are satisfied by symmetry. This is accomplished by the distortion of the molecular symmetry so as to reduce the total energy of the molecule. The Jahn-Teller effect happens when the highest-occupied molecular orbitals (HOMO) of the molecule are degenerate, and the direct product of the irreducible representations of the HOMO and LUMO belongs to the irreducible representations of the vibrations modes,

i.e.,

$$\Gamma_{HOMO} \otimes \Gamma_{LUMO} \in \Gamma_{vib} \tag{A.21}$$

5. *Pseudo-Jahn-Teller effect*: When two states approach, the mutual distortion of the electronic configurations will lead to, instead of a crossing, the deviation of the potential energy curves from each other (e.g. vibronic coupling). This is in fact the typical response deduced by the quasi-degenerate perturbation theory.

Bibliography

[1] M. Born, R. Oppenheimer, *Ann. Phys.* **84**, 457 (1927).

[2] B. E. Applegate, T. A. Barckholtz, T. A. Miller, *Chem. Soc. Rev.* **32**, 38 (2003).

[3] G. A. Worth, L. S. Cederbaum, *Ann. Rev. Phys. Chem.* **55**, 127 (2004).

[4] B. H. Bransden, C. J. Joachain, *Quantum Mechanics*, 2nd edition, Prentice Hall, New York, 2000; Chapter 8.

[5] J. von Neumann, E. Wigner, *Phys. Z.* **30**, 467 (1929).

[6] S. S. Gershtein, V. D. Krivchenkov, *Sov. Phys. JETP* **13**, 1044 (1961).

[7] J. D. Power, *Phil. Trans. R. Soc. London Ser. A* **274**, 663 (1973).

[8] G. J. Hatton, W. L. Lichten, N. Ostrove, *J. Chem. Phys.* **67**, 2169 (1977).

[9] Q. C. Shi, S. Kais, F. Remacle, R. D. Levine, *J. Chem. Phys.* **114**, 9697 (2001).

[10] G. Hunter, H. O. Pritchard, *J. Chem. Phys.* **46**, 2146 (1967).

Appendix B

Double Group Symmetry

B.1 Introduction

It has been shown in Chapter 8 that a new set of symmetry labels, which are completely different from the conventional symbols Λ and S deduced in the Russell-Saunders coupling or jj-coupling schemes, are used to assign the symmetry of electronic states in relativistic calculations. This new set of designation, called the double group, was first introduced by Bethe [1] in order to take into account the spin-orbit coupling effect that may lead to the electronic states in point-group symmetry of the crystalline field corresponding to half-integral angular momenta.

The derivations in the theory of double groups are complicated and tedious. For more information concerning comprehensive details of the theory, one is referred to the original reference by Bethe [1] and some excellent reviews by Cotton [2], Bunker and Jensen [3], and Balasubramanian [4]. In this appendix, only the simplified procedures for the determination of the relativistic term symbol for an electronic state of a diatomic molecule will be outlined.

The relativistic term symbol of an electronic state for a diatomic molecule is composed of both the spin and spatial parts. The designation for the spin part is determined according to the table B.1. s in the double-group label D^s is the spin quantum number of the electronic state of an diatomic molecule.

The symmetry assignment for the spatial part is identical to that for the non-relativistic counterpart. Once these symbols are determined, the final relativistic

Table B.1: Spin states correlation for diatomics

D^s	$D^2_{\infty h}$ or $C^2_{\infty v}$
D^0	Σ^+
$D^{1/2}$	$E_{1/2}$
D^1	$\Sigma^- \oplus \Pi$
$D^{3/2}$	$E_{1/2} \oplus E_{3/2}$
D^2	$\Sigma^+ \oplus \Pi \oplus \Delta$
$D^{5/2}$	$E_{1/2} \oplus E_{3/2} \oplus E_{5/2}$
D^3	$\Sigma^- \oplus \Pi \oplus \Delta \oplus \Phi$

term labels can be deduced as the direct product of the two representations based on the following multiplication rules:

$$\Sigma^-(\text{spin}) \otimes \Pi(\text{spatial}) = \Pi \tag{B.1}$$

$$\Pi(\text{spin}) \otimes \Pi(\text{spatial}) = \Sigma^- \oplus \Sigma^+ \oplus \Delta \tag{B.2}$$

$$\Sigma^-(\text{spin}) \otimes \Sigma^-(\text{spatial}) = \Sigma^+ \tag{B.3}$$

$$\Pi(\text{spin}) \otimes \Sigma^-(\text{spatial}) = \Pi \tag{B.4}$$

$$E_{1/2}(\text{spin}) \otimes \Pi(\text{spatial}) = E_{1/2} \oplus E_{3/2} \tag{B.5}$$

$$E_{3/2}(\text{spin}) \otimes \Pi(\text{spatial}) = E_{1/2} \oplus E_{5/2} \tag{B.6}$$

Note that the direct multiplication of any irreducible representation and Σ^+ will generate the original irreducible representation.

$$\Sigma^+ \otimes \Sigma^- = \Sigma^- \tag{B.7}$$

$$\Sigma^+ \otimes \Pi = \Pi \tag{B.8}$$

$$\Sigma^+ \otimes \Delta = \Delta \tag{B.9}$$

The double-group irreducible representations of diatomic molecules are translated to their corresponding $\omega - \omega$ state representations as listed in table B.2.

As an illustrative example, let's consider the $^3\Pi$ state of AgH. The spin part of this state is transformed to, according to table B.1, $\Sigma^- \oplus \Pi$, and the spatial part is transformed to Π. Therefore, the direct products of these two sets of irreducible

Table B.2: Irreducible representations of double groups of diatomics and their $\omega - \omega$ state designation

Irreducible Representation	$\omega - \omega$ State Designation
Σ^+	0^+
Σ^-	0^-
Π	1
Δ	2
Φ	3
Γ	4
$E_{1/2}$	1/2
$E_{3/2}$	3/2
$E_{5/2}$	5/2

representations are:

$$(\Sigma^- \oplus \Pi) \otimes \Pi = \Sigma^+ \oplus \Sigma^- \oplus \Pi \oplus \Delta \tag{B.10}$$

which correspond, respectively, to 0^+, 0^-, 1 and 2 states in $\omega - \omega$ scheme. Note that both 1 and 2 states are doubly degenerate. Therefore, when the spin-orbit coupling is taken into account in the calculations, the $^3\Pi$ state will split into six energy levels, among which two pairs are degenerate.

Bibliography

[1] H. A. Bethe, *Ann. Physik.* **3**, 133 (1929).

[2] F. A. Cotton, *Chemical Applications of Group Theory*, 3rd edition, Wiley Interscience, New York, 1990; Chapter 9.

[3] P. R. Bunker, P. Jensen, *Molecular Symmetry and Spectroscopy*, 2nd edition, NRC Research Press, Ottawa, 1998; Chapter 18.

[4] K. Balasubramanian, *Relativistic Effects in Chemistry: Part A*, Wiley Interscience, New York, 1997; Chapter 5.